NORTHWEST GEOLOGY

The Journal of The Tobacco Root Geological Society

Volume 48, July 2019

44th Annual Field Conference

Geology of the Deer Lodge and Boulder Areas

July 26–28, 2019

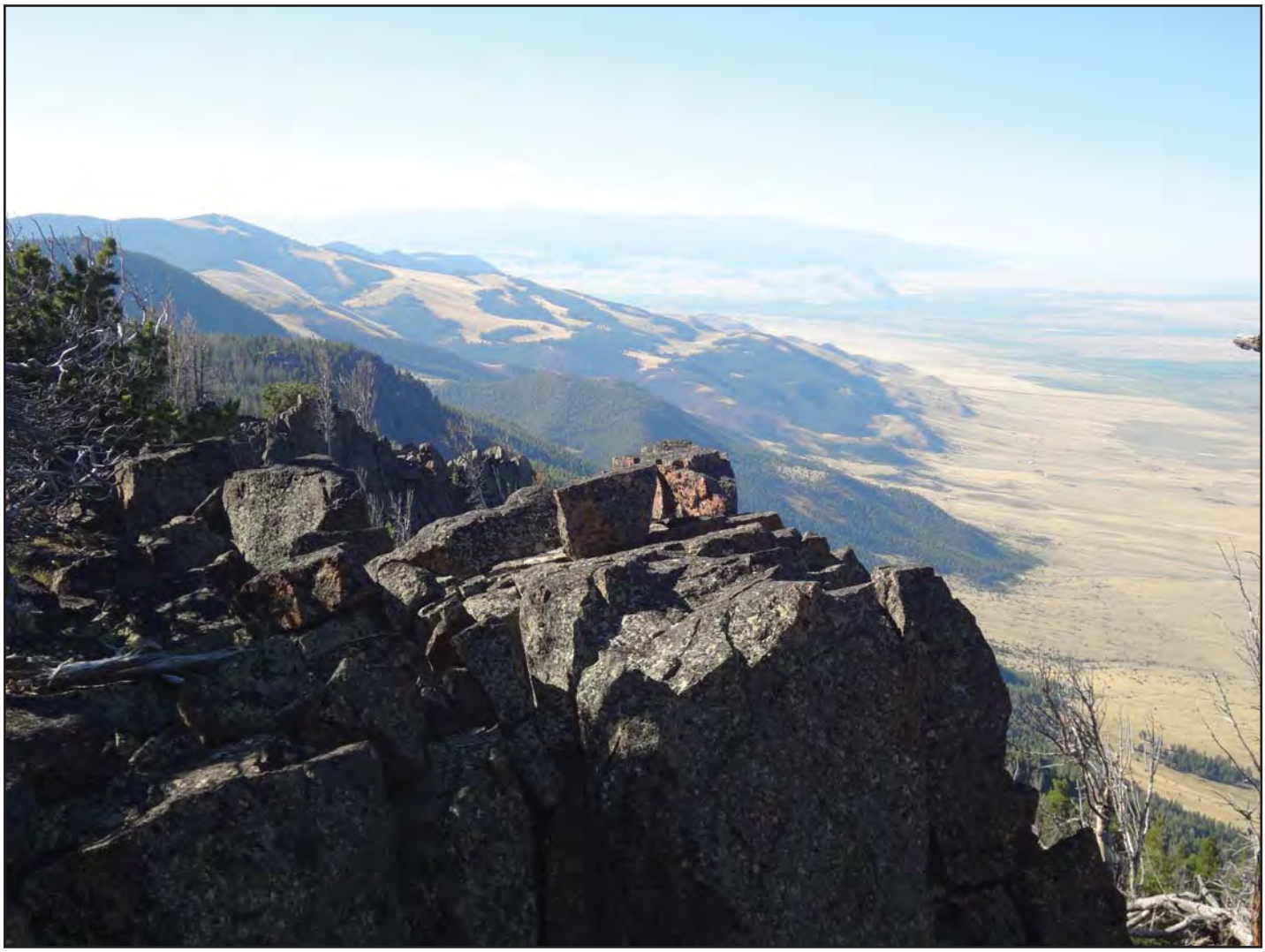

Published by The Tobacco Root Geological Society, Inc.
P.O. Box 118
Butte, Montana 59703

http://trgs.org

Edited by: Kaleb Scarberry

Cover photo by Kaleb Scarberry, MBMG.

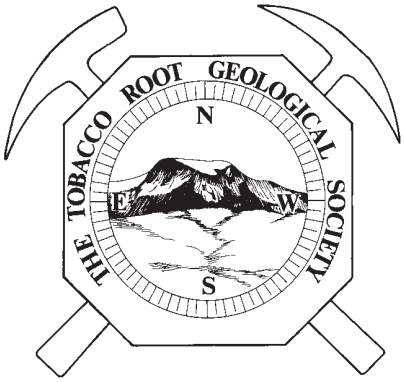

NORTHWEST GEOLOGY

The Journal of The Tobacco Root Geological Society

Volume 48, July 2019

44th Annual Field Conference

Geology of the Deer Lodge and Boulder Areas

July 26–28, 2019

Published by The Tobacco Root Geological Society, Inc.
P.O. Box 118
Butte, Montana 59703

http://trgs.org

Edited by: Kaleb Scarberry

The Tobacco Root Geological Society, Inc.

P.O. Box 118
Butte, Montana 59703

Officers, 2018:

President: Jesse Mosolf, Montana Bureau of Mines and Geology, Butte, MT
Vice-President: Alan English, Montana Bureau of Mines and Geology, Butte, MT
Treasurer: Katie McDonald, Montana Bureau of Mines and Geology, Butte, MT
Secretary: Sandy Underwood, Bozeman, MT
Corresponding Secretary: Lara Strickland, Columbus, MT
Webmasters: Petr Yakovlev, Montana Bureau of Mines and Geology, Butte, MT

Board of Directors, 2018:

Ted Antonioli, Geologist, Missoula, MT
Bruce E. Cox, Geologist (semi-retired), Missoula, MT
Larry Johnson, Consultant, Missoula, MT
Larry N. Smith, Dept. of Geological Engineering, Montana Tech, Butte, MT
Mike Stickney, Montana Bureau of Mines and Geology, Butte, MT
John Childs, Childs Geoscience Inc., Bozeman, MT
Emily Geraghty Ward, Geology Dept., Rocky Mountain College, Billings, MT

2019 Conference Organizers:

Kaleb Scarberry, Colleen Elliott, and Petr Yakovlev, Montana Bureau of Mines and Geology, Butte, MT

Editors: Kaleb Scarberry (MBMG)

Layout and Editing: Susan Barth (MBMG)

Printed by Insty-Prints, Butte, Montana

ISSN: 0096-7769

http://trgs.org

NORTHWEST GEOLOGY

The Journal of The Tobacco Root Geological Society

Volume 48, July 2019

Geology of the Deer Lodge and Boulder Areas

TABLE OF CONTENTS

TRGS 2019 SCHOLARSHIP AWARD WINNERS

* Caden Howlett (Foster), Montana State University
  Determining the relationship between magmatism, exhumation, and gold mineralization in the Anaconda Metamorphic Core Complex using detrital and igneous zircon geochronology, western Montana
* Crenshaw (Skipp), University of Montana
  Petrogenesis and tectonic implications of gedrite-anthophyllite-cordierite gneisses in the NW Wyoming Province
* Joel Dietrich (TRGS), Montana Tech
  Stratigraphic and structural analysis of the North Flint Creek Range near Gold Creek, Montana
* Matthew Ellison (Harrison), Utah State
  How complete is the Snowball Earth record in SE Idaho? Sequence stratigraphy and facies analysis of the Pocatello Formation
* Eve Lalor (Skipp), Western Washington University
  Scaling of environmental responses to multiple Eocene global warming events in the Bighorn Basin, Wyoming
* Kelly Helmer (Foster), Montana State University
  Structural geology of hydrothermal breccia pipes as potential hosts for mineral deposits and hydrocarbon reservoirs in central Montana
* Jacob Milton (Harrison), Idaho State University
  Geologic relations of the Neoproterozoic and Cambrian Wilbert Formation, Lost River Range, east-central Idaho
* Michael Kipp (Harrison), University of Washington
  A stable isotope study of nutrient cycling in the Cryogenian Pocatello Formation, Idaho
* Brandi Lawler (TRGS), University of Wyoming
  A spatial and temporal study of mafic volcanism across the Yellowstone plateau: Petrology, geochemistry, and geochronology of the basalts
* Nate Mitchell (TRGS), Indiana University
  Field mapping of fracture density within Mesoproterozoic Gneiss of the Belt Supergroup and its relationship with Bedrock River Morphology and erosion near Shoup, ID
* Jacob Palmer (TRGS), Montana Tech
  Structural analysis of the Gold Creek area
* Brianna Rick (Kleinkopf), Colorado State University
  Rock glaciers as climate resilient cold-water reservoirs in Rocky Mountain alpine basins
* Justin Rosenblume (TRGS), University of Iowa
  Tectono-stratigraphic history and multi-proxy provenance of a Cretaceous broken foreland basin in southwest Montana
* Grace Sutherland (TRGS), Western Washington University
  Thresholds in fluvial response to ancient global warming events in Bighorn Basin, Wyoming
* Megan Tarmichael (TRGS), University of Montana-Western
  The effects of beaver on lateral channel migration in Southwest Montana
* Kelly Thomson (TRGS), UT Austin
  Effects of hydraulic sorting on detrital zircon age spectra and sediment mixture modeling: Insights from the Upper Missouri River
* Rachelle Turnier (Harrison), University of Wisconsin-Madison
  Genesis and timing of corundum formation in southwest Montana
* Allie Ann Wolverton (TRGS), Rocky
  The growth of Earth's early continents: Kinematics and timing of a suture zone within the northern Wyoming Province of North America

TRGS CHARTER MEMBERS

Stanley W. Anderson
Clyde Cody
William S. Cordua
Lanny H. Fisk
Richard I. Gibson†
Thomas Hanley
Stephen W. Henderson
Thomas E. Hendrix
Mac R. Hooton
Inda Immega
Steven W. Koehler
Marian Millen Lankston†
Robert W. Lankston†
J. David Lazor
Joe J. Liteheiser, Jr.
Judson Mead*
Marvin R. Miller
Vicki M. Miller*
Allen H. Nelson
Alfred H. Pekarek
Patricia Price*
Donald L. Rasmussen
Raymond M. Rene

TRGS LIFETIME MEMBERS

John Childs
Rob Foster
Joan (Mrs. Jack) Harrison*
Karen Keefer
Layaka Mann
Chris Pool

† = co-founder
* = deceased

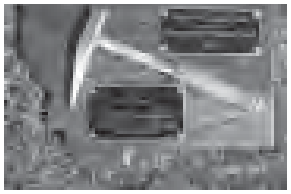

TRGS HAMMER AWARD RECIPIENTS

Awarded for distinguished achievement in the study of the geology of the Northern Rocky Mountains

1993: Ed Ruppel*
1994: Dick Berg
2003: Don Winston
2004: Dean Kleinkopf*
2009: Betty Skipp
2010: Jim Sears
2011: John Childs
2012: J. Michael O'Neill
2013: Paul Karl Link
2014: Reed Lewis
2015: Jeff Lonn
2016: Bruce Cox
2019: Susan Vuke

TRGS HONORARY MEMBERS

1980: Charles J. Vitaliano*
2008: Elizabeth Younggren*
(also honorary Board member)
2010: Dick Berg
2010: Bruce Cox
2010: Dean Kleinkopf*
2010: Dave Lageson
2011: Marie Marshall Garsjo
2011: Paul Link
2011: Rob Thomas
2012: Jeff Lonn
2012: Mitch Reynolds
2013: Reed Lewis
2015: Don Winston

DEDICATION

ELIZABETH "LIZ" BRENNER YOUNGGREN (1941–2019)

Liz was born in Butte, Montana on January 8, 1941, and was raised on the family ranch at Horse Prairie southwest of Dillon. She enjoyed natural sciences, animal care, art, and life on "the Prairie." Liz's love of science blossomed into a passion for geology. After graduating from Roland Hall in Salt Lake City, she attended and graduated from Wellesley College. With her geology degree in hand and adventure in her heart, she and a dear college friend traveled around the globe after graduation.

Liz then moved to Denver to start her professional career as a geologist for the United States Geological Survey. Her work at the USGS was diverse, including professional papers on topics such as uranium deposits, lithium occurrences in the western U.S., copper deposits in sedimentary and volcanic rocks, and black shale geochemical investigations.

Liz left the USGS in the late 1970s, returned to Dillon, Montana, and shortly thereafter launched her own business, X-Min Analytical Lab, providing x-ray diffraction analyses for industry and government clients. In the 1980s, Liz and her husband Tom Younggren returned to Horse Prairie and operated the Lazy E4 Cattle Company (Brenner Ranch). They made a winter home in Boulder City Nevada where they explored hectorite occurrences near Lake Meade and became geology volunteers for the Lake Meade National Recreation Area. During summers in Montana, Liz evaluated and promoted numerous mining properties in southwest Montana, including: the Chinatown gold lode and placer project, Argenta District properties, the Tamarack mine in the Tobacco Root Mountains, and zeolite deposits on Grasshopper Creek.

Throughout her life, Liz continued her interest and work in geology, including attaining credentials from the Gemological Institute of America and recently co-authoring the Geologic Map of the Coyote Creek 7.5' Quadrangle, Southwestern Montana (a return to her beloved Horse Prairie).

For more than three decades, interwoven with her professional work and ranch work, Liz was an active member of several professional organizations, most notably devoting countless hours and positive energy to TRGS, serving as an officer, director (and Honorary Board Member), scholarship committee member, and contributor to Northwest Geology.

The science of geology had a bright, enthusiastic friend in Liz. A visit to Horse Prairie might bring you a sense of her geologic inspiration.

2019 TRGS HAMMER AWARD

SUSAN VUKE

Susan Vuke was born in the upper midwest, but was destined for a life of Montana geology. Her childhood in Indiana and Michigan was a running exploration of all things biologic and earthy, including a 4H project in geology. Susan was awarded a geology scholarship to Indiana University and received her BS degree in Biology from IU in 1972. When she took the geologic field mapping course at the IU Geologic Field Station (IUGFS) in the Tobacco Root Mountains, the Montana hook was set. After graduation, Susan returned to Montana in a Volkswagen bug to become the Field Camp secretary for the IUGFS. After a brief stint at Betty's Café in Ennis, Susan attended graduate school at the University of Montana and earned her MS in Geology in 1979.

Susan began her professional career with a Montana geological consulting company focused on petroleum exploration mapping in the Montana disturbed belt. Having added industry experience to her résumé, she sought more challenging work.

Susan was hired by the Montana Bureau of Mines and Geology (MBMG) in 1981 as an Assistant Research Geologist and began a geologic mapping career that would cover most of the State. Her legacy is the superb geologic maps she published, including many quadrangle maps for eastern Montana where Susan's contributions to the stratigraphy and structure significantly improved on the previous generation of mapping. Susan was committed to balancing her work and family life, and camped with her children (Emily and Ben) during many of her eastern Montana field projects.

In 2005, Susan became an Associate Research Geologist with the MBMG and in 2014 was promoted to Senior Research Geologist. She guided compilation and was senior author for the revised Geologic Map of Montana (2007). Susan also published the popular Geologic Road Map of Montana (2015) and was recognized as a Lifetime Distinguished Researcher by the MBMG that same year. Susan"retired" in 2017, but continues to contribute to the STATEMAP program and the MBMG Centennial volume. This is fortunate, because we would be hard-pressed to find anyone who knows more about Montana regional geology than Susan.

The Tobacco Root Geological Society is pleased to honor Susan Vuke with the 2019 Hammer Award for her lifetime of excellence in geologic field work and in recognition of her incredible knowledge of Montana's geology. Thank you, Susan.

PAPERS

GEOLOGIC SUMMARY OF THE BUTTE NORTH 30' X 60' QUADRANGLE, SOUTHWESTERN MONTANA

Kaleb C. Scarberry, Colleen G. Elliott, and Petr V. Yakovlev

Montana Bureau of Mines and Geology

INTRODUCTION

The Montana Bureau of Mines and Geology (MBMG) recently completed the Geologic Map of the Butte North 30' x 60' quadrangle (Scarberry and others, in preparation). The Butte North 30' x 60' quadrangle contains abundant Late Cretaceous and Tertiary igneous rocks (fig. 1) formed during volcanic arc magmatism followed by orogenic collapse in western Montana. Interest in metallic mineral deposits associated with the igneous rocks has driven geologic research in the Butte North 30' x 60' quadrangle since the 1890s. Mineral resource exploration associated with the Butte, Welcome Creek, and Rock Creek mining districts was the focus of early geologic investigations (e.g. Weed, 1912; Blackwelder and Atwood, 1917). Geologic mapping efforts in the 1960s and 1970s by the USGS focused on the Boulder Batholith, in part to explore for mineral deposits (Becraft, 1960a,b; Becraft and Pinckney, 1961; Smedes and others, 1962; Ruppel, 1963; Wanek and Barclay, 1966; Weeks, 1974). Mapping efforts were limited from the 1960s onwards with the MBMG completing one quadrangle (Derkey and Bartholomew, 1988), and a 1:250,000 compilation (Lewis, 1998).

In 2004, in conjunction with the STATEMAP advisory committee, the MBMG selected the Butte North 30' x 60' quadrangle as a priority because it has world-class ore deposits, is transected by two major transportation corridors, has seen increased development in the valleys, and is within a major superfund site with ongoing reclamation. STATEMAP-funded mapping at 1:24,000 and 1:50,000 scale over the fol-

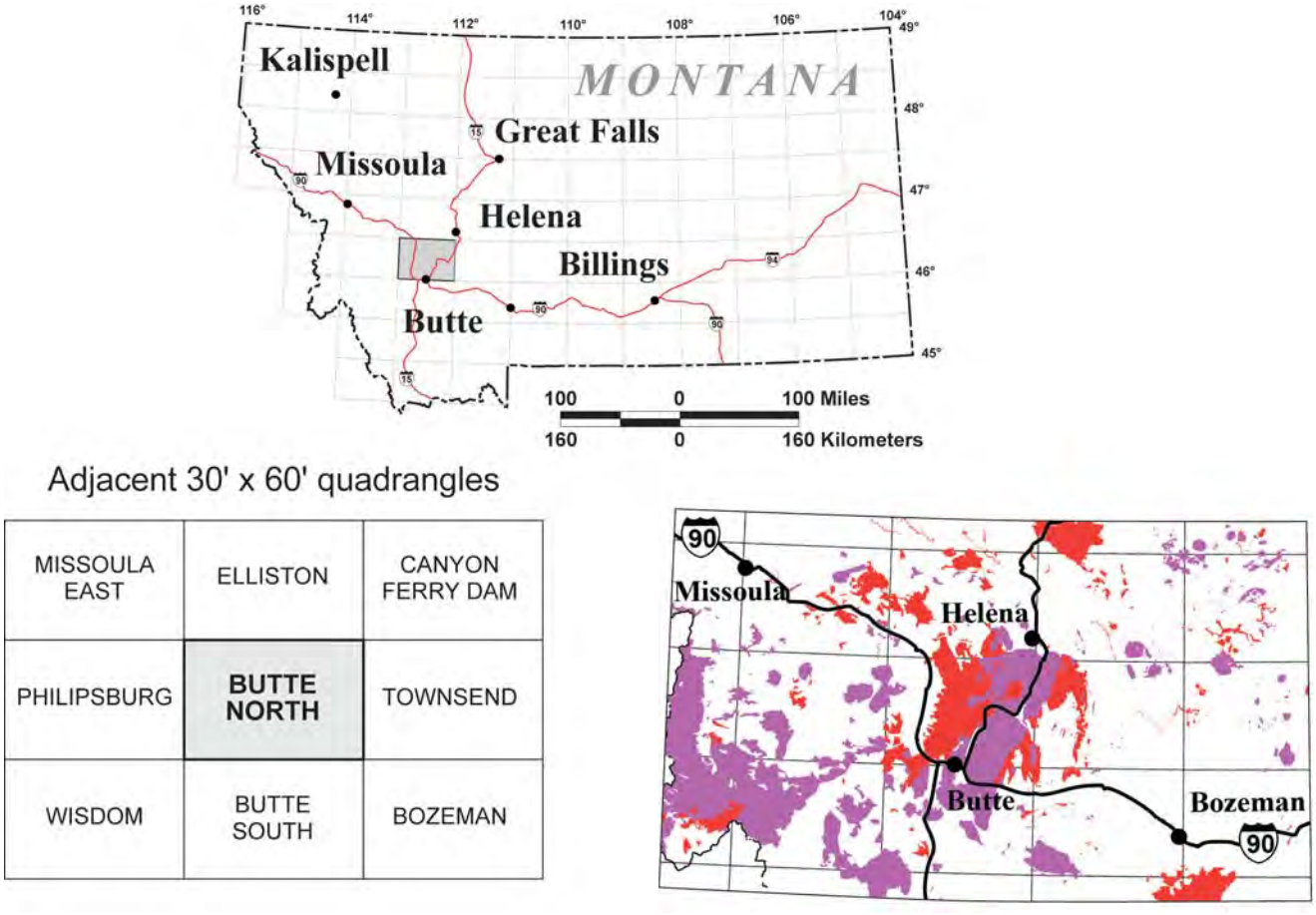

Figure 1. Location of the Butte North 30' x 60' quadrangle in southwestern Montana. The bottom right panel shows the distribution of volcanic (red) and plutonic (purple) rocks. Geology from Vuke (2015).

lowing 12 years significantly advanced knowledge of structural and igneous development of the area (Berg and Hargrave, 2004; Hargrave and Berg, 2013; Elliott and others, 2013; Scarberry and Elliott, 2016; Scarberry, 2016a,b, 2019; Scarberry and others, 2017, 2018). Other important contributions to mapping in the quadrangle include: (1) a geologic hazard assessment at 1:50,000 scale for Silver Bow County (Elliott and McDonald, 2009), (2) three 7.5' quadrangle maps produced as student EDMAP projects (Feeney and others, 2009; Olson and others, 2016, 2017), and (3) a detailed map and study of the Butte mining district (Houston and Dilles, 2013a,b).

The Butte North 30' x 60' quadrangle lies in a geologically complex area of southwestern Montana. Mesoproterozoic through Cretaceous metasedimentary and sedimentary rock, Cretaceous through Tertiary intrusive and volcanic rock, and Tertiary and Quaternary valley-fill and surficial deposits are all exposed in the quadrangle (figs. 2, 3). A major objective of new MBMG mapping and map compilation for Butte North was to better constrain the age and composition of the Late Cretaceous and Tertiary magma systems and to unravel the tectonic processes that contributed to Tertiary–Quaternary basin formation and sedimentation.

The dominant rock types in the quadrangle are igneous rocks of the Late Cretaceous Boulder Batholith and co-magmatic Elkhorn Mountains Volcanic Field, the Eocene Lowland Creek Volcanic Field, and Eocene–Oligocene volcanic deposits. The Boulder Batholith hosts two world-class porphyry Cu-Mo deposits, which are cut by polymetallic lode veins at Butte (Lund and others, 2002; Houston and Dilles, 2013a; Reed and others, 2013) .

Glacial deposits are particularly abundant in the north-central part of the quadrangle, and on the western margin of the Deer Lodge Valley. The quadrangle is characterized by high elevation, low relief topography in the Boulder Mountains, and rugged alpine topography in the Flint Creek and Anaconda ranges at its western edge. The continental divide crosses the central portion of the quadrangle, separating the Clark Fork and Missouri watersheds.

LATE CRETACEOUS–EOCENE MAGMATISM AND VOLCANIC STRATIGRAPHY

Volcanic arc magmatism accompanied Mesozoic contraction in the continental interior at the eastern edge of the U.S. Cordillera in Montana. In southwestern Montana, contraction culminated locally with Laramide basement-cored uplifts and significant erosion (summary in Yonkee and Weil, 2015). Radiometric ages indicate that near Butte compressional deformation from 79 Ma to 58 Ma was replaced by extension and normal faulting by 54 Ma (Foster and others, 2010; Houston and Dilles, 2013a).

The Elkhorn Mountains Volcanic Field

The Elkhorn Mountains Volcanic Field (EMVF) was named for volcanic deposits described in the Elkhorn Mountains (Klepper and others, 1957). The EMVF is exposed over an area greater than 25,000 km^2 that includes both flanks of the Boulder Batholith and roof pendants in the batholith (fig. 2). Together, the EMVF and Boulder Batholith represent a rare and well-preserved record of continental magmatism (e.g., Lipman, 1984). USGS geologists mapped and described much of the EMVF during the 1950s through the 1970s (Robertson, 1953; Klepper and others, 1957; Ruppel, 1961, 1963; Becraft and others, 1963; Prostka, 1966; Smedes, 1966; Klepper and others, 1971; Weeks, 1974). Smedes (1966) divided the deposits into three members:

(1) A lower member characterized by basaltic andesite to rhyodacite lavas, and pyroclastic and epiclastic volcanic deposits. In the northern Elkhorn Mountains the lower member consists of about 650 m of andesitic epiclastic and volcaniclastic sedimentary deposits that are intruded by mafic sills, and interstratified with andesite tuffs and amygdaloidal basaltic lavas (Smedes, 1966).

(2) A middle member with at least seven welded rhyolite ignimbrite sheets intercalated with epiclastic volcanic debris derived from erosion of the lower member that is around 1,500 m thick near Elkhorn (Klepper and others, 1971).

(3) An upper member consisting of bedded and water-laid tuff and andesitic epiclastic volcanic rocks (Smedes, 1966) that are exposed in the larger roof pendants to the Boulder batholith north of the town of

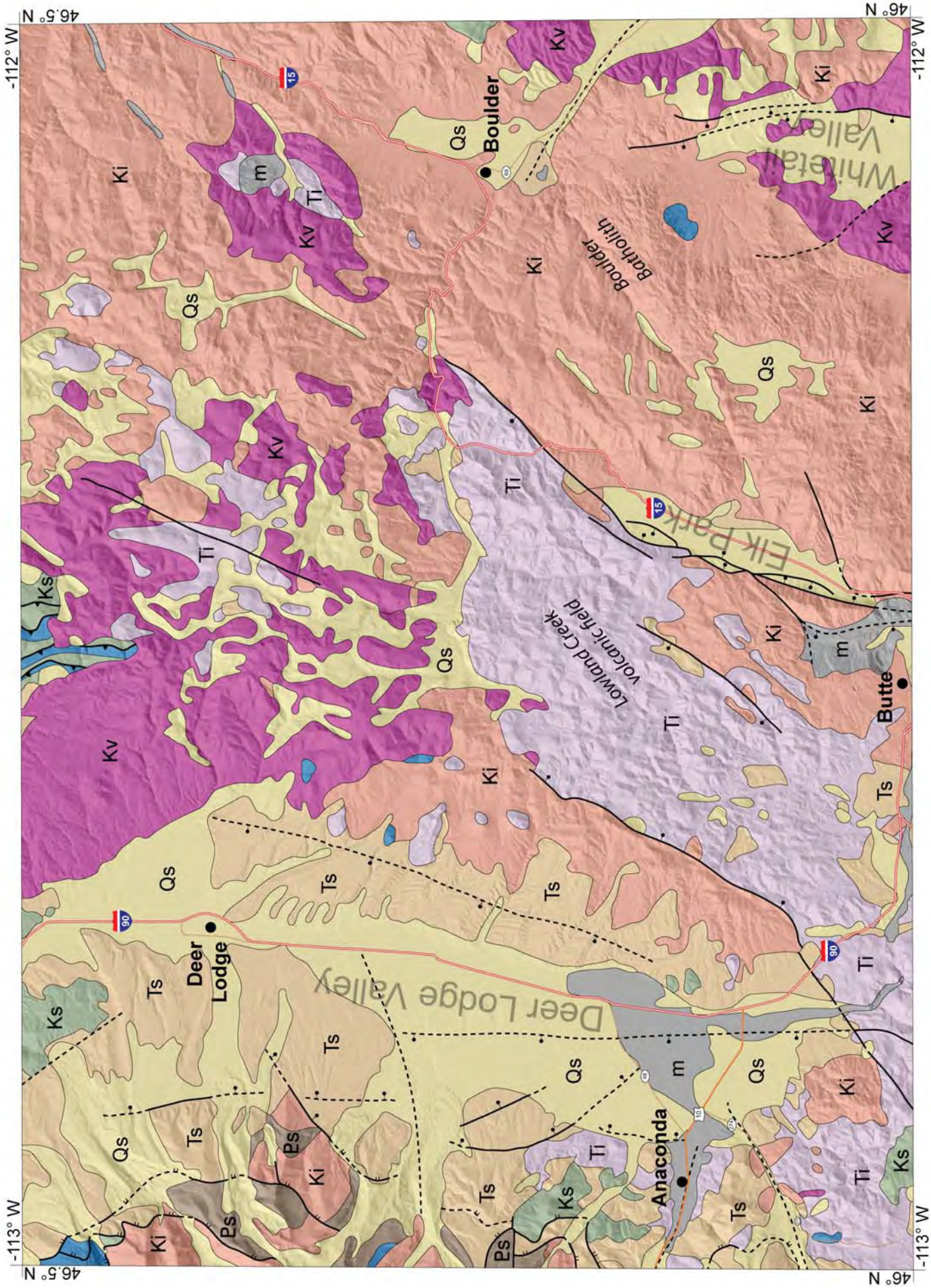

Figure 2. Simplified geologic map of the Butte North 30' x 60' quadrangle. Figure 3 shows a correlation diagram for the rock types.

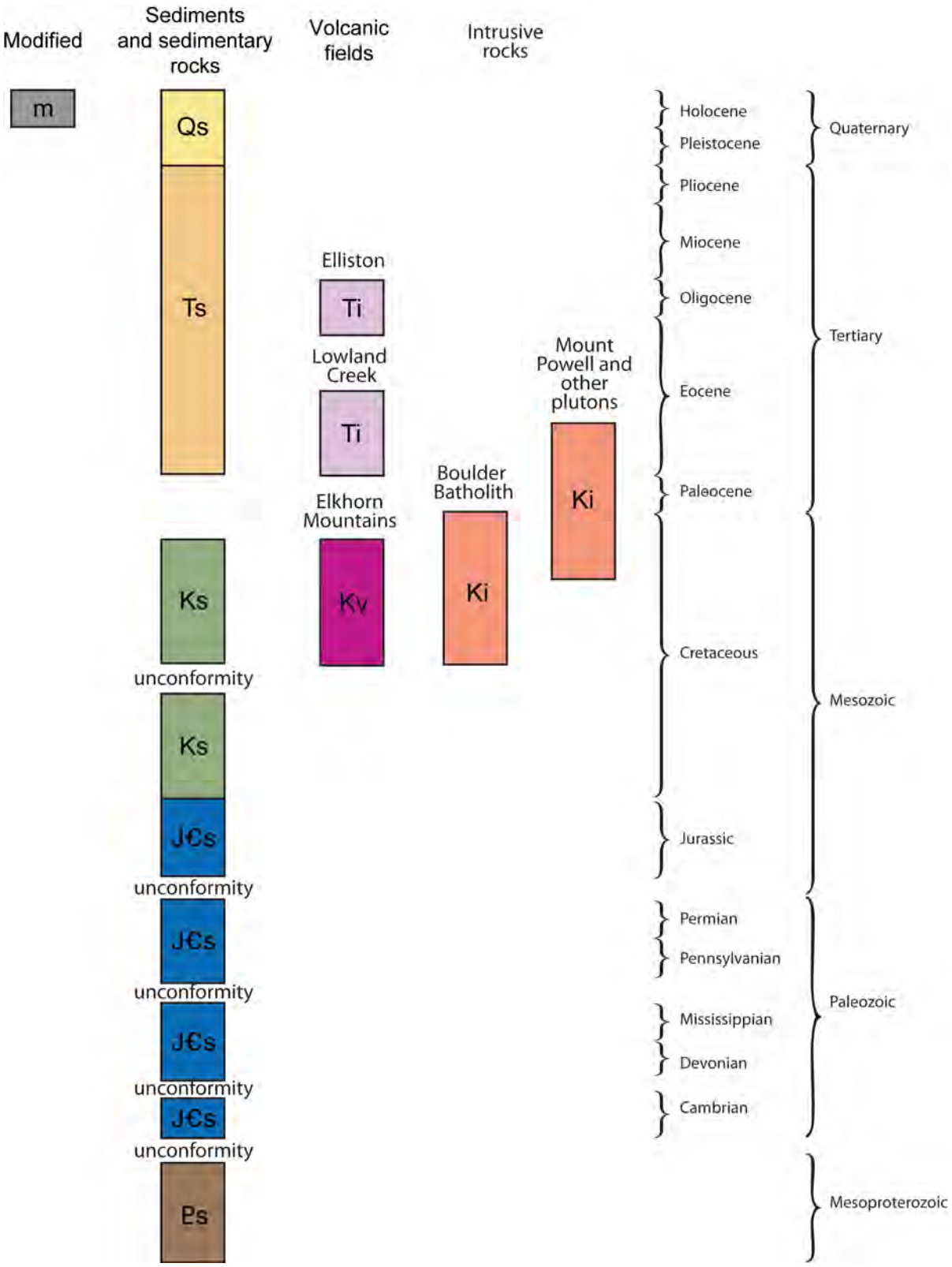

Figure 3. Correlation diagram for the rock types shown on the simplified geologic map of the Butte North 30’ x 60’ quadrangle.

Boulder (fig. 2; Becraft and others, 1963; Olson and others, 2017).

Recent mapping in the EMVF has focused on the age (fig. 4), composition, and emplacement history of the igneous deposits. The EMVF consists of basalt–rhyolite (SiO_2 about 49 to 78 wt. percent) compositions that fall within the range of compositions of Boulder Batholith plutons (fig. 5). Late Cretaceous basalt–andesite lava flows and gabbro–diorite plutons are some of the most mafic compositions (SiO_2 about 49 to 60 wt. percent) in the Butte North 30' x 60' quad-

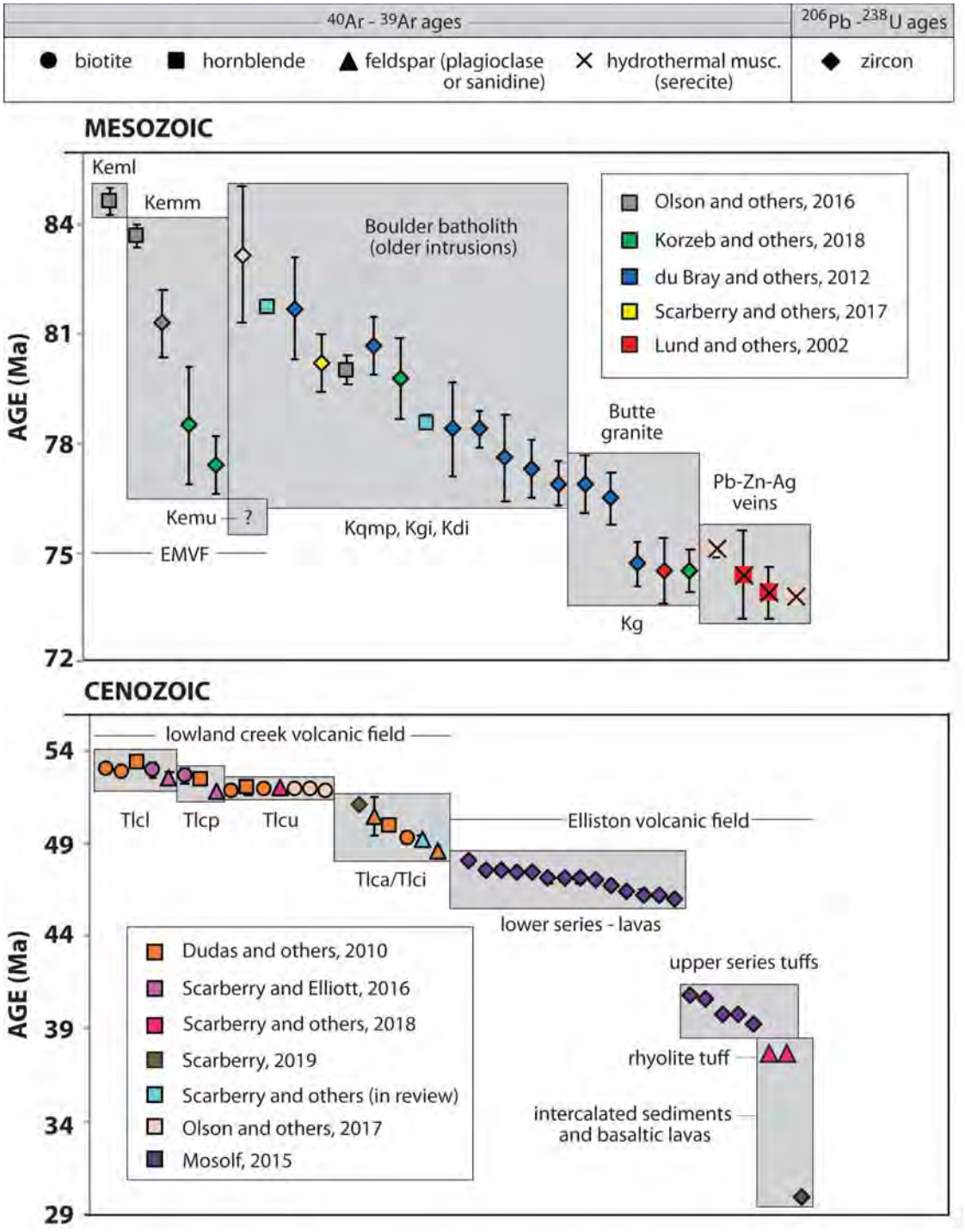

Figure 4. Summary of published and unpublished radiometric age determinations from igneous rocks within and adjacent to the Butte North 30' x 60' quadrangle.

rangle. A notable difference between the co-magmatic EMVF and Boulder Batholith rock suites is a compositional gap in the EMVF, from around 66 to 70 wt. percent SiO_2 (fig. 5). Rocks in the EMVF are predominantly metaluminous and calc-alkaline.

The lower member EMVF is older than about 84 Ma, constrained by radiometric ages from the overlying middle member rhyolite ignimbrites. On the west side of the Boulder Batholith ignimbrite eruptions occurred between about 80 Ma and 76 Ma (Korzeb and others, 2018), whereas on the east side of the batholith ignimbrite eruptions occurred between 85 Ma and 81 Ma (Olson and others, 2016). These ages imply that the middle member ignimbrites are either younger on the west side of the batholith than they are on the east side, or that the young ignimbrites on west side of the batholith are interstratified with the upper member of the EMVF. In the main roof pendant to the Boulder Batholith, located north of Boulder (fig. 1), upper member volcanic sandstones and middle member

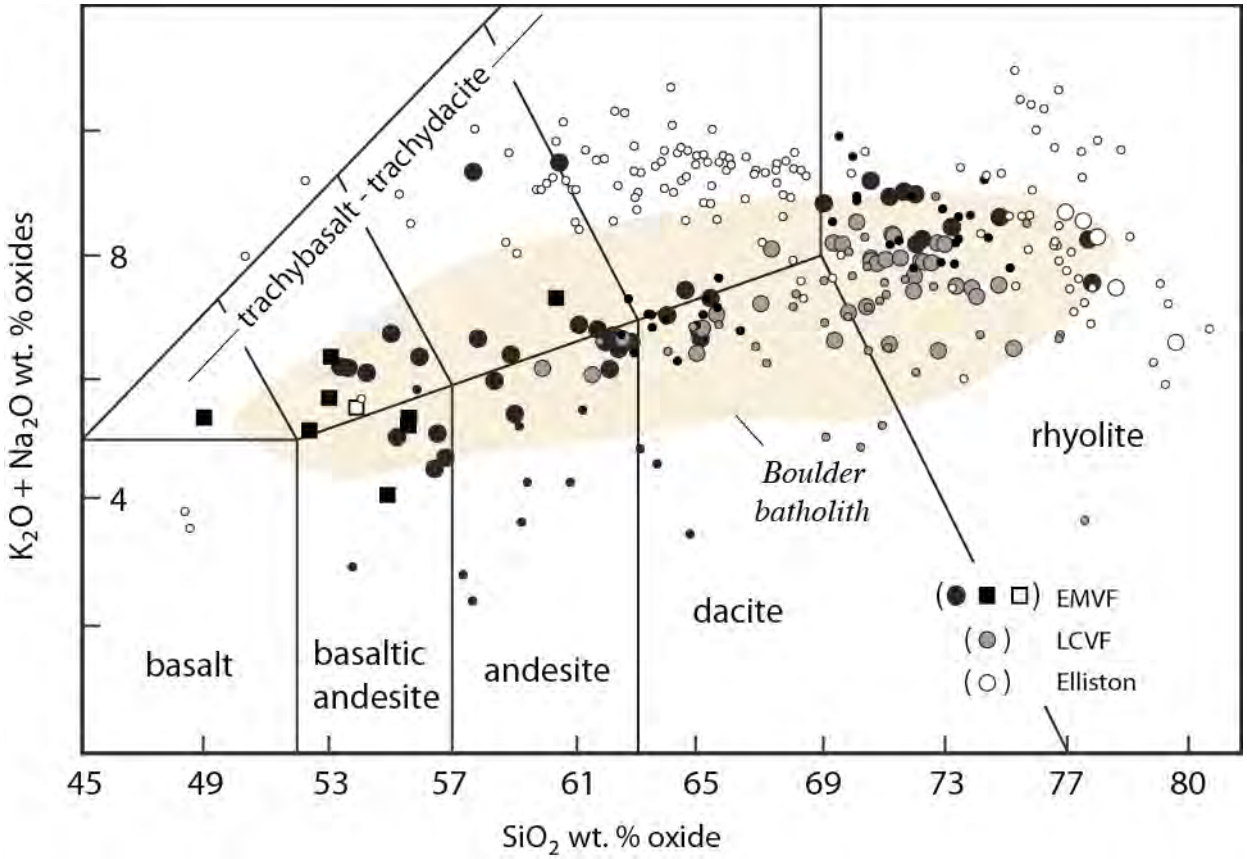

Figure 5. Total alkali vs. silica diagram (Le Bas and others, 1986) for rocks in the Butte North 30' x 60' quadrangle. Data from this study shown as large symbols. Squares are EMVF gabbro–diorite intrusions and lamprophyres. Previous work (small symbols) includes: Becraft and others (1963), Ruppel (1963), Smedes (1966), Dudas and others (2010), Derkey and Bartholomew (1988), Mosolf (2015), and Olson and others (2016, 2017). The Boulder Batholith field (tan), encompasses >95% of the data presented by du Bray and others (2009).

ignimbrites are crosscut by 83 Ma granite porphyry intrusions (Olson and others, 2017). High-K dikes and sills, some that are lamprophyres, intruded the lower and middle members of the EMVF between about 82 Ma and 76 Ma (DeWitt and others, 1996; Sears and others, 1998; Olson and others, 2016; Scarberry and others, in preparation).

Middle member ignimbrites on the eastern flank of the Boulder Batholith (fig. 1) were correlated over distances of tens of kilometers using the stratigraphic nomenclature of Prostka (1966; also Olson and others, 2016; Scarberry and others, 2017, this volume). These efforts determined that three of the ignimbrites are regionally extensive, rheomorphic, and have minimum eruption volumes of 200–400 km^3. Rheomorphic flow indicators show NNE–SSW and E–W movement of the units during cooling (Olson and others, 2016; Scarberry and others, 2016). Most of the EMVF vents are probably lost to erosion, but vent-proximal deposits are described on the western flank of the batholith (Scarberry, 2016b; Scarberry and others, this volume) and also along its eastern flank (DeWitt and others, 1996; Olson and others, 2016; Scarberry and others, 2017).

The Lowland Creek Volcanic Field

The 53 to 49 Ma Eocene Lowland Creek volcanic field is exposed north and west of Butte in a 10-km-wide, 65-km-long, NE-trending belt that cuts the Late Cretaceous Boulder Batholith and the EMVF (fig. 2) (Smedes, 1962; Smedes and Thomas, 1965; Dudas and others, 2010). Eocene andesite–rhyolite and related subvolcanic intrusions in the Lowland Creek volcanic field (LCVF) form a continuous suite, from SiO_2 of about 60 to 76 wt. percent (fig. 5). The LCVF suite is predominately peraluminous and calc-alkaline. The LCVF is distinct relative to the EMVF and the Eocene–Oligocene Elliston volcanic field because it is dominated by dacite–rhyolite compositions, with rare andesite compositions and basalt compositions absent (fig. 5). Volcanic products include rhyolite tuffs, porphyry rhyodacite lavas, and small piles of crystal-poor andesite. Lavas collectively have a maximum regional thickness of 1,830 m (Smedes, 1962) and original volume of about 310 km^3.

The Elliston Volcanic Field

Mosolf (2015) described an approximately 1-km-thick sequence of Late Eocene to Oligocene lavas and fragmental volcanic rocks exposed between Missoula and Helena in the Elliston 30' x 60' quadrangle (fig. 1). These rocks occur in the northern quarter of the Butte North 30' x 60' quadrangle but remain understudied. Rocks in the Elliston volcanic field are metaluminous, particularly for basalt–andesite compositions, to peraluminous and are more alkaline than the EMVF or the LCVF suites. These rocks post-date the LCVF (fig. 4) and are informally referred to here as the Elliston volcanic field. The Elliston volcanic field consists of a 48 Ma to 46 Ma lower series that is dominantly intermediate composition lavas, and a 41 Ma to 39 Ma upper series that consists mainly of voluminous rhyolite lavas and tuffs. Bimodal, basalt–rhyolite lavas and ash-flow tuffs erupted between 37 and 30 Ma and are interstratified with Renova Formation sediments (fig. 4; Mosolf, 2015; Scarberry and others, 2018).

Geochemistry

We examined the bulk compositions of 91 igneous rock samples from the Butte North quadrangle: 41 samples of the Late Cretaceous EMVF, 8 samples of Late Cretaceous gabbro–diorite dike rocks, 37 samples from the Eocene LCVF, and 5 samples of rocks related to the Late Eocene–Oligocene Elliston volcanic field. Most of our samples fall within range of published results (fig. 5) with only a few exceptions. Our work adds to what is known about mafic plutonic rocks in the Boulder Batholith and extends the mafic end of the LCVF compositions to around 60 wt. percent silica. Trace element enrichments in Late Cretaceous–Eocene rocks are consistent with magma generation in a volcanic arc. However, the Eocene LCVF suite is enriched in fluid-mobile elements (Th, Rb) compared to less mobile elements (Nb, Zr) relative to the EMVF. Relative enrichments of fluid-mobile elements in the LCVF is consistent with magma generation in a non-typical volcanic arc setting characterized by melting of a metasomatized lithospheric mantle (e.g., Feeley, 2003). The Tertiary ignimbrite associated with the Elliston Volcanic Field shows an enrichment pattern opposite to that of LCVF, suggesting that primary mantle melts began to play an important role in magma generation.

Radiometric Ages

New ^{40}Ar-^{39}Ar age dates add to the understanding of magmatic episodes in the quadrangle (fig. 4). Gabbro–diorite plutons and lamprophyric dikes, sills, and laccoliths formed in the EMVF–Boulder Batholith magma system between about 82 and 76 Ma. It is unclear how these plutons relate to basalt–basaltic andesite lavas in the lower member EMVF. The gabbro–diorite plutons appear to be several Myr younger than the lower member EMV lavas despite compositional similarities (fig. 5; SiO_2 about 53 to 60 wt. percent). Gabbro–diorite plutons and lamprophyre cuts the lower EMVF on the west side of the batholith (Scarberry and others, 2018; Sears and others, 1998), and the lower and middle EMVF on the east side of the batholith (DeWitt and others, 1996; Scarberry, 2016a; Olson and others, 2016).

New ages from the LCVF (fig. 4) confirm that the upper ignimbrite (Dudas and others, 2010; Olson and others, 2017) formed at about 52 Ma and erupted from vents north of Butte (Houston and Dilles, 2013a) and west of Jefferson City (Olson and others, 2017). North of Ramsay outcrops of rhyodacite porphyry lava flows and dikes crosscut the two major ignimbrite units and are interpreted as intercaldera deposits (Scarberry, 2019). One of the dikes yielded a U-Pb zircon age of about 51 Ma and probably formed during resurgent doming of a caldera floor (e.g., Hargrave and Dresser, 2000). A 37 Ma ignimbrite mapped in the Butte North quadrangle (Scarberry and others, 2018) is related to the Elliston volcanic field (e.g., Mosolf, 2015). The top and base of the 250-m-thick ignimbrite sequence formed during one eruption, and its thickness alone suggests that it formed near a vent.

New U-Pb detrital zircon spectra from five outcrops of sediments interlayered with the Lowland Creek Volcanic Field document maximum depositional ages ranging from 52.9 ± 1.8 Ma to 49.97 ± 0.22 Ma. A depositional age greater than 50 Ma would be the oldest for Cenozoic sediments and sedimentary rocks in western Montana, giving them a North American Land Mammal (NALMA) age of Wasatchian (Barnosky and others, 2014). A U-Pb detrital zircon analysis for Renova strata at Robinson Ridge near the west side of the Butte North quadrangle yielded zircons with concordant ages of ~25 and 26 Ma, and one with a discordant age of 26 Ma, all of which fall within the Arikareean NALMA age range. A thin tuff

layer interbedded with fluvial deposits on the east side of the Deer Lodge Valley yielded a maximum U-Pb zircon age of 9.69 ± 0.19 Ma, the youngest recorded from the region.

TECTONIC HISTORY

Cretaceous and older rocks along the western edge of the Butte North quadrangle (fig. 2) were deformed and metamorphosed during Sevier contraction in Late Cretaceous through early Paleocene times (Harlan and others, 1988; Lageson and others, 2002). In the Philipsburg 30' x 60' quadrangle to the west of Butte North (fig. 1; Lonn and others, 2003), there is evidence of as many as five generations of Sevier deformation structures, including extensional faults and top to the west shear zones and nappe folds, as well as the more commonly recognized east to northeast verging folds and thrust faults (Lonn and others, 2003; Berger and Elliott, 2004, 2007; Lonn and Elliott, 2011). In the Butte North quadrangle, signs of this complex deformation history are found in refolded folds in metamorphosed Blackleaf and Kootenai Formations north of Anaconda, in transposed amphibolite facies fabrics in Piegan Group calc-silicates on Mount Powell, and in the large stack of east-dipping, upside down, Ravalli Group quartzite north of Mount Powell.

Map relationships within the Butte North quadrangle show that the Boulder Batholith was emplaced during orogenesis. A gently folded, north-plunging anticline at the eastern margin of the Boulder Batholith is 30° oblique from the eastern margin of the batholith (Scarberry and others, this volume), suggesting that folding occurred before intrusion. The northern margin of the Boulder Batholith near Helena (fig. 1) is aligned with the hinge of a tight, south-plunging anticline (see map of Stickney and Vuke, 2007) suggesting a genetic connection between the batholith and folding. A penetrative cleavage within the Butte Pluton is a strong indication that contraction continued after intrusion of the batholith. The contact between the east side of the batholith and the Elkhorn Mountains Volcanic Field cuts straight through rugged topography for about 150 km, which suggests that the eastern Boulder Batholith margin was intruded along a preexisting high-angle fault (Schmidt and O'Neill, 1982; Schmidt and others, 1990; Berger and others, 2011).

Extensional structures that formed after Sevier contraction dominate the large-scale architecture of the Butte North 30' x 60' quadrangle. The most extension occurred above the Anaconda Metamorphic Core Complex (AMCC), which is exposed along the western edge of the quadrangle (O'Neill and others, 2004; Foster and others, 2007, 2010; Kalakay and others, 2014). The core of the AMCC is a thinned sequence of Mesoproterozoic to Cretaceous metasediments intruded by Late Cretaceous to Paleocene plutons, dikes and sills, the youngest of which were intruded during AMCC formation (Foster and others, 2010). Extension, which occurred from about 54 to 27 Ma (Foster and others, 2010), was accomplished by movement onset of shallowly dipping, weakly mylonitic detachment faults, collectively called the Anaconda Detachment Zone (Elliott, this volume). The faults dip northeast, east, and southeast, and extend into the subsurface below the Deer Lodge Valley and probably much farther east (Foster and others, 2010). Extension was initially described as towards the east–southeast direction (O'Neill and others, 2004; Foster and others, 2010; Kalakay and others, 2014), but our work identifies more than one extension direction and a more complex history (Elliott, this volume). The Anaconda Detachment Zone likely forms the base of valley fill in the Deer Lodge Valley where six oil and gas exploration wells penetrated over 2 mi (3.3 km) of Tertiary sediments and volcanic rocks (McLeod, 1987). Three of the wells bottomed out in granite, and one intersected granite mylonite at 11,605 ft (3,537 m; McLeod, 1987).

Low-angle extension and uplift of the AMCC was followed by high-angle faulting that shaped the northeast-trending Deer Lodge, Whitetail, and Elk Park Valleys (fig. 1). The presence of the Eocene to early Miocene sediments in the Deer Lodge Valley (fig. 2) suggests it was a topographic low since at least Eocene time, and an early high-angle normal fault is now buried beneath the east flank of the Deer Lodge Valley (fig. 2), as revealed by gravity data (Konizeski and others, 1968; Hanna and others, 1994). The buried fault, or faults, appears to offset Eocene through early Miocene sediments whose presence at depth is verified by drill hole data (McLeod, 1987). The overlying Middle Miocene and younger sediments are not faulted. It is possible that the older sediments are locally missing due to non-deposition and that movement on the buried fault or faults occurred even earlier.

The Deer Lodge, Whitetail, and Elk Park Valleys largely owe their current geometries to Basin and

Range style extension on high-angle normal faults from about 15 Ma onwards (Sears and Thomas, 2007). The widely variable strikes of normal faults in Butte North reflect reactivation of preexisting structures as well as rotation of the crustal stress field associated with the passage of the Yellowstone Hotspot (Sears and others, 2009).

Normal faulting still occurs in southwestern Montana, and the P–T axes of earthquakes reflect both northeast–southwest-directed Basin and Range style extension and north–south extension attributed to the Yellowstone hotspot (Stickney and Bartholomew, 1987). Apparent offsets on Quaternary deposits in Elk Park, which is a north–northeast-trending half graben (fig. 2), suggests that some faults in Butte North are still active. Faults on the west side of Elk Park include a primary east-dipping normal fault and an antithetic west-dipping normal fault. Potential fault scarps on the east-dipping fault are up to 18 m (60 ft) high and commonly contain bedrock in the footwall and Quaternary deposits in the hanging wall. Fault scarps on the antithetic west-dipping fault are up to 1.5 m (5 ft) high and offset Quaternary debris flow deposits.

Active faulting is also suggested by prominent triangular facets in parts of the western Deer Lodge Valley, but it is not clear that Quaternary sediments are offset. Similarly, there are no Quaternary faults occuring in the Whitetail Valley (fig. 1). Olson and others (2016) described a fault scarp in Quaternary sediments along the west side of the valley near Ratio Mountain. The Bull Mountain western border fault (Stickney and others, 2000), a Quaternary structure, bounds the east side of the Whitetail Valley and may be capable of generating a magnitude 7 earthquake (see Scarberry and others, this volume).

The earthquake record in the Butte North 30' x 60' quadrangle is dominated by a 1986 earthquake swarm in the eastern Boulder Valley. The largest earthquake occurred on October 24th, 1986, and had a magnitude of 3.5. Inferred focal mechanisms associated with this earthquake swarm are predominantly strike-slip, with sinistral motion on a north–south nodal plane. A subset of focal mechanisms is consistent with movement on a north- to northwest-striking normal fault. Overall, focal mechanisms associated with the 1986 Boulder earthquake cluster are consistent with NE–SW-directed extensional strain (Scarberry and others, 2017).

DISCUSSION AND SUGGESTIONS FOR FURTHER RESEARCH

Our map compilation (Scarberry and others, in preparation) and this overview aim to incorporate previous studies with new observations to provide a modern synopsis of geologic knowledge in the Butte North quadrangle. It is our hope that these efforts will provide a useful resource for future studies in this geologically fascinating part of the world. Here are some suggestions for future research:

1. The timing and style of faulting during Boulder Batholith crystallization and emplacement is still a topic of great debate (Schmidt and O'Neill, 1982; Schmidt and others, 1990; Kalakay and others, 2001; Berger and others, 2011; Houston and Dilles, 2013a,b). Modern thermos-geochronology across the batholith and its host rocks should provide age, pressure, and temperature constraints.

2. New geochronologic and geochemical data shed light on the eruption of the Lowland Creek Volcanic Field. Future work should focus on comparing and correlating them with adjacent volcanic fields (see fig. 2; unit Ti).

3. The extension history of the AMCC and bounding detachment zone is not well understood. Further research could include detailed mapping and thermochronology of transects across the Pikes Peak detachment zone, across the southwestern continuation of the detachment zone in the Big Hole Valley, and along the length of the detachment zone. Data from such studies would complement the work of Foster and others (2010). Another line of research is provenance and transport studies of Cenozoic units in the Deer Lodge Valley and Big Hole Valley to the south like those of Schwartz and others (2013, 2019) and Schwartz and Graham (2017). These will contribute to knowledge of basin evolution in the hanging wall of the AMCC.

4. Late, high-angle normal faults have a variety of orientations, and their ages of initiation, how they accommodate regional extension, how they interact to produce modern topography, and whether they are currently active are not well understood. While some high-angle normal faults likely formed during Eocene development of the AMCC, others likely initiated in Miocene time or later as part of regional Basin and Range style extension (Sears and Ryan, 2003; Sears and others, 2009).

5. The new Quaternary fault system identified in Elk Park adds to previously identified potentially active faults in southwestern Montana (Stickney and others, 2000). The faults on the west side of Elk Park produced scarps in modern sediments and therefore have the potential to rupture. The minimum estimated magnitude for surface ruptures in the Basin and Range is Mw 6.5 (dePolo, 1994). The Butte North quadrangle likely contains additional Quaternary faults that may pose a seismic hazard to nearby populations and infrastructure. No detailed paleoseismic studies have been carried out in the Butte North quadrangle, leaving seismic hazards poorly constrained. Additional field investigations, supported by high-resolution topographic data, would shed light on the presence or absence of Quaternary normal faults in the Elk Park, Deer Lodge, and Whitetail Valleys. No paleoseismic investigations have been carried out in the Butte North 30' x 60' quadrangle, leaving earthquake recurrence intervals and maximum potential earthquakes on Quaternary faults unknown, and a target for future research.

REFERENCES CITED

Barnosky, A.D., Holmes, M., and Kirchholtes, R., 2014, Prelude to the Anthropocene: Two new North American Land Mammal Ages (NALMAs): The Anthropocene Review, v. 1, p. 225–242, doi:10.1177/2053019614547433.

Bartholomew, M.J., Bone, M.J., Rittenour, T.M., Mickelson, A.M., and Stickney, M.C., 2009, "Stress switching" along the Lima Reservoir Fault in Yellowstone's wake: Geological Society of America Abstracts with Programs v. 41, p. 55.

Becraft, G.E., 1960a, Preliminary geologic map of the southern half of the Jefferson City quadrangle, Jefferson County, Montana: U.S. Geological Survey Mineral Investigations Field Studies Map MF-172, 1 sheet, scale 1:24,000.

Becraft, G.E, 1960b, Preliminary geologic map of the northern half of the Jefferson City quadrangle, Jefferson County, Montana: U.S. Geological Survey Mineral Investigations Field Studies Map MF-171, 1 sheet, scale 1:24,000.

Becraft, G.E., and Pinckney, D.M., 1961, Preliminary geologic map of the northwest quarter of the Boulder quadrangle, Montana: U.S. Geological Survey Mineral Investigations Field Studies Map MF-183, 1 sheet, scale 1:24,000.

Becraft, G.E., Pinckney, D.M., and Rosenblum, S., 1963, Geology and mineral deposits of the Jefferson City Quadrangle, Jefferson and Lewis and Clark Counties, Montana: U.S. Geological Survey Professional Paper 428, 101 p.

Berg, R.B., and Hargrave, Phyllis, 2004, Geologic map of the Upper Clark Fork Valley, southwestern Montana: Montana Bureau of Mines and Geology Open-File Report 506, 10 p., 2 sheets, scale 1:50,000.

Berger, A., and Elliott, C.G., 2004, Synchronous extension and contraction in the Anaconda Metamorphic Complex: Geological Society of America Abstracts with Programs, v. 36, no. 4.

Berger, A., and Elliott, C.G., 2007, Detailed structural geology of the central part of the West Valley 7.5′ quadrangle, southwest Montana: Montana Bureau of Mines and Geology Open-File Report 560, 11 p., 1 sheet, scale 1:24,000.

Berger, B.R., Hildebrand, T.G., and O'Neill, J.M., 2011, Control of Precambrian basement deformation zones on emplacement of the Laramide Boulder Batholith and Butte Mining District, Montana, United States: U.S. Geological Survey Scientific Investigations, v. 2011–5016.

Blackwelder, E., and Atwood, W.W., 1917, Physiographic conditions and copper enrichment (discussion): Economic Geology, v. 12, p. 541–547.

Constenius, K.N., 1996, Late Paleogene extensional collapse of the Cordilleran foreland fold and thrust belt: Geological Society of America Bulletin, v. 108, p. 20–39.

dePolo, C.M., 1994, The maximum background earthquake for the Basin and Range Province, western North America: Bulletin of the Seismological Society of America, v. 84, p. 466–472.

Derkey, P.D., and Bartholomew, M.J., 1988, Geologic map of the Ramsay quadrangle, Montana: Montana Bureau of Mines and Geology Geologic Map 47, 1 sheet, scale 1:24,000.

DeWitt, Foord, E.E., Zartman, R.E., Pearson, R.C., and Foster, F., 1996, Chronology of Late Cretaceous Igneous and hydrothermal events at the Golden Sunlight gold–silver breccia pipe, southwestern Montana: U.S. Geological Survey Bulletin 2155, 48 p.

du Bray, E.A., Lund, K., Tilling, R.I., Denning, P.D.,

and DeWitt, E., 2009, Geochemical database for the Boulder batholith and its satellitic plutons, southwest Montana: U.S. Geological Survey Data Series 454.

du Bray, E.A., Aleinikoff, J.N., and Lund, K., 2012, Synthesis of Petrographic, geochemical, and isotopic data for the Boulder Batholith, Southwest Montana: U.S. Geological Survey Professional Paper 1793, 39 p.

Dudas, F.O., Ispolatov, V.O., Harlan, S.S., and Snee, L.W., 2010, $^{40}Ar/^{39}Ar$ geochronology and geochemical reconnaissance of the Eocene Lowland Creek volcanic field, west-central Montana: Journal of Geology, v. 118, no. 3, p. 295–304.

Elliott, C.G., and McDonald, C., 2009, Geologic map and geohazard assessment of Silver Bow County, Montana: Montana Bureau of Mines and Geology Open-File Report 585, 88 p., 3 sheets, scale 1:50,000.

Elliott, C.G., Smith, L.N., and Lonn, J.D., 2013, Geologic map of the Mount Powell 7.5' quadrangle, southwestern Montana: Montana Bureau of Mines and Geology Open-File Report 635, 22 p., 1 sheet, scale 1:24,000.

Feeley, T.C., 2003, Origin and tectonic implications of across-strike geochemical variations in the Eocene Absaroka Volcanic Province, United States: The Journal of Geology, v. 111, p. 329–346.

Feeney, C.M., Ryan. C.B., O'Connell, M., and Hendrix, M.S., 2009, Geologic map of the Rock Creek 7.5' quadrangle, Powell County, Montana: Montana Bureau of Mines and Geology ED-MAP-2, 6 p., 2 sheets, scale 1:24,000.

Foster, D.A., Doughty, P.T., Kalakay, T.J., Fanning, C.M., and Grice, W.C., 2007, Kinematics and timing of exhumation of metamorphic core complexes along the Lewis and Clark fault zone, northern Rocky Mountains, USA: Special Paper 434: Exhumation Associated with Continental Strike-Slip Fault Systems, v. 2434, p. 207–232.

Foster, D.A., Grice, W.C., and Kalakay, T.J., 2010, Extension of the Anaconda metamorphic core complex: $^{40}Ar/^{39}Ar$ thermochronology and implications for Eocene tectonics of the northern Rocky Mountains and the Boulder batholith: Lithosphere, v. 2, p. 232–246.

Gaschnig, R.M., Vervoort, J.D., Lewis, R.S., and McClelland, W.C., 2010, Migrating magmatism in the northern US Cordillera: In situ U-Pb geochronology of the Idaho batholith: Contributions to Mineralogy and Petrology, v. 159, p. 863–883.

Hanna, W.F., Hassemer, J.H., Elliott, I.E., Wallace, C.A., and Snyder, S.L., 1994, Maps showing gravity and aeromagnetic anomalies in the Butte 1° x 2° quadrangle, Montana: U.S. Geological Survey Miscellaneous Investigations Series Map I-2050-I, scale 1:250,000.

Hargrave, P.A., and Berg, R.B., 2013, Geologic map of the Lockhart Meadows 7.5′ quadrangle, west central Montana: Montana Bureau of Mines and Geology Open-File 629, 1 sheet, scale 1:24,000.

Hargrave, P., and Dresser, H., 2000, Stereo picture guidebook to Intrusive Tuff at "The Rocks": Tobacco Root Geological Society, Annual Meeting, Butte, MT, August 3–6, 2000, 32 p.

Harlan, S.S., Geissman, J.W., Lageson, D.R., and Snee, L.W., 1988, Paleomagnetic and isotopic dating of thrust-belt deformation along the eastern edge of the Helena salient, northern Crazy Mountains Basin, Montana: Bulletin of the Geological Society of America, v. 100, p. 492–499, doi:10.1130/0016-7606(1988)100<0492:PAIDOT>2.3.CO;2.

Houston, R.A., and Dilles, J.H., 2013a, Geology of the Butte mining district, Montana: Montana Bureau of Mines and Geology Open-File Report 627, 1 sheet, scale 1:24,000.

Houston, R.A., and Dilles, J.H., 2013b, Structural geologic evolution of the Butte District, Montana: Economic Geology, v. 108, p. 1397–1424.

Kalakay, T.J., Foster, D.A., and Lonn, J.D., 2014, Polyphase collapse of the Cordilleran hinterland: The Anaconda metamorphic core complex of western Montana—The Snoke symposium field trip: Geological Society of America Field Guides, p. 145–159.

Kalakay, T.J., John, B.E., and Lageson, D.R., 2001, Fault-controlled pluton emplacement in the Sevier fold-and-thrust belt of Southwest Montana, USA: Journal of Structural Geology, v. 23, p. 1151–1165, doi:10.1016/S0191-8141(00)00182-6.

Klepper, M.R., Weeks, R.A, and Ruppel, E.T., 1957, Geology of the southern Elkhorn Mountains, Jef-

ferson and Broadwater Counties, Montana: U.S. Geological Survey Professional Paper 292, 82 p.

Klepper, M. R., Ruppel, E. T., Freeman, V. L., and Weeks, R. A., 1971, Geology and mineral deposits, east flank of the Elkhorn Mountains, Broadwater County, Montana: U.S. Geological Survey Professional Paper 665, scale 1:48,000.

Konizeski, R.L., McMurtrey, R.G., and Brietkrietz, A., 1968, Geology and ground-water resources of the Deer Lodge Valley, Montana: USGS Water Supply Paper 1862, 55 p., 2 sheets, scale 1:62,500.

Korzeb, S.L., Scarberry, K.C., and Zimmerman, J.L., 2018, Interpretations and genesis of Cretaceous age veins and exploration potential for the Emery Mining District, Powell County, Montana: Montana Bureau of Mines and Geology Bulletin 137, 60 p., 1 sheet, scale 1:24,000.

Lageson, D.R., Schmitt, J.G., Horton, B.K., Kalakay, T.J., and Burton, B.R., 2002, Influence of Late Cretaceous magmatism on the Sevier orogenic wedge, western Montana: Geology, v. 29, p. 723–726, doi:10.1130/0091-7613(2001)029<0723:IOLCMO>2.0.CO;2.

Le Bas, M.J., LeMaitre, R.W., Streckeisen, A., and Zanettin, B., 1986, A chemical classification of volcanic rocks based on the total alkali silica diagram: Journal of Petrology, v. 27, p. 745–750.

Lewis, R.S., 1998, Geologic map of the Butte 1º x 2º quadrangle, southwestern Montana: Montana Bureau of Mines and Geology Open-File Report 363, 16 p., 1 sheet, scale 1:250,000.

Lipman, P.W., 1984, The roots of ash flow calderas in western North America: Windows into the tops of granitic batholiths: Journal of Geophysical Research, v. 89, p. 8801–8841.

Lonn, J.D., McDonald, C., Lewis, R.S., Kalakay, T.J., O'Neill, J.M., Berg, R.B., and Hargrave, P., 2003, Geologic map of the Philipsburg 30' x 60' quadrangle, western Montana: Montana Bureau of Mines and Geology Open-File Report 483, 1 sheet, scale 1:100,000.

Lonn, J., and Elliott, C.G., 2011, Cretaceous synorogenic and Eocene post-orogenic extension in the Sevier hinterland, southwestern Montana: Geological Society of America, Rocky Mountain Section, Logan, UT.

Lund, K., Aleinikoff, J.N., Kunk, M.J., Unruh, D.M., Zeihen, G.D., Hodges, W.C., Du Bray, E.A., and O'Neill, M.J., 2002, SHRIMP U-Pb and $^{40}Ar/^{39}Ar$ age constraints for relating plutonism and mineralization in the Boulder batholith region, Montana: Economic Geology, v. 97, p. 241–267.

McLeod, P. J., 1987, The depositional history of the Deer Lodge Basin, Western Montana: Missoula, University of Montana, M.S. Thesis.

McQuarrie, N., and Wernicke, B.P., 2005, An animated tectonic reconstruction of southwestern North America since 36 Ma: Geosphere 1, p. 147–172.

Mosolf, J.G., 2015, Geologic field guide to the Tertiary volcanic rocks in the Elliston 30′ x 60′ quadrangle, west-central Montana, Northwest Geology, v. 44, p. 213–231.

Olson, N.H., Dilles, J.H., Kallio, I.M., Horton, T.R., and Scarberry, K.C., 2016, Geologic map of the Ratio Mountain 7.5′ quadrangle, southwest Montana: Montana Bureau of Mines and Geology EDMAP-10, 1 sheet, scale 1:24,000..

Olson, N.H., Sepp, M.D., Dilles, J.H., Mankins, N.E., Blessing, J.M., and Scarberry, K.C., 2017, Geologic map of the Mount Thompson 7.5′ quadrangle, southwest Montana: Montana Bureau of Mines and Geology EDMAP-11, 13 p., 11 sheets, scale 1:24,000.

O'Neill, J.M., Lonn, J.D., Lageson, D.R., and Kunk, M.J., 2004, Early Tertiary Anaconda metamorphic core complex, southwestern Montana: Canadian Journal of Earth Sciences, v. 41, p. 63–72.

Pardee, J.T., 1950, Late Cenozoic block faulting in western Montana: Geological Society of America Bulletin, v. 61, p. 359–406.

Prostka, H.J., 1966, Igneous geology of the Dry Mountain quadrangle, Jefferson County, Montana: U.S. Geological Survey Bulletin 1221-F, scale 1:24,000.

Reed, M., Rusk, B., and Palandri, J., 2013, The Butte magmatic-hydrothermal system: One fluid yields all alteration and veins: Economic Geology, v. 108, p. 1379–1396, doi:10.2113/econgeo.108.6.1379.

Reynolds, M.W., 1979. Character and extent of Basin-Range faulting, western Montana and east-central Idaho, *in* Newman, G., and Goode, H. eds., 1979 Basin and Range Symposium: Rocky Mountain

Association of Geologists and Utah Geological Association, p. 185–193.

Robertson, F.S., 1953, Geology and mineral deposits of the Zosell (Emery) mining district, Powell County, Montana: Montana Bureau of Mines and Geology Memoir 34, 29 p.

Ruppel, E.T., 1961, Reconnaissance geologic map of the Deer Lodge quadrangle, Powell and Jefferson Counties, Montana: U.S. Geological Survey Mineral Investigations Map MF-174, 1:48,000 scale.

Ruppel, E.T., 1963, Geology of the Basin quadrangle Jefferson, Lewis and Clark, and Powell Counties, Montana: U.S. Geological Survey Bulletin 1151, 121 p., 1 sheet, scale 1:48,000.

Scarberry, K.C. and Elliott, C., 2016, Geologic map of the Opportunity 7.5' quadrangle, southwestern Montana: Montana Bureau of Mines and Geology Open-File Report 683, 1 sheet, scale 1:24,000.

Scarberry, K.C., Elliott, C.G., and Yakovlev, P., in preparation, Geologic map of the Butte North 30' x 60' quadrangle, southwestern Montana: Montana Bureau of Mines and Geology Geologic Map.

Scarberry, K.C., Kallio, I.M., Olson III, N., Dilles, J.H., Older, C.W., Horton, T., and English, A.R., 2016, Large-volume pyroclastic deposits along the eastern edge of the Boulder Batholith, southwestern Montana: Geological Society of America Abstracts with Programs.

Scarberry, K.C., 2016a, Geologic map of the Wilson Park 7.5' quadrangle, southwestern Montana: Montana Bureau of Mines and Geology Geologic Map 66, 1 sheet, scale 1:24,000.

Scarberry, K.C., 2016b, Geologic map of the Sugarloaf Mountain 7.5' quadrangle, Deer Lodge, Powell, and Jefferson Counties, Montana: Montana Bureau of Mines and Geology Open-File Report 674, 1 sheet, scale 1:24,000.

Scarberry, K.C., Kallio. I.M., and English, A.R., 2017, Geologic map of the Boulder East 7.5' quadrangle, southwest Montana: Montana Bureau of Mines and Geology Geologic Map 68, 1 sheet, scale 1:24,000.

Scarberry, K.C., Coppage, E.L., and English, A.R., 2018, Geologic map of the Bison Mountain 7.5' quadrangle, Powell and Jefferson Counties, Montana: Montana Bureau of Mines and Geology Geologic Map 71.

Scarberry, K.C., 2019, Geologic map of the Ramsay 7.5' quadrangle, Silver Bow County, MT: Montana Bureau of Mines and Geology Geologic Map 72, 1 sheet, scale 1:24,000.

Schmidt, C.J., and O'Neill, J.M., 1982, Structural evolution of the southwest Montana transverse zone, *in* Powers, R.B., ed., Geologic studies of the Cordilleran thrust belt (v. 1): Denver, Colo., Rocky Mountain Association of Geologists, p. 193–218.

Schmidt, C.J., Smedes, H.W., and O'Neill, J.M., 1990, Syncompressional emplacement of the Boulder and Tobacco Root batholiths (Montana-USA) by pull-apart along old fault zones: Geological Journal, v. 25, p. 305–318.

Schwartz, T.M., and Graham, S.A., 2017, Depositional history and provenance of Paleogene strata in the Sage Creek basin, southwestern Montana: Geosphere, v. 13, p. 1285–1309, doi:10.1130/GES01450.1.

Schwartz, T.M., Methner, K., Chamberlain, C.P., Mulch, A., and Graham, S.A., 2019, Paleogene topographic and climatic evolution of the Northern Rocky Mountains from integrated sedimentary and isotopic data: GSA Bulletin, p. 1–21, doi:10.1130/b32068.1.

Schwartz, T.M., and Schwartz, R.K., 2013, Paleogene postcompressional intermontane basin evolution along the frontal Cordilleran fold-and-thrust belt of southwestern Montana: Bulletin of the Geological Society of America, v. 125, p. 961–984, doi:10.1130/B30766.1.

Sears, J.W. , Hendrix, M.S. , Webb, B., and Archibald, D.A., 1998 [abstract], Constraints on deformation of the northern Rocky Mountain fold-thrust belt in Montana from $^{40}Ar/^{39}Ar$ geochronology of andesite sills: American Association of Petroleum Geologists, *in* Bridges to Discovery (1 CD-ROM): American Association of Petroleum Geologists Annual Convention, Salt Lake City, Utah, May 17–29, 1998.

Sears, J.W., and Ryan, P.C., 2003, Cenozoic evolution of the Montana Cordillera: Evidence from Paleovalleys: Cenozoic Systems of the Rocky Mountain Region, p. 289–301.

Sears, J.W., Hendrix, M.S., Thomas, R.C., and Fritz, W.J., 2009, Stratigraphic record of the Yellowstone hotspot track, Neogene Sixmile Creek

Formation grabens, southwest Montana: Journal of Volcanology and Geothermal Research, v. 188, p. 250–259.

Sears, J.W., and Thomas, R.C., 2007, Extraordinary middle Miocene crustal disturbance in southwest Montana: Birth record of the Yellowstone hot spot, *in* Introduction to the geology of the Dillon area: Northwest Geology: Dillon Field Conference, v. 36, p. 133–142.

Simonsen, S.W., 1997, $^{40}Ar/^{39}Ar$ ages of Eocene dikes and the age of extension in a Tertiary magmatic arc Idaho and Montana: Missoula, University of Montana, M.S. thesis, 121 p.

Smedes, H.W., 1962, Lowland Creek volcanics, an Upper Oligocene formation near Butte, Montana: The Journal of Geology, v. 70, no. 2, p. 255–266.

Smedes, H.W., Klepper, M.R., Pinckney, D.M., Becraft, G.E., and Ruppel, E.T., 1962, Preliminary geologic map of the Elk Park quadrangle, Jefferson and Silver Bow Counties, Montana: U.S. Geological Survey Mineral Investigations Field Studies Map MF-246, 1 sheet, scale 1:48,000.

Smedes, H.W., and Thomas, H.H., 1965, Reassignment of the Lowland Creek Volcanics to Eocene age: Journal of Geology, v. 73, no. 3, p. 508–510.

Smedes, H.W., 1966, Geology and igneous petrology of the northern Elkhorn Mountains Jefferson and Broadwater counties, Montana: U.S. Geological Survey Professional Paper 510, 116 p.

Stickney, M.C., and Bartholomew, M.J., 1987, Seismicity and late Quaternary faulting of the northern Basin and Range province, Montana and Idaho: Bulletin of the Seismological Society of America, v. 77, p. 1602–1625.

Stickney, M.C., and Vuke, S.M., 2017, Geologic map of the Helena Valley, west-central Montana: Montana Bureau of Mines and Geology Open-File Report 689, 11 p., 1 sheet, scale 1:50,000.

Stickney, M.C., Haller, K., and Machette, M., 2000, Quaternary faults and seismicity in western Montana: Montana Bureau of Mines and Geology Special Publication 114, 1 sheet, scale 1:750,000.

Vuke, S.M., Porter, K.W., Lonn, J.D., and Lopez, D.A., 2007, Geologic map of Montana: Montana Bureau of Mines and Geology Map 62A, scale 1:500,000.

Vuke, S.M., 2015, Geologic road map of Montana: Montana Bureu of Mines and Geology Geologic Map 65, scale 1:1,000,000.

Wanek, A.A., and Barclay, C.S.V., 1966, Geology of the northwest quarter of the Anaconda quadrangle, Deer Lodge County, Montana: U.S. Geological Survey Bulletin 1222-B, 1 sheet, scale 1:24,000.

Weed, W.H., 1912, Geology and ore deposits of the Butte district, Montana: U.S. Geological Survey Professional Paper 74, 262 p.

Weeks, R. A., 1974, Geologic map of the Bull Mountain area, Jefferson County, Montana: U.S. Geological Survey Open-File Report 74-354, scale 1:48,000.

Yonkee, W.A., and Weil, A.B., 2015, Tectonic evolution of the Sevier and Laramide belts within the North American Cordillera orogenic system: Earth Science Reviews, v. 150, p. 531–593.

EMPLACEMENT OF LARGE-VOLUME FELSIC PLUTONS IN ACTIVE FOLD-THRUST BELTS: A REVIEW OF MODELS FOR THE BOULDER BATHOLITH (MONTANA) AND NEW IDEAS

David R. Lageson,[1,*] Thomas J. Kalakay,[2] and David A. Foster[3]

[1]Montana State University, [2]Rocky Mountain College, and [3]University of Florida
**Speaker*

Pluton emplacement within convergent tectonic settings has been a fertile topic of research for many years. In the absence of *in situ* melting of the upper crust (anatexis), how do large batholiths find space in a crustal environment that is undergoing orogenic compression and shortening? This question takes on direct significance in western Montana and adjacent Idaho where major composite plutonic centers include the Idaho, Boulder, and Pioneer batholiths, and magmatism was broadly synchronous with crustal shortening and thickening between 85 and 55 Ma (Foster and Fanning, 1997; Kalakay and others, 2001). These plutonic centers define a west-to-east corridor of Cretaceous–Paleogene magmatism that spans west-central Montana from the Bitterroot Lobe of the Idaho batholith on the west, to the Castle Mountains and Crazy Mountains Basin on the east (Bitterroot–Boulder tectono-magmatic channel). However, unlike mid-crustal magmatic systems exposed in the Idaho batholith, emplacement of plutons further east occurred within the evolving fold-and-thrust belt and foreland basin at relatively shallow depths (1–10 km), mostly as thin (meter- to kilometer-scale) tabular sheets or laccoliths (Hyndman and others, 1988; Sears and others, 1989; Kalakay and others, 2001). Many intrusive bodies spatially overlap with major contractional structures (Kalakay and others, 2001). Regional cross sections have depicted the granitoid sheets as occupying major thrust zones (e.g., Hyndman and others, 1988; Kalakay and others, 2001), or superjacent to major thrust surfaces (Burton and others, 1998).

It has always been a major question as to how the "main phase" of the Boulder batholith found accommodation space during crustal shortening and, specifically, during emplacement of the Eldorado–Lombard thrust system (e.g., Schmidt and others, 1990; Kalakay and others, 2001). Underscoring this point is the fact that, although the Boulder batholith includes at least 15 distinct plutons, emplacement of roughly ninety percent of the exposed Butte Granite occurred between 81 and 76 Ma, comprising the Butte quartz monzonite (granodiorite by modern classification). Given the dimensions of the Boulder batholith (4,500 km^2 x ~10 km thick), in addition to the enormous volume of magma represented by its cogenetic volcanic carapace (Elkhorn Mountains Volcanic succession; 5–6 km thick), it is difficult to reconcile an igneous mass this large being "squeezed" into an actively forming fold-thrust belt. Many previous investigators have tried to construct models for intrusion of the Boulder batholith into the evolving fold-thrust belt based on geological and geophysical data (e.g., Tilling and others, 1968; Hamilton and Meyers, 1974; Hyndman and Chase, 1979; Lageson and others, 1994; Vejmelek and Smithson, 1995; Burton and others, 1998; Kalakay and others, 2001; Berger and others, 2011; Sears, 2016). For example, the NE-trending rhombic shape of the Boulder batholith was used to suggest a "pull-apart" model of emplacement by some workers (Schmidt and others, 1990), a model that has been championed by more recent authors, albeit with significant modification (Berger, 2011; Sears, 2016). Others have proposed that emplacement of the Boulder batholith and other plutons in southwest Montana (e.g., Pioneer batholith, McCartney Mountain, Bannack) occurred at the top of major footwall ramps within the evolving fold-and-thrust belt (Burton and others, 1998; Kalakay and others, 2001). Still others have emphasized the role of Paleoproterozoic structural inheritance along the Great Falls Tectonic Zone, involving a hypothesized deep-seated shear zone that facilitated "pull-apart" emplacement of the batholith, although a geometric or kinematic model was not presented to show how this might work (Berger and others, 2011).

Field relationships in southwest Montana show a clear spatial correlation between plutons and the top of major footwall thrust ramps. Thrust ramps demonstrate many key structural elements that may facilitate pluton emplacement by providing dilatant accommodation space for pluton nucleation and growth

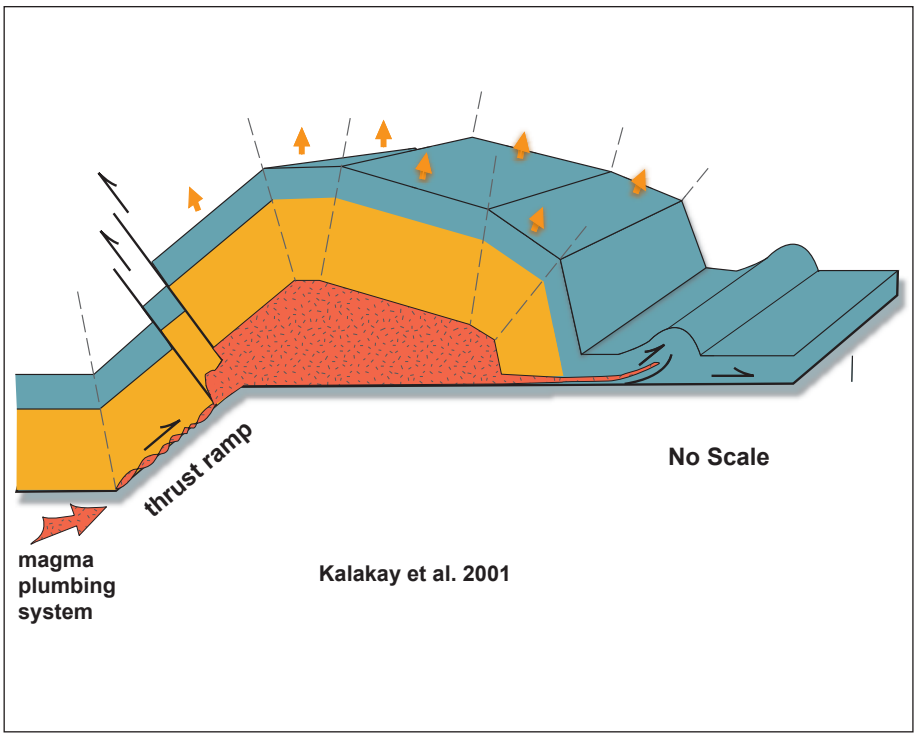

Figure 1. Ramp-top model for Late Cretaceous emplacement of felsic plutons in southwest Montana (from Kalakay and others, 2001). Mid-crustal pulses of magma migrate up-dip to dilatant areas at the top of major, regional-scale footwall ramps. Ramp-top space is provided by the flexural rigidity of the hanging wall ("releasing-step"), by back-thrusts shown by experimental and field data, and by mode-1 (extensional) joints in hanging wall competent layers. Magma emplacement is not a sudden, one-time event, but rather involves pulses of synkinematic sill emplacement at the top of the ramp, triggered by incremental over-pressuring in the mid-crustal magma source area.

(fig. 1): (1) extensional strains along the ramp interface produced by incremental plane-strain simple shear; (2) a dilatant space or "releasing-step" at the top of the ramp; and (3) antithetic back-thrusts that may assist in pluton emplacement. Regardless of whether the pluton is synkinematic (*sensu stricto*), post-kinematic, or some combination thereof, there is abundant experimental and field evidence that frontal ramp tops create a dilatant environment where plutons are initially emplaced and grow (Morse, 1977; Serra, 1977; Chester and others, 1991; Ferré and others, 2012). Several Montana intrusive centers are located at ramp-top structural positions, including Bannack, McCartney Mountain, the Pioneer batholith, and the Boulder batholith.

The Boulder batholith was overprinted by significant Eocene extension during development of the Anaconda metamorphic core complex, unlike ramp-top plutons in the McCartney Mountain salient. Based on regional cross sections, movement on the east-dipping Anaconda detachment carried the batholith in its hanging wall and displaced it several kilometers east of its original location (Foster and others, 2010; Kalakay and others, 2014). This Eocene translation must be considered when reconstructing the location of the batholith within the fold-and-thrust belt at the time of its intrusion. The footwall of the Anaconda detachment exposes Late Cretaceous and Eocene plutons that intruded a high-grade metamorphic sequence of deformed Belt and Paleozoic sedimentary units (Foster and others, 2010, Kalakay and others, 2014). Deformation in the footwall is characterized by extreme attenuation of the Belt section associated with a collapsed thrust ramp system that formed structurally beneath the Georgetown thrust. This collapsed ramp coincides, along strike, with ramps in the Pioneer batholith complex and those farther south, near Bannack (Kalakay and others, 2001, 2014; Lonn and others, 2003; Ruppel and others, 1993; Fraser and Waldrop, 1972). By restoring the Boulder batholith westward along the Anaconda detachment back to its original position, it ends up on top of the collapsed ramp system just described. Thus, it remains plausible that the Boulder batholith, like plutons to the south, was emplaced near the top of a major, regional footwall ramp in the Sevier orogenic system as previously proposed (figs. 2, 3; Burton and others, 1998; Kalakay and others, 2001).

Although the ramp-top model of emplacement appears to be a geometrically and volumetrically viable emplacement model, there is a bigger picture that may have bearing on emplacement of plutons within the Bitterroot–Boulder tectono-magmatic channel. Synconvergent channel flow is a tectono-magmatic model that has evolved from decades of research in the Greater Himalaya (fig. 4), involving the lateral extrusion or flow of mid-crustal rocks and melt towards an orogenic foreland (Godin and others, 2006). However, channel flow is a physical process (e.g., largely driven by lateral stress gradients) that is not restricted to large-magnitude collisional orogens, just as fold-and-thrust belts are not restricted to one tectonic environment. We propose herein that channel flow is equally viable for the Mesozoic magmatic arc environment of western Montana. Channel flow is a time-dependent,

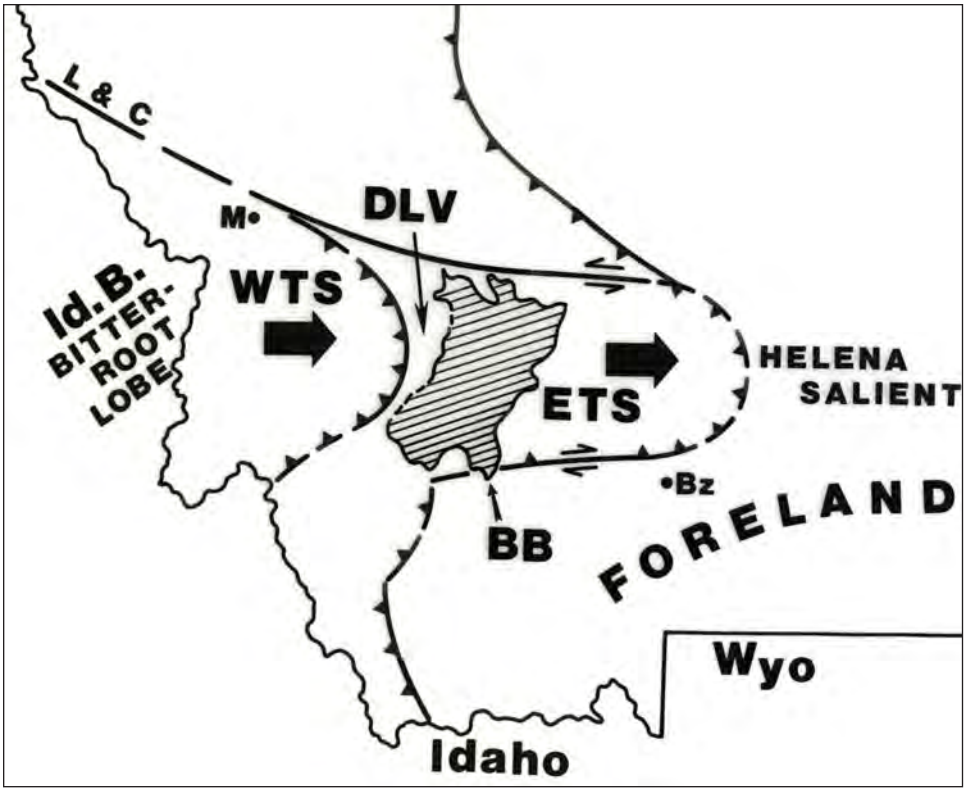

Figure 2. Map of southwest Montana showing the Bitterroot lobe of the Idaho batholith, western thrust belt (WTS), Lewis and Clark fault zone (L&C), Deer Lodge Valley (DLV), Boulder batholith (BB), and eastern thrust belt salient (ETS). Towns for reference are Missoula (M) and Bozeman (Bz).

thermo-mechanical process that dynamically couples the metamorphic hinterland to an evolving, shallow fold-thrust belt in the foreland (Godin and others, 2006). More specifically, channel flow is defined as a "viscous fluid-filled channel lying between two rigid sheets" (Godin and others, 2006), undergoing flow induced by lateral stress gradients within the channel (fig. 4). Lateral stress gradients can be caused by differential lithostatic loading over broad areas, high rates of erosion along the topographic crest of the orogen (Zeitler and others, 2001), changes in thickness of the orogenic wedge as it adjusts to critical taper conditions through time (Lageson and others, 2001), or some combination of all.

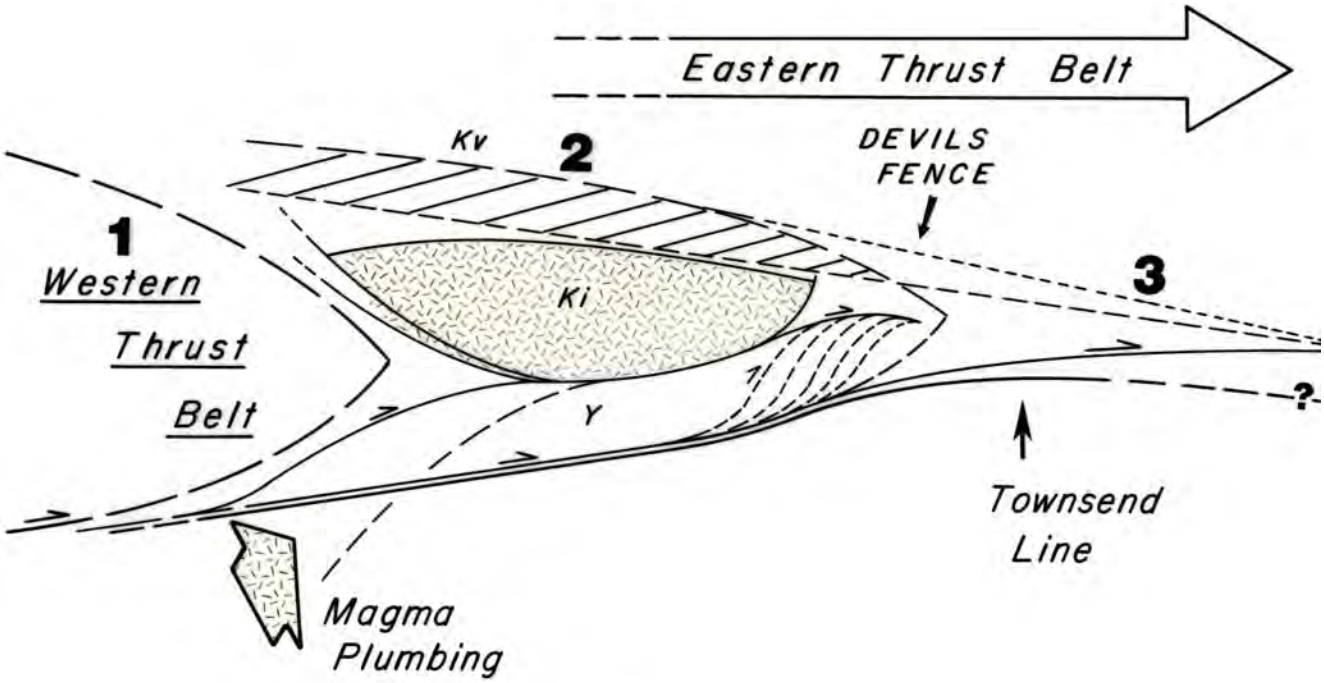

Figure 3. Highly schematic cross section (not to scale) showing the Boulder batholith (Ki) and superjacent Elkhorn Volcanic field (Kv) in a "central position" within the western Montana fold-and-thrust belt. Zone 1 is the western thrust belt (Flint Creek and Anaconda Ranges), zone 2 is the Boulder batholith at the top of a regional footwall ramp, and zone 3 is the eastern thrust belt that extends as a pronounced salient into the western Crazy Mountains Basin. Metamorphosed and intruded Belt rocks (Mesoproterozoic, Y) are in the footwall of the Boulder batholith. Townsend Line is from Winston (1986). The western margin of the Boulder batholith diagrammatically reflects ramp-top back-thrusts, overprinted by down-to-the-east detachment faulting from the Eocene Anaconda metamorphic core complex immediately west. The thick and extensive Elkhorn Volcanic field (Kv) would have comingled with other cogenetic volcanic centers to the west and southwest, creating a highland region in western Montana during Campanian–Maastrichtian time, herein named Montanaplano. Montanaplano would be tectonically and geomorphically similar to the mid-Cretaceous Nevadaplano in the hinterland of the Sevier orogen to the southwest and the Andean Altiplano-Puna Plateau, except it would have directly overlapped the Sevier fold-thrust belt in western Montana, rather than lying in the distant hinterland.

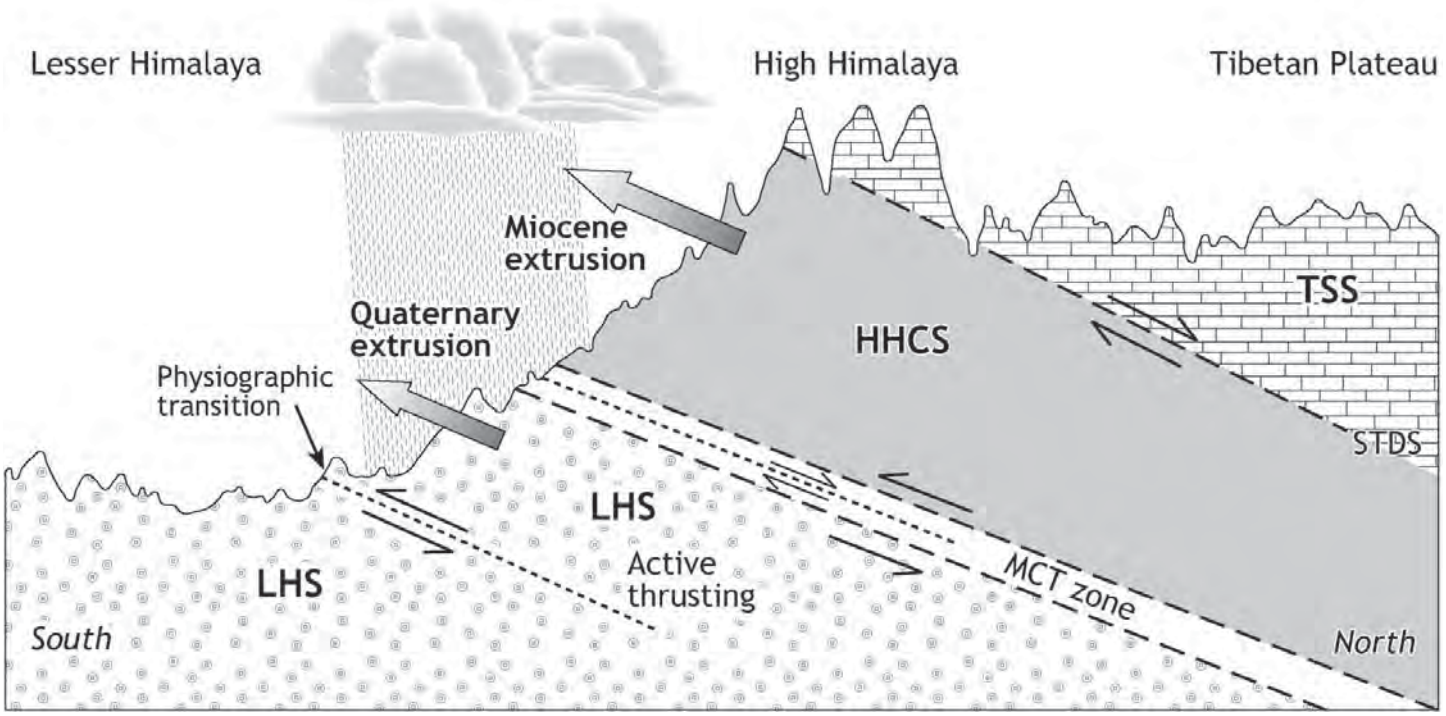

Figure 4. Schematic model for the Miocene mid-crustal channel (HHCS, gray shading) exposed in the High Himalaya. HHCS, Higher Himalayan Crystalline Series; TSS, Tethyan Sedimentary Series; LHS, Lesser Himalayan Series; MCT, Main Central Thrust; STDS, South Tibetan Detachment System. Channel flow is depicted to be the result of lateral pressure gradients in the crust induced by the seasonal summer monsoon and extensive erosion of south-facing slope of the Higher Himalaya. A similar monsoonal scenario has been proposed for the North American Cordillera during the mid- to late Cretaceous, whereby summer moisture in the atmosphere was carried upslope to the northwest from the Western Interior Cretaceous Seaway, first hitting the front of the Sevier orogenic wedge (Yonkee and Weil, 2015).

In western Montana, transverse fault zones with opposite sense of shear flank the central magmatic channel at the north and south margins of the Helena salient, while the lower channel boundary was the basal décollement of the fold-thrust belt that climbed up-section to the east along a series of footwall ramps (Burton and others, 1998). The upper boundary of the channel is uncertain, but may be represented by later detachment faults of the Bitterroot and Anaconda metamorphic core complexes (Eocene reactivation), as has been suggested for the Monashee core complex in the SE Canadian Cordillera (Gervais and Brown, 2011). Channel flow has been proposed for the south-eastern Canadian Cordillera by several authors (Brown and Gibson, 2006; Carr and Simony, 2006; Kuiper and others, 2006; Gervais and Brown, 2011), but until now has not been applied to the magmatically inflated thrust belt of western Montana.

The Bitterroot–Boulder tectono-magmatic channel obliquely intersects the Great Falls Tectonic Zone in central Montana, where deep-seated, northeast-trending basement structures related to the Big Sky orogen may have further controlled the emplacement and location of Late Cretaceous and early Tertiary igneous rocks (O'Neill and Lopez, 1985; Berger and others, 2011; Sears, 2016). Therefore, on a much broader scale of observation, the Bitterroot–Boulder magmatic corridor may only be a subset of regional channel flow processes that operated, in one form or another, from central Idaho to central Montana and involved several discrete centers of pluton emplacement at successively higher levels to the east through time (Sears, 2016). There were obviously several tectonic factors, both near-field and far-field, associated with the eastward, diachronous movement of magmatism into western and west-central Montana during the Late Cretaceous–Paleogene. However, despite the long geologic history and inherited complexity of the region, we believe that channel flow should also be considered in tectono-magmatic models applied to western Montana.

REFERENCES CITED

Berger, B.R., Hildenbrand, T.G., and O'Neill, J.M., 2011, Control of Precambrian basement deformation zones on emplacement of the Laramide Boulder batholith and Butte Mining District, Montana, United States: U.S. Geological Survey Scientific Investigations Report 2011-5016, 29 p.

Brown, R.L., and Gibson, H.D., 2006, An argument for channel flow in the southern Canadian Cordil-

lera and comparison with Himalayan tectonics, *in* Law, R.D., Searle, M.P., and Godin, L., eds., Channel flow, ductile extrusion and exhumation in continental collision zones: The Geological Society of London Special Publication 268, p. 543–559.

Burton, B.R., Lageson, D.R., Schmidt, C.J., Ballard, D.W., and Warne, J.R., 1998, Large magnitude shortening of the Lombard thrust system, Helena salient of the Montana thrust belt: Implications for reconstruction of the Belt Basin and emplacement of the Boulder batholith, *in* Berg, D., ed., Proceedings of Belt Symposium III, Montana Bureau of Mines and Geology Special Publication 112, p. 229–243.

Carr, S.D., and Simony, P.S., 2006, Ductile thrusting versus channel flow in the southeastern Canadian Cordillera: Evolution of a coherent crystalline thrust sheet, *in* Law, R.D., Searle, M.P., and Godin, L., eds., Channel flow, ductile extrusion and exhumation in continental collision zones: The Geological Society of London Special Publication 268, p. 561–587.

Chester, J.S., Logan, J.M., and Spang, J.H., 1991, Influence of layering and boundary conditions on fault-bend and fault-propagation folding: Geological Society of America Bulletin, v. 103, p. 1059–1072.

Ferré, E.C., Galand, O., Montanari, D. and Kalakay, T.J., 2012, Granite magma migration and emplacement along thrusts: International Journal of Earth Science, doi: 10.1007/s00531-012-0747-6

Foster, D.A., and Fanning, C.M., 1997, Geochronology of the northern Idaho batholith and Bitterroot metamorphic core complex: Magmatism preceding and contemporaneous with extension: Geological Society of America Bulletin, v. 109, p. 379–394.

Foster, D.A., Grice, W.C., and Kalakay, T.J., 2010, Extension of the Anaconda metamorphic core complex: $^{40}Ar/^{39}Ar$ thermochronology with implications for Eocene tectonics of the northern Rocky Mountains and the Boulder batholith: Lithosphere, v. 2, p. 232–246, doi: 10.1130/L94.1.

Fraser, G.D., and Waldrop, H.A., 1972, Geologic map of the Wise River quadrangle, Silver Bow and Beaverhead counties, Montana. U.S. Geological Survey Geologic Quadrangle Map GQ-988.

Gervais, F., and Brown, R.L., 2011, Testing modes of exhumation in collisional orogens: Synconvergent channel flow in the southeastern Canadian Cordillera: Lithosphere, v. 3, no. 1, p. 55–75.

Godin, L., Grujic, D., Law, R.D., and Searle, M.P., 2006, Channel flow, ductile extrusion and exhumation in continental collision zones: An introduction, *in* Law, R.D., Searle, M.P., and Godin, L., eds., Channel flow, ductile extrusion and exhumation in continental collision zones: The Geological Society of London Special Publication 268, p. 1–23.

Hamilton, W., and Meyers, W., 1974, The nature of the Boulder batholith of Montana: Geological Society of America Bulletin 85, p. 365–378.

Hyndman, D.W., Alt, D., and Sears, J.W., 1988, Post-Archean metamorphic and tectonic evolution of western Montana and northern Idaho, *in* Ernst, W.G., ed., Metamorphism and Crustal evolution of the western United States, Rubey volume VII, Prentice Hall, p. 333–361.

Hyndman, D.W., and Chase, R.B., 1979, Major tectonic elements and tectonic problems along the line of section from northeastern Oregon to west-central Montana: Geological Society of America Map and Chart Series MC-28C, scale 1:250,000.

Kalakay, T.J., Foster, D.A., and Lonn, J.D., 2014, Polyphase collapse of the Cordilleran hinterland: The Anaconda metamorphic core complex of western Montana—The Snoke Symposium Field Trip, *in* Shaw, C.A., and Tickoff, B., eds., Exploring the northern Rocky Mountains: Geological Society of America Field Trip Guide 37, p. 145–159, doi: 10.1130/2014.0037(07).

Kalakay, T.J., John, B.E., and Lageson, D.R., 2001, Fault-controlled pluton emplacement in the Sevier fold-and-thrust belt of southwest Montana, USA: Journal of Structural Geology, v. 23 (6–7), p. 1151–1165.

Kuiper, Y.D., Williams, P.F., and Kruse, S., 2006, Possibility of channel flow in the southern Canadian Cordillera: A new approach to explain existing data, *in* Law, R.D., Searle, M.P., and Godin, L., eds., Channel flow, ductile extrusion and exhumation in continental collision zones: The Geological Society of London Special Publication 268, p. 589–611.

Lageson, D.R., Schmitt, J.G., and Burton, B.R., 1994, Upper Cretaceous magmatism and development of a super-critically tapered wedge in the Sevier orogenic belt of western Montana: Geological Society of America Abstracts with Programs 26, p. 316.

Lageson, D.R., Schmitt, J.G., Horton, B.K., Kalakay, T.J., and Burton, B.R., 2001, Influence of Late Cretaceous magmatism on the Sevier orogenic wedge, western Montana: Geology, v. 29, p. 723–726, doi: 10.1130/0091 -7613(2001)029<0723:IOLCMO>2.0.CO;2.

Lonn, J.D., McDonald, C., Lewis, R.S., Kalakay, T.J., O'Neill, J.M., Berg, R.B., and Hargrave, P., 2003, Geologic map of the Philipsburg 30' x 60' quadrangle, western Montana: Montana Bureau of Mines and Geology Open-File Report 483, 1 sheet, scale 1:100,000.

Morse, J., 1977, Deformation in ramp regions of overthrust faults: Experiments with small-scale rock models, *in* Rocky Mountain Thrust Belt Geology and Resources: Wyoming Geological Association 29th Annual Field Conference Guidebook (in conjunction with Montana Geological Society and Utah Geological Society), p. 457–470.

O'Neill, M.J., and Lopez, D.A., 1985, Character and regional significance of the Great Falls tectonic zone, east-central Idaho and west-Central Montana: American Association of Petroleum Geologists Bulletin, v. 69, no. 3, p. 437–447.

Ruppel, E.T., O'Neill, J.M., and Lopez, D.A., 1993, Geologic map of the Dillon 1°x2° quadrangle, Idaho and Montana: U.S. Geological Survey Map I-1803-H.

Schmidt, C.J., Smedes, H.W., and O'Neill, J.M., 1990, Syncompressional emplacement of the Boulder and Tobacco Root Batholiths (Montana-USA) by pull-apart along old fault zones: Geological Journal, v. 25, p. 305–318.

Sears, J.W., 2016, Belt-Purcell Basin: Template for the Cordilleran magmatic arc and its detached carapace, Idaho and Montana, *in* MacLean, J.S., and Sears, J.W., eds., Belt Basin: Window to Mesoproterozoic Earth: Geological Society of America Special Paper 522, p. 365–384, doi: 10.1130/2016.2522(14).

Sears, J.W., Schmidt, C.J., Dresser, H.W., and Hendrix, T., 1989, A geological transect from the Highland Mountains foreland block, through the southwest Montana thrust belt, to the Pioneer batholith: Northwest Geology, v. 18, p. 1–20.

Serra, S., 1977, Styles of deformation in the ramp regions of overthrust faults, *in* Rocky Mountain Thrust Belt geology and resources: Wyoming Geological Association 29th Annual Field Conference Guidebook (in conjunction with Montana Geological Society and Utah Geological Society), p. 487–498.

Tilling, R.I., Klepper, M.R., and Obradovich, J.D., 1968, K-Ar ages and time span of emplacement of the Boulder Batholith: American Journal of Science, v. 266, p. 671–689.

Vejmelek, L., and Smithson, S.B., 1995, Seismic reflection profiling in the Boulder batholith, Montana: Geology, v. 23, p. 811–814.

Winston, D., 1986, Middle Proterozoic tectonics of the Belt Basin, western Montana and northern Idaho, *in* Roberts, S., ed., Belt Supergroup: A guide to Proterozoic rocks of western Montana and adjacent areas: Montana Bureau of Mines and Geology Special Publication 94, p. 245–257.

Yonkee, W.A., and Weil, A.B., 2015, Tectonic evolution of the Sevier and Laramide belts within the North American Cordillera orogenic system: Earth-Science Reviews, v. 150, p. 531–593.

Zeitler, P.K., Meltzer, A.S., Koons, P.O., Craw, D., Hallet, B., Chamberlain, C.P., Kidd, W.S.F., Park, S.K., Seeber, L., Bishop, M., and Shroder, J., 2001, Erosion, Himalayan geodynamics, and the geomorphology of metamorphism: Geological Society of America, GSA Today, January issue, p. 4–9.

STRUCTURAL INHERITANCE FOR THE LARAMIDE, CENTRAL MONTANA UPLIFT: A WRENCH-FAULT TECTONIC MODEL RELATED TO PROTEROZOIC OROGENESIS IN THE FORELAND OF THE NORTH AMERICAN CORDILLERA

Jeffrey W. Bader

North Dakota Geological Survey

ABSTRACT

The Central Montana uplift of eastern Montana lies adjacent to the Northern Rocky Mountains on the western edge of the Northern Great Plains Physiographic Province, and just north of the Laramide belt of the Central Rockies. The origins of this deformed region have received little attention relative to Laramide tectonism and Precambrian basement interrelations, particularly within the overall context of plate tectonic evolution of the North American Cordillera.

The Central Montana uplift is characterized at the surface by six well-defined fault zones with general trends to the WNW and NE. Previous work attributes development of these fault zones to transcurrent motion on basement-rooted faults that deformed the sedimentary cover during Laramide orogenesis.

A Paleoproterozoic origin for these fault zones is proposed/argued herein, with the faults initially forming in cratonic basement as pure-shear conjugates during convergence at the northeastern margin of the Wyoming Province. It is further proposed that the conjugate shears were reactivated as simple shears during the Laramide orogeny under similar SW–NE stress conditions as those in the Precambrian.

Structural analysis of basement fabrics of the western Beartooth Mountains and Laramide surface structures (compiled from previously published data) indicate that these major, and likely regional, crustal anisotropies (conjugate shears) may have guided Laramide deformation across eastern Montana. Isostatic gravity data support these interpretations. Precambrian development of conjugate shears was likely related to Trans-Hudson (1.78–1.74 Ga) orogenesis along the eastern Wyoming Province boundary. Data also indicate that these structures were reactivated as wrench faults during the Laramide orogeny, forming the Central Montana uplift. Results of this study may be used to guide future field efforts to build upon conclusions presented herein.

INTRODUCTION

The Laramide belt is a distinctive tectonic feature located on the eastern side of the North American Cordillera (fig. 1a; Yonkee and Weil, 2015). This classic orogenic system included an active trench with an accretionary complex, forearc basin, magmatic arc, retroarc hinterland, thin-skinned fold and thrust belt, foreland basin, and thick-skinned (basement involved) Laramide belt. The Laramide belt formed in cratonic basement from the Late Cretaceous through the Oligocene (Copeland and others, 2017), disrupting formation of the southwestern portion of the foreland basin (Weil and others, 2016). It extends SW–NE from Arizona to southern Montana and corresponds with the flat-slab subduction zone of the southwestward-moving North American Plate and the subducting oceanic Farallon Plate (fig. 1a; Saleeby, 2003; Lacombe and Bellahsen, 2016; Weil and others, 2016; Wright and others, 2016). This work proposes that the Central Montana uplift (fig. 1b) is the northern extension of Laramide belt deformation and has Precambrian origins.

Using previously published and available geologic, structural, and geophysical data, this study presents a structural analysis of the northern portion of the Wyoming Province (fig. 1b) that shows evidence for the development of pure-shear-related Precambrian anisotropies that were reactivated as simple-shear wrench faults during Laramide orogenesis (Wilson, 1936; Wilcox and others, 1973; Reid and others, 1975; Nelson, 1993; Bader, 2018). A hypothesis for the development of a set of basement fabrics (conjugate shears) that formed in a Paleoproterozoic convergent deformation system is presented herein as a companion paper prepared in conjunction with recent work (Bader, 2018). In that paper, Bader (2018) postulated that a Late Archean convergent deformation system formed within the inner core of the Wyoming Province, developing a preferred orientation of basement fabrics (NNW, WNW, and NE) that were subsequently reactivated during Laramide tectonism, resulting in

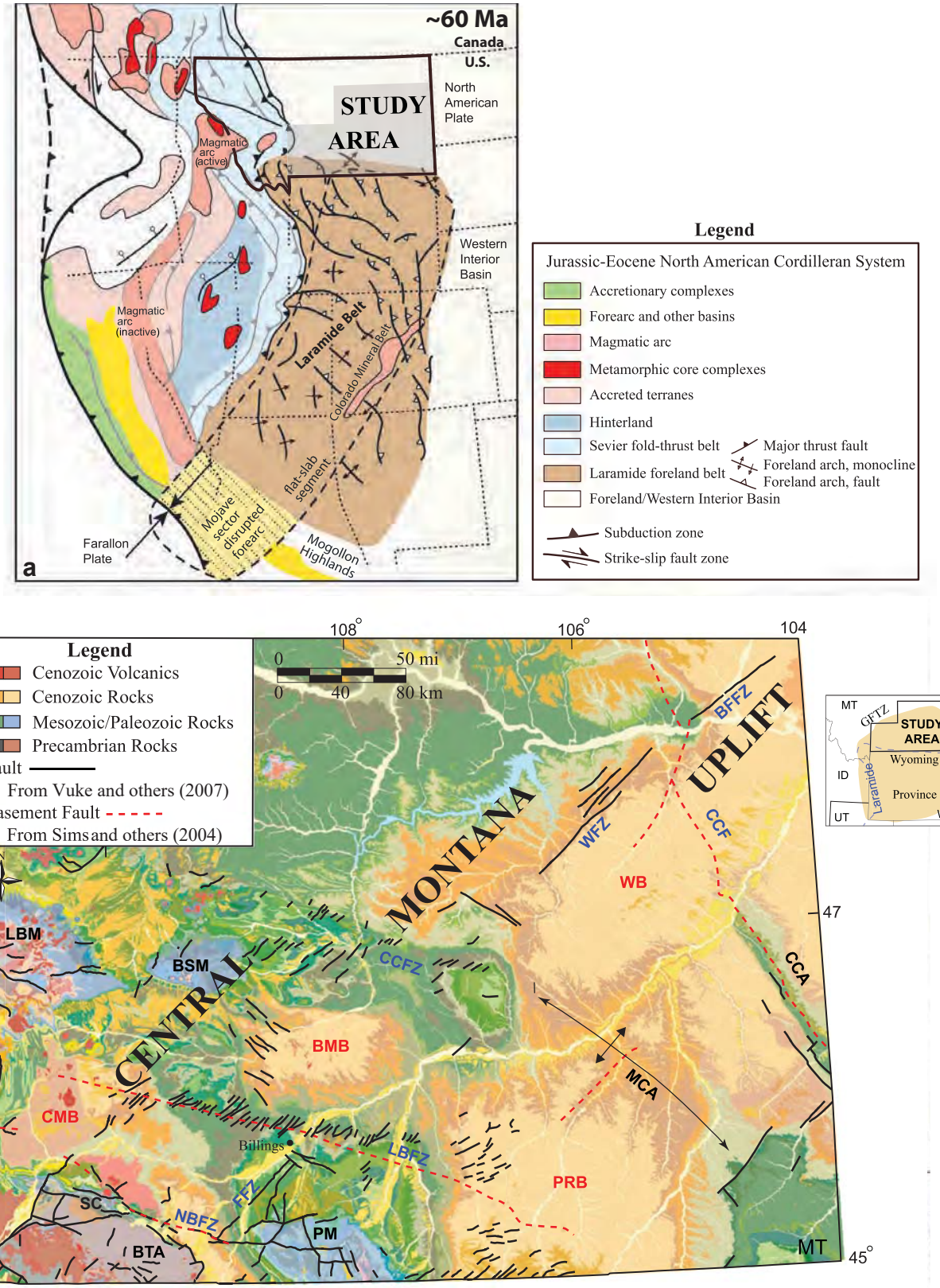

Figure 1. (a) Generalized tectonic map of North American Cordillera at ~60 Ma showing major components including the Laramide belt and zone of flat-slab subduction relative to study area. Modified from Weil and others (2016). (b) Geologic map of eastern Montana, showing physiographic features and major tectonic elements of the Central Montana uplift (study area). BFFZ, Brockton–Froid fault zone; BMB, Bull Mountains Basin; BSM, Big Snowy Mountains; BTA, Beartooth arch; CCA, Cedar Creek anticline; CCF, Cedar Creek fault; CCFZ, Cat Creek fault zone; CMB, Crazy Mountains Basin; FFZ, Fromberg fault zone; GFTZ, Great Falls tectonic zone; LBFZ, Lake Basin fault zone; LBM, Little Belt Mountains; MCA, Miles City arch; NBFZ, Nye–Bowler fault zone; PM, Pryor Mountains; PRB, Powder River Basin; SC, Stillwater Complex; WB, Williston Basin; WFZ, Weldon fault zone. Surface geology/tectonic elements are after Vuke and others (2007). Please note that some surface/near-surface faults (black lines) may be basement-rooted. Inset map delineates the Laramide belt of Wyoming relative to the Wyoming Province boundary in the study area. State abbreviations: ID, Idaho; MT, Montana; NE, Nebraska; ND, North Dakota; SD, South Dakota; UT, Utah; WY, Wyoming.

major arches and uplifts of north-central Wyoming. A similar set of Precambrian (Paleoproterozoic) fabrics oriented WNW and NE are present in the western Beartooth Mountains of south-central Montana (Reid and others, 1975). These fabrics are sub-parallel to the major surface-fault zones of eastern Montana that also trend WNW and NE (Wilson, 1936; Wilcox and others, 1973; Thomas, 1974; Nelson, 1993; Lopez, 2000a,c; Wilde and Smith, 2003). Therefore, as described by Bader (2018) for northern Wyoming, reactivation of these fabrics during the Laramide orogeny is proposed, forming the Central Montana uplift across the northern portion of the Wyoming Province (fig. 1b). This hypothesis is evaluated by: (1) analyzing pertinent geophysical data to identify possible basement-rooted structures in Archean rocks of eastern Montana, and comparing those results to Laramide structural features; (2) reviewing spatial distributions, orientations, and kinematics of available Proterozoic fabrics (shear zones and foliations) exposed in Archean gneissic rocks of the western Beartooth Mountains, and comparing those results to Laramide structural features; and (3) briefly reviewing and integrating plate tectonic evolution data related to development of the North American Cordillera.

BACKGROUND

Regional Topography and Geology

The study area lies dominantly in the Northern Great Plains Physiographic Province of eastern Montana (fig. 1; Norwood, 1965), which topographically is in stark contrast to the Central Rocky Mountain Physiographic Province at the extreme southern end of the study area, near the Montana–Wyoming border. The study area is dominated by the Central Montana uplift, a zone of discrete and slightly uplifted regions in the southwest portion, and rolling hills and prairies of the northern and eastern portions.

Geologically, the eastern portion of the study area is situated on the southwestern flank of the Williston Basin and the northern portion of the Powder River Basin. These two basins are separated by the northwest-trending Miles City arch (fig. 1b). In the western portion of the study area, three distinct, rectilinear fault zones (Cat Creek, Lake Basin, and Nye–Bowler) characterize the area to the NNE of the NNW-trending Laramide Bighorn arch. Northeasterly striking fault zones include the Fromberg and Weldon/Brockton–Froid systems (figs. 1b, 2). These fault zones have been mapped in detail by the Montana Bureau of Mines and Geology (Vuke and others, 2007).

Previous Work

Numerous studies of central and eastern Montana structures have been conducted in the last century (Bowen, 1914; Chamberlin, 1919; Hancock, 1919, 1920; Reeves, 1927; Wilson, 1936; Dobbin and Erdmann, 1955; Wilcox and others, 1973; Thomas, 1974; Reid and others, 1975; Robinson and Barnum, 1986; Mogk and others, 1988; Nelson, 1993; Lopez and others, 2007; Sims, 2009), along with geologic mapping conducted by the Montana Bureau of Mines and Geology (Porter and Wilde, 1993, 1999; Bergantino and Wilde, 1998a,b; Berg and others, 2000; Lopez, 2000a,b,c, 2001; Vuke and others, 2000a,b, 2001a,b, 2003a,b; Wilde and Porter, 2000, 2001; Wilde and Smith, 2003; Vuke and Wilde, 2004; Wilde and Vuke, 2004a,b). Most of these studies were local in nature and in some cases general structural interpretations were presented. However, the regional tectonic significance and the potential genetic relationship between Laramide surface structures and Precambrian basement fabrics has only been addressed superficially (Thomas, 1974). In addition, the significance of these structures in relation to lithospheric architecture and both Precambrian and Laramide plate boundary dynamics has received minimal attention. The more relevant of these studies are discussed below.

West–Northwest-Striking Fault Zones

Western Beartooth Mountains and the Stillwater Complex

The Stillwater Complex is exposed on the northwestern edge of the Beartooth Mountains (figs. 1b, 2; Van Gosen and others, 2000). This igneous intrusive consists of layered mafic to ultramafic rocks that are Archean in age (DePaolo and Wasserburg, 1979; Nunes, 1981; Premo and others, 1990). The complex is rectilinear, strikes west–northwest, and extends approximately 48 km. It is cut by several high-angle reverse faults that strike subparallel to the strike of the layered intrusives (Turner and others, 1985). Due west of the Stillwater Complex, major WNW-striking sinistral faults (Davis Creek and Basin Creek) are present (Reid and others, 1975; Mogk and others, 1988).

Cat Creek Fault Zone

The Cat Creek fault zone shows well-developed en échelon normal faults across much of its 206 km

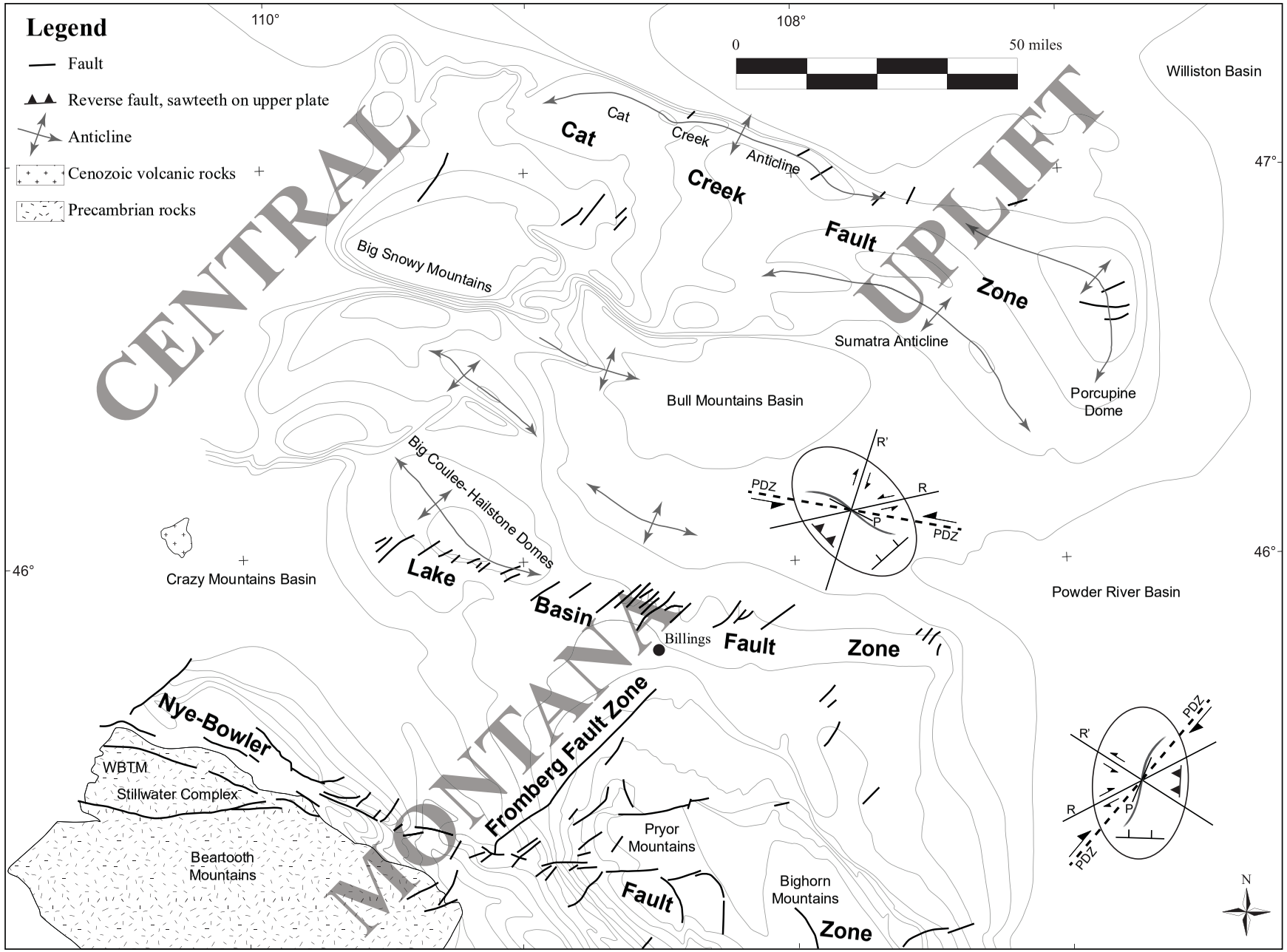

Figure 2. Generalized structure contour map for the Central Montana uplift after Dobbin and Erdmann (1955). Simple-shear strain ellipse for sinistral wrench fault oriented N80°W, and a dextral wrench fault oriented N40°E, provided for comparison. Contours are on the base of the Cretaceous (e.g., Fall River Sandstone). Contour interval = 1000 ft. WBTM, western Beartooth Mountains; PDZ, principal displacement zone/master fault; P, P shear; R, Riedel shear/synthetic-strike slip fault; R', Riedel shear/antithetic-strike slip fault.

trend and includes the Cat Creek anticline, a major curvilinear (reverse-S shape) fold oriented northwest to southeast subparallel to the fault zone (figs. 1b, 2; Dobbin and Erdmann, 1955). Bowen (1914) first studied the fault system while investigating coalfields in central Montana. Reeves (1927) also investigated the system during his studies of the Cat Creek and Devils Basin oil fields. The Reeves (1927) study was very descriptive in nature and identified the Cat Creek fault zone, but did not provide an interpretation for its genesis. However, Reeves (1930) studied the Big Snowy Mountains and attributed their formation, along with the corridor of en échelon normal faults of the Cat Creek system, to lateral crustal movement in the basement.

Nelson (1993) used borehole data to document the presence of the Cat Creek fault in his study of the Cat Creek anticline. He described it as a south-dipping (~60°), high-angle structure that cuts the basement with opposing senses of displacement and a long history of movement, after forming as a proposed rift-related normal fault in the Proterozoic. The Cat Creek fault was reactivated as a reverse, left-lateral oblique-slip fault during the Laramide orogeny (Nelson, 1993), with equal amounts of reverse and strike-slip displacement totaling approximately 1,200 m. Oil production is from structural traps found in northwest-trending en échelon domes/anticlines created from interpreted Laramide left-lateral slip along the Cat Creek fault zone.

Lake Basin Fault Zone

Hancock (1919, 1920) studied the geology and oil and gas prospects of the Lake Basin and Huntley fields located across the trend of the Lake Basin fault zone (Chamberlin, 1919). Hancock (1919) interpreted northeast-striking en échelon normal faults to be related to "a great belt of shearing" that formed the rectilinear zone of deformation along a 320 km, west–northwest trend just north of Billings, Montana (figs. 1b, 2). Wilcox and others (1973) inferred left-lateral shear on a buried, basement-rooted fault based on the well-developed en échelon normal faults similar to those seen at the surface of the Cat Creek fault zone. This zone was also mapped in the subsurface by Dobbin and Erdmann (1955). Robinson and Barnum (1986) studied additional normal faulting in the Paleocene Fort Union Formation. These were interpreted to be the result of left-lateral slip on a previously unidentified southeast extension of the Lake Basin zone. In the subsurface, Sims (2009) identified the Lake Basin fault as a basement-rooted Precambrian structure. Seismic profiles across the fault zone indicate the master fault dips steeply to the south (~87°) with minimal vertical basement offset (<8 m), and cuts Precambrian to Lower Cretaceous rocks (Lopez and others, 2007).

Nye–Bowler Fault Zone

The Nye–Bowler fault zone extends from northwest of Livingston, Montana southeast a distance of approximately 400 km and into the Powder River Basin of Wyoming. The Pryor Mountains and associated compressional structures (reverse faults and curvilinear, en échelon folds) are located in the central portion of the fault zone (figs. 1b, 2; Dobbin and Erdmann, 1955). Wilson (1936) performed detailed mapping of surface structures in south-central Montana and interpreted that deformation was related to movement on a basement-rooted sinistral wrench fault (fig. 2). The subsidiary structures formed in the sedimentary cover above the master fault, including en échelon folds oriented to the northwest, were identified as potential structures for petroleum entrapment.

Northeast-Striking Fault Zones

Little previous work has been published on the Fromberg and Weldon/Brockton–Froid fault zones other than mapping performed by the Montana Bureau of Mines and Geology (figs. 1b, 2; Bergantino and Wilde, 1998a,b; Lopez, 2000a,b,c; Wilde and Smith, 2003; Wilde and Vuke, 2004a).

Fromberg Fault Zone

The Fromberg system strikes NE and is located just south of Billings, Montana, between the Nye–Bowler and Lake Basin zones. It extends for approximately 66 km where it terminates against the Nye–Bowler/Lake Basin systems (Lopez, 2000a,b). The main throughgoing fault has been classified as a right-lateral strike-slip fault with splays off the main fault forming an anastomosing pattern up to 6 km wide.

Weldon/Brockton–Froid Fault Zone

The Weldon/Brockton–Froid fault zone is located in northeastern Montana extending from 50 km southwest of Weldon, Montana, to where it terminates approximately 16 km northeast of Froid, Montana (fig. 1b; Bergantino and Wilde, 1998a,b; Wilde and Smith,

2003; Wilde and Vuke, 2004a). This deformation corridor is generally linear in plan view and as much as 18 km wide with some splays off the main fault. Weldon-zone faults are nearly vertical, down mainly on the northeast side, and have up to 46 m of throw (Wilde and Smith, 2003).

Other Faults

In the western Beartooth Mountains, major faults include the NNE-striking, dextral Blacktail Lake and West Boulder faults, along with the Marten Peak and Luccock Park faults (Reid and others, 1975). Reid and others (1975) interpreted these faults, along with the WNW-striking faults in the western Beartooths, as shear zones originating from Paleoproterozoic (1.7 Ga) compressional stress from the NE.

Subsurface

Figure 2 is a structure contour map on the base of the Cretaceous (e.g., Fall River Sandstone) for the southern portion of the Central Montana uplift (Dobbin and Erdmann, 1955). Several of the Laramide structures discussed earlier have been delineated in the subsurface including the Cat Creek, Lake Basin, Nye–Bowler, and Fromberg fault zones, as well as Laramide basins including the larger Williston and Powder River, and smaller Crazy Mountains and Bull Mountains basins.

METHODS

This work was an evaluation of existing disparate datasets, completed in conjunction with Bader (2018). Fieldwork to collect additional data to support this effort is warranted, but was not possible; however, significant previously published material exists to present the aforementioned hypothesis and, in conjunction with Bader (2018), provides a baseline for future field investigations.

Geophysical data were used to help identify areas of basement uplift and potential basement anisotropy. These areas were then compared to: (1) previously mapped Laramide surface and subsurface structures (Porter and Wilde, 1993, 1999; Bergantino and Wilde, 1998a,b; Berg and others, 2000; Lopez, 2000a,b,c, 2001; Vuke and others, 2000a,b, 2001a,b, 2003a,b; Wilde and Porter, 2000, 2001; Wilde and Smith, 2003; Vuke and Wilde, 2004; Wilde and Vuke, 2004a,b); and (2) data from the western Beartooth Mountains (Reid and others, 1975; Van Gosen and others, 2000), in order to assess the relationship between Precambrian fabrics in proximity to major Laramide structures along the two hypothesized directions of potential basement weakness. These include the Nye–Bowler, Lake Basin, and Cat Creek fault zones (WNW strike); and the Fromberg and Weldon/Brockton–Froid fault zones (NE strike). Surface deformations along these fault zones were compared to the strain ellipse for simple-shear systems to ascertain the potential for wrench deformation across the Central Montana uplift area.

DATA AND RESULTS

Geophysical Data

The USGS (2019) developed an isostatic gravity map of Montana (fig. 3a). Calculation of the isostatic model used averaged digital topography, crustal thickness of 30 km, crustal density of 2.67 g/cc, and a density contrast between the crust and upper mantle of 0.35 g/cc (USGS, 2019).

The Central Montana uplift is readily identified by the positive anomaly oriented SW–NE at ~N40°E that extends from south-central to northeastern Montana. The Williston and Powder River basins are also easily discerned as gravity lows throughout eastern Montana. Contrast between the gravity highs and lows define WNW-, NNE-, and NNW-striking linear anomalies (fig. 3a).

Geological Data

Precambrian Fabrics

Archean basement exposures are extremely rare in the study area and are limited to the Beartooth Mountains of south-central Montana. Basement fabric data (foliations and shear zones) were compiled from a preexisting map for the western Beartooth Mountains (fig. 2; Reid and others, 1975) and synthesized, and plots were created on equal-area, lower-hemisphere projections from which rose diagrams were constructed for the area using Stereonet 10 (figs. 4, 5). These plots were used for comparison to data from Laramide structures discussed below (figs. 6–11).

Western Beartooth Mountains and the Stillwater Complex. Fabric data collected from the pervasively foliated Mount Delano gneiss over an area of approximately 38 km^2 are shown in figures 4a and 4b. Foliations (n = 264) are distinctly unimodal with an average strike of N45°E. This is consistent with

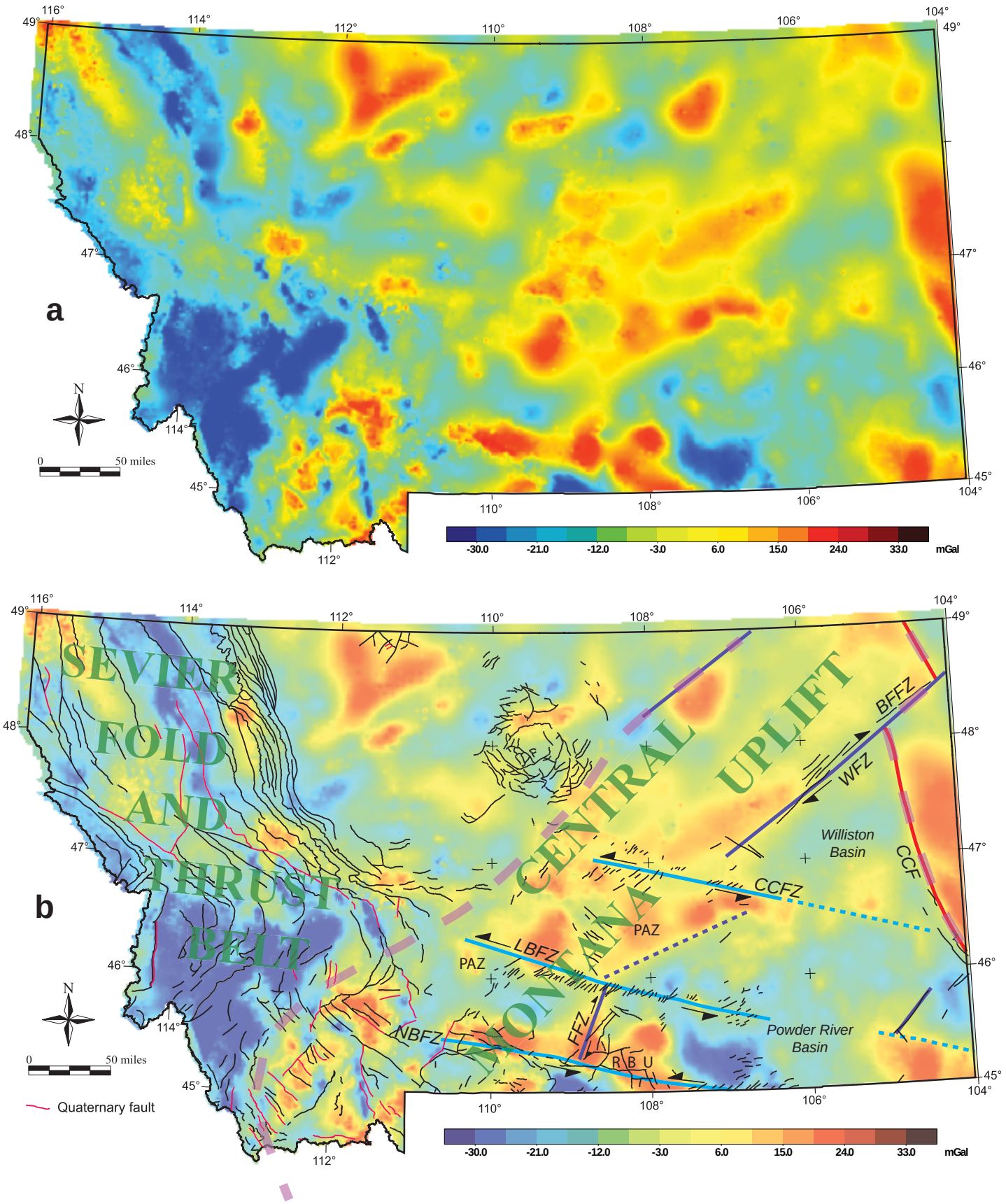

Figure 3. (a) Isostatic residual gravity map of Montana (USGS, 2019). (b) Interpretation of isostatic residual gravity map of Montana. PAZ, pull-apart zone; RBU, restraining bend uplift. See figure 1 for other abbreviations. See text and figures 14 and 15 for discussion. Surface faults after Vuke and others (2007).

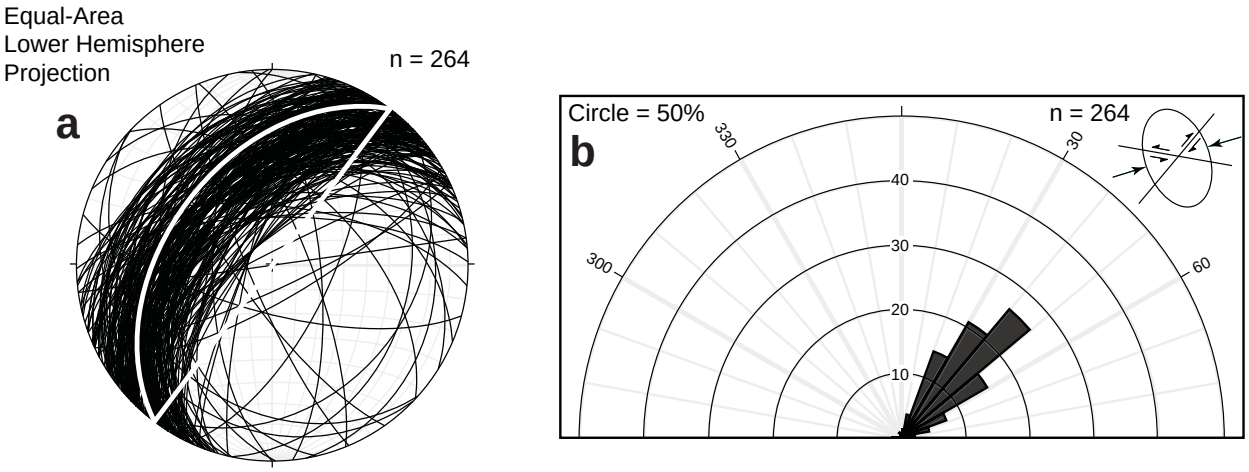

Figure 4. (a) Equal-area lower-hemisphere projection showing attitude of foliations for the Mount Delano gneiss in the western Beartooth Mountains; avg. N38°E, 55°NW (white line). (b) Rose diagram showing strikes of foliations for the Mount Delano gneiss in the western Beartooth Mountains. Data are after Reid and others (1975). Pure-shear strain ellipse with principal horizontal stress at N70°E provided for comparison.

data for shears in the western Beartooth Mountains (Luccock Park, Marten Peak, Blacktail Lake, and West Boulder faults) where the average strike is ~N35°E (fig. 5). These NNE-trending zones of basement anisotropy are subparallel with overall strikes of the Fromberg and Weldon Brockton–Froid systems at ~N40°E (figs. 9–11). Other shears in the western Beartooth Mountains include the Davis Creek and Basin Creek faults that strike ~N75°W (fig. 5), and are subparallel to the Cat Creek, Lake Basin, and Nye–Bowler fault zones at ~N80°W (figs. 6–8).

In general, major faults in the Stillwater Complex have a unimodal distribution striking to the WNW at ~N70°W, parallel to the complex itself. However, faults of the Stillwater Complex may represent Archean and/or Laramide tectonism, whereas shears of the western Beartooth Mountains likely represent Proterozoic orogenesis (Reid and others, 1975). Therefore, faults of the Stillwater Complex are not included in figure 5.

Laramide Structures

Available Laramide fault strike-data were compiled from pre-existing maps (Porter and Wilde, 1993, 1999; Bergantino and Wilde, 1998a,b; Berg and others, 2000; Lopez, 2000a,b,c, 2001; Vuke and others, 2000a,b, 2001a,b, 2003a,b; Wilde and Porter, 2000, 2001; Wilde and Smith, 2003; Vuke and Wilde, 2004; Wilde and Vuke, 2004a,b) and synthesized, and plots were created on equal-area, lower-hemisphere projections from which rose diagrams were constructed for each fault zone (figs. 6–11).

West-Northwest-Striking Fault Zones. Surface fault data for the WNW-striking zones of the Central Montana uplift are shown in figures 6–8. Faults of the Cat Creek fault zone (n = 200) have a dominant strike of N55°E and are unimodal (fig. 6). Faults of the Lake Basin fault zone (n = 34) show similar trends to the Cat Creek system with dominant strikes to the NE at N45°E; however, some faults also strike WNW (fig. 7). Faults of the Nye–Bowler zone (n = 319) are multidirectional (fig. 8), but have a dominant strike of N50°E.

Northeast-Striking Fault Zones. The Weldon (n = 10) and Brockton–Froid (n = 8) fault zones are distinctly unimodal as compared to the WNW-striking systems and show very similar strikes of N45°E and N55°E (figs. 10, 11). Faults of the Fromberg zone (n = 25) are multidirectional (fig. 9), but have a dominant strike of N45°E.

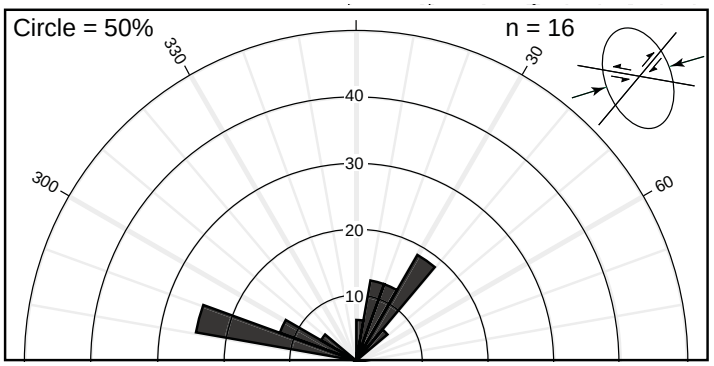

Figure 5. Rose diagram showing strikes of major shear zones in the western Beartooth Mountains. Data are after Reid and others (1975) and Van Gosen and others (2000). Pure-shear strain ellipse with principal horizontal stress at N70°E provided for comparison.

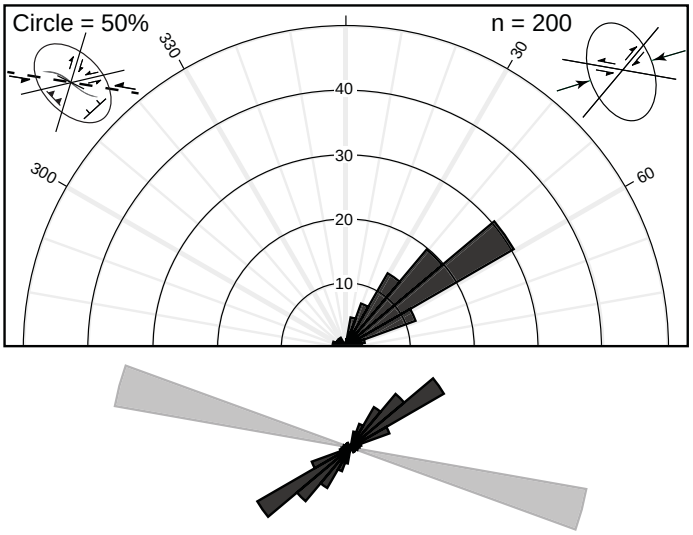

Figure 6. Rose diagram showing strikes of major faults of the Cat Creek fault zone (dark gray) as compared to the strike of the Cat Creek fault (light gray). Data are after Porter and Wilde (1993, 1999), Vuke and others (2003a), and Vuke and Wilde (2004). Simple-shear strain ellipse for sinistral wrench fault oriented N80°W, and pure-shear strain ellipse with principal horizontal stress at N70°E, provided for comparison.

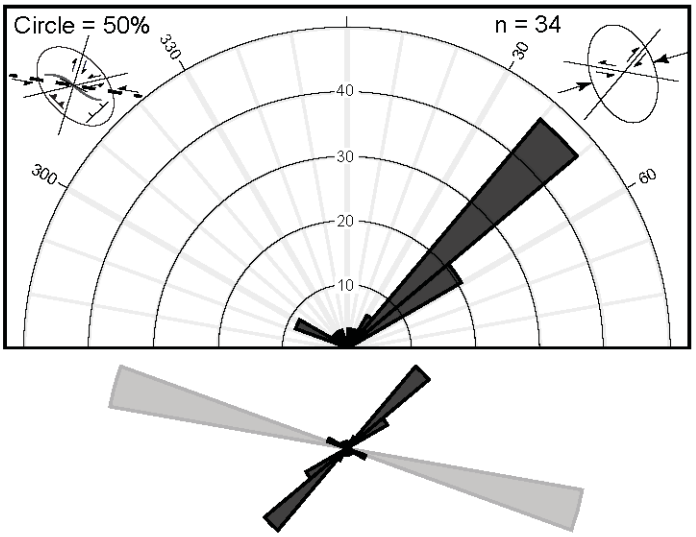

Figure 7. Rose diagram showing strikes of major faults of the Lake Basin fault zone (dark gray) as compared to the strike of the Lake Basin fault (light gray). Data are after Lopez (2000a,b), Vuke and others (2000a, 2001b), and Wilde and Porter (2001). Simple-shear strain ellipse for sinistral wrench fault oriented N80°W, and pure-shear strain ellipse with principal horizontal stress at N70°E, provided for comparison.

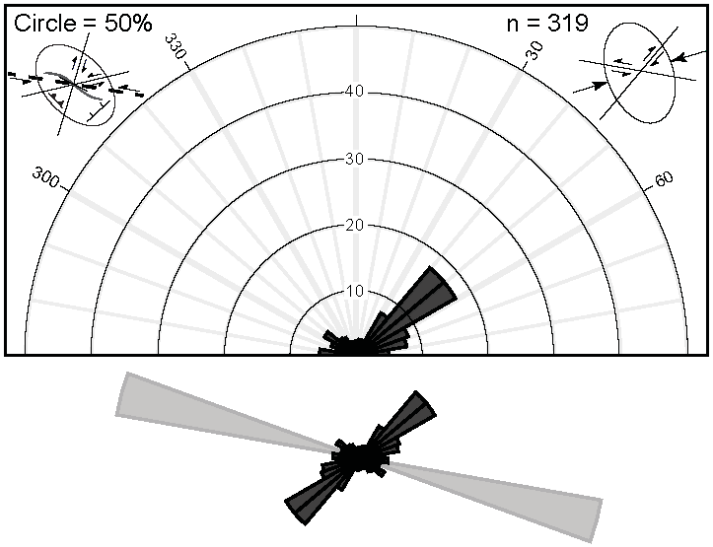

Figure 8. Rose diagram showing strikes of major faults of the Nye–Bowler fault zone (dark gray) as compared to the strike of the Nye–Bowler fault (light gray). Data are after Berg and others (2000), Lopez (2000c, 2001), and Vuke and others (2000b, 2001a). Simple-shear strain ellipse for a sinistral wrench fault oriented N80°W, and pure-shear strain ellipse with principal horizontal stress at N70°E, provided for comparison.

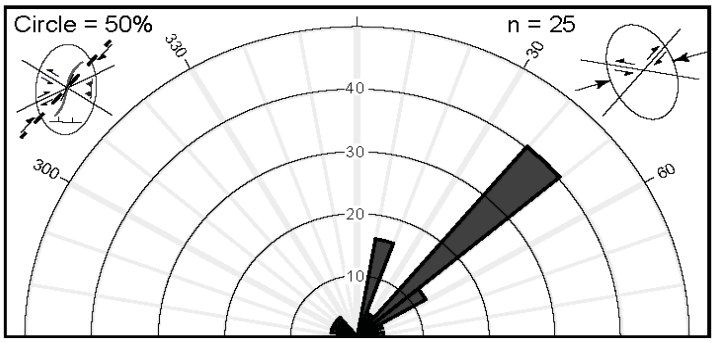

Figure 9. Rose diagram showing strikes of major faults of the Fromberg fault zone. Data are after Lopez (2000a,b,c). Simple-shear strain ellipse for a dextral wrench fault oriented N40°E, and pure-shear strain ellipse with principal horizontal stress at N70°E, provided for comparison.

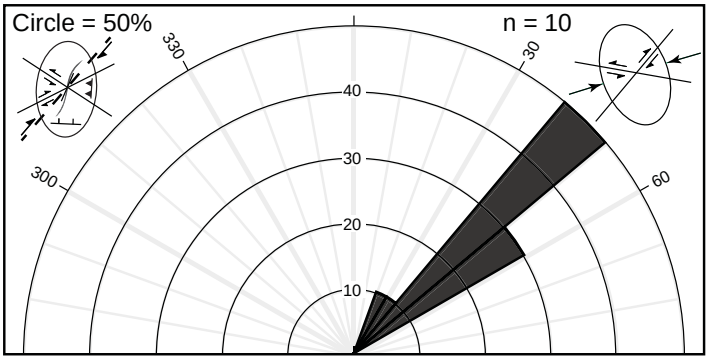

Figure 10. Rose diagram showing strikes of major faults of the Weldon fault zone. Data are after Wilde and Smith (2003) and Wilde and Vuke (2004a). Simple-shear strain ellipse for a dextral wrench fault oriented N40°E, and pure-shear strain ellipse with principal horizontal stress at N70°E, provided for comparison.

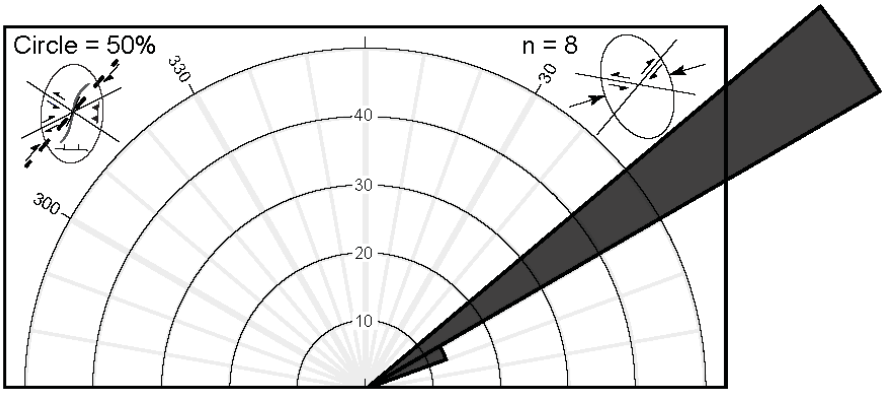

Figure 11. Rose diagram showing strikes of major faults of the Brockton–Froid fault zone. Data are after Bergantino and Wilde (1998a,b). Simple-shear strain ellipse for a dextral wrench fault oriented N40°E, and pure-shear strain ellipse with principal horizontal stress at N70°E, provided for comparison.

INTERPRETATIONS

Geophysical Data

An interpretation of the geophysical data is presented as figure 3b. Potential basement-rooted structures can be inferred where gravity anomalies are present and provide possible evidence for Precambrian anisotropies in support of the limited Precambrian fabric data available for eastern Montana. Figure 3b also includes surface fault traces (Vuke and others, 2007) of the previously described fault zones for comparison.

West–Northwest Anomalies

Several distinct, linear, WNW-trending anomalies are interpreted to represent the basement expression of major fault zones. The Nye–Bowler fault zone is clearly discernable as positive gravity anomalies separating gravity lows of the surrounding basin areas. The Pryor Mountains uplift is defined by gravity highs along the central portion of the Nye–Bowler trend, which extends well into the Powder River Basin of Wyoming. The Lake Basin system also shows distinct gravity contrasts between basins and uplifted areas, and may also extend to the SE into southeastern Montana. The Cat Creek fault zone is defined by gravity highs from east to west, and contributes to the overall positive gravity trends seen from central to northeastern Montana. This system could also extend to the east across the southern Williston Basin.

Northeast and North–Northwest Anomalies

The Fromberg, Weldon, and Brockton–Froid fault zones are also distinct and define uplifted areas lateral to both the Powder River and Williston basins.

In addition to the WNW- and NE-trending anomalies, eastern Montana is characterized by significant gravity highs. These areas are interpreted to define the Wyoming Province/Trans-Hudson orogen boundary, where rocks of the Archean Wyoming craton are juxtaposed against Proterozoic terranes along the NNW-striking Cedar Creek fault/suture (fig. 3b).

Geological Data–Rectilinear Deformation Zones

In and of itself, the isostatic gravity data and seismic data from previous studies support previous interpretations of the presence of potential basement-rooted faults across eastern Montana, oriented WNW and possibly NE (fig. 3b). Additionally, surface mapping of fault zones across the Central Montana uplift suggests that Laramide structures in the study area are related to simple shear reactivation of basement-rooted features (figs. 1b, 2, 3b; Wilson, 1936; Wilcox and others, 1973; Nelson, 1993). Structural analysis of surface deformations in the Central Montana uplift as compared to the strain ellipse for a simple-shear system, and Precambrian fabric data collected from the western Beartooth Mountains for the current study, were used to see if interpreted basement faults observed on the gravity map may have originated in the Proterozoic.

Cat Creek Fault Zone

Previous workers have interpreted the NW-striking corridor of en échelon faults of the Cat Creek system to be normal faults related to Laramide left-lateral shear in underlying basement rocks (e.g., Nelson, 1993). Structural analysis utilizing the strain ellipse for a simple-shear sinistral wrench fault is consistent

with that interpretation (figs. 1b, 2, 6), as documented in the field by Nelson (1993). Faults of the Cat Creek system are dominantly NE-striking normal faults with a few NE-striking synthetic strike-slip faults. Very few reverse and antithetic strike-slip faults are present (Porter and Wilde, 1993, 1999; Vuke and others, 2003a; Vuke and Wilde, 2004). NW–SE-trending curvilinear (reverse S-shape) drag folds (Cat Creek and Sumatra anticlines and Porcupine Dome) are prevalent across the area and likely related to sinistral shear on the Cat Creek fault (fig. 2).

Lake Basin Fault Zone

Like the Cat Creek fault, NE-striking normal faults dominate across the entire trend of the inferred basement fault (figs. 1b, 2, 7; Chamberlin, 1919; Robinson and Barnum, 1986; Lopez, 2000a,b; Vuke and others, 2000a, 2001b; Wilde and Porter, 2001), but the Lake Basin system has less synthetic/antithetic strike-slip faults based on comparison to the strain ellipse. Some minor reverse faults and P-shears striking to the NW are also present along the Lake Basin trend. To the SE, synthetic strike-slip and normal faults predominate as documented in the field by Robinson and Barnum (1986), and as predicted by the strain ellipse (fig. 7). Big Coulee and Hailstone domes also indicate sinistral shear on the Lake Basin fault based on northwesterly trend and sigmoidal shape (fig. 2).

Nye–Bowler Fault Zone

The multidirectional distribution of faults along the Nye–Bowler zone is consistent with sinistral shear along its NW–SE trend, based on the strain ellipse. Synthetic/antithetic strike-slip (NE strike), and reverse faults (NW strike) are significant along the central and western portions of the system (figs. 1b, 2, 8; Berg and others, 2000; Lopez, 2000c, 2001), with some smaller P-shears (NW strike) connecting the antithetic faults. Normal faults (NE strike) are more predominate southeast of the central zone (Vuke and others, 2000b, 2001a) along the Wyoming–Montana border.

Fromberg, Weldon, and Brockton–Froid Fault Zones

Surface deformations for these fault zones were compared to the strain ellipse for a simple-shear dextral wrench fault. Unimodal distributions for the NE-striking Weldon and Brockton–Froid fault zones suggest that the master fault may be present at or near surface and slip on the master fault has been minimal, thus creating a relatively narrow corridor of deformation with less subsidiary structures (faults and folds) as compared to the WNW-trending deformations (figs. 1b, 10, 11; Bergantino and Wilde, 1998a,b; Wilde and Smith, 2003; Wilde and Vuke, 2004a). The Fromberg zone is also relatively narrow aerially, but shows a multidirectional distribution of faults including synthetic/antithetic strike-slip faults along with several P-shears connecting the synthetic faults, especially near the NE-terminus of the fault (figs. 1b, 2, 9; Lopez, 2000a,b,c).

Comparison of Precambrian Fabrics to Laramide Structural Patterns

West–Northwest-Striking Fault Zones

Major sinistral shears of Paleoproterozoic age (Reid and others, 1975) in the western Beartooth Mountains (~N75°W) are subparallel to the strike of the Nye–Bowler, Lake Basin, and Cat Creek fault zones (~N80°W). This suggests that the proximal Nye–Bowler fault, and possibly the Lake Basin and Cat Creek faults, may have formed in the Proterozoic, and then were reactivated during the Laramide orogeny. Faults of the Archean Stillwater Complex, and layered mafic intrusions of the complex as a whole, have a similar strike (~N70°W) that may be related to, and/or affected by, Paleoproterozoic tectonism discussed herein; thus the Stillwater Complex is also in conducive alignment to contribute to Laramide deformation along the northwest portion of the Nye–Bowler trend.

North–Northeast-Striking Fault Zones

Foliation in the Mount Delano gneiss (N45°E, fig. 4) is nearly parallel to the major NE-striking fault zones (~N40°E, figs. 9–11) of the Central Montana uplift and likely indicates a preferred orientation of weakness to the NE. Foliation along with northeast-striking shears in the western Beartooth Mountains (~N35°E), suggest that Laramide development of the NE-striking Fromberg fault zone, and possibly the Weldon and Brockton–Froid fault systems, may have been guided by Precambrian fabrics. This also likely explains the structural grain to the NE, from the western Beartooth Mountains to NE Montana (figs. 1, 3).

Summary

Data presented herein indicate that WNW and NE directions of potential basement weakness are present in the Central Montana uplift, and are defined by several well-developed surface fault zones. Evidence

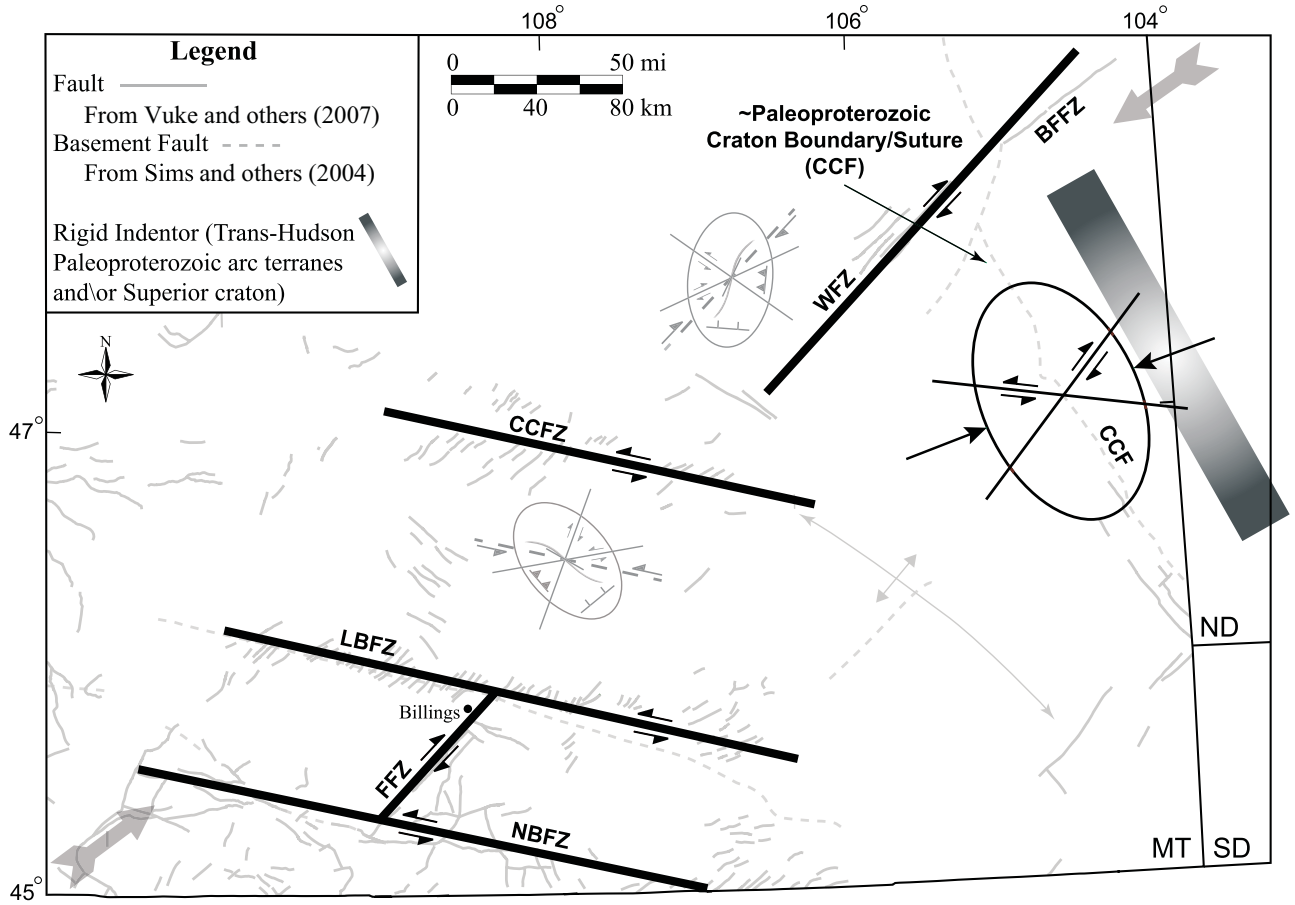

Figure 12. Study area showing interpreted Paleoproterozoic convergent-deformation-system and wrench-fault zones of the Central Montana uplift. Pure-shear strain ellipse with kinematic indicators and general Paleoproterozoic timing for convergent-zone deformations are presented for comparison. Shaded back area showing Laramide and basement deformations with simple-shear strain ellipse for sinistral wrench fault oriented N80°W, and a dextral wrench fault oriented N40°E, also provided for comparison. Large gray arrows indicate the approximate Laramide principal horizontal stress direction (~N60°E). See figure 1 for abbreviations. Tectonic elements are from Vuke and others (2007) and this paper. Some surface/near-surface faults (gray lines) may also be basement rooted.

that basement anisotropies control formation of these major Laramide surface structures is suggested, based on surface and subsurface structure, seismic data, gravity data, Precambrian fabrics, and regional structural grain. Deformation corridors define an apparent conjugate shear pattern that is regional in extent, and is very well displayed across the Central Montana uplift (fig. 12).

DISCUSSION

Paleoproterozoic Orogenic Hypothesis

Collectively, the proposed WNW- and NE-striking basement-rooted faults kinematically define a nearly perfect conjugate shear pattern with WNW faults striking ~N80°W and NE faults striking ~N40°E. However, a principal horizontal stress oriented ~N70°E is required if the proposed faults of the Central Montana uplift are truly Precambrian conjugate shears. This bearing is roughly transverse to the orientation of the major NNW-striking Cedar Creek fault (~N25–30°W; figs. 1b, 3b), the likely suture between the Archean Wyoming craton and Proterozoic terranes to the east (Brewer and others, 1982; Whitmeyer and Karlstrom, 2007; McCormick, 2010). Therefore, orientation of the Cedar Creek fault and proposed conjugate shears is consistent with a convergence model and is evidence that the rectilinear fault zones of the Central Montana uplift may be reactivated basement fabrics originally formed during Paleoproterozoic contraction along the NE Wyoming craton boundary (fig. 12; Reid and others, 1975; Mueller and others, 2005). Kinematically, the conjugate shear set would be expected to form at an active continental margin in-board of a convergent plate boundary (Sylvester, 1988; Bader, 2018). Therefore, a relationship between Paleoproterozoic continent to continent/arc terrane collision during the Trans-Hudson orogeny (circa 1.78–1.74 Ga) and the development of a Proterozoic convergent deformation system within the northern Wyoming craton is pro-

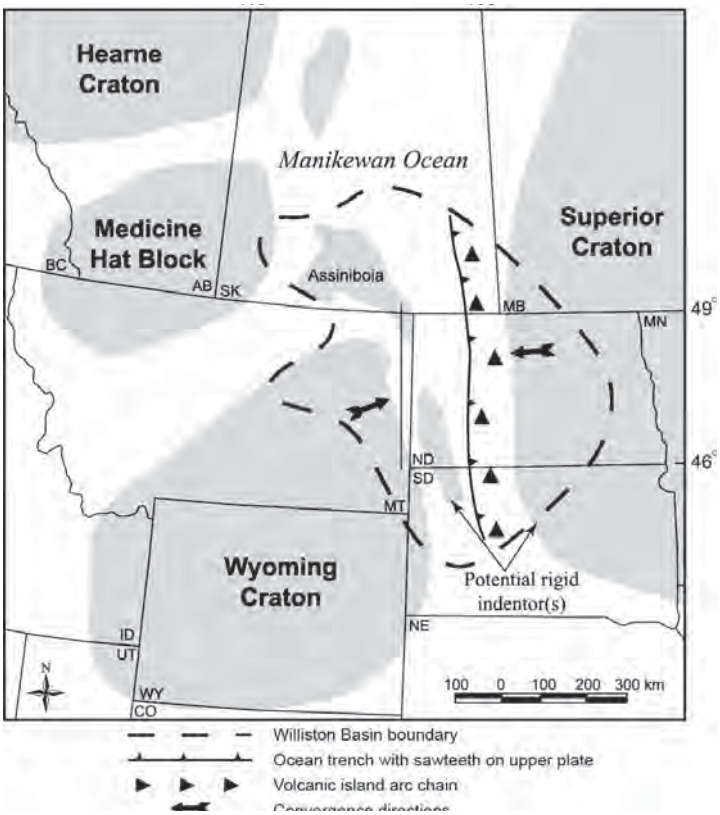

Figure 13. Hypothetical schematic showing plate tectonic setting of the Trans-Hudson orogen with major lithotectonic elements. Modified from Mueller and others (2005), Corrigan and others (2009), and Bader (2018). State abbreviations in figure 1. Province abbreviations: AB, Alberta; BC, British Columbia; MB, Manitoba; SK, Saskatchewan.

posed. This relationship is temporally consistent with Bader's (2018) hypothesis of SW-directed convergence beginning in the Late Archean for this region, as well as other studies related to Trans-Hudson orogenesis (fig. 13; Mueller and others, 2005; Corrigan and others, 2009). The WNW Cedar Creek fault is the likely paleo-suture, and WNW (e.g., Cat Creek, Lake Basin, and Nye–Bowler faults) and NE (e.g., Fromberg, Weldon, and Brockton–Froid faults) deformations are conjugate shears formed within the Wyoming craton during the docking event(s), as shown in figs. 12 and 13.

Contrasting arguments of Nelson (1993) indicated that the Cat Creek fault originated at ~1.5 Ga in the Mesoproterozoic during rifting events that were prevalent at that time. The Cat Creek fault was likely involved in these rifting events, but probably formed earlier in the Paleoproterozoic as discussed herein, and was reactivated later in the Proterozoic and into the Phanerozoic as well (Nelson, 1993). This same argument would also apply to the work of Marshak and others (2000), who suggested that Laramide structures of the northern Rocky Mountains were related to inversion of WNW-striking rift zones that formed in the Mesoproterozoic.

Lack of Precambrian exposures in Laramide belt basement-cored arches/uplifts in the study area is likely due to a change in the paleostress/strain boundary related to flat-slab subduction. In addition, NNE-striking anisotropies that characterize the major arches in the core of the Wyoming Province in north-central Wyoming (Beartooth, Wind River, Bighorn, and Laramie arches) have not been observed within the Wyoming Province of eastern Montana, where only two directions (WNW and NE) of major anisotropy are postulated, versus three directions (NNE, WNW, and NE) in the core of the Wyoming Province. Thus, by inference, NNE-striking anisotropies that facilitated formation of major arches in north-central Wyoming are not likely present in the Wyoming Province of central and eastern Montana. However, WNW-trending structures of central Montana, such as the Pryor Mountains, Big Snowy Mountains, and Little Belt Mountains, probably are basement cored. They would be analogous to WNW-oriented structures in north-central Wyoming/south-central Montana (western end of Beartooth Mountains, Tensleep fault zone, Owl Creek fault zone, Sweetwater uplift) and thus should be characterized as uplifts rather than arches, as per Bader (2018). Therefore, this work suggests that significant stress was transmitted well north of the Laramide belt into Montana and deformation was basement involved, thus making the Central Montana uplift the northern extension of the Laramide belt.

Laramide Structural Inheritance

Conjugates formed from pure shear during Proterozoic convergence directed from the NE (figs. 4, 5) were likely reactivated as wrench faults (simple shear) during the Laramide orogeny (figs. 6–11) as shown in figure 12. Limited strike-slip/shear may have occurred across the basement-rooted Laramide wrench faults (Nelson, 1993), with most of both lateral and vertical displacement taken up on subsidiary faults (e.g., synthetic/antithetic strike-slip, reverse, and normal faults) of the WNW- and NE-striking system(s). However, even with minimal lateral slip, the sedimentary cover provides a clear record of wrench faulting across these zones (Wilcox and others, 1973; Bader, 2008, 2009, 2018). In addition to matching Proterozoic convergent deformation and Laramide contractional structures,

other subsidiary surface deformational features (e.g., rectilinear deformation zones with en échelon and right-stepping normal faults across the zone, curvilinear drag folds, documented steep, high-angle master faults, etc.), also strongly suggest basement-rooted wrenching during the Laramide.

The reactivation of Precambrian fabrics during Laramide orogenesis is likely because the principal horizontal stress of N70°E during hypothesized Paleoproterozoic contraction is very similar to that of Laramide shortening at ~N60°E (Bird, 1978; Erslev and Koenig, 2009; Weil and Yonkee, 2012), thus facilitating Laramide wrench deformation across the six basement-rooted fault zones of the Central Montana uplift.

Pull-Apart Zones and Restraining Bend Uplifts

Based on the interpretations presented, the presence of left-stepping WNW-striking, sinistral wrench systems would suggest that releasing bends/stepovers and restraining bends/stepovers may be present along these transcurrent features. Smaller sedimentary basins in the study area include the Bull Mountains Basin, an apparent WNW extension of the Powder River Basin, and the Crazy Mountains Basin, a smaller basin WNW of the Bighorn Basin of north-central Wyoming (fig. 1b). Significant structural highs, other than the Beartooth Mountains, include a smaller uplift, the Pryor Mountains, present just east of the Beartooths, and along the Nye–Bowler trend (fig. 1b).

Dooley and McClay (1995) presented models for pull-apart basin formation along basement-seated, simple parallel-wrench faults (i.e., no transpression or transtension) that support the hypothesis of basement-rooted left-stepping sinistral wrench zones across the Central Montana uplift. Dooley and McClay's (1995) model for an overlapping-150° sidestep (their figs. 2, 7, 8, 9c) is a representative analog for development of the Bull Mountains Basin, and possibly the Crazy Mountains Basin, during Laramide sinistral wrenching (fig. 14).

A significant restraining stepover/bend along the Nye–Bowler trend is likely responsible for the Pryor Mountains and associated structures created as a result of localized contraction at the stepover/bend (McClay and Bonora, 2001; their figs. 3, 5). Analog models for a 90° restraining stepover geometry for a right-stepping sinistral system produced a nearly identical rhomboidal uplift as seen in the Pryor Mountains; however, the Pryor Mountains are likely related to a restraining bend (~60°), rather than a restraining stepover (fig. 15).

CONCLUSIONS

This study confirms the genetic interpretations of previously mapped and studied structures across the Central Montana uplift. Evidence indicates that the major Laramide fault zones (Cat Creek, Lake Basin, Nye–Bowler, Fromberg, Weldon, and Brockton–Froid) of eastern Montana are related to transcurrent movement on basement-rooted wrench faults. Consistent orientation of these wrench corridors within the northern Wyoming Province appear to be fundamentally related to the intracratonic nature of Paleoproterozoic anisotropies striking WNW and NE (i.e., proposed convergent deformation system).

Fabrics of this Proterozoic convergent deformation system likely underwent reactivation during Laramide orogenesis, as shallow-angle Farallon plate subduction to the SW formed the Laramide belt due south of the study area (Bader, 2018). WSW–ENE-directed regional shortening during the Laramide reactivated basement weaknesses forming the Central Montana uplift. Small rhomboid/sigmoidal basins (e.g., Bull Mountains) formed as releasing stepovers adjacent to left-stepping sinistral faults that developed as the system evolved during the Laramide. Restraining bend uplifts such as the Pryor Mountains also formed along the Nye–Bowler trend, where wrench geometry facilitated formation of compressive structures.

This paper incorporates nearly all available published material regarding the Laramide for the Central Montana uplift and presents new and current interpretations, thus providing a useful baseline for conducting future research into Laramide orogenesis. Bader (2018) has shown the important role that basement anisotropies may have played in Laramide tectonism for the central core of the Wyoming Province in north-central Wyoming. Along those lines, the current study presents a hypothesis and model that is geologically, and, more importantly, temporally consistent with the work of Bader (2018), as well as others (Mueller and others, 2005; Corrigan and others, 2009) for the northern portion of the Wyoming Province. The current study and Bader's (2018) work contribute to a better understanding of the origins and nature of Neoarchean

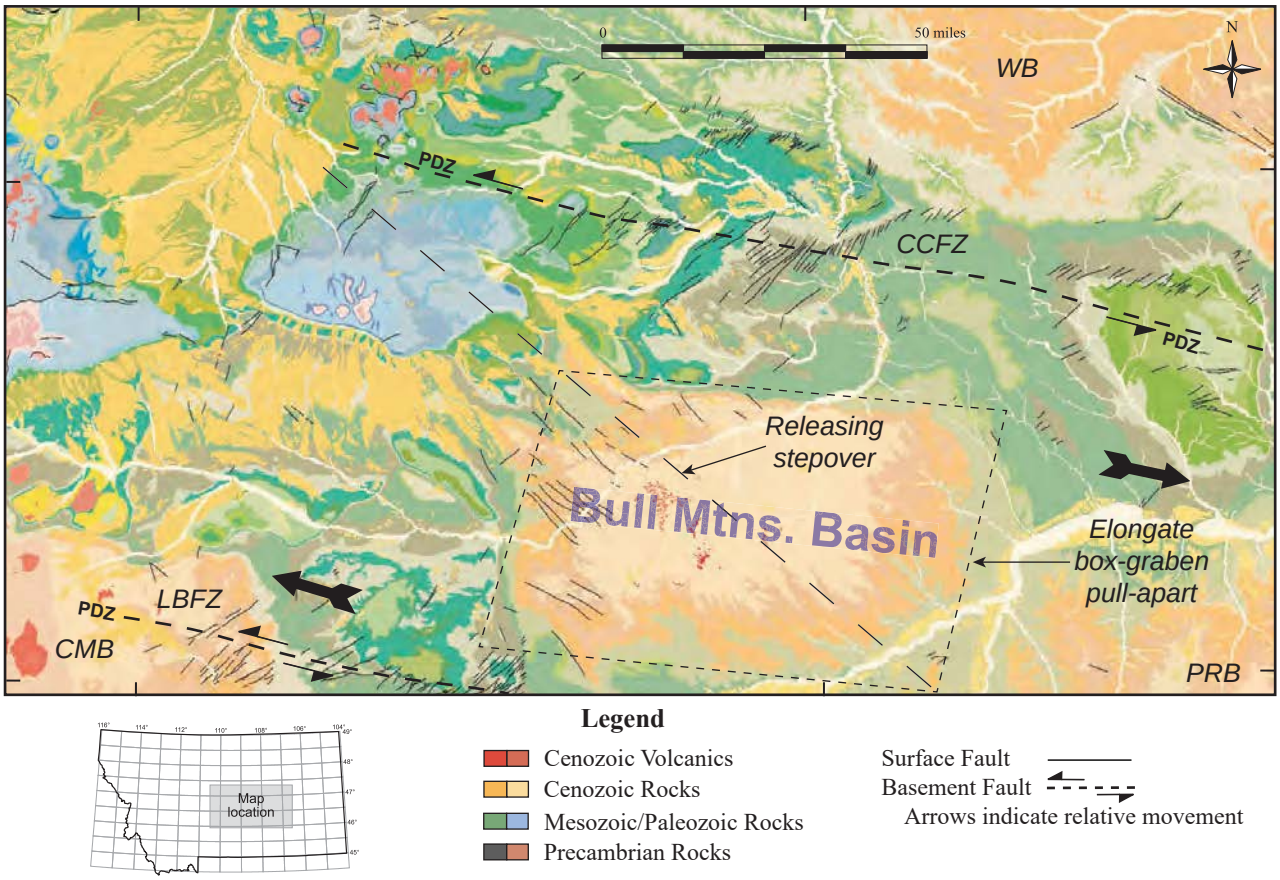

Figure 14. Sinistral 90° releasing sidestep for the Bull Mountains Basin. See Dooley and McClay (1995), their figures 2, 7, 8, and 9c for comparison. PDZ, principal displacement zone/master fault. See figure 1 for other abbreviations. Large black arrows indicate dilatation direction. Modified from Vuke and others (2007).

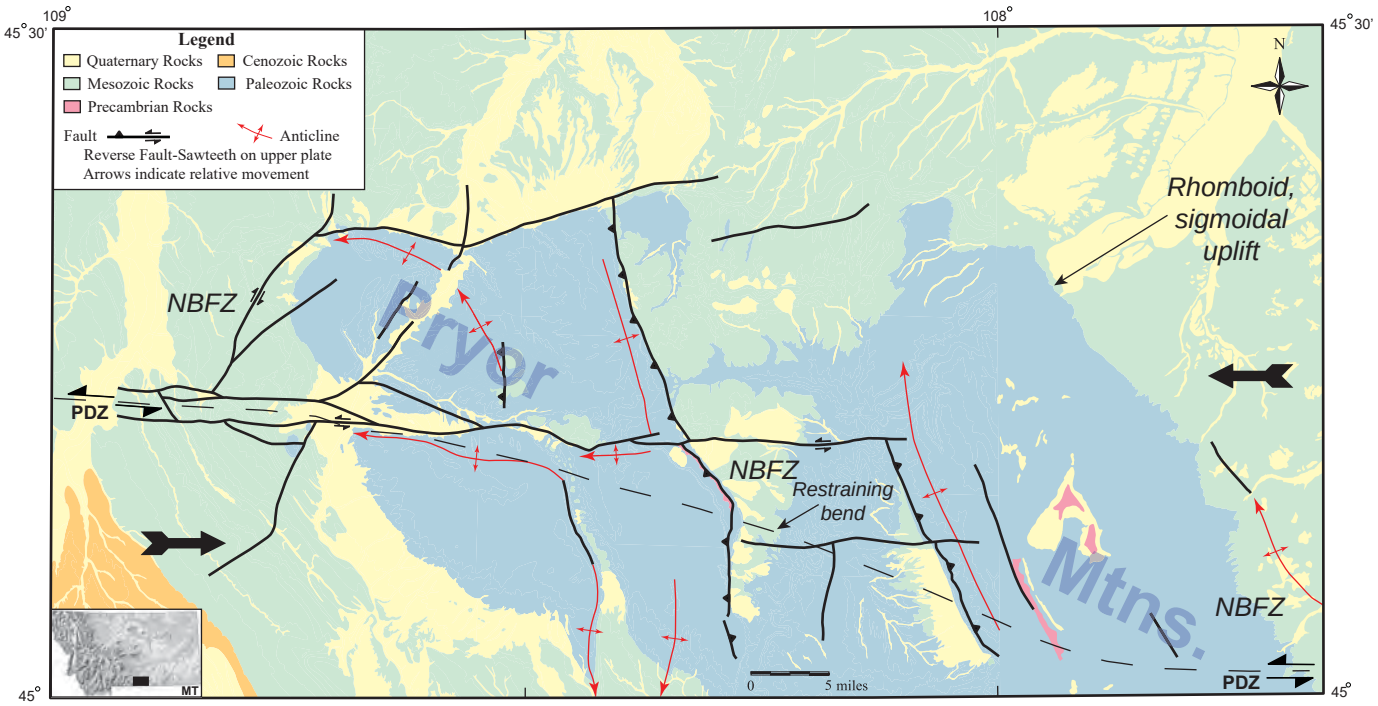

Figure 15. Sinistral ~60° restraining bend for the Pryor Mountains uplift. See McClay and Bonora (2001), their figures 3 and 5 for comparison. PDZ, principal displacement zone/master fault; NBFZ, Nye-Bowler fault zone. Large black arrows indicate contraction direction. Modified from Lopez (2000c), and Vuke and others (2000b).

and Paleoproterozoic anisotropies along active Precambrian continental margins, and how these preexisting and primary basement heterogeneities controlled subsequent deformational events in the northern Laramide belt. Finally, this work provides insight into Neoarchean terrane amalgamation and later Paleoproterozoic convergent episodes related to the development and possible final assembly of Laurentia.

ACKNOWLEDGMENTS

I would like to especially thank Steve Nordeng for early reviews and encouragement to move forward with this entire project. His moral support has been invaluable, both in regard to this topic, as well as work and life in general. I also thank Alan English, Oliver Lacombe, and an anonymous reviewer for their detailed reviews. In addition, I express appreciation to all of the geologists at the Montana Bureau of Mines and Geology, and specifically Susan Barth. This work could not have been completed without the detailed maps they provide on-line and the materials Susan provided me for Figures 14 and 15. Finally, I am indebted to the hundreds, if not thousands, of scientists that have published Laramide-related works over the last century. Every one of them had something to contribute to this project. Regardless of their interpretations, where the valuable information is often lost, their keen observations and data were precious, and "not lost for the trees." My work in this arena would not have been possible without them.

All of the people above contributed to this paper and enhanced it greatly; however, interpretations and conclusions are solely those of the author.

REFERENCES

Bader, J.W., 2008, Structural and tectonic evolution of the Cherokee Ridge arch, south-central Wyoming: Implications for recurring strike-slip along the Cheyenne Belt suture zone: Rocky Mountain Geology (The University of Wyoming), v. 43, no. 1, p. 23–40.

Bader, J.W., 2009, Structural and tectonic evolution of the Douglas Creek arch, the Douglas Creek fault zone, and environs, northwestern Colorado and northeastern Utah: Implications for petroleum accumulation in the Piceance and Uinta basins: ocky Mountain Geology (The University of Wyoming), v. 44, no. 2, p. 121–145.

Bader, J.W., 2018, Structural inheritance and the role of basement anisotropies in the Laramide structural and tectonic evolution of the North American Cordilleran foreland, Wyoming: Lithosphere, v. 11, no. 1, p. 129–148, https://doi.org/10.1130/L1022.1.

Berg, R.B., Lopez, D.A., and Lonn, J.D., 2000, Geologic map of the Livingston 30' x 60' quadrangle, south-central Montana: Montana Bureau of Mines and Geology Open-File Report 406, 21 p., 1 sheet, scale 1:100,000.

Bergantino, R.N., and Wilde, E.M., 1998a, Preliminary geologic map of the Culbertson 30' x 60' quadrangle, northeastern Montana and northwestern North Dakota: Montana Bureau of Mines and Geology Open-File Report 359, 5 p., 1 sheet, scale 1:100,000.

Bergantino, R.N., and Wilde, E.M., 1998b, Preliminary geologic map of the Wolf Point 30' x 60' quadrangle: Montana Bureau of Mines and Geology Open-File Report 358, 5 p., 1 sheet, scale 1:100,000.

Bird, P., 1978, Kinematic history of the Laramide orogeny in latitudes 35-49N, western United States: Tectonics, v. 17, no. 5, p. 780–801.

Bowen, C.F., 1914, Coal discovered in a reconnaissance survey between Musselshell and Judith, Montana: U.S. Geological Survey Bulletin 541, p. 39–47.

Brewer, J.A., Allmendinger, R.W., Brown, L.D., Oliver, J.E., and Kaufman, S., 1982, COCORP profiling across the Rocky Mountain front in southern Wyoming: Part 1. Laramide structure: Geological Society of America Bulletin, v. 93, no. 12, p. 1242–1252, doi: https://doi.org/10.1130/0016-7606(1982)93<1242:CPATRM>2.0.CO:2.

Chamberlin, R.T., 1919, A peculiar belt of oblique faulting: Journal of Geology, v. 27, no. 8, p. 602–613.

Copeland, P., Currie, C.A., Lawton, T.F., and Murphy, M.A., 2017, Location, location, location: The variable lifespan of the Laramide orogeny: Geology, v. 45, no. 3, p. 223–226.

Corrigan, D., Pehrsson, S., Wodicka, N., and de Kemp, E., 2009, The Palaeoproterozoic Trans-Hudson orogen: A prototype of modern accretionary

processes: Geological of London Special Publications, v. 327, p. 457–479.

DePaolo, D.J., and Wasserburg, G.J., 1979, Sm-Nd age of the Stillwater Complex and the mantle evolution curve for neodymium: Geochimicha et Cosmochimica Acta, v. 43, p. 999–1008.

Dobbin, C.E., and Erdmann, C.E., 1955, Structure contour map of the Montana plains: U.S. Geological Survey Oil and Gas Investigations Map OM 178-B, scale 1:1,000,000.

Dooley, T., and McClay, K., 1995, Analogue models of pull-apart basins: Geology, v. 23, no. 8, p. 711–714, doi: https://doi.org/10.1130/0091-7613(1995)0232.3.CO;2.

Erslev, E.A., and Koenig, N.B., 2009, 3D kinematics of Laramide, basement-involved Rocky Mountain deformation, U.S.A.: Insights from minor faults and GIS-enhanced structure maps, *in* Kay, S., Ramos, V., and Dickinson, W.R., eds., Backbone of the Americas: Shallow subduction, plateau uplift and ridge and terrane collision: Geological Society of America Memoir 204, p. 125–150.

Hancock, E.T., 1919, Geology and oil and gas prospects of the Lake Basin field, Montana: U.S. Geological Survey Bulletin 691-D, p. 101–147.

Hancock, E.T., 1920, Geology and oil and gas prospects of the Huntley field, Montana: U.S. Geological Survey Bulletin 711, p. 105–148.

Lacombe, O., and Bellahsen, N., 2016, Thick-skinned tectonics and basement-involved fold-thrust belts: Insights from selected Cenozoic orogens: Geological Magazine, v. 153, no. 5/6, p. 763–810.

Lopez, D.A., 2000a, Geologic map of the Big Timber 30' x 60' quadrangle, south-central Montana: Montana Bureau of Mines and Geology Open-File Report 405, 17 p., 1 sheet, scale 1:100,000.

Lopez, D.A., 2000b, Geologic map of the Billings 30' x 60' quadrangle, Montana: Montana Bureau of Mines and Geology Geologic Map 59, 1 sheet, scale 1:100,000.

Lopez, D.A., 2000c, Geologic map of the Bridger 30' x 60' quadrangle, Montana: Montana Bureau of Mines and Geology Geologic Map 58, 1 sheet, scale 1:100,000.

Lopez, D.A., 2001, Preliminary geologic map of the Red Lodge 30' x 60' quadrangle, south-central Montana: Montana Bureau of Mines and Geology Open-File Report 423, 17 p., 1 sheet.

Lopez, D.A., VanDelinder, S.W., Hendricks, M.L., Bayliss, G.S., and Ewert, W.L., 2007, The Tensleep play of south-central Montana: A part of the Permo-Pennsylvanian petroleum system of Montana and Wyoming: Montana Bureau of Mines and Geology Report of Investigation 18, 78 p.

Marshak, S., Karlstrom, K.E., and Timmons, J.M., 2000, Inversion of Proterozoic extensional faults: An explanation for the pattern of Laramide and Ancestral Rockies intracratonic deformation, United States: Geology, v. 28, no. 8, p. 735–738.

McClay, K., and Bonora, M., 2001, Analogue models of restraining stepovers in strike-slip fault systems: American Association of Petroleum Geologists Bulletin, v. 85, no. 2, p. 233–260.

McCormick, K.A., 2010, Precambrian basement terrane of South Dakota: South Dakota Geological Survey Bulletin 41, 37 p., 1 sheet, scale 1:100,000.

Mogk, D.W., Mueller, P.A., and Wooden, J.A., 1988, Archean tectonics of the North Snowy Block, Beartooth Mountains, Montana: Journal of Geology, v. 96, no. 2, p. 125–141.

Mueller, P.A., Burger, H.R., Wooden, J.L., Brady, J.B., Cheney, J.T., Harms, T.A., Heatherington, A.L., and Mogk, D.W., 2005, Paleoproterozoic metamorphism in the northern Wyoming Province: Implications for the assembly of Laurentia: Journal of Geology, v. 113, no. 2, p. 169–179.

Nelson, W.J., 1993, Structural geology of the Cat Creek anticline and related features, central Montana: Montana Bureau of Mines and Geology Memoir 64, 44 p., 4 plates.

Norwood, E.E., 1965, Geological history of central and south-central Montana: American Association of Petroleum Geologists Bulletin, v. 49, no. 11, p. 1824–1832.

Nunes, P.D., 1981, The age of the Stillwater Complex: A comparison of U-Pb zircon and Sm-Nd isochron systematics: Geochimica et Cosmochimica Acta, v. 45, p. 1961–1963.

Porter, K.W., and Wilde, E.M., 1993, Geologic map of the Winnett 30' x 60' quadrangle, central Montana: Montana Bureau of Mines and Geol-

ogy Open-File Report 307, 16 p., 2 sheets, scale 1:100,000.

Porter, K.W., and Wilde, E.M, 1999, Geologic map of the Musselshell 30' x 60' quadrangle, central Montana: Montana Bureau of Mines and Geology Open-File Report 386, 22 p., 1 sheet, scale 1:100,000.

Premo, W.R., Helz, R.T., Zientek, M.L., and Langston, R.B., 1990, U-Pb and Sm-Nd ages for the Stillwater Complex and its associated dikes and sills, Beartooth Mountains, Montana: Identification of a parent magma: Geology, v. 18, p. 1065–1068.

Reeves, F., 1927, Geology of the Cat Creek and Devils Basin oil fields and adjacent areas in Montana: U.S. Geological Survey Bulletin 786, p. 39–98.

Reeves, F., 1930, Geology of the Big Snowy Mountains, Montana: U.S. Geological Survey Professional Paper 165-D, p. 135–149.

Reid, R.R., McMannis, W.J., and Palmquist, J.C., 1975, Precambrian geology of the North Snowy block, Beartooth Mountains Montana: Geological Society of America Special Paper 157, 135 p.

Robinson, L.N., and Barnum, B.E., 1986, Southeastern extension of the Lake Basin fault zone in south-central Montana: Implications for coal and hydrocarbon exploration: The Mountain Geologist, v. 23, no. 2, p. 37–44.

Saleeby, J., 2003, Segmentation of the Laramide slab—Evidence from the southern Sierra Nevada region: Geological Society of America Bulletin, v. 115, no. 6, p. 665–668.

Sims, P.K, 2009, The Trans–Rocky Mountain Fault System—A fundamental Precambrian strike-slip system: U.S. Geological Survey Circular 1334, 13 p.

Sylvester, A.G., 1988, Strike-slip faults: Geological Society of America Bulletin, v. 100, no. 11, p. 1666–1703, doi: https://doi.org/10.1130/0016-7606(1988)1002.3.CO;2.

Thomas, G.E., 1974, Lineament block tectonics: Williston-Blood Creek Basin: American Association of Petroleum Geologists Bulletin, v. 58, no. 7, p. 1305–1322.

Turner, A.R., Wolfgram, D., and Barnes, S.J., 1985, Geology of the Stillwater County sector of the J-M reef, including the Minneapolis adit, *in* Czamanske, G.K., and Zientek, M.L., eds., Stillwater Complex: Montana Bureau of Mines and Geology, Special Publication 92, p. 210–230.

U.S. Geological Survey (USGS), 2019, Montana isostatic gravity anomaly map: https://pubs.usgs.gov/of/1998/ofr-98-0333/mt_iso.html [Accessed May 2019].

Van Gosen, B.S. (compiler), Elliott, J.E., LaRock, E.J., Du Bray, E.A., Carlson, R.R., and Zientek, M.L., 2000, Generalized geologic map of the Absaroka-Beartooth study area, south-central Montana: U.S. Geological Survey Miscellaneous Field Studies Map 2338, scale 1:250,000.

Vuke, S.M., and Wilde, E.M., 2004, Geologic map of the Melstone 30' x 60' quadrangle, eastern Montana: Montana Bureau of Mines and Geology Open-File Report 513, 12 p., 1 sheet, scale 1:100,000.

Vuke, S.M., Porter, K.W., Lonn, J.D., and Lopez, D.A., 2007, Geologic Map of Montana: Montana Bureau of Mines and Geology Geologic Map 62-A, 73 p., 2 sheets, scale 1:500,000.

Vuke, S.M., Wilde, E.M., and Bergantino, R.N., 2000a, Geologic map of the Hardin 30' x 60' quadrangle, Montana: Montana Bureau of Mines and Geology Geologic Map 57, 1 sheet, scale 1:100,000.

Vuke, S.M., Wilde, E.M., and Bergantino, R.N., 2003a, Geologic map of the Angela 30' x 60' quadrangle, eastern Montana: Montana Bureau of Mines and Geology Open-File Report 485, 10 p., 1 sheet, scale 1:100,000.

Vuke, S.M., Wilde, E.M., and Bergantino, R.N., 2003b, Geologic map of the Hysham 30' x 60' quadrangle, eastern Montana: Montana Bureau of Mines and Geology Open-File Report 486, 10 p., 1 sheet, scale 1:100,000.

Vuke, S.M., Wilde, E.M., Lopez, D.A., and Bergantino, R.N., 2000b, Geologic map of the Lodge Grass 30' x 60' quadrangle, Montana: Montana Bureau of Mines and Geology Geologic Map 56, 1 sheet, scale 1:100,000.

Vuke, S.M., Heffern, E.L., Bergantino, R.N., and Colton, R.B., 2001a, Geologic map of the Birney 30' x 60' quadrangle, eastern Montana: Montana Bureau of Mines and Geology Open-File Report 431, 12 p., 1 sheet, scale 1:100,000.

Vuke, S.M., Heffern, E.L., Bergantino, R.N., and Colton, R.B., 2001b, Geologic map of the Lame Deer 30' x 60' quadrangle, eastern Montana: Montana Bureau of Mines and Geology Open-File Report 428, 8 p., 1 sheet, scale 1:100,000.

Weil, A.B., and Yonkee, W.A., 2012, Layer parallel shortening across the Sevier fold-thrust belt and Laramide foreland of Wyoming: Spatial and temporal evolution of a complex geodynamic system: Earth and Planetary Science Letters, v. 357–358, p. 405–420.

Weil, A.B., Yonkee, W.A., and Schultz, M., 2016, Tectonic evolution of a Laramide transverse structural zone: Sweetwater arch, south central Wyoming: Tectonics, v. 35, no. 5, p. 1090–1120, doi: https://doi.org/10.1002/2016TC004122.

Whitmeyer, S.J., and Karlstrom, K.E., 2007, Tectonic model for the Proterozoic growth of North America: Geosphere, v. 3, no. 4, p. 220–259, doi: https://doi.org/10.1130/GES00055.1.

Wilcox, R.E., Harding, T.P., and Seely, D.R., 1973, Basic wrench tectonics: American Association of Petroleum Geologists Bulletin, v. 57, no. 1, p. 74–96.

Wilde, E.M., and Porter, K.W., 2000, Geologic map of the Roundup 30' x 60' quadrangle, central Montana: Montana Bureau of Mines and Geology Open-File Report 404, 14 p., 1 sheet, scale 1:100,000.

Wilde, E.M., and Porter, K.W., 2001, Geologic map of the Harlowton 30' x 60' quadrangle, central Montana: Montana Bureau of Mines and Geology Open-File Report 434, 20 p., 1 sheet, scale 1:100,000.

Wilde, E.M., and Smith, L.N., 2003, Geologic and structure contour map of the Richey 30' x 60' quadrangle, eastern Montana: Montana Bureau of Mines and Geology Open-File Report 475, 9 p., 1 sheet, scale 1:100,000.

Wilde, E.M., and Vuke, S.M., 2004a, Geologic map of the Jordan 30' x 60' quadrangle, eastern Montana: Montana Bureau of Mines and Geology Open-File Report 514, 8 p., 1 sheet, scale 1:100,000.

Wilde, E.M., and Vuke, S.M., 2004b, Geologic map of the Sand Springs 30' x 60' quadrangle, eastern Montana: Montana Bureau of Mines and Geology Open-File Report 515, 8 p., 1 sheet, scale 1:100,000.

Wilson, C.W., Jr., 1936, Geology of the Nye–Bowler lineament, Stillwater and Carbon Counties, Montana: American Association of Petroleum Geologists Bulletin, v. 20, no. 9, p. 1161–1188.

Wright, N.M., Seton, M., Williams, S.E., and Muller, R.D., 2016, The Late Cretaceous to recent tectonic history of the Pacific Ocean basin: Earth-Science Reviews, v. 154, p. 138–173.

Yonkee, W.A., and Weil, A.B., 2015, Tectonic evolution of the Sevier and Laramide belts within the North American Cordillera orogenic system: Earth Science Reviews, v. 150, p. 531–593.

DEPOSITIONAL ENVIRONMENT OF *HORODYSKIA* ('STRING OF BEADS') FROM THE EARLY MESOPROTEROZOIC GREYSON AND SPOKANE FORMATIONS OF THE BELT SUPERGROUP, NEAR HELENA, MONTANA, U.S.A.

Ray H. Breuninger

Consulting Geologist, Helena, Montana

ABSTRACT

Horodyskia 'strings of beads' were collected at seven Helena-area localities across the marine-to-nonmarine transition from the upper Greyson to lower Spokane formations (1.4–1.5 GA), in the Belt Supergroup. The collections expand *Horodyskia*'s geographic range in Montana from Glacier National Park south 250 km to the northern Big Belt Mountains and the North Hills near Helena.

Horodyskia williamsii is locally abundant, while the larger-beaded *H. moniliformis* is rare. *Horodyskia* beads are preserved as molds, or as flattened biconvex lens shapes, usually infilled with argillaceous silt or clay. No bead wall or interior structures are preserved. Shallow depressions, probably scoured out by currents, ring many beads; they are evidence that the beads were well-attached to the sediment substrate. The absence of clear-cut examples of strings crossing one another suggests that during life *Horodyskia* lay prostrate on the substrate. Sedimentary structures indicate that in quiet water, strings grew in random orientations, or developed arcuate, branching, and crude net patterns. Where strings lie subparallel to one another, it is possible that growth was parallel to currents.

Horodyskia is found in very shallow marine Greyson siltstone beds, which cyclically interfinger with and grade upward into subaerial, desiccation-cracked Spokane redbeds. Measured sections document seven transgressive–regressive cycles. *Horodyskia* strings grew along the west side of a sand-flat and beach complex, flourishing along a low-relief, muddy to fine-grained sandy shore out onto a shallow, silt-dominated marine shelf. Tides were negligible; waves and currents from minor storms brought in and deposited suspended mud and very fine-grained sand; infrequent major storms left distinctive laminated to thin-bedded silt beds with hummocky cross-stratification. Farther west and farther from a source of sand, *Horodyskia* was absent in tracts of microlaminated, mostly calcareous muds.

INTRODUCTION AND PREVIOUS WORK

Horodyskia, informally termed 'string of beads,' occurs as discoidal bodies arranged in uniserial chains resembling strings of beads, as in a necklace. The biologic origin of *Horodyskia* is accepted by most but not all reseachers.

Horodyski (1982) described 'Strings of Beads' near the base of the Mesoproterozoic Appekunny Formation (1.4–1.5 Ga) of Glacier National Park, Montana (fig. 1). The specimens were in shallow marine argillaceous siltstone and fine-grained sandstone beds, which are similar to the string-bearing beads near Helena. The Appekunny probably correlates lithostratigraphically with the Greyson (Slotznick and others,

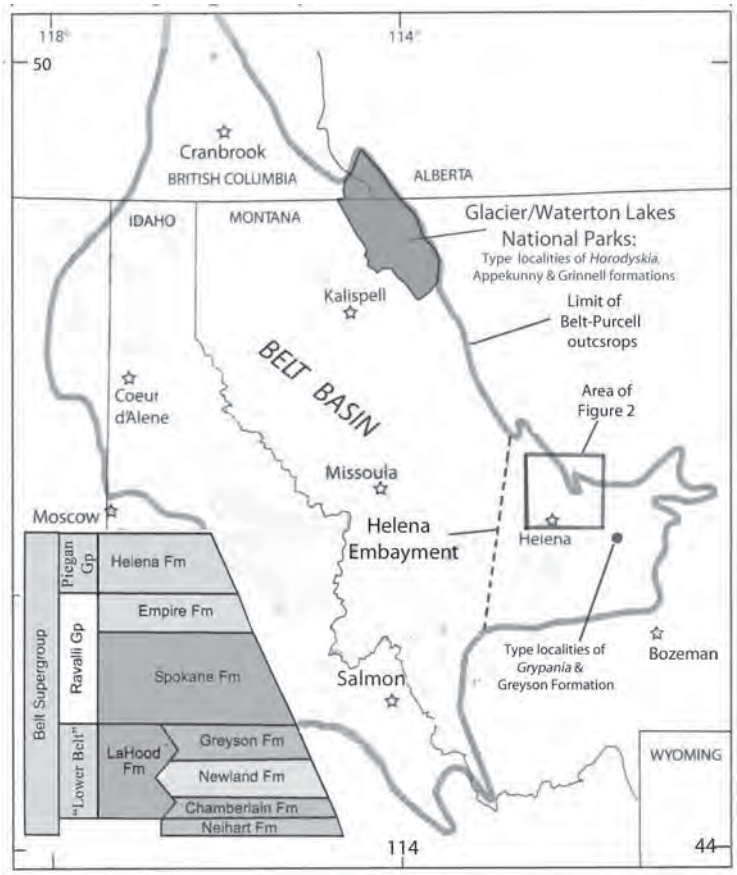

Figure 1. Regional map showing the extent of the Belt Supergroup outcrops and the location of the Helena study area. Stratigraphic column shows Belt Supergroup formations in the Helena Embayment. Modified from figure 1 of Burmester and others (2013).

2015), and together they are the uppermost formations of the lower Belt Supergroup. Skeptical of their organic origin, Horodyski presented them as "problematic bedding-plane markings." After sectioning new specimens, Horodyski (1989) modified his view slightly, suggesting the strings were "...best regarded as dubiofossils." Working with Appekunny specimens, Yochelson and Fedonkin (2000) suggested the strings were the oldest tissue-grade colonial eukaryote. Fedonkin and Yochelson (2002) established the new genus and species, *Horodyskia moniliformis*.

Grey and Williams (1990) found Middle Proterozoic bedding-plane markings in the Manganese Group, Bangemall Supergroup of Western Australia. They compared the markings with biologic and inorganic structures, concluding that evidence favored a biogenic origin. Using Australian specimens, Grey and others (2001) expanded the evidence for biogenicity, and described (Grey and others, 2010) a new species, *H. williamsii*, distinguished from *H. moniliformis* by its smaller diameter (beads typically 1 to 3 mm in diameter), with a central node in each bead. Martin (2004) interpreted the depositional environment and taphonomy of *Horodyskia* in the Bangemall Supergroup of Western Australia. Calver and others (2010) described *H. williamsii* from the Balfour Subgroup of northwest Tasmania. Halpin and others (2014) reported detrital zircon and authigenic monazite ages constraining the lower and middle units of the Proterozoic Rocky Cape Group of Tasmania to about 1450 Ma and 1330 Ma. This includes *Horodyskia*-bearing beds in the Balfour Subgroup.

Gonzalez-Alvarez and others (2003) described questionably organic bedding marks throughout the Belt Supergroup in Glacier National Park, identical to *Horodyskia* moniliformis. The marks were clay-filled, lenticular beads arranged randomly, as well as in (unfigured) strings and regular nets. Retallack and others (2013) collected new specimens of *Horodyskia* from the Appekunny in Glacier National Park, and reexamined specimens in the park's museum. They found evidence for tubes within beads, tubes between beads, and tubes extending from beads into the sediment below. Rule (2012, 2014) described *Horodyskia* from Glacier National Park, noting that many specimens with strings also have many isolated beads, and that strings frequently lie on or in microbial mats and related microbial structures. Rule (2014) proposed that beads are inorganic, aggregated, or flocculated clumps of clay, some of which are aligned into strings with the assistance of microbial mats.

Mathur and Srivastava (2004) described *Horodyskia* in an Ediacaran siltstone-shale sequence in the Kauriyala Formation of the Krol Group, Garwhal Syncline, Lesser Himalaya, Uttaranchal, India. Dong and others (2008) described chains of small silicified beads in the Ediacaran of China, and erected a third species, *H. minor.* Serial cross sections suggested that thin filaments connect spherical beads. The Ediacaran age of Indian and Chinese specimens and the Mesoproterozoic age of Montana and Australian specimens imply a range exceeding 800 My for *Horodyskia*.

GEOLOGICAL SETTING

Belt Basin

Sears (2007a) interpreted the Belt Basin (fig. 1) as a Mesoproterozoic intracratonic rift (fig. 3 of Sears, 2007b). Ross and Villeneuve (2003) suggest that most clastic sediments of Ravalli and Piegan groups (which include *Horodyskia*-bearing Greyson and Spokane formations near Helena) were probably derived from a non-American, western source. Feldspathic quartz sandstones served as key beds for local correlations near Helena; the sandstones are also abundant in the Appekunny Formation of Glacier National Park, and were probably sourced from the Laurentian craton, now east of the Belt Basin (Smith, 1963; Barnes, 1963; Kuhn, 1987; Bloomfield, 1983).

Winston (1986a,b) proposed that Belt rocks were deposited on a basin-wide megafan, dominated by sheetflood transport of sediment from a western source to an intermittent interior lake complex. Winston's lacustrine model could very well be correct for portions of the Piegan Group and Helena Formation (fig. 1). However, the subaqueous strata of the Greyson and Appekunny formations are more likely marine than lacustrine.

Adam and others (2017) described the eukaryote Tapannia microfossil assemblage from the middle of the Greyson Formation in the Helena Embayment, and briefly reviewed age constraints on the Greyson. It is older than a 1454 ± 9 Ma bentonite from the Helena Formation, and approximately the same age as sills dated 1470–1460 Ma from the Lower Belt (Prichard Formation) in western Montana. The Prichard correlates with the lower Belt of the Helena Embayment.

They pointed out that the Tappania assemblage zone has worldwide distribution, as do the macrofossils *Horodyskia* (Fedonkin and Yochelson, 2002) from the lower Appekunny of Glacier National Park and Grypania (Walter and others, 1976) from the lower Greyson in the Helena Embayment (fig. 2). This is strong evidence that the Belt Basin was connected to the world ocean during deposition of the Greyson and Appekunny formations.

The new Helena localities of *Horodyskia* are in the northwest part of the Helena Embayment (figs. 1, 2), which is a southeast extension of the Belt Basin. Mueller and others (2016) briefly review the origin, age, tectonics, and stratigraphy of the lower Belt in and near the Helena Embayment. The floor of the embayment was faulted downward along the south and north sides of the Helena Embayment. An Archaean igneous–metamorphic terrain was uplifted to the south, and shed coarse-grained clastics (LaHood Formation) to the north into the embayment, where they interfingered with mostly fine-grained, basinal clastics and carbonates of the lower Belt.

Greyson and Spokane Formations

The Greyson, along with the Appekunny (its lateral equivalent in Glacier National Park), are the uppermost formations in the lower Belt (figs. 1, 2; see also fig. 1 of Winston, 2016). Shelf-to-basin deposits of the lower and middle Greyson are unoxidized and mostly medium to dark gray in color. These pass up into shallow, fine-grained shelf deposits of the upper Greyson. The upper 200 m of the Greyson consists of argillaceous siltstone and mudstone, often with a greenish-gray color, and sandstone, along with thin, nonmarine interbeds and carbonate-bearing intervals.

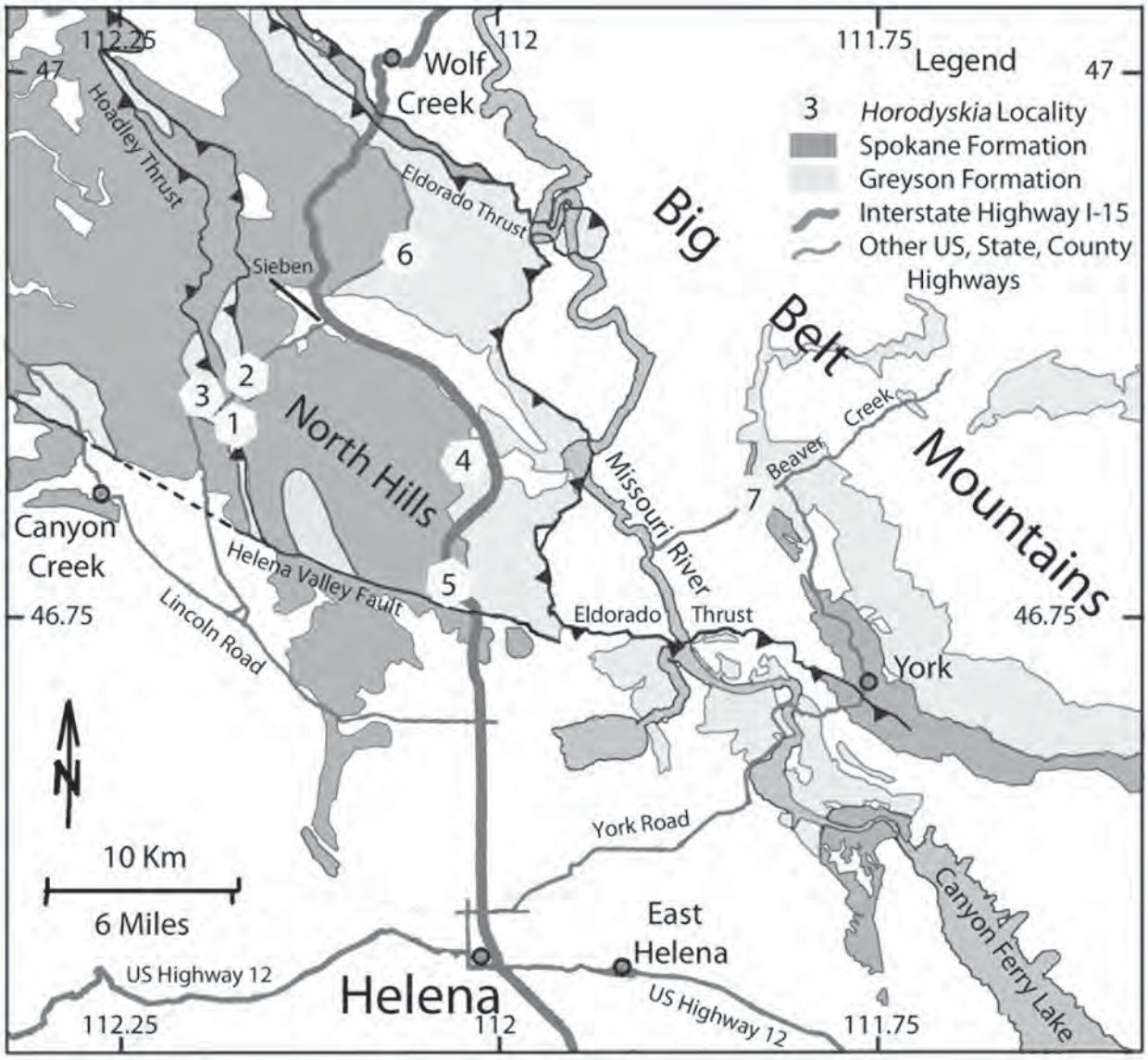

Figure 2. Geologic map showing the seven *Horodyskia* localities north of Helena, Montana. Base map is modified from Vuke and others (2007). All localities are along the Greyson–Spokane contact.

However, thick shale and silty shale intervals are uncommon in the upper Greyson. In the study area north of Helena (including *Horodyskia* locations 1 to 6), the Greyson is about 1,700+ m thick (Bregman, 1981). The Eldorado thrust fault cuts off the basal beds of the Greyson. In the northern Big Belt Mountains (including *Horodyskia* Location 7), Reynolds and Brandt (2005) estimated the Greyson as about 1,550 m thick.

The Spokane (figs. 1, 2), along with its Glacier National Park equivalent, the Grinnell, are the lowest formations in the Ravalli Group, which overlies the lower Belt. Beds in the lower 150 m of the Spokane are mostly purplish maroon, nonmarine clastics (mudstone and siltstone), and feldspathic quartz sandstone, with many ripples, desiccation cracks, and rip-up clasts. To the north of Helena, the Spokane is about 1,830+ m thick (Bregman, 1981). In the Big Belt Mountains, the Spokane ranges from 0 to 1,480 m thick (Reynolds and Brandt, 2005); post-Belt erosion truncates the uppper part.

NEW *HORODYSKIA* LOCALITIES NORTH OF HELENA, MONTANA

Horodyskia was found at seven localities near Helena, Lewis and Clark County, Montana (fig. 1), in the upper Greyson Formation and lower Spokane Formation. Specimens were collected mostly from float.

Locality 1: Tributary Gulch of Little Prickly Pear Creek. Well-preserved *Horodyskia williamsii* is in talus and a cliffy west-dipping outcrop near the top of a 22-m measured section. The site is southeast up an unnamed gulch branching from the canyon of Little Prickly Pear Creek. The area has both private and public land.

Locality 2: Little Prickly Pear Creek Canyon North of Little Sheep Creek. Cliffs of west-dipping upper Greyson and lower Spokane lie on private land west of Little Prickly Pear Creek, north of its confluence with Little Sheep Creek. A well-exposed section 90 m long was measured.

Locality 3: Little Prickly Pear Creek Canyon at Little Sheep Creek. *Horodyskia williamsii* and uncommon *H. moniliformis* are in cliffs and talus of west-dipping upper Greyson, on private and public land just south of the mouth of Little Sheep Creek. A 175-m section was measured up to the base of Spokane redbeds; offsets were made across several normal faults.

Locality 4: Rattlesnake Mountain, Northeast Ridge. A 102-m measured section follows the northeast ridge of the mountain, in west-dipping, *Horodyskia*-bearing Greyson and Spokane outcrops on private land. A microwave tower tops the summit. A second section, 190 m long, runs along the gulch northeast of the mountain. Poorly exposed normal faults complicate the stratigraphic interpretation. A graded private road gives access.

Locality 5: North Hills Summit. Strings of beads were collected in place and as float from the northwest-dipping, lowest marine unit in the Spokane Formation. The site is in a roadcut along Interstate Highway 15 (I-15) north of Helena. The site has both *H. moniliformis* (rare) and *H. williamsii.*

Locality 6: Ridge Crest between Heads of Rose and Levings Gulches. This remote site is in a thin marine tongue of the lower Spokane, on public land north of the Hilger valley. Access is by the steep Wood Siding Road, which may be closed by the Bureau of Land Management for game management at times. A 5.8-m section was measured.

Locality 7: Beaver Creek, Big Belt Mountains. A single specimen with three *Horodyskia* strings was collected from float from west-dipping beds of the upper Greyson 1.4 km west of Hunter's Gulch, near the mouth of a small gulch entering Beaver Creek Canyon. A 225-m section was measured from that gulch west to the Spokane (redbeds) contact. Bloomfield (1983) measured a shorter (120 m) section, mostly along and close to the county road. The two sections are in close agreement. Spectacular exposures of Laramide (about 74 to 59 Ma) thrust faults and folds are displayed along Beaver Creek.

DESCRIPTION OF HELENA AREA *HORODYSKIA*

Beads are circular to oval or somewhat irregular in top view, and lenticular in vertical cross section. Beads range from 0.6 to 6.3 mm in diameter, with most from 0.8 to 1.7 mm and 2.0 to 3.2 mm. The break in bead size between 1.7 and 2.0 mm may be a statistical artifact. Bead diameters and distance between adjacent beads remain about the same along the entire length of a string.

According to Grey and others (2010), *H. williamsii* is characterized by bead diameters typically less than

3.0 mm, and the common presence of small 'nodes' or 'dimples.' See their illustration of the paratype of *H. williamsii* (Grey and others, 2010; fig. 3). Helena-area strings with beads from 0.8 to 3.2 mm are considered *H. williamsii*, on the basis of bead diameter and common dimples (figs. 3, 4). Strings with large beads (diameters in the range of 3.3 to 6.3 mm) were found in three specimens, two at Locality 3 and one at Locality 5. Following Grey and others (2010), these specimens are assigned to *Horodyskia moniliformis*, on the basis of large bead diameter and absence of central dimples (fig. 5).

Most *Horodyskia* beads are preserved as three-dimensional, biconvex, lens-shaped bodies. Before burial and compaction, the beads may have been spherical or lenticular. Beads are also preserved as positive and negative molds. No bead wall structures are preserved. No filaments or tubes were observed connecting adjacent beads. The beads are typically filled with silt (as in fig. 5), clayey silt, or clay of the same or finer size grade as the adjoining rock matrix. Beads may be ringed with dark halos, and halos may join to form irregularly bounded dark ribbons (fig. 3).

Many strings lie in random or near random orientation on flat, slightly rippled, or wavy to mounded siltstone bedding surfaces (figs. 3–5). Microbial mat wrinkle structures are sometimes found with these strings, as is unidirectional ripple cross-lamination in the underlying bed. These strings typically developed complex arcuate, often branching and net-like patterns (figs. 3, 4). Compare with figure 2c of Grey and others (2001), and with the complexly sinuous, very weakly oriented strings in plate 1, image 3a of Horodyski (1982).

A second common group of strings is found in siltstone and sandy siltstones; these strings show strong sub-parallel orientation to one another (fig. 6). Beds with this group of strings are commonly less argillaceous and less thinly laminated than those containing randomly oriented strings. Beds with these strings may interbed with nonmarine deposits containing desiccation mud cracks or salt casts. For example, on Rattlesnake Mountain (Locality 4, visible in fig. 10), subparallel *Horodyskia* strings at 37 m and 39 m are in thin marine beds sandwiched with non-marine beds.

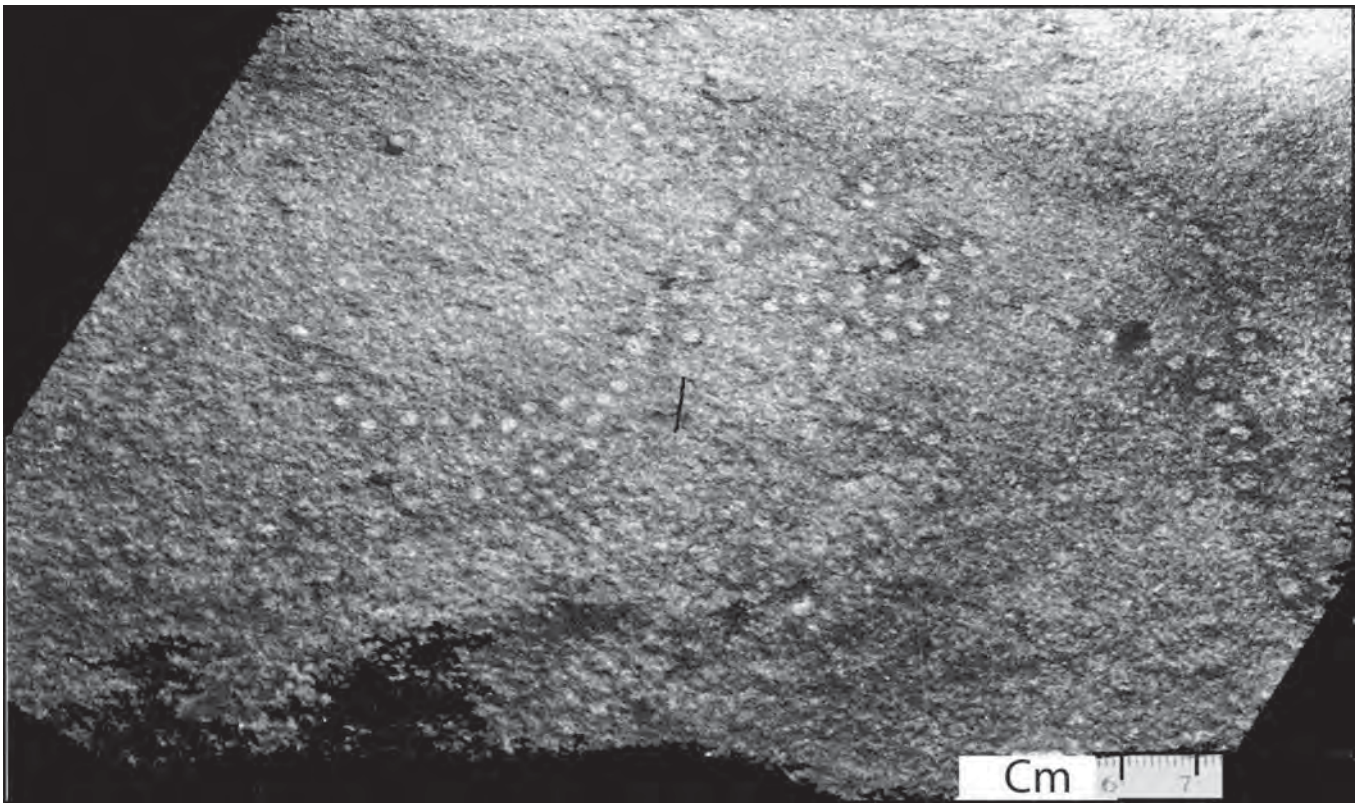

Figure 3. Sinuous to arcuate strings of *H. williamsii* on gently rippled siltstone, Locality 1, Cycle 1. The strings spray out from common points, or lead away from a tangle of tight bead loops or bead clusters. With some imagination, a crude, open net pattern extends over the bedding surface. Dark halos ring each bead, with halos joining to form an irregularly-bounded dark ribbon in which the beads are centered.

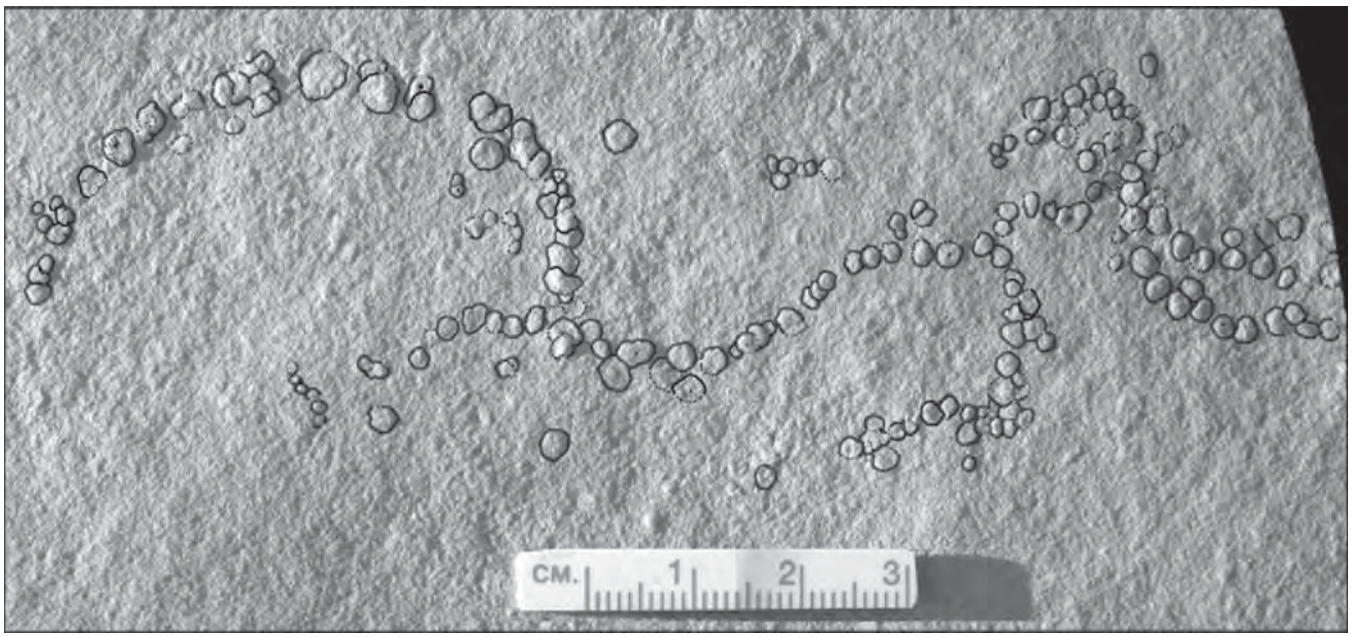

Figure 4. Arcing strings of beads of *H. williamsii* and possibly a few large beads of *H. moniliformis* on a flat bedding plane of thinly laminated siltstone, Locality 1, Cycle 1. Lighting is from the left, and black ink traces the beads. Strings radiate from several centers; they may also branch. Also, there are many isolated beads, some partly concealed beneath beads of the obvious strings. Some adjacent beads overlap within a single string. Many isolated beads are not traced, with more problematic beads visible under magnification.

Figure 5. Horodyskia moniliformis on top (left) and bottom (right) of a split piece of argillaceous, thinly laminated siltstone from Locality 5, Cycle 6. Lighting is from the upper right. On the left, a ring-shaped depression surrounds each bead; on the right, shadowing brings out in relief some of the silty, fine-grained sand that filled the ring depressions. The rings are interpreted as scours. In the right image, most rings are wider to the upper right and lower left, suggesting back-and-forth wave oscillations.

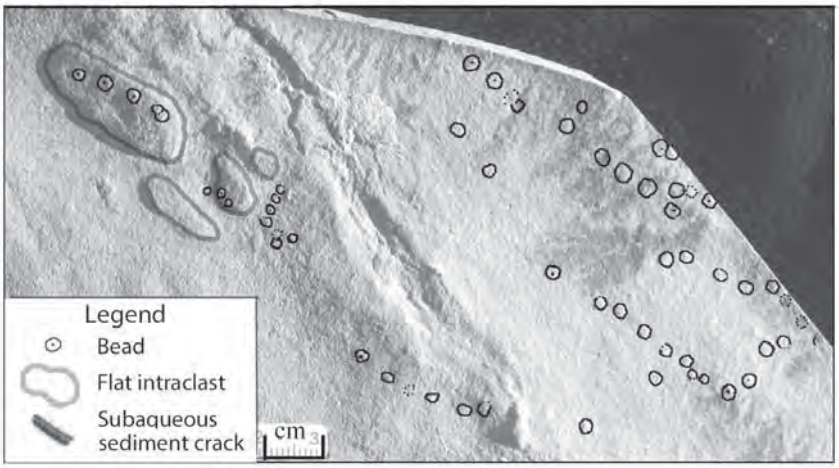

Figure 6. Tracing on photograph showing sub-parallel *H. williamsii*, in association with thin, oval siltstone intraclasts and a subaqueous shrinkage crack, on laminated argillaceous siltsones at Locality 5, Cycle 6.

STRATIGRAPHY AND SEDIMENTOLOGY OF *HORODYSKIA*-BEARING BEDS NEAR HELENA

Shallow marine beds of the uppermost Greyson interfinger with the lowermost mostly nonmarine redbeds of the Spokane. In a 135-m-thick *Horodyskia*-bearing interval, seven mini-regressions and transgressions were studied. They are designated informally as cycles 1 through 7. Several more unnumbered cycles, including one at Locality 6, are higher in the Spokane Formation; in total, *Horodyskia* occurs in a stratigraphic packet about 230 m thick across the Greyson–Spokane boundary. The cycles document a north-to-south (present-day coordinates) prograding shoreline. *Horodyskia* occurs in at least five of the marine intertongues.

Horodyskia is limited to siltstone beds, often shaley or sandy (fine-grained). The siltstone beds are usually flaggy-weathering, microlaminated to thinly bedded, and greenish-gray to medium-light gray. Laminae are planar to gently wavy or with low hummocks. Unidirectional ripples, microbial mat structures, subaqueous shrinkage cracks (fig. 6), and oscillation ripples are locally common. At one site (Location 3, fig. 7), strings-of-beads lie on the sloping side of a siliciclastic dome. Deep scour structures and large-scale cross-statification are absent. Table 1 tabulates the rich array of sedimentary structures found with *Horodyskia*.

Representative segments of measured sections are presented in figs. 8 and 10, with *Horodyskia* beds

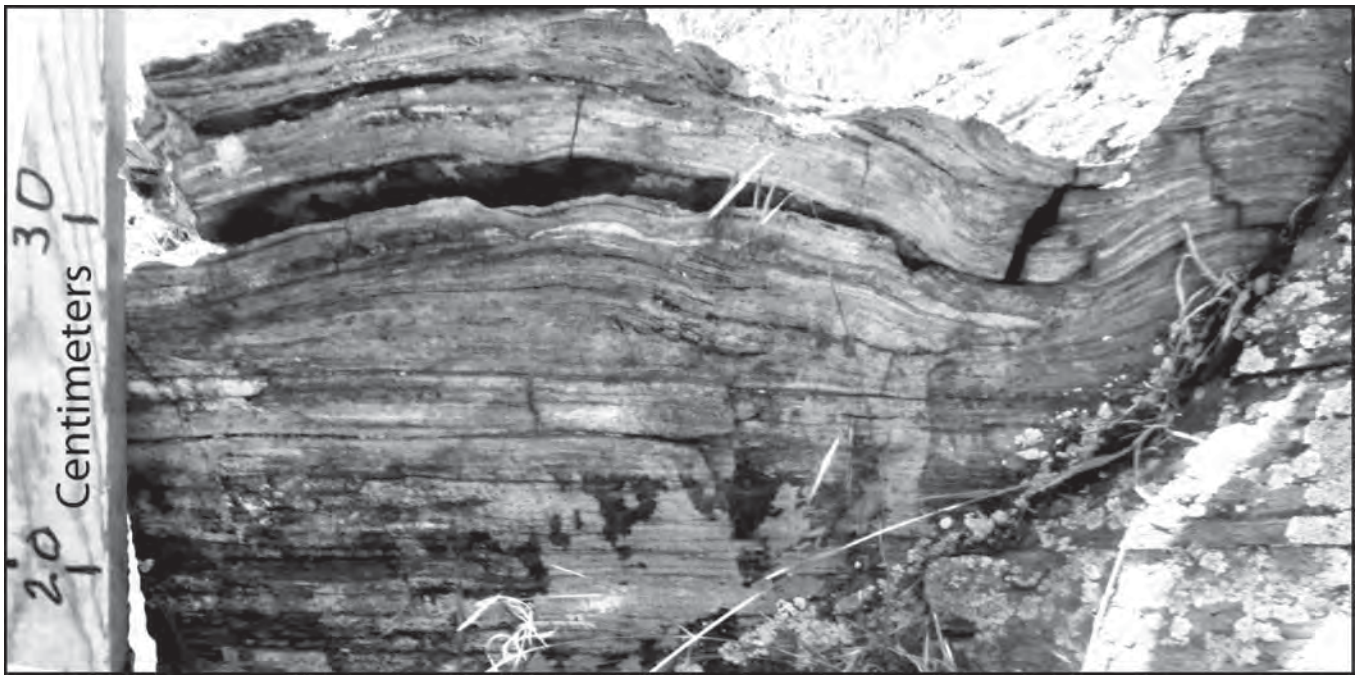

Figure 7. Outcrop photo of vertical section of a siliciclastic dome, and to the right, part of a second dome, in Cycle 2, Locality 2, 15.2–15.4 m in measured section. The domes are thinly laminated siltite, underlain by a unit of planar microlaminated siltite. A shallow channel, 2 to 5 cm deep, separates the domes, and is filled with laminated siltite and granule-sized siltite intraclasts. *H. williamsii* strings, not shown in the photo, lie on lamination planes on the back side of the main dome.

Table 1. Sedimentary structures directly associated with *Horodyskia*.

Laminae, flat	X-laminae, small-scale	Laminae, wavy, low amplitude	Sediment cracks, subaqueous	Microbial mats	Ripple marks, oscillation	'Ribbon' (film) along string	Hummocks & swales, low	Other*
13	8	7	7	5	4	2	2	--

*Other: Structures found with *Horodyskia* but not listed in table—siliciclastic dome (fig. 7); large, flat mud clasts (fig. 6). Structures with dubious association to beads—bead identification is questionable: desiccation mud cracks (2); rip-up clasts (mud chips) (1); calcite microspar intraclasts, probably mostly molar-tooth fragments (1); salt casts (1); carbonate-cored blebs (1).

Note. The observations were made of 27 representative specimens, collected at each stratigraphic horizon containing strings of beads, at Localities 1, 3, 4, and 6. A few of the specimens were collected from outcrops, but most were float found on slopes below but within several meters of the string source beds.

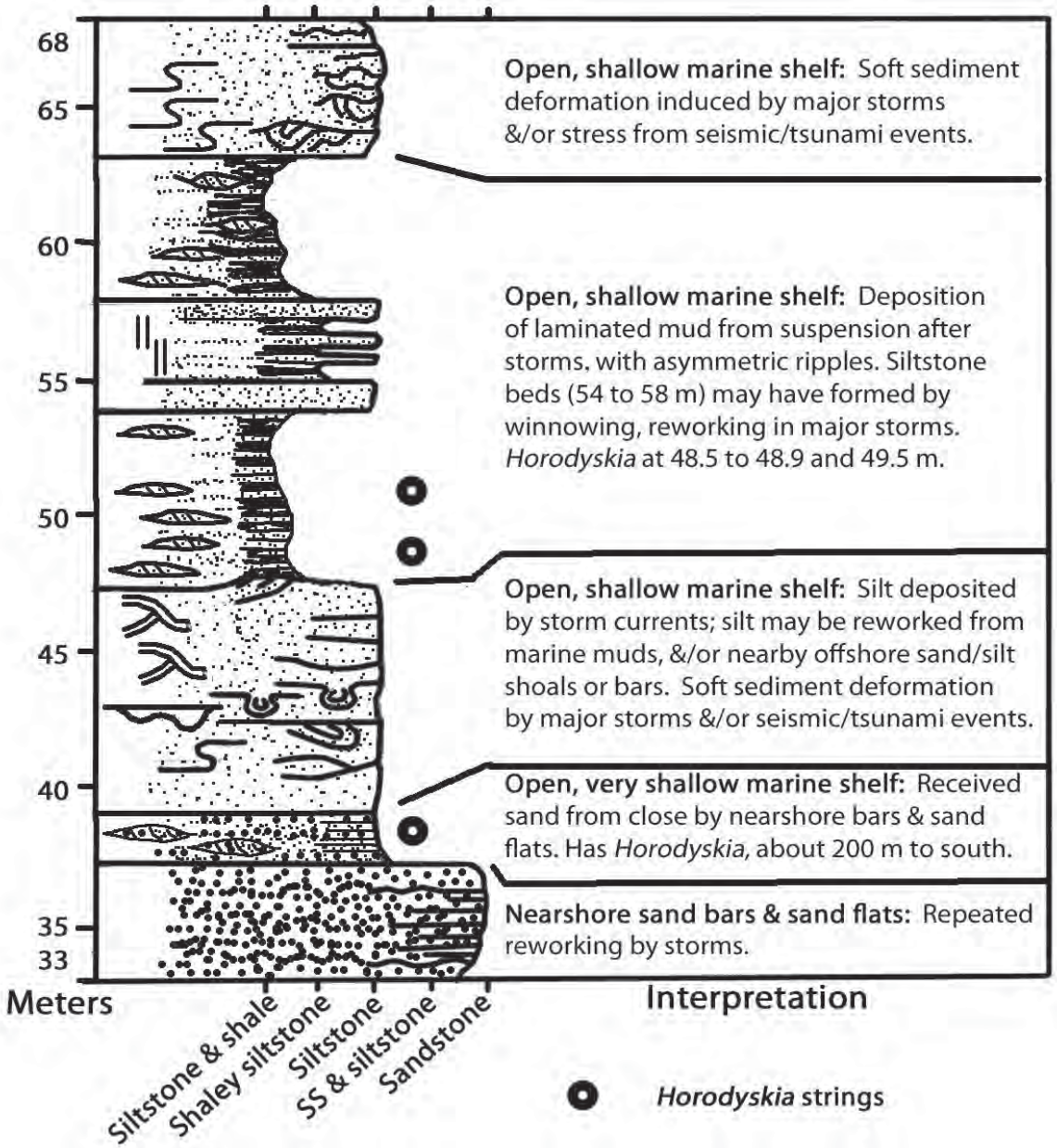

Figure 8. Lower half of Cycle 1 at Locality 3. *Horodyskia* (both species) are found in siltstone and sandy siltstone beds, which were deposited on a shallow, quiet marine shelf subject to rare storm or seismic events.

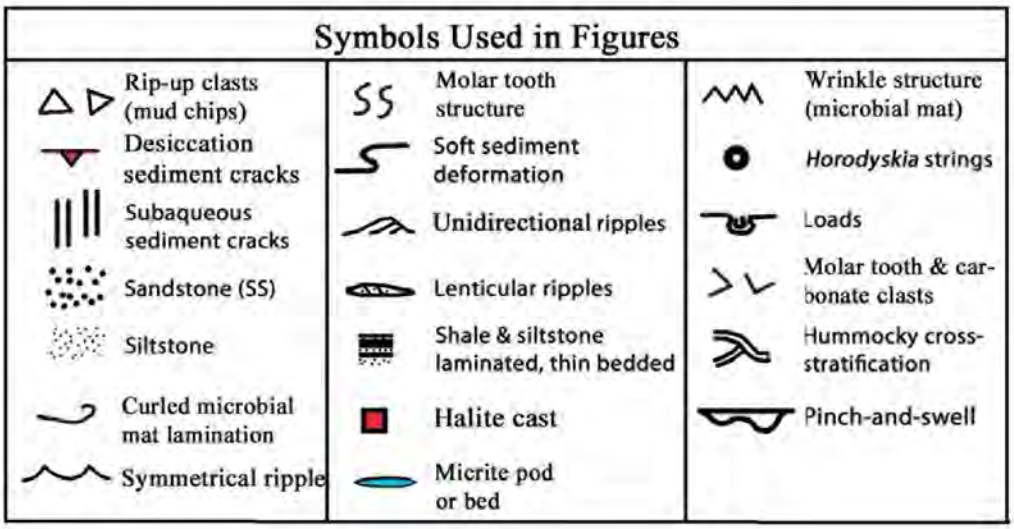

Figure 9. Key to symbols used in the graphic columns of figures 8 and 10.

indicated with black circles (fig. 9). Working in the Big Belt Mountains, Spokane Hills, and Wolf Creek area, Bloomfield (1983) recognized four cycles, which correspond to Helena-area cycles 3, 4, 5, and 6/7.

The sedimentary structures and lithologies indicate a mostly calm depositional environment, with low depositional relief. The lack of typical tidal deposits such as tidal channels and flasers suggests that tides had a very low range. Ordinary storm currents moved mud and fine-grained sand by traction and suspension, while rare major storms formed hummocky structures and brought in thin sheets of sand and silt, probably from nearby sand flats and beaches (Locality 1, fig. 8; Locality 4, fig. 10). The siltstones mostly fall into the microlamina and plane-laminated silt-and-clay sediment types of Winston (1986b) and Winston and Link (1993). Many of the microlaminates are likely microbial boundstones, deposited in very shallow near-shore sites.

Horodyskia is absent from tabular, mostly medium-grained quartz sandstone beds. These sandstones, along with interbedded siltstones, are interpreted as deposits on beaches, near-shore sand bars, and sand flats. See, for instance, the basal and capping sandstone units of Cycle 3 (fig. 10, colored orange). These sandstones are thin- to medium-bedded, feldspathic, weather in light tones, and stand out as key beds in outcrop. The sandstones may contain upper-flow-regime planar lamination and cross-bedding on a 2- to 4-decimeter-scale, grading up to lower-flow-regime unidirectional ripples. Winston (1989) and Bloomfield (1983) studied the Greyson–Spokane transition to the east and north of the present study area; their interpretations of depositional environments agree with mine. As discussed above, the sand probably derived from the Laurentian craton to the northeast (present coordinants).

Nonmarine beds contain no *Horodyskia*, although *Horodyskia* can be found within a few meters or even decimeters above or below desiccation-cracked, nonmarine beds. In this study, desiccation cracks (polygonal to irregular, downward-tapering, sediment-filled mud cracks) are considered indicators of subaerial drying of muddy sediment. Salt casts and redbeds are generally nonmarine in Greyson and Spokane rocks, but are used with caution as indexes of non-marine deposition. At the study sites, salt casts are scattered on bedding planes, and probably formed through evaporation of ephemeral coastal ponds. The salt casts do not merge into continuous beds as would be expected in a marginal marine setting, such as a lagoon connected hydraulically to the Belt Basin.

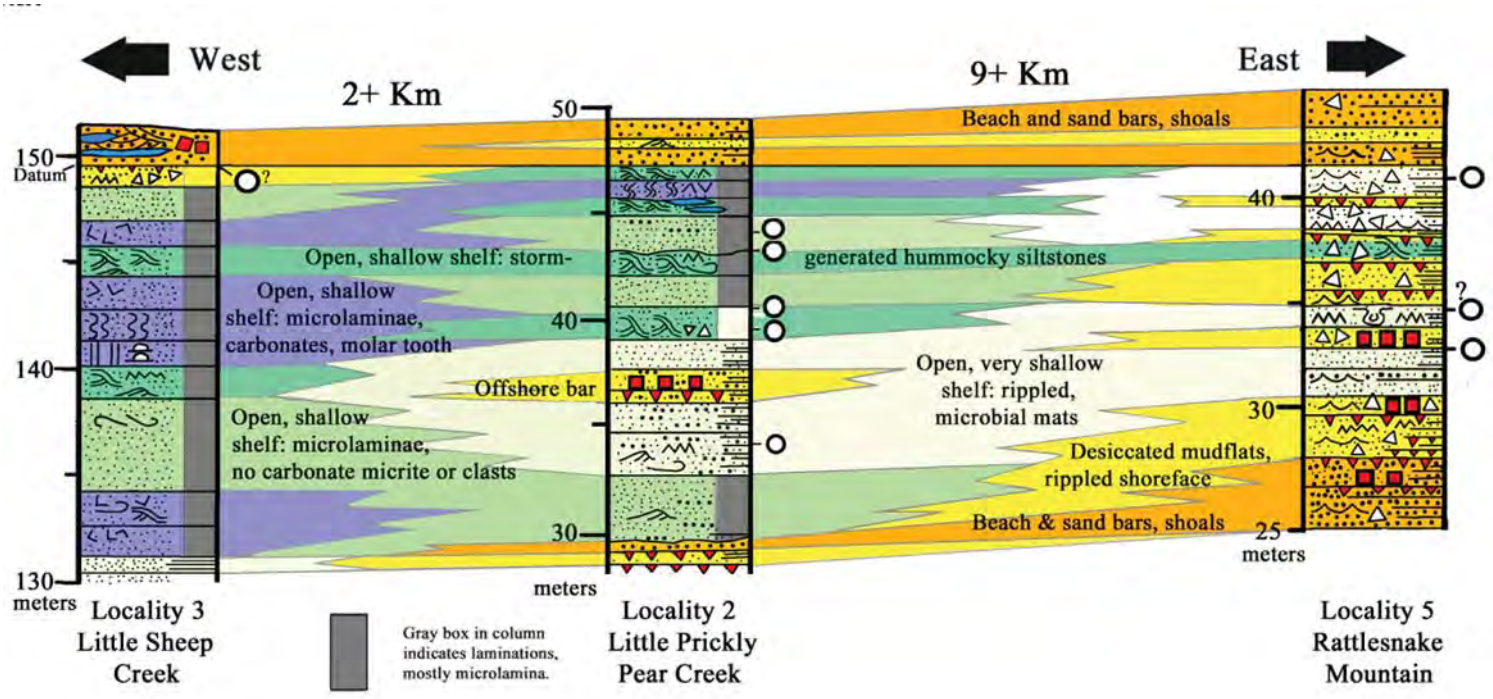

Figure 10. Cross-section of Cycle 3. The environment most favorable for growth of *Horodyskia* was at Locality 2, with five *Horodyskia* occurences, in offshore, microlaminated to thin-bedded siltstone. Locality 2 is transitional between coastal deposits (mudflats, sandy beaches, sand bars) to the east, and laminated, carbonate-rich, suspension-deposited muds on a shallow marine shelf to the west. The horizontal scale of the cross section is approximate, and not corrected for displacement on two branches of the Hoadley thrust fault (fig. 2), just east and west of Locality 2.

Horodyskia is found near but not in direct association with stromatolites and micritic limestone pods and beds, dolomitic or calcitic mud, and syndepositional molar-tooth structures (fig. 10). This implies that much of the Helena-area *Horodyskia* was tolerant of suspended mud but not of carbonate-rich, slighty siliciclastic-starved conditions.

DISCUSSION

The seven new Helena-area sites expand *Horodyskia*'s geographic range in Montana from Glacier National Park 250 km southeast into the Helena Embayment of the Belt Basin, and expand its stratigraphic range upward in the Mesoproterozoic Belt Basin, to the upper Greyson and lower Spokane formations.

Horodyskia Growth in Shallow Water, Offshore of Low-Relief Sand Flats, Mud Flats, and Beaches

Many *Horodyskia* beds are in repetitive, marine-to-nonmarine depositional cycles (fig. 10), with beds containing subaerial desiccation cracks, halite casts, and redbeds in close juxtaposition with beds containing *Horodyskia*. In this case, *Horodyskia* probably carpeted a gentle slope just off the shore-face. *Horodyskia* also grew farther off shore, just above or below (and rarely in) beds with low hummocky cross-bedding (figs. 8, 10). The depth of water on the shelf is not known, but the presence of hummocks does not necessarily indicate depths of tens of meters deep or more. Hummocks typically develop above but near storm wave base (Dumas and Arnott, 2006), but also have been recorded in shallower shelf conditions and up to the shore-face.

Prostrate Growth Habit; Scouring

A growth habit free of the bottom or anchored by a holdfast is rejected. If *Horodyskia* was free-floating, then upon death the strings should settle to the bottom, with many strings criss-crossing. Likewise, if strings were eroded and then redeposited, many strings should cross one another, or drape around low obstacles on the bottom, or settle out in tangled or subparallel masses in depressions such as ripple troughs. The Helena area lacks examples of string cross-overs and drapes, but cases (unfortunately, poorly preserved) of groups of many strings side-by-side, touching one another, were found at Locality 4 (fig. 2). Better specimens are needed before concluding that intact strings were commonly eroded, transported, and redeposited.

No systematic study of paleocurrent indicators in relation to string orientation was done. An obvious working hypothesis is that strings tended to grow parallel to the dominant current direction; for instance, many Bangemal Supergroup (Western Australia) specimens show sub-parallel growth generally but not always corresponding current direction (Grey and others, 2001; their fig. 2b). But sub-parallel Tasmanian strings (Calver and others, 2010; their fig. 4) are of unknown orientation in relation to current directions.

Beads at many Helena sites are ringed by shallow depressions. If these depressions were current-scoured, then it is likely that the beads were well attached to the sediment substrate during growth. Fedonkin and Yochelson (2002) also proposed a prostrate growth habit. Beads with ring- and scoop-shaped depressions are common in western Australia (for instance, Grey and others, 2010), but the structures have not been documented as parallel to other paleocurrent indicators. This is also the case with some Helena-area specimens. In summary, the ring depressions are probably scour structures, but more work is needed.

Nets and Branching; Dark Halos and Ribbons

The strings shown in figures 3 and 4 are tightly to loosely arcuate, and they seem to repeatedly branch. No single split of a string is proof of branching, but collectively the pattern is fairly convincing. However, better and larger specimens are needed to determine if the strings branch or form net patterns. In figure 4, most of the string segments curve to the left from each branching point; this further suggests a reproducible pattern. Compare figures 3 and 4 to Horodyski's (1982) figure 3a of Plate 1, also reproduced as figure 3c in Horodyski (1989).

Halos and ribbon-like films (fig. 3) may be organic and part of *Horodyskia*, or post-depositional mineral stains localized by some property of the beads. Alternatively, they could be poorly preserved, delicate, crustose algal thalli, originally only a few cells thick. If so, the beads might be reproductive structures such as conceptacles, which are common, for example, in red algae.

REFERENCES CITED

Adam, Z.A., Skidmore, M.L., Mogk, D.W., and Butterfield, N.J., 2017, A Laurentian record of the earliest fossil eukaryotes: Geology, v. 45, p. 387–390.

Barnes, W.C., 1963, Geology of the northeast Whitefish range, Northwest Montana: Princeton, Princeton University, Ph.D. Thesis, 166 p.

Bloomfield, S.L., 1983, The Proterozoic Greyson–Spokane transition sequence: A stratigraphic and gravity study, west-central Montana: Missoula, University of Montana, M.S. Thesis, 107 p.

Bregman, M.L., 1981, Geologic map of the Sheep Creek and Rattlesnake Mountain quadrangles, Lewis and Clark County, Montana: Montana Bureau of Mines and Geology Geologic Map 26, 1 plate.

Burmester, R.F., Lonn, J.D., Lewis, R.S., and McFaddan, M.D., 2013, Toward a grand unified theory for stratigraphy of the Lemhi subbasin of the Belt Supergroup, *in* Lewis, R.S., Garsjo, M.M, and Gibson, R.I., eds., 38th Annual Field Conference Belt Symposium V: Northwest Geology, v. 42, p. 1–20.

Calver, C.R, Grey, K., and Laan, M., 2010, The 'string of beads' fossil (*Horodyskia*) in the mid-Proterozoic of Tasmania: Precambrian Research, v. 180, p. 18–25.

Dong, L., Xiao, S., Shen, B., and Zhou, C., 2008, Silicified *Horodyskia* and *Palaeopascichnus* from upper Ediacaran cherts in South China: Tentative phylogenetic interpretation and implications for evolutionary stasis: Journal of the Geologic Society, London, v. 165, p. 367–378.

Dumas, S., and Arnott, R.W.C., 2006, Origin of hummocky and swaley cross-stratification—The controlling influence of unidirectional current strength and aggradation rate: Geology, v. 34, p. 1073–1076.

Fedonkin, M.A., and Yochelson, E.L., 2002 , Middle Proterozoic (1.5 Ga) *Horodyskia moniliformis* Yochelson and Fedonkin, the oldest known tissue-grade colonial eucaryote: Smithsonian Contributions to Paleobiology, 94, 29 p.

Grey, K., and Williams, I.R, 1990, Problematic bedding-plane markings from the Middle Proterozoic Manganese Subgroup, Bangemall Basin, Western Australia: Precambrian Research, v. 46, p. 307–327.

Grey, K., Williams, I.R., Martin, D. McB., Fedonkin, M.A., Gehling, J.G., and Runnegar, B.N., and Yochelson, E.L., 2001, New occurrences of 'strings of beads' in the Bangemall supergroup: A potential biostratigraphic marker horizon: Geological Survey of Western Australia, 2000–01 Annual Review, p. 69–73.

Grey, K., Yochelson, E.L., Fedonkin, M.A., and Martin, D. McB., 2010, *Horodyskia williamsii* new species, a Mesoproterozoic macrofossil from Western Australia: Precambrian Research, v. 180, p. 1–17.

Gonzalez-Alvarez, I.J., Pratt, B.R., and Kerrich, R., 2003, Putative metazoans in a Mesoproterozoic shallow marine environment, Belt Supergroup, western North America: Organic versus inorganic?: Abstracts Book 22nd IAS Meeting of Sedimentology—Opatija 2003, p. 67

Halpin, J.A, Jensen, T., McGoldrick, P., Meffre, S., Berry, R.F., Everard, J.L, Calver, C.R., Thompson, J., Goemann, K., and Whittaker, J.M, 2014, Age constraints from the Rocky Cape Group: Putting Tasmania on the Mesoproterozoic map: Abstracts of the 22nd Australian Earth Sciences Convention 2014, 7–10 July 2014, Newcastle, Australia, p. 207–208.

Horodyski, R.J., 1982, Problematic bedding-plane markings from the Middle Proterozoic Appekunny Argillite, Belt Supergroup, northwestern Montana: Journal of Paleontology, v. 56, p. 882–889.

Horodyski, R.J., 1989, Paleontology of the Middle Proterozoic Belt Supergroup, *in* Winston, D., Horodyski. R.J., and Whipple, J.W., eds., Middle Proterozoic Belt Supergroup, western Montana, Geological Society of America, Northwest Section Trip Guidebook T334, p. 7–26.

Kuhn, J.A., 1987, The stratigraphy and sedimentology of the Middle Proterozoic Grinnell Formation, Glacier National Park and the Whitefish Range NW Montana: Missoula, University of Montana, M.S. Thesis, 122 p.

Martin, D. McB., 2004, Depositional environment and taphonomy of the 'strings of beads': Mesoproterozoic multicellular fossils in the Bangemall

Supergroup, Western Australia: Australian Journal of Earth Sciences, v. 51, p. 555–561.

Mathur, V.K, and Srivastava, D.K,. 2004, Record of tissue grade colonial eukaryote and microbial mat associated with Ediacaran fossils in Krol Group, Garhwal Syncline, Lesser Himalaya, Uttaranchal: Journal of the Geological Society of India, v. 63, p. 100–102.

Mueller, P., Mogk, D., Wooden, J., and Spake, D, 2016, U-Pb ages of zircons from the Lower Belt Supergroup and proximal crystalline basement: Implications for the early evolution of the Belt Basin, *in* MacLean, J.S., and Sears, J.W., eds., Belt Basin: Window to Mesoproterozoic Earth: Geological Society of America Special Paper 522, p. 283–303.

Retallack, K.L., Dunn, P.L, and Saxby, J., 2013, Problematic Mesoproterozoic fossil *Horodyskia* from Glacier National Park, USA: Precambrian Geology, v. 226, p. 125–142.

Reynolds, M.W., and Brandt, T.R., 2005, Geologic map of the Canyon Ferry Dam 30' x 60' quadrangle, west-central Montana: U.S. Geological Survey Scientific Investigations Map 2860, 32 p., 3 sheets, scale 1:100,000.

Ross, G.M., and Villeneuve, M., 2003, Provenance of the Mesoproterozoic (1.45 Ga) Belt basin (western North America): Another piece in the pre-Rodinia paleogeographic puzzle: Geological Society of America Bulletin, v. 165, p. 1191–1217.

Rule, R., 2012, *Horodyskia* from the Belt Supergroup (~1.45 Ga) of Montana: Animal, mineral, or vegetable?: Abstract, 2012 Geological Society of America Annual Meeting in Charlotte, Abstracts with Programs, v. 44, no. 7, p. 87.

Rule, R., 2014, *Horodyskia moniliformis* of the Belt Supergroup: A case study of the relationships between Precambrian microbially induced and physical sedimentary structures in a flocculating muddy environment: Abstract, 2014 Geological Society of America Annual Meeting, Vancouver, British Columbia (19–22 October 2014), Paper no. 171-9.

Sears, J.W., 2007a, Belt-Purcell Basin: Keystone of the Rocky Mountain fold-and-thrust belt, United States and Canada, *in* Sears, J.W., Harms, T.A., and Evenchick, C.A., eds., Whence the Mountains? Inquires into the evolution of orogenic systems: Geological Society of America Special Paper 433, p. 147–166.

Sears, J.W., 2007b, Rift destabilization of a Proterozoic epicontinental pediment: A model for the Belt-Purcell basin, North America, *in* Link, P.K., and Lewis, R.S., eds., Proterozoic geology of Western North America and Siberia: Society of Economic Paleontologists and Mineralogists Special Publication 86, p. 55–64.

Slotznick, S.P., Zieg, J., Webb, S.M, Kirschvink J.L., and Fischer, W.W., 2015, Iron mineralogy and redox chemistry of the Mesoproterozoic Newland Formation in the Helena embayment, Belt Supergroup, Montana, *in* Mosolf, J., and McDonald, C., eds., 40th annual field conference, Geology of the Elliston area, Montana and other papers, Tobacco Root Geological Society, Butte, Montana: Northwest Geology, v. 44, p. 55–72.

Smith, A.G., 1963, Structure and stratigraphy of the Northwest Whitefish Range, Lincoln County, Montana: Princeton, Princeton University, Ph.D. Thesis, 151 p.

Walter, M.R., Oehler, J.H., and Oehler, D.Z., 1976, Megascopic algae 1300 million years old from the Belt Supergroup, Montana: A reinterpretation of Walcott's *Helminthoidichnites*: Journal of Paleontology, v. 50, p 872–881.

Winston, D., 1986a, Stratigraphy and nomenclature of the Middle Proterozoic Belt Supergroup, Montana, Idaho and Washington, *in* Roberts, S.M., ed., A guide to Proterozoic rocks of western Montana and adjacent areas: Montana Bureau of Mines and Geology Special Publication 94, p. 69–84.

Winston, D. 1986b, Sedimentology of the Ravalli Group, middle Belt carbonate and Missoula Group, Middle Proterozoic Belt Supergroup, Montana, Idaho and Washington, *in* Roberts, S.M., ed., Belt Supergroup: A guide to Proterozoic rocks of western Montana and adjacent areas: Montana Bureau of Mines and Geology Special Publication 94, p. 85–124.

Winston, D., 1989, A sedimentologic and tectonic interpretation of the Belt: International Geological Congress Field Trip T334, 1989, p. 47–69.

Winston, D., 2016, Sheetflood sedimentology of the Mesoproterozoic Revett Formation, Belt Super-

group, northwestern Montana, USA, *in* MacLean, J.S., and Sears, J.W, eds., Belt Basin: Window to Mesoproterozoic Earth, Boulder, Colorado, Geological Society of America Special Paper 522, p. 1–56.

Winston, D., and Link, P.K., 1993, Middle Proterozoic rocks of Montana, Idaho, and eastern Washington: The Belt Supergroup, *in* Reed, J.C., Jr., Bickford, M.E., Houston, R.S., Link, P.K., Rankin, R.W., Sims, P.K., and Van Schmus, W.R., eds., Precambrian: Conterminous U.S.: Boulder, Colorado, Geological Society of America, v. C2, p. 487–517.

Yochelson, E.L., and Fedonkin, M.A., 2000, A new tissue-grade organism, 1.5 billion years old from Montana: Proceedings of the Biological Society of Washington, v. 113, p. 843–847.

Vuke, S.M., Porter, K.W., Lonn, J.D, and Lopez, D.A., 2007, Geologic map of Montana: Montana Bureau of Mines and Geology Geologic Map 62A, 73 p., 2 sheets, scale 1:500,000.

EVIDENCE FOR A PERMAFROST CREEP-ROCK GLACIER ORIGIN FOR SOME PROTALUS RAMPARTS IN WESTERN MONTANA

Jeff Lonn

Montana Bureau of Mines and Geology

ABSTRACT

Protalus ramparts, also called pronival ramparts, are commonly explained as relict accumulations of rockfall debris that fell onto a steep snow slope and slid or rolled down to accumulate at the base of the now-melted snowfield. However, four protalus ramparts examined in western Montana lack the characteristics of ramparts that form from rockfall on snowfields. Instead, they exhibit evidence of a permafrost creep origin, the same process by which rock glaciers move. There is broad support in the recent literature for this alternative origin, suggesting that many, if not most, protalus ramparts are actually small rock glaciers. The most recent literature now uses the term "pronival ramparts" for rockfall on snowfield ramparts and restricts "protalus ramparts" to those with permafrost creep origins.

INTRODUCTION

Protalus ramparts, also called pronival ramparts, are ridges of angular boulders at the toes of talus slopes. They are commonly explained as relict accumulations of rockfall debris near the base of a cliff that fell onto a steep snow slope and slid or rolled down to accumulate at the base of the now-melted snowfield (fig. 1). They have been considered distinctly different from ridges and ramparts formed on rock glaciers, in that downslope creep has not been considered to be an important process in their formation. However, examination of four protalus ramparts in western Montana calls the conventional rockfall theory into question, and suggests instead a permafrost creep origin similar to the processes that form rock glaciers (fig. 2). A literature review revealed numerous recent studies from the European Alps that support similar alternative origins for protalus rampart formation, (e.g., Barsch, 1996; Haeberli, 1985; Scapozza and others, 2011; Scapozza, 2015; Wilson, 1990). In fact, Barsch (1996) stated "in most cases, 'protalus ramparts' are nothing but embryonal talus rock glaciers (active, inactive, or fossil ones). They can be explained as the creep of mountain permafrost." Subsequently, talus ridges

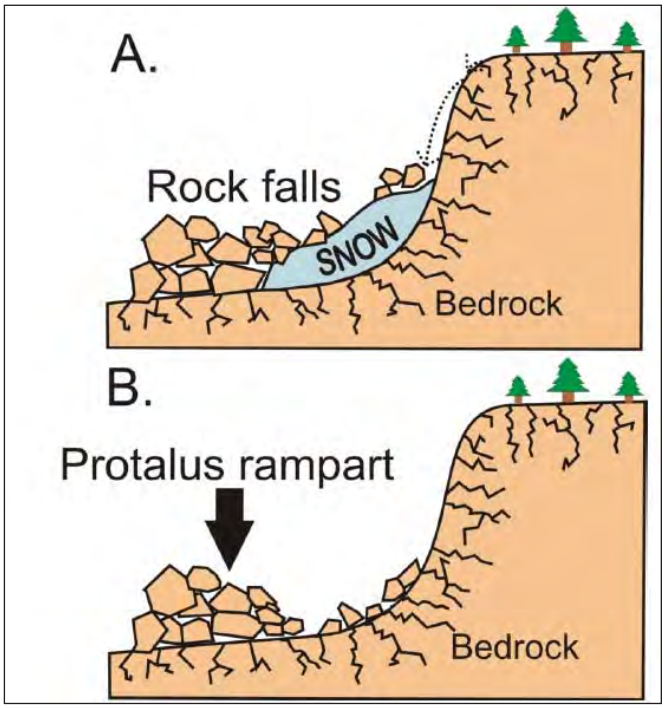

Figure 1. Conventional explanation of protalus or pronival rampart formation by rockfall accumulation at the base of on a now-melted snowfield. From Orr and others, 2009.

that form through the conventional rockfall origin described above are now termed "pronival ramparts" (Matthews and others, 2011; Hedding, 2011, 2016). The new term is derived from "nival," which means "pertaining to snowfields." The term "protalus rampart" now refers to talus ridges that form from permafrost creep processes (Haeberli, 1985; Barsch, 1996; Scapozza and others, 2011), although Scapozza (2015) recommends that this terminology be abandoned and that they simply be called rock glaciers.

The conventional rockfall explanation for the origin of protalus—now pronival—ramparts requires that:

1. The slope be steep enough for angular boulders to slide or roll down;
2. There be a source area, such as a cliff, upslope;
3. The outer slope of the rampart be no steeper than the angle of repose;
4. The ridge be composed completely of angular

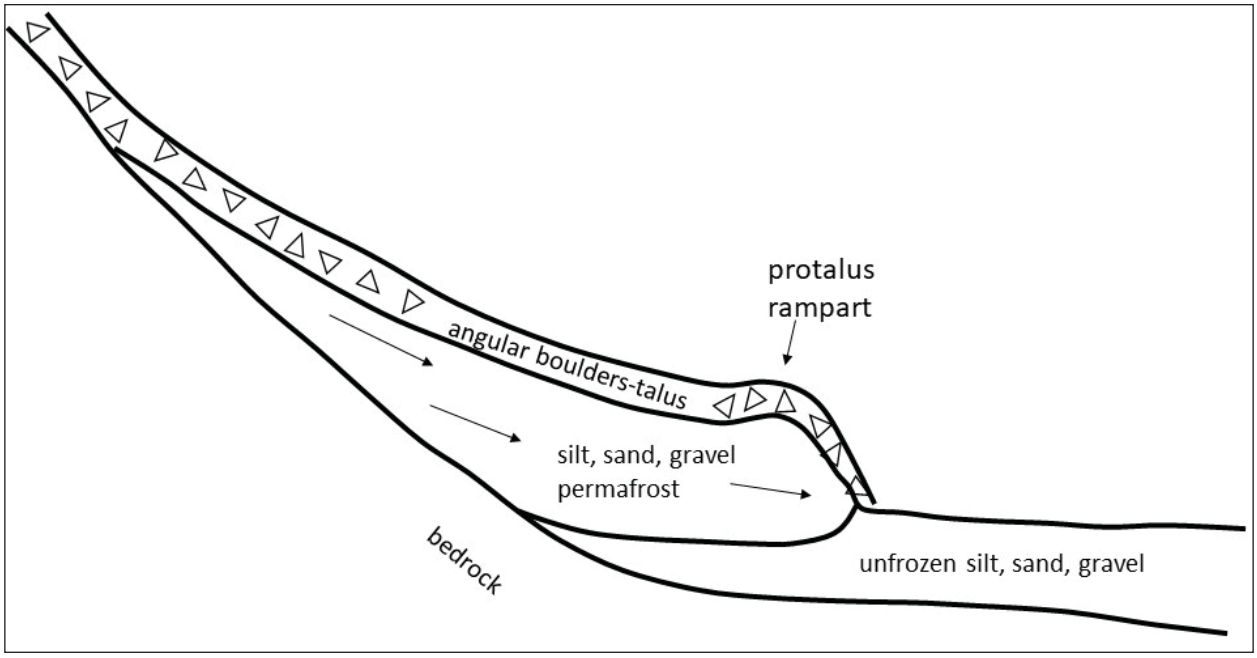

Figure 2. Permafrost creep-rock glacier model of protalus rampart formation where a 1-5-m-thick veneer of angular talus is carried downslope by an underlying layer of perennially frozen finer-grained material. Haeberli (1985) used drillhole and seismic data to confirm the typical rock glacier geometry shown above, which is modified from his work.

boulders and incorporate no soil or fine-grained material;

5. The ridge crest be oriented at a high angle to the fall line in map view;

6. The outer edge of the ridge be indistinct as a result of boulders of different shapes and sizes rolling variable distances.

Here I describe four protalus ramparts in western Montana that do not obey these rules. I speculate that many, if not most, talus ramparts in the northern Rockies formed through creep or flow, not rockfall on snow processes.

RESULTS

Rampart #1

Rampart #1 is a small protalus rampart (fig. 3) developed at the foot of a quartzite talus field on a north aspect at 8,200 ft in the southern Sapphire Mountains (46.03195, -113.77396). Soil is deformed in front of the ridge and incorporated into the ridge itself. The leading edge is very abrupt, with no stray boulders beyond the front. Some boulders along the front appear to be rotated to overhang the soil beyond the leading edge. Although there is a cliff source area above, the occurrence of fine-grained material in the rampart and its distinct leading edge show that the boulders did not simply roll down to form the rampart, but instead crept downhill along with the underlying fine-grained material.

Figure 3. Rampart #1 has an abrupt front and contains both angular boulders and fine-grained soil (covered by vegetation). Note the lack of stray boulders downslope of the rampart and the rotated boulders at the front of the rampart.

Rampart #2

Rampart #2 is a small ridge (fig. 4) developed at the lower end of a granite talus field on an ENE aspect at 7,960 ft in the southern Bitterroot Mountains (46.15346, -114.29180). The talus field above it is only 17–21° in steepness. Above the talus field is a nearly flat bench that provides no source for boulders sliding or rolling downhill, and the slope itself is too gentle to support those processes. In map view, the trace of the rampart is oriented at acute angles (26–39°) to the fall lines (fig. 5). The features all suggest that a rockfall origin is unlikely. Note also that the outer slope of the ridge is steeper than the angle of repose, about 45° (fig. 4), a characteristic of permafrost creep protalus ramparts (Scapozza, 2015). The gently sloping blockfield above the rampart probably formed from in-place frost heaving or wedging, and moved downslope through permafrost creep to form the small protalus rampart.

Figure 4. Views of rampart #2. Note that the gentle talus slope above the rampart has no rock fall source, and the leading edge is steep and abrupt.

Figure 5. Thick white lines show locations of ramparts #2, #3, and #4 on a Google Earth image. Arrows show the orientations and slope angles of fall lines above rampart #2. Note that ramparts #3 and #4 are part of the same talus field, and could be interpreted as concentric flow features in a rock glacier.

Figure 6. Rampart #3 curves upslope on its southern end (see white arrow in upper right), becoming sub-parallel to the fall line. Person in lower left for scale.

Figure 7. The leading edge of rampart #4 is abrupt and much steeper than the angle of repose.

Figure 8. Boulder 0.7 m long and weighing more than 100 kg probably slid down a deep, late spring snowpack or was carried within a snow avalanche to its present perch. The visible scar on the tree above the boulder suggests high-speed impact. Obviously, rockfall–snow interactions do create some unusual features that may include some protalus/pronival ramparts, but permafrost creep is probably a more common origin for these ramparts. Photo from the northern Beaverhead Mountains, Idaho.

Rampart #3

Rampart #3 (fig. 6) is partway down a granite talus slope on an east aspect at 7,760 ft in the southern Bitterroot Mountains (46.15265, -114.2902). Although the ridge is beneath a steep slope with a boulder source area in the cliff above, the rampart is curved and outlines a lobe-shaped tongue of talus. The rampart's trace curves up the slope on its south end (figs. 5, 6), becoming nearly parallel to the fall line and flanking the side of the talus field. This end of the rampart has no rockfall source area, and its parallelism with the fall line suggests that the ridge is part of a rock glacier that moved through permafrost creep.

Rampart #4

Rampart #4 is a small talus ridge (fig. 7), downslope from rampart #3, at 7,710 ft on an east aspect in the southern Bitterroot Mountains (46.15299, -114.2896). It has a very steep, abrupt front containing elongate, tabular boulders that appear to have been rotated into vertical orientations. Rock glacier creep offers the best explanation for these features. The talus field above rampart #4 is continuous with rampart #3, and the two subparallel ramparts might outline concentric lobes within a rock glacier (fig. 5).

CONCLUSIONS

Four protalus ramparts examined in western Montana lack the characteristics of pronival ramparts that form from rockfall collecting at the base of snowfields. Instead, they exhibit evidence of a permafrost creep origin, the same process by which rock glaciers move. There is broad support in the recent literature for this alternative origin, suggesting that many, if not most, protalus ramparts are actually small rock glaciers. Field geologists can use the simple observations presented here to test this theory.

REFERENCES CITED

Barsch, D., 1996, Rockglaciers: Indicators for the present and the former geoecology in high mountain environments: Springer, Berlin Heidelberg, Germany, 331 p., 1996.

Colucci, R.R., Boccali, C., Žebre, M., and Guglielmin, M., 2012, Rock glaciers, protalus ramparts and pronival ramparts in the south-eastern Alps:

Geomorphology, v. 269, p. 112–121, doi: http://dx.doi.org/10.1016/j.geomorph.2016.06.039

Haeberli, W., 1985, Creep of mountain permafrost: Internal structure and flow of alpine rock glaciers: Mitteilungen der Versuchsanstalt für Wasserbau, Hydrologie und Glaziologie, ETH Zurich, v. 77, p. 5–142. https://www.ethz.ch/content/dam/ethz/special-interest/baug/vaw/vaw-dam/documents/das-institut/mitteilungen/1980-1989/077.pdf [Accessed May 2019]

Hedding, D.W., 2011, Pronival rampart and protalus rampart: A review of terminology: Journal of Glaciology., v. 57, p. 1179–1180.

Hedding, D.W., 2016, Pronival ramparts: Origin and development of terminology: Erdkunde, v. 70, no. 2, p. 141–151.

Matthews, J.A., Shakesby, R.A., Owen, G., and Vater, A.E., 2011, Pronival rampart formation in relation to snow-avalanche activity and Schmidt-hammer exposure-age dating (SHD): Three case studies from southern Norway: Geomorphology, v. 130, p. 280–288, doi: http://dx.doi.org/10.1016/j.geomorph.2011.04.010.

Orr, I.M., Mohr, A.R., Syverson, K.M., and Jol, H.M., 2009, Sedimentology of the Blue Hills Felsenmeer State Natural Area, Wisconsin: Geological Society of America Abstracts with Programs, v. 41, no. 4, p. 63.

Scapozza, C., 2015, Investigation on protalus ramparts in the Swiss Alps: Geographica Helvetica, v. 70, P. 135–139, https://www.geogr-helv.net/70/135/2015/ [Accessed May 2019]

Scapozza, C., Lambiel, C., Baron, L., Marescot, L., and Reynard, E., 2011, Internal structure and permafrost distribution in two alpine periglacial talus slopes, Valais, Swiss Alps: Geomorphology, v. 132, p. 208–221, doi: 10.1016/j.geomorph.2011.05.010, 2011.

Shakesby, R.A., Matthews , J.A., McEwen, L.J., and Berriford, M.S., 1999, Snow-push processes in pronival (protalus) rampart formation: Geomorphological evidence from Smørbotn, Romsdal-salpane, southern Norway: Geografiska Annaler: Series A, Physical Geography 81, p. 31–45, doi: 10.1111/j.0435-3676.1999.00047.x

Wilson, P., 1990, Characteristics and Significance of Protalus ramparts and fossil rock glaciers on Errigal Mountain, County Donegal: Proceedings of the Royal Irish Academy, Section B: Biological, Geological, and Chemical Science, v. 90B, p. 1–21, https://www.jstor.org/stable/20494540 [Accessed May 2019]

FIELD GUIDE TO THE GEOLOGY AND METALLIC MINERAL DEPOSITS ALONG THE WESTERN CONTACT BETWEEN THE BOULDER BATHOLITH AND THE LOWER AND MIDDLE MEMBERS OF THE ELKHORN MOUNTAINS VOLCANIC FIELD

Kaleb C. Scarberry,[1] Ethan L. Coppage,[2] and Alan R. English[1]

[1]*Montana Bureau of Mines and Geology*
[2]*Geologic Engineering, Montana Technological University*

*Note that the odometer values were done using Google Earth, so may be slightly off.

INTRODUCTION

This field guide examines igneous rocks and metallic mineral deposits along a portion of the western contact between the comagmatic Late Cretaceous Boulder Batholith and the Elkhorn Mountains volcanic field (Elkhorn Mountains Volcanics, EMVF) west of Helena, MT. Although EMVF stratigraphy is emphasized in this field trip guide, aspects of mine production and Tertiary geology are also addressed. The field trip begins in Elliston, MT and travels west to MacDonald Pass to observe volcanic features of a middle member EMVF ignimbrite where it is in contact with Boulder Batholith granodiorite. The trip then backtracks towards Elliston and heads south into the Little Blackfoot River drainage to look at mineral deposits and the age and geochemical stratigraphy of the lower and middle member EMVF section in the Bison Mountain 7.5′ quadrangle. The trip ends with a short hike in semi-challenging terrain (<1 mi, with about 600 ft elevation gain) to look at a 37 Ma rhyolite ignimbrite and discuss evidence for Tertiary block faulting in the region.

GEOLOGIC SETTING

Tectonic shortening, intrusion of the Boulder Batholith, and coeval eruption of the EMVF (fig. 1) thickened the Paleozoic–Cretaceous sedimentary thrust wedge in Montana by around 16–17 km between about 85 and 74 Ma (Lageson and others, 2001). Late Cretaceous Cordilleran arc magmatism (e.g., Rutland and others, 1989) produced the EMVF between about 85 and 77 Ma (Olson and others, 2016; Korzeb and others, 2018). A detailed overview of Boulder Batholith plutons and the stratigraphic relationships in the EMVF is provided by Scarberry and others (this volume). Precious and base metal mineral deposits formed during Late Cretaceous emplacement of the Boulder Batholith into the EMVF, its volcanic carapace.

High-angle normal faulting contributed to exhumation of the Late Cretaceous magma system (Ruppel, 1963; Wallace and others, 1990; Schmidt and others, 1994). Block faulting may have initiated in the Tertiary (Ruppel, 1963), and Basin and Range extension was ongoing in the Bison Mountain 7.5′ quadrangle by the Middle Miocene (Reynolds, 1979). The Bison Mountain 7.5′ quadrangle (scale 1:24,000) is located at the junction between the Lewis and Clark Zone and the Intermountain Seismic Belt, two major belts of regional seismicity, and several small magnitude earthquakes (magnitude 2.5–3.5) have occurred in the region since 1982 (Stickney and others, 2000).

Pleistocene valley glaciers occupied the main river drainages and many of their tributaries during the last glaciation. Valley glaciers were part of an ice cap in the Boulder Mountains that attained a thickness of more than 300 m locally, and covered around 520 km^2 between Butte and Helena (Ruppel, 1962). Some of the most prominent terminal features of the ice cap occur in the Bison Mountain 7.5′ quadrangle (fig. 1) (Mahoney and others, 2015).

ROAD LOG

The road log begins in Elliston, MT, located along Highway 2 approximately 8 mi east of Avon and 23 mi west of Helena. The road log has two parts: Part 1 examines features of middle member EMVF ignimbrite where it is in contact with Boulder Batholith granodiorite. Part 2 is focused on the geology of the Boulder Batholith–EMVF magma system, related mineral deposits, and possible evidence for Tertiary block faulting in the Bison Mountain 7.5′ quadrangle. Scarberry and others (2018) mapped the Bison Mountain 7.5′ quadrangle and reported geochemical and radiometric age data for a reconnaissance sampling of the EMVF and Tertiary ignimbrite. Set your odometer to 0.0 mi at the convenience store in Elliston and follow Highway 2 east towards Helena.

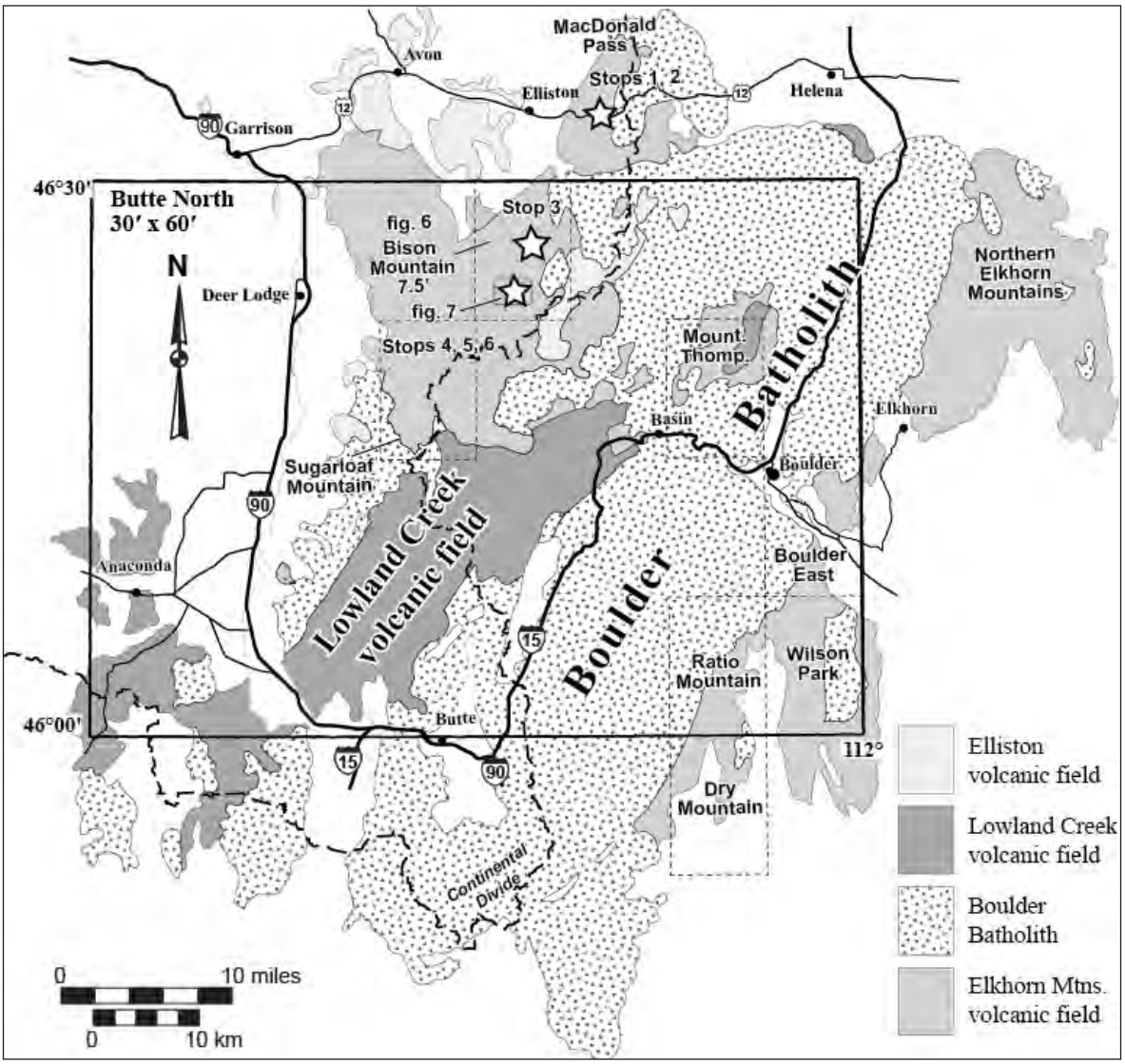

Figure 1. General location of the field- trip stops and simplified igneous geology of the Boulder Batholith–– Elkhorn Mountains Volcanic Field magma system (after Vuke and others, 2007).

Part 1: The Middle Member of the Elkhorn Mountains Volcanic Field

The middle member of the EMVF (fig. 2) is characterized by rhyolite ignimbrite deposits and intercalated epiclasitic volcanic debris that averages 1,650 m thick. At least three of the ignimbrites are regionally extensive, rheomorphic, and exhibit features of both lateral shear and syn-crystallization flow-folding (Olson and others, 2016).

On the west side of the Boulder Batholith, the middle member EMVF thins from about 0.7 km to 1 km thick in the Bison Mountain and Sugarloaf Mountain 7.5′ quadrangles, respectively, to less than 0.5 km thick in the Mount Thompson 7.5′ quadrangle to the east (figs. 1, 2). Radiometric ages from the middle member EMVF sequences have large errors (fig. 2), but the rocks appear to be older than about 81.5 Ma and possibly as young as around 79 Ma. On the east side of the Boulder Batholith, Klepper and others (1971) described 1.5 km of the middle member EMVF near Elkhorn, MT, located on the eastern flank of the Boulder Batholith (fig. 1). The Elkhorn section has not been stratigraphically correlated with more recent studies of the middle member EMVF along its eastern contact with the Boulder Batholith, where a 0.7-km-thick section formed between about 83.5 and 84.5 Ma (Olson and others, 2016; Scarberry and others, this volume).

From Highway 2 heading east, turn right (south) after 6.4 mi at MacDonald Pass (46.56141°N, 112.30889°W). Take the main road south and then up the hill towards the Continental Divide Trail jump-off.

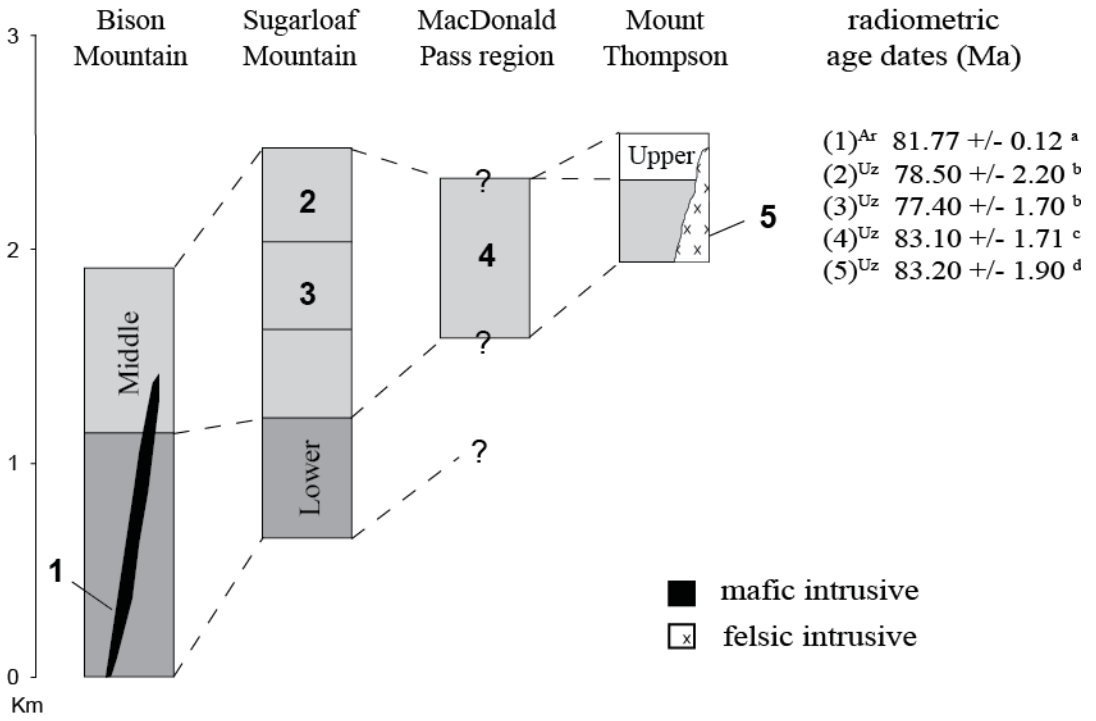

Figure 2. Correlation diagram illustrating the continuity of the lower, middle, and upper member EMVF rocks over a distance of about 30 km along the western margin of the Boulder Batholith. Volcanic stratigraphy: Sugarloaf Mountain 7.5′ (Scarberry, 2016); Bison Mountain 7.5′ (Scarberry and others, 2018); Mount Thompson 7.5′ (Becraft and others, 1963; Olson and others, 2017). The thickness and stratigraphic position of the EMVF at MacDonald Pass is uncertain. Ar, 40Ar/39Ar age; Uz, U/Pb age from zircon. Data sources: (a) Scarberry and others, 2018; (b) Korzeb and others, 2018; (c) Mahoney and others, 2015; (d) Olson and others, 2017.

STOP 1A: MacDonald Pass–Along the Road to the Continental Divide Trail Jump-Off

Outcrops of middle member EMVF welded ignimbrite occur along the right (south) side of the road at: (a) odometer: 6.8 mi; 46.55702°N, 112.31004°W, and (b) odometer: 6.9 mi; 46.55802°N, 112.30826°W. At this stop you can see rheomorphic flow-bands in the ignimbrite that formed near the base of a hot pyroclastic density flow under ductile shear conditions (fig. 3). The ignimbrite is crystal-rich (about 20–25%) with plagioclase laths that are up to 7 mm long. Conspicuous biotite constitutes 2–5% of the crystal population. Flow-bands and planar exsolution parting surfaces are oriented roughly N5°E and dip about 20°NW. Stretching lineations indicate approximately N–S bi-directional flow. Look for rotated porphyroclasts (fig. 3) to determine flow direction.

STOP 1B: MacDonald Pass–Continental Divide Trail Jump-Off (Odometer: 7.0 mi; 46.55749°N, 112.30830°W)

At this stop crystal-rich welded ignimbrite of the middle member EMVF is intruded by granodiorite satellite plutons of the Boulder Batholith. Mahoney and others (2015) reported U-Pb zircon ages of 83.1 ± 1.7 Ma for the ignimbrite and 81.4 ± 1.9 Ma and 81.7 ± 1.4 for granodiorite at MacDonald Pass. The age of the ignimbrite at MacDonald Pass correlates with ages for the middle member EMVF (fig. 2; Olson and others, 2016; Scarberry and others, this volume). The granodiorite plutons at MacDonald Pass are roughly the same age as the Unionville Granodiorite (Lund and others, 2002), located about 10 mi (16 km) south of MacDonald Pass.

Return to Highway 2, turn left (west) and head back towards Elliston. Pull off to the right (north) side of Highway 2 at the MacDonald Pass Spring.

STOP 2: MacDonald Pass Spring (Odometer: 9.5 mi; 46.55919°N, 112.34398°W)

At this stop you can see banded pumice (fig. 4A) in massive, vitroclastic, crystal-rich (20%) ignimbrite. Abundant pyroclasts are up to 7 cm long and encased in a devitrified matrix with abundant small 1–2 mm plagioclase, hornblende and pyroxene phenocrysts, and 2–5% accessory magnetite. The mafic minerals

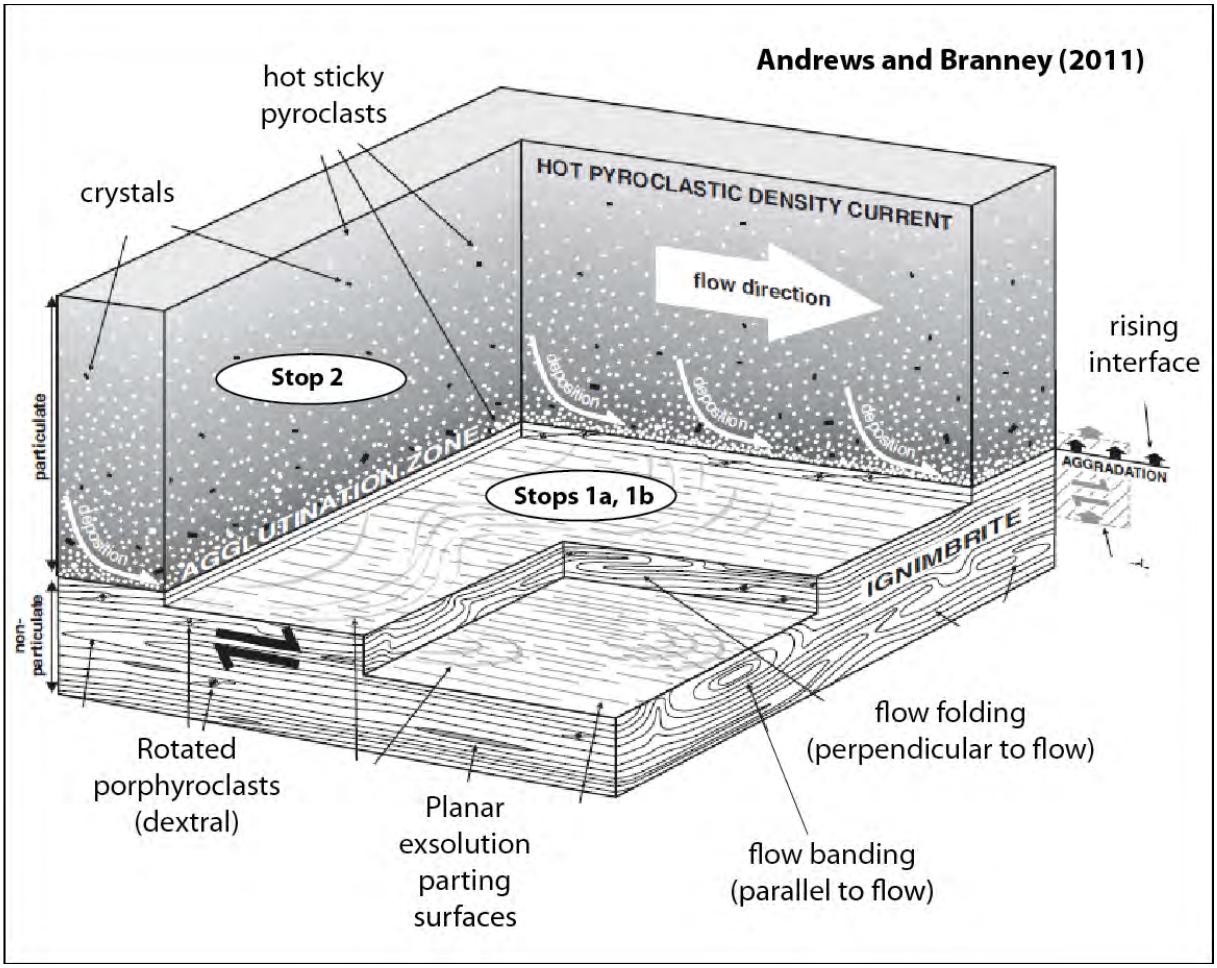

Figure 3. Components of a hot pyroclastic density current, or ignimbrite, after Andrews and Branney (2011).

are semi-chloritized. Leucocratic granitic clasts and partially resorbed red and glassy scoria pyroclasts are fragmental and 1–2 cm long.

Walk down the north side of the highway, to the west, and look at another outcrop of this ignimbrite. Crude flow-banding is visible and oriented about N80°E, dipping 15°SE. Bidirectional flow lineations are oriented about N50°E. Look for rotated porphyroclasts (fig. 3) to determine shear-sense and flow direction of the ignimbrite. The relatively coarse nature of pyroclasts in the ignimbrite at this stop suggests that the unit is a facies of a lag breccia deposit, which is a coignimbrite lithic breccia that forms from a collapsing eruption column, and during caldera collapse (e.g., Walker, 1985; Druitt and Bacon, 1985).

Part 2: The Lower Member of the Elkhorn Mountains Volcanic Field

The lower member of the EMVF consists largely of pyroxene-bearing andesitic lavas, flow-banded rhyodacite lavas, and pyroclastic and epiclastic volcanic deposits that are about 85 Ma or older. Lower member EMVF sequences are about 1.2 km and 0.5 km thick in the Bison Mountain and Sugarloaf Mountain 7.5′ quadrangles, respectively, but the lower member pinches out entirely to the east, towards Mount Thompson (fig. 2).

Reconnaissance geochemical sampling of the EMVF section in the Bison Mountain 7.5′ quadrangle shows that the top of the section correlates with lower member EMVF dacite porphyry flow-dome complexes and the base of the middle member EMVF ignimbrite “A” from the east flank of the Boulder Batholith (fig. 5). In the Bison Mountain 7.5′ quadrangle, a sequence of locally coarse volcanic breccia (fig. 4B) forms the top 450 m of the lower member EMVF and the bottom 500 m consist of andesitic lava flows. Many of the lava flows contain amygdule zones consisting of elliptical vesicles filled with amorphous calcite and quartz.

In the northern Elkhorn Mountains, between Boulder and Helena (fig. 1), Smedes (1966) described about 650 m of andesitic epiclastic and volcaniclastic sedimentary deposits that are intruded by mafic sills, and interstratified with andesite tuffs and amygdaloidal

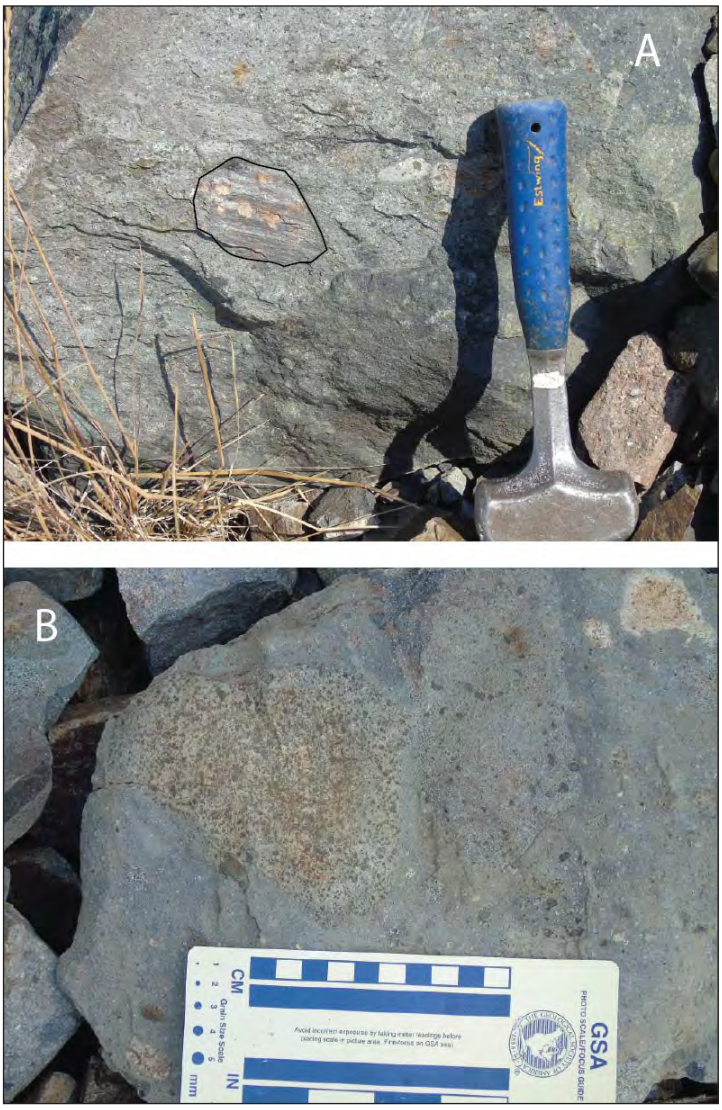

Figure 4. (A) Banded pumice in ignimbrite at Stop 2. (B) Coarse volcanogenic breccia collected from the Big Dick Mine on the east side of the Little Blackfoot River (see fig. 5 for location).

basaltic lavas. Anywhere from 1.7 to 2.2 km of the lower member EMVF is continuously exposed on the east side of the Boulder Batholith, near Dry Mountain (Prostka, 1966), where it thins rapidly northward to about 0.5 km thick in the Ratio Mountain 7.5′ quadrangle (fig. 1). Olson and others (2016) dated the top of the lower member EMVF at around 84.5 Ma, which currently is the only radiometric age reported from lower member EMVF rocks.

Continue west on Highway 2 towards Elliston. Turn left (south) on to the Little Blackfoot River Road just before entering Elliston (odometer: 13.2 mi; 46.55663°N, 112.41354°W). Continue south on the Little Blackfoot River Road. After about 3.0 mi the road forks; stay right (west; odometer: 16.2 mi; 46.51800°N, 112.39296°W). Continue for another 5.4 mi, where the road forks again; stay right (west) to-

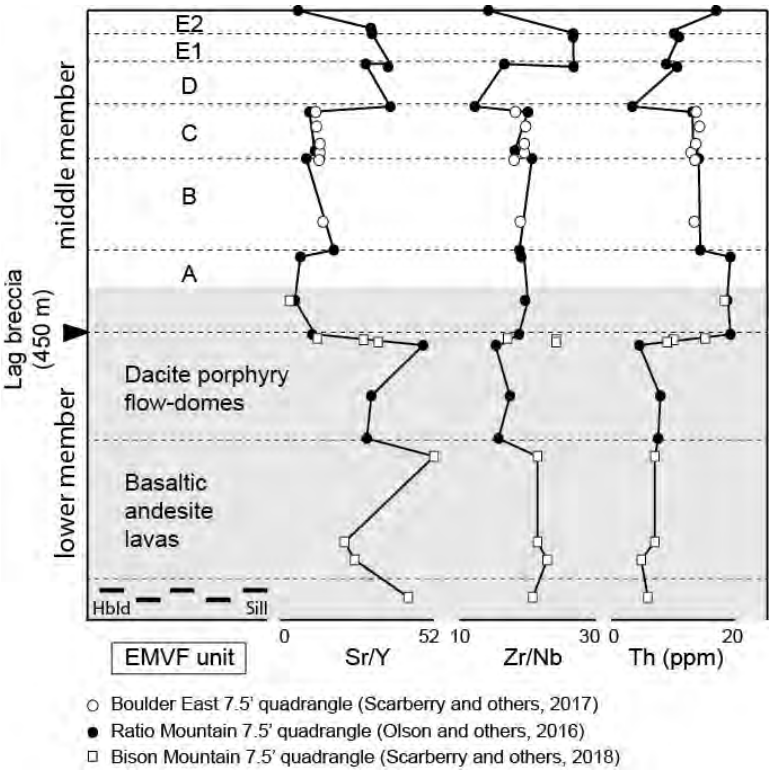

Figure 5. Simplified geologic map highlighting the major faults, veins, and distribution of mines in the Bison Mountain 7.5′ quadrangle, after Scarberry and others (2018).

wards Kading Campground. Pull into the parking area on the right (west) side of the road, about 0.1 mi past the fork in the road.

STOP 3: Kimball Mine Dumps and Middle EMVF Basaltic Andesite–Dacite Breccia and Welded Tuff (Odometer: 21.7 mi; 46.45753°N, 112.41946°W)

Hike north along the Little Blackfoot River Road for about 275 ft, then walk up the road to the left (west) about 200 ft to the Kimball Mine. The ore bin is on the left (west) side of the path just as you turn the corner to the mine bench. The Kimball Mine is one of several Ag–Zn–Pb lode mines that exploit predominately E–W-trending vein systems that occupy the Boulder Batholith–EMVF contact zone in the Bison Mountain 7.5′ quadrangle (fig. 6). Collectively these lode mines have produced Au, Ag, Cu, Pb, and Zn (table 1) valued today at around 15 million dollars.

Follow the mine bench to the north and hike northwest through the forest for about a fifth of a mile to another sulfide-bearing mine dump. The adit here, although now caved, is on a vein oriented N80°W. Ore minerals include chalcopyrite, galena, arsenopyrite, pyrite ± tetrahedrite.

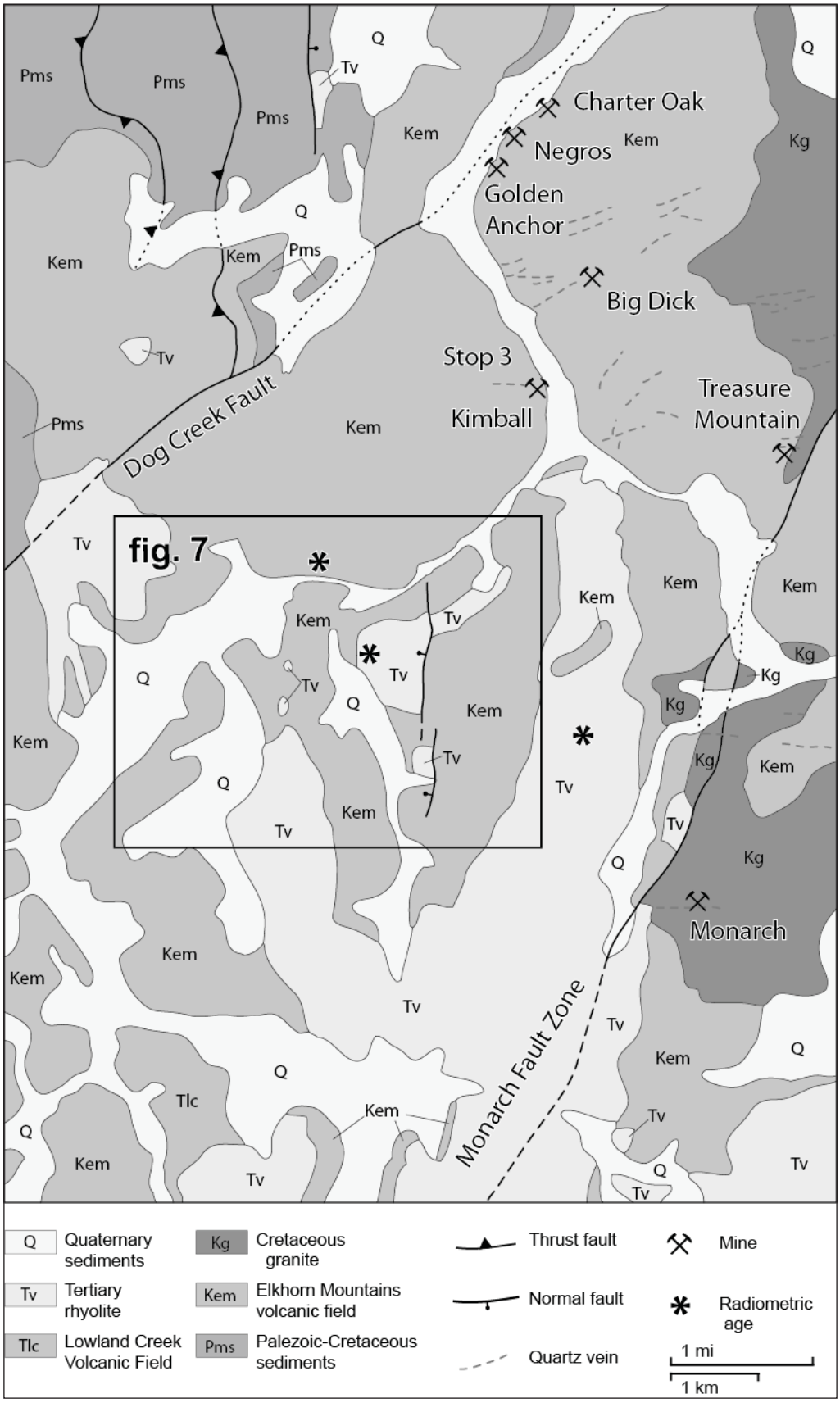

Figure 6. Simplified geologic map of the Larabie Gulch region in the Bison Mountain 7.5′ quadrangle, after Scarberry and others (2018).

Table 1. Historic precious and base metal production from lode mines in the Bison Mountain 7.5' quadrangle.

Mine	Au (oz.)	Ag (oz.)	Cu (lbs.)	Pb (lbs.)	Zn (lbs.)	Operating Date	Host Rock
Monarch (Mine and Mill)	157	10,677	25,034	96,514	48	1894–1909, 1916	BB/EMVF
Kimball Mine	-	-	-	-	-	-	EMVF
Treasure Mountain Mine	-	-	-	-	-	-	BB/EMVF
Big Dick (Mill and Tailings)	7,687	51,236	1,870	716,553	3,800	1902–1954	EMVF
Charter Oak (Mine and Mill)	382	39,146	10,041	672,046	168,270	1916–1966	EMVF
Negros Mine	170	6,118	808	132,026	10,083	1946–1968	EMVF
Golden Anchor	-	-	-	-	-	Active in 1973	EMVF
Totals	**8,396**	**107,177**	**37,753**	**1,617,139**	**182,201**	**1894–1973**	

Note. Compiled from Hargrave and others (1998). BB, Boulder Batholith; EMVF, Elkhorn Mountains Volcanic Field.

Continue west up the hill for about a tenth of a mile to examine outcrops of basaltic andesite–dacite breccia. In many places these rocks appear to be sub-angular to sub-rounded, and poorly sorted volcanogenic sediments; possibly lahar deposits. In other places, particularly in the northeastern corner of the Bison Mountain quadrangle, near the Big Dick Mine (fig. 6), these rocks are clearly a coarse lithic breccia (fig. 4B), which is up to 450 m thick (Scarberry and others, 2018). Weathered surfaces appear to show polylithic clast populations (fig. 4B), but the clast populations are generally monolithic when fresh surfaces are compared. The clasts and matrix are andesitic–dacitic compositions that have been affected to various degrees by greenschist- (chlorite and epidote) and hornfels-type metamorphic conditions (P <2 kbars; T ~300–700°C). We interpret these rocks to represent lag deposits that formed during caldera collapse and were subsequently reworked, metamorphosed, and locally mineralized during emplacement of the Boulder Batholith.

Hike back to the vehicle and continue south on the Little Blackfoot River Road. Basaltic andesite lavas are present on the right (west) side of the road after about 1.3 mi. Continue for another 0.7 mi and park on the left (east) side of the road next to the Little Blackfoot River (odometer: 23.5 mi). Hike about 300 ft up the road to the west, cross the road to the north, and then hike another 350 ft northwest up the hill.

STOP 4: Coarse Hornblende Lamprophyre Intruding a Lower Member EMVF Lava Package (Odometer: 23.5 mi.; 46.43984°N, 112.44764°W)

At this stop you can see a coarse hornblende diorite lamprophyre sill that intrudes andesitic lava flows of the lower member EMVF. The sill has 3- to 5-mm-long hornblende crystals, and smaller quartz and plagioclase phenocrysts set in a blue to gray groundmass. A coarse hornblende separate from the intrusion has a ^{40}Ar-^{39}Ar age of 81.77 ± 0.21 Ma (Scarberry and others, 2018; Scarberry and others, this volume).

Stops 5 and 6 are located in Larabee Gulch (fig. 7), which can be seen directly to the south at stop 4. Larabee Gulch was created by glacial ice movement during the last Pleistocene glacial advance about 25,000 to 21,000 years ago (Ruppel, 1962). The lower member EMVF andesite lava sequence is visible in the hillside to the SSW, on the west side of Larabee Gulch, where the section strikes NNW and dips about 25° towards the west.

From Stop 4 head south on foot and cross the Little Blackfoot River, then hike south along the lowest ridge on the east side of Larabee Gulch for about 0.4 mi to Stop 5A.

STOP 5A: Lower Member EMVF Lava Section (46.43372°N, 112.45035°W)

At stop 5A you will see cliffy and massive outcrops of vesicular and amygdaloidal lower member EMVF lava flows. The lavas are two-pyroxene andesites that contain plagioclase phenocrysts and secondary reddish-purple hematite in places. Calcite is a common phase in the amygdules, which record low-temperature hydrothermal alteration, perhaps related to caldera resurgence following eruption of the middle member EMVF from a nearby vent. Lower member EMVF lavas are also characterized by autobreccia, horizontal vesicular zones, and steeply dipping vesicle pipes. At this stop, the lava section is oriented about N45°E and dips around 20° to the NW.

Continue southwest on foot for another 370 ft to Stop 5B (fig. 7)

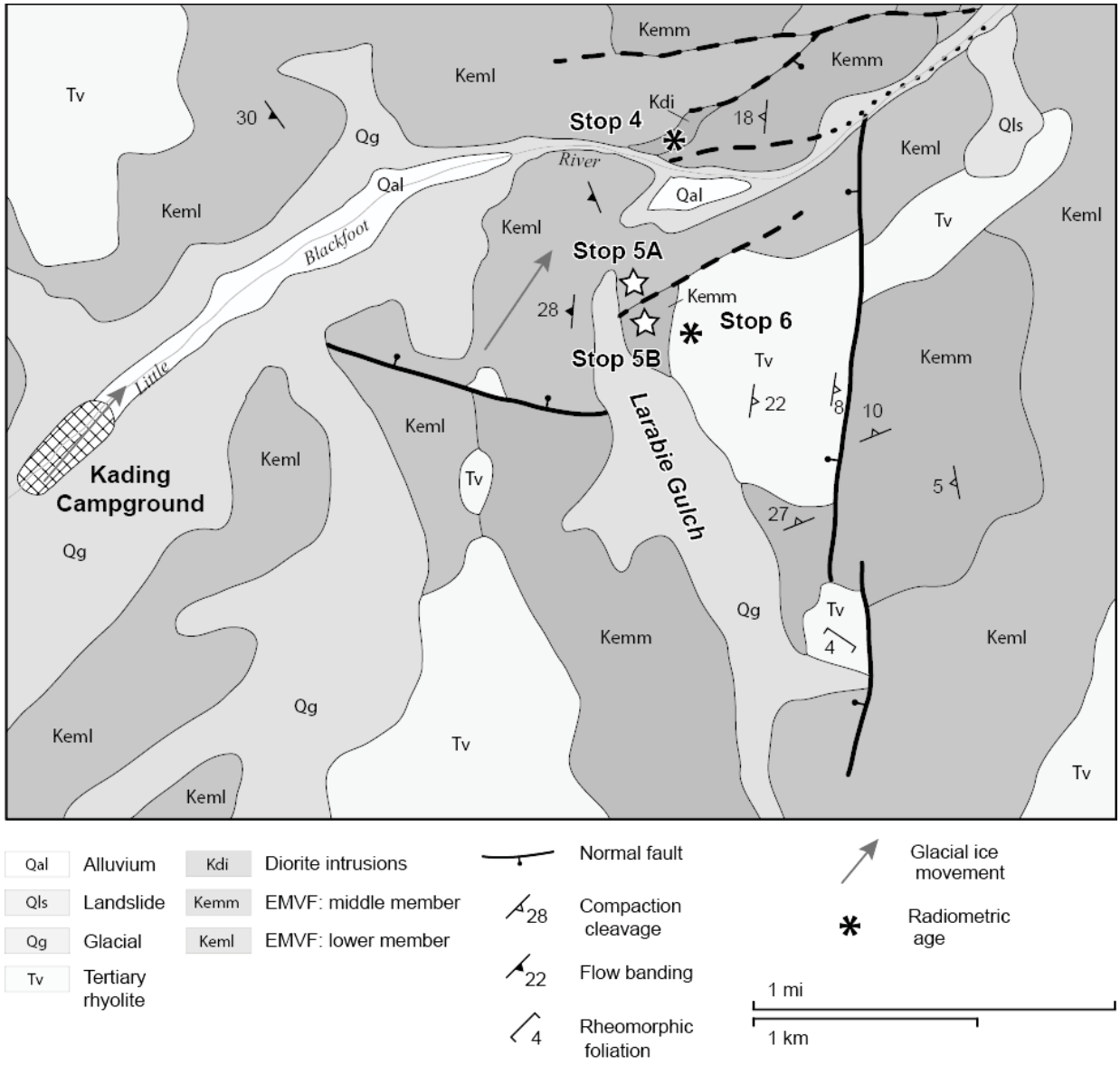

Figure 7. Geochemical stratigraphy of the middle and lower members of the EMVF.

STOP 5B: Middle Member EMVF Rhyolite Flow-Dome with Lower Member EMVF Basaltic Andesite Lava Rip-Up (46.43292°N, 112.44945°W)

At Stop 5B you can see "oatmeal" textured, flow-banded rhyolite lavas that cap the andesitic lava flow sequence. The oatmeal rhyolites cap andesite lavas at isolated locations throughout the Bison Mountain 7.5′ quadrangle. These oatmeal rhyolite deposits may represent small flow-dome complexes related to caldera resurgence because they are often in proximity to amygdule-rich sections of andesite lava flows. Blocks of pyroxene andesite up to 2 m wide occur in the oatmeal-textured flow domes at this stop. Some of the rhyolite has been polished and striated by Pleistocene glacial ice. The glacial striations trend about N65°W.

Continue west–southwest for about 600 ft to Stop 6 (fig. 7).

STOP 6: Tertiary Rhyolite Ignimbrite–Hike (46.43222°N, 112.44712°W)

At stop 6 you can see the base of a Tertiary rhyolite ignimbrite. The rock is white and crystal-rich (25%) and contains sanidine, smoky quartz, biotite phenocrysts, and glass. Lithic fragments in the base of the ignimbrite are up to 6 cm wide (Ruppel, 1963). The ignimbrite is up to 250 m thick in the Bison Mountain 7.5′ quadrangle and likely formed during a single explosive eruption at about 37 Ma. A sanidine separate obtained from rhyolite collected at this stop yielded a ^{40}Ar-^{39}Ar age of 37.42 ± 0.05 Ma, whereas a sanidine separate from a sample of the top of the ignimbrite, to the east (see fig. 6), yielded a ^{40}Ar-^{39}Ar age of 37.43 ± 0.05 Ma (Scarberry and others, 2018).

Ruppel (1963) proposed that as much as 430 m of paleotopography channeled the movement of Tertiary silicic lavas and tuffs in the region. Observations from mapping in the Bison Mountain 7.5′ quadrangle support this interpretation because the tuffs are rheomorphic and complexly deformed where they erupted through uneven terrain, crystallized, and continued to flow. In the Monarch Fault Zone, located in the eastern quarter of the Bison Mountain 7.5′ quadrangle (fig. 6), about 75 m of rheomorphic ignimbrite is buttressed into late Cretaceous granite along a N–S-trending zone that we interpret as a pre-ignimbrite normal fault. Stretching lineations in the ignimbrite mimic the orientation of its contact with the granite. Based on these observations, we propose that as much as 250 m of normal slip occurred along predominantly N–S-trending faults prior to about 37 Ma in the Bison Mountain 7.5′ quadrangle.

ACKNOWLEDGMENTS

We thank Bruce Cox for sharing his mapping in the Bison Mountain quadrangle. These maps were made by Bruce when he worked for Earthworks, Inc., and was consulting for Homestake Mining Company to examine the geology of part of the Bison Mountain 7.5′ quadrangle. Susan Smith (MBMG) helped immensely with developing figures.

REFERENCES CITED

Andrews, G.D.M., and Branney, M.J., 2011, Emplacement and rheomorphic deformation of a large, lava-like rhyolitic ignimbrite: Gray's Landing, southern Idaho: Geologic Society of America Bulletin, v. 123, p. 725–743.

Becraft, G.E., Pinckney, D.M., and Rosenblum, S., 1963, Geology and mineral deposits of the Jefferson City Quadrangle, Jefferson and Lewis and Clark Counties, Montana: U.S. Geological Survey Professional Paper 428, 101 p.

Druitt, T.H., and Bacon, C.R., 1985, Lithic breccia and ignimbrite erupted during the collapse of Crater Lake Caldera, Oregon: Journal of Volcanology and Geothermal Research, v. 29, p. 1–32.

Hargrave, P.A., Bowler, T.P., Lonn, J.D., Madison, J.P., Metesh, J.J., and Wintergerst, R., 1998, Abandoned–inactive mines of the Blackfoot and Little Blackfoot River drainages, Helena National Forest Volume II: Montana Bureau of Mines and Geology Open-File Report 368, 159 p.

Klepper, M.R., Ruppel, E.T., Freeman, V.L., and Weeks, R.A., 1971, Geology and mineral deposits, east flank of the Elkhorn Mountains, Broadwater County, Montana: U.S. Geological Survey Professional Paper 665, 1:48,000 scale.

Korzeb, S.L., Scarberry, K.C., and Zimmerman, J.L., 2018, Interpretations and genesis of Cretaceous age veins and exploration potential for the Emery mining district, Powell County, Montana: Montana Bureau of Mines and Geology Bulletin 137, 49 p., map plate.

Lageson, D., Schmitt, J., Horton, B., Kalakay, T., and Burton, B., 2001, Influence of Late Cretaceous magmatism on the Sevier orogenic wedge, western Montana: Geology, v. 29, p. 723–726.

Lund, K., Aleinikoff, J., Kunk, M., Unruh, D., Zeihen, G., Hodges, W., duBray, E., and O'Neill, J., 2002, SHRIMP U-Pb and $^{40}Ar/^{39}Ar$ age contrasts for relating plutonism and mineralization in the Boulder Batholith region, Montana: Economic Geology, v. 97, p. 241–267.

Mahoney, J.B., Pignotta, G.S., Ihinger, P.D., Wittkop, C., Balgord, E.A., Potter, J.J., and Leistikow, A., 2015, Geologic relationships in the northern Helena Salient, Montana: Geology of the Elliston Region: Northwest Geology, v. 44, p. 109–136.

Olson, N.H., Dilles, J.H., Kallio, I.M., Horton, T.R., and Scarberry, K.C., 2016, Geologic map of the Ratio Mountain 7.5′ quadrangle, southwest Montana: Montana Bureau of Mines and Geology EDMAP 10, 1 sheet, scale 1:24,000.

Olson, N.H., Sepp, M.D., Dilles, J.H., Mankins, N.E., Blessing, J.M., and Scarberry, K.C., 2017, Geologic map of the Mount Thompson 7.5′ quadrangle, southwest Montana: Montana Bureau of Mines and Geology EDMAP 11, 13 p., 11 sheets, scale 1:24,000.

Prostka, H.J., 1966, Igneous geology of the Dry Mountain quadrangle, Jefferson County, Montana: U.S. Geological Survey Bulletin 1221-F, scale 1:24,000.

Reynolds, M.W., 1979, Character and extent of Basin–Range faulting, western Montana and east-central Idaho, *in* Newman, G., and Goode, H., eds., 1979 Basin and Range Symposium: Rocky Mountain Association of Geologists and Utah Geological

Association, p. 185–193.

Ruppel, E.T., 1962, A Pleistocene ice sheet in the northern Boulder Mountains, Jefferson, Powell, and Lewis and Clark Counties, Montana: U.S. Geological Survey Bulletin 1141-G, 22 p.

Ruppel, E.T., 1963, Geology of the Basin quadrangle, Jefferson, Lewis and Clark, and Powell Counties, Montana: U.S. Geological Survey Bulletin 1151, 121 p., scale 1:62,500.

Rutland, C., Smedes, H., Tilling, R., and Greenwood, W., 1989, Volcanism and plutonism at shallow crustal levels: The Elkhorn Mountains Volcanics and the Boulder Batholith, southwestern Montana, *in* Henshaw, P., ed., Volcanism and plutonism of western North America, vol. 2, Cordilleran volcanism, plutonism, and magma generation at various crustal levels, Montana and Idaho: Field trips for the 28th International Geological Congress: American Geophysical Union, Monograph, p. 16–31.

Scarberry, K.C., 2016, Geologic map of the Sugarloaf Mountain 7.5′ quadrangle, Deer Lodge, Jefferson, and Powell Counties, Montana: Montana Bureau of Mines and Geology Open-File Report 674, 1 sheet, scale 1:24,000.

Scarberry, K.C., Coppage, E.L., and English, A.R., 2018, Geologic map of the Bison Mountain 7.5′ quadrangle, Powell and Jefferson Counties, Montana: Montana Bureau of Mines and Geology Geologic Map 71, 10 p., 1 sheet, scale 1:24,000.

Schmidt, R.G., Loen, J.S., Wallace, C.A., and Mehnert, H.H., 1994, Geology of the Elliston region, Powell and Lewis and Clark Counties, Montana: U.S. Geological Survey Bulletin 2045, 25 p., scale 1:62,500.

Smedes, H.W., 1966, Geology and igneous petrology of the northern Elkhorn Mountains, Jefferson and Broadwater counties, Montana: U.S. Geological Survey Professional Paper 510, 116 p.

Stickney, M.C., Haller, K.M., and Machette, M.N., 2000, Quaternary faults and seismicity in western Montana; Montana Bureau of Mines and Geology Special Publication 114, 1 sheet, scale 1:750,000.

Vuke, S.M., Porter, K.W., Lonn, J.D., and Lopez, D.A., 2007, Geologic map of Montana: Montana Bureau of Mines and Geology Geologic Map 62A, scale 1:500,000.

Walker, G.P.L., 1985, Origin of coarse lithic breccias near ignimbrite source vents: Journal of Volcanology and Geothermal Research, v. 25, p. 157–171.

Wallace, C.A., Lidke, D.J., and Schmidt, R.G., 1990, Faults of the central part of the Lewis and Clark line and fragmentation of the Late Cretaceous foreland basin in west-central Montana: Geological Society of America Bulletin, v. 102, p. 1021–1037.

MULTIPHASE EXTENSION IN THE HANGING WALL OF THE ANACONDA DETACHMENT ZONE

Colleen Elliott

Montana Bureau of Mines and Geology

INTRODUCTION

The purpose of this field trip is to examine unconformity-bounded sequences in the hanging wall of the Anaconda Detachment Zone to learn about the extension history of the Anaconda Metamorphic Core Complex (AMCC). We will see evidence for two to three phases of Cenozoic extension, adding new dimension to current interpretations of the Cenozoic history of southwest Montana.

Stops are in or near the town of Anaconda, which has been the locale for previous AMCC field trips (O'Neill and Lageson, 2003; Kalakay and others, 2003; Lonn and Elliott, 2010). There are two very good reasons to return to Anaconda: the excellent exposures and the excellent access. Together they reveal a devilishly complicated geologic history that would be impossible to work out anywhere else.

BACKGROUND

The AMCC forms the high peaks of the Flint Creek and Anaconda Ranges. It is separated from the valley floor by the Anaconda Detachment Zone, whose known extent is at least 60 mi, from Gold Creek at the north end of the Flint Creek Range to beyond Pintler Lake on the south side of the Anaconda Range (fig. 1). It is a detachment zone rather than a detachment fault because for much of its length two or more fault strands that dip between 10° and 20° separate the valleys from the ranges. The different detachment strands

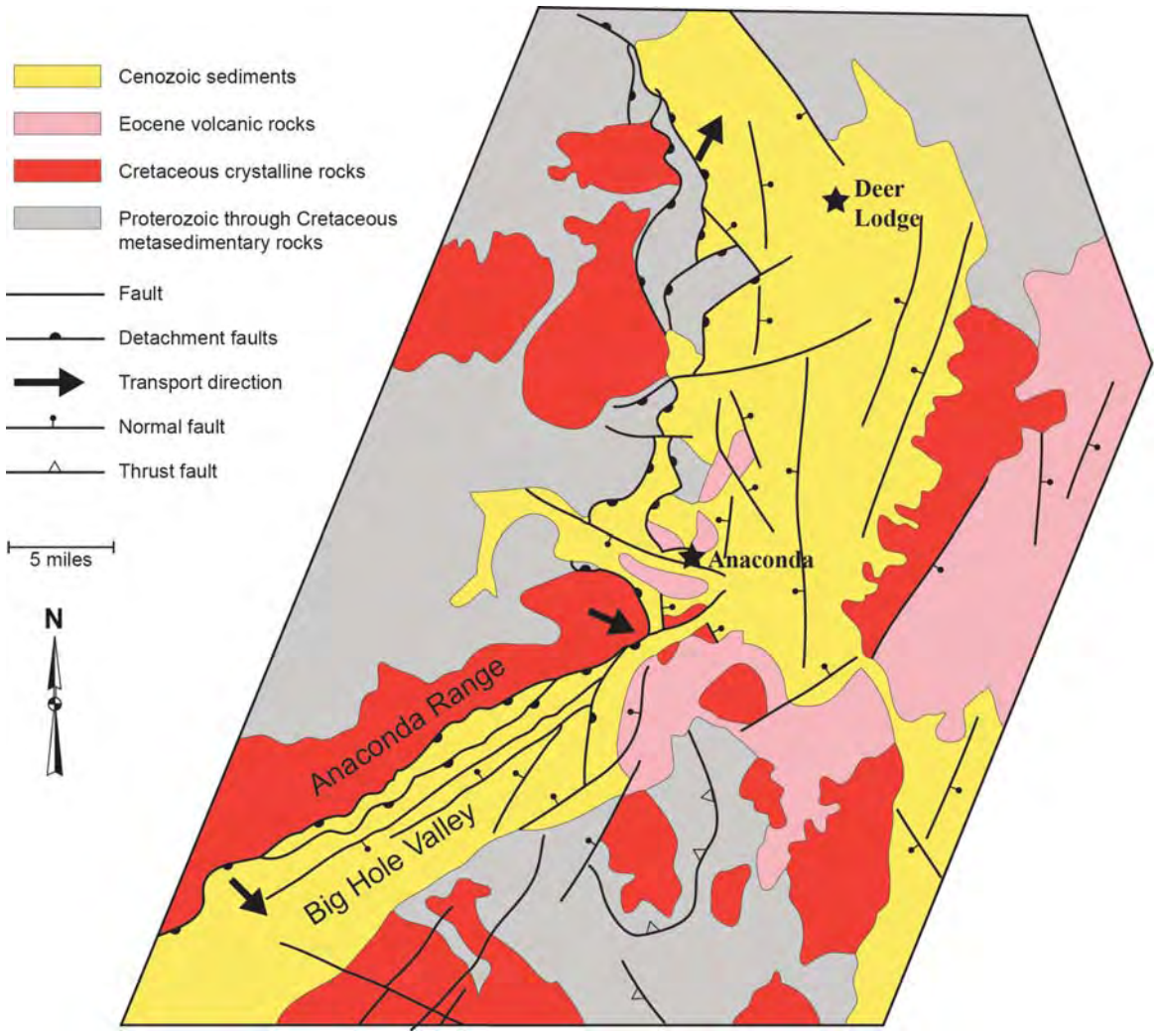

Figure 1. Generalized regional geologic map showing the known extent of the Anaconda Detachment zone.

and steep antithetic and synthetic normal faults bound small and large sedimentary basins, some of which have unique depositional histories. We will visit some of these basins to see what each reveals about extensional tectonics.

The AMCC is one of a series of core complexes that extend south from southern British Columbia to Mexico that formed as contraction on the North American Cordillera waned (Coney, 1980; Foster and others, 2007, 2010; Yonkee and Weil, 2015). It is also the most recently identified (O'Neill and others, 2004), although Emmons and Calkins (1913) recognized over a century ago that the Anaconda and Flint Creek ranges had undergone extension on shallowly dipping faults. The AMCC is composed of metamorphosed Mesoproterozoic through Early Cretaceous sedimentary rocks and Cretaceous through Eocene igneous rocks, all of which enjoyed a multifaceted tectonic history (Lonn and others, 2003; Berger and Elliott, 2007; Lonn and Elliott, 2010, 2011). Cretaceous amphibolite facies metamorphism (Haney, 2008) was followed by one or more retrograde metamorphic events (Berger and Elliott, 2007). This means that, unlike the ideal core complex described by Coney (1980), there are high-grade metamorphic rocks in both the hanging wall and footwall of the AMCC.

Absolute ages of exhumation and extension of the AMCC come from multi-mineral $^{40}Ar/^{39}Ar$ thermochronology data that demonstrate that rapid extension began around 53 Ma and continued to about 39 Ma (Eocene; Foster and others, 2007, 2010). Apatite fission-track data indicate that footwall exhumation continued to about 27 Ma (Oligocene; Foster and others, 2010). The youngest dated rocks offset by the Anaconda Detachment are latest Oligocene sediments of the upper Renova Group (Scarberry and others, in review). New mapping in the Big Hole Valley (Elliott and Lonn, in review) indicates that extension there continued into the Pliocene. Overall, evidence is strong for more than 25 Ma of extension and exhumation of the AMCC.

O'Neill and others (2004), Grice (2006), and Foster and others (2010) report extension toward about 115° based on lineations measured in the greenschist facies mylonites of the detachment zone. New mapping at the north and south ends of the detachment zone, however, tells a more complicated story: between Mount Powell to the north end of the Flint Creek Range, extension lineations plunge shallowly toward about 025° (Scarberry and others, in review; fig. 1). At the base of Mount Powell there are two sets of lineations—one that trends towards 025°, and an overprinting set that trends towards about 115° (Elliott and others, 2013). In the Big Hole Valley, extension lineations trend 140–160° (Elliott, 2015; Elliott and Lonn, in review; Howlett and others, in review). The simplest explanation for this variation is sequential change of extension direction from top northeast to top east–southeast to top southeast, though the relative timing of the three phases of extension are not well established.

On this trip, we will look at three volcanic and sedimentary packages that are separated by angular unconformities. In figure 2 they are distinguished as "Lower volcanic sequence," "Middle volcanic sequence," and "upper volcanic sequence."

ROAD LOG

This road log starts in Anaconda. Stops are shown on figures 2 and 3. Most stops are close to the road, but some will require scrambles on steep slopes.

Drive west on Commercial Street through town to Linden Street. Turn right on Linden Street, bearing right at the Y junction with Cable Road, and pull into the parking lot on the north side of the road (it's only about 600 ft from Commercial Street to parking).

STOP 1. Lorry Thomas Urban Wildlife Area (46.140092°, -112.981248°; toilet available)

The Lorry Thomas Urban Wildlife viewing area is on Cable Road near the intersection with Linden Street. It has an accessible parking lot and a toilet. A covered bridge crosses Warm Springs Creek and leads to a short graveled walking loop around a wetland complex. The wetland is bounded on the north and east by a steep scarp of faulted and slickenlined quartzite. This outcrop was mapped as Quadrant Formation by Csejtey (1962) and Kootenai Formation by Wanek and Barclay (1966). The protolith may have been Quadrant or another clean quartzite, but the rock is now a cataclasite that is shot through with fault planes and slickenlines of many orientations. We will take the trail to the north past the duck pond. Near the left bend in the trail (near the first bench), we will go off the trail to the right and across a spring. There is a vague path here, though mid-summer vegetation might

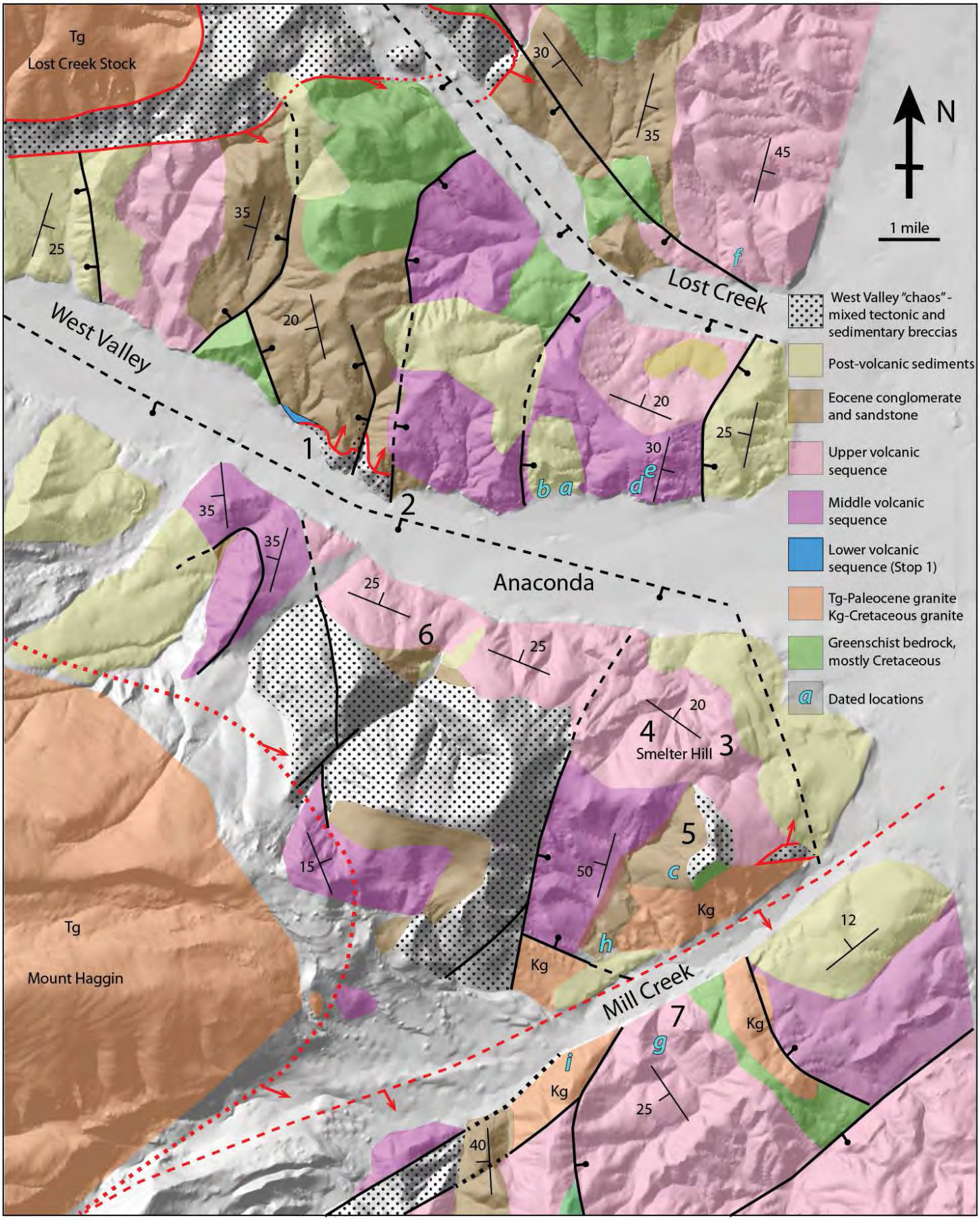

Figure 2. Generalized geologic map of Anaconda area. Uncolored areas are Quaternary sediments. Strike and dip symbols represent orientations averaged over outcrop area. Red lines are low-angle extensional faults, with arrows on the hanging wall plate showing transport direction. Black lines are faults. Bars and balls are drawn on the downthrown sides of normal faults. Field log stops are shown in large numbers (1–7).

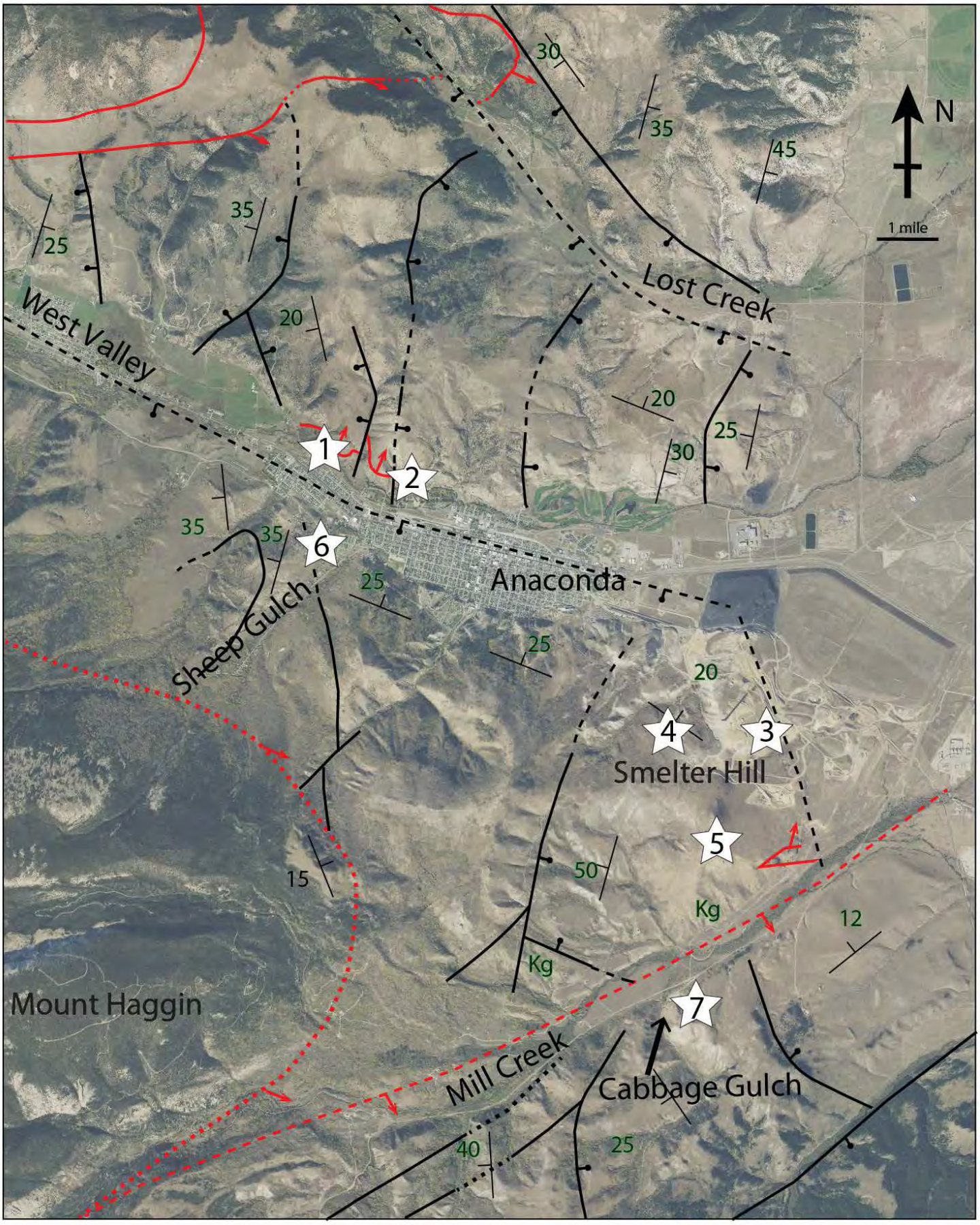

Figure 3. Aerial photographic view of Anaconda Area showing stop locations and faults.

make it hard to find. Follow the base of the scarp about 250 ft (75 m) and angle up the slope to the top of a block of quartz cataclasite that has been down-faulted towards the creek.

The cataclasite is shot through with slickenlined fault planes of all orientations, and overlain by broken quartzite–cobble conglomerate. The conglomerate appears to be resting on a shallowly dipping fault surface with northeast-trending slickenlines (fig. 4). It is possible that this is a piece of an early low-angle fault that was exposed long enough for gravel to be deposited directly on it. The fact that the cobbles are now thoroughly fractured and re-cemented attests to the deformation they later enjoyed.

If we wind our way up the slope through more cataclasite and gravel, we will see spectacular examples of fractured and re-cemented cobbles and boulders. As we angle up and to the left (west), we will begin to find cobbles and boulders cemented by a felsic volcanic matrix. Further to the west, there is more felsic volcanic matrix and less conglomerate. The volcanic material might be the base of the Lowland Creek volcanic sequence because it and the conglomerate/gravel are unconformably overlain by flows and sediments ("Lower volcanic sequence" in fig. 2) that are themselves unconformably overlain by a tuff and sediments ("Middle volcanic sequence" in fig. 2).

We can side-slope down across the volcanic rocks and muse on their significance, until one last steep skid takes us back to the valley floor and the trail.

Figure 4. Gravel on quartz cataclasite at Stop 1. Slickenlines on the top surface of the cataclasite plunge shallowly towards the north–northeast. The steep faults offsetting the slickenlines surface are down-dropped towards the valley. Orange notebook is 7.5 in long.

STOP 2. Fault Relationships at the West End of Washoe Park (46.135520°, -112.968593°)

From Stop 1, drive east on Cable Road, which merges with McCarthy Alley in about 0.25 mi. In another 0.25 mi turn left (north) and then immediately right (east) onto West Pennsylvania Avenue. Take the next left (north) onto Washoe Park Road and cross the bridge over Warm Springs Creek. Park on southeast side of road across from the large outcrop on your left.

Figure 5 shows my interpretation of the geologic relations exposed at Stop 2. The cataclasite we saw at the first stop is exposed right on the road. A vertical fault with vertical slickenlines separates the cataclasite from sandstone and shale dipping towards the fault. The sandstone underlies a generally east-dipping series of interlayered sediments, Lowland Creek pyroclastic deposits, and felsic flows (Middle volcanic sequence). There are no age data for the volcanic rocks here, but I interpret them to be equivalent to the lower Lowland Creek sequence, which erupted between 53 Ma and 52 Ma (Dudás and others, 2010; Scarberry and others, 2015).

It is a fairly easy walk up the fault scarp to the top of the ridge, which is covered with broken clasts of the quartzite-rich conglomerate ('gravel-slaw') that we saw at Stop 1.

We will stop at Washoe Park (across the street from Stop 2) for lunch and restrooms.

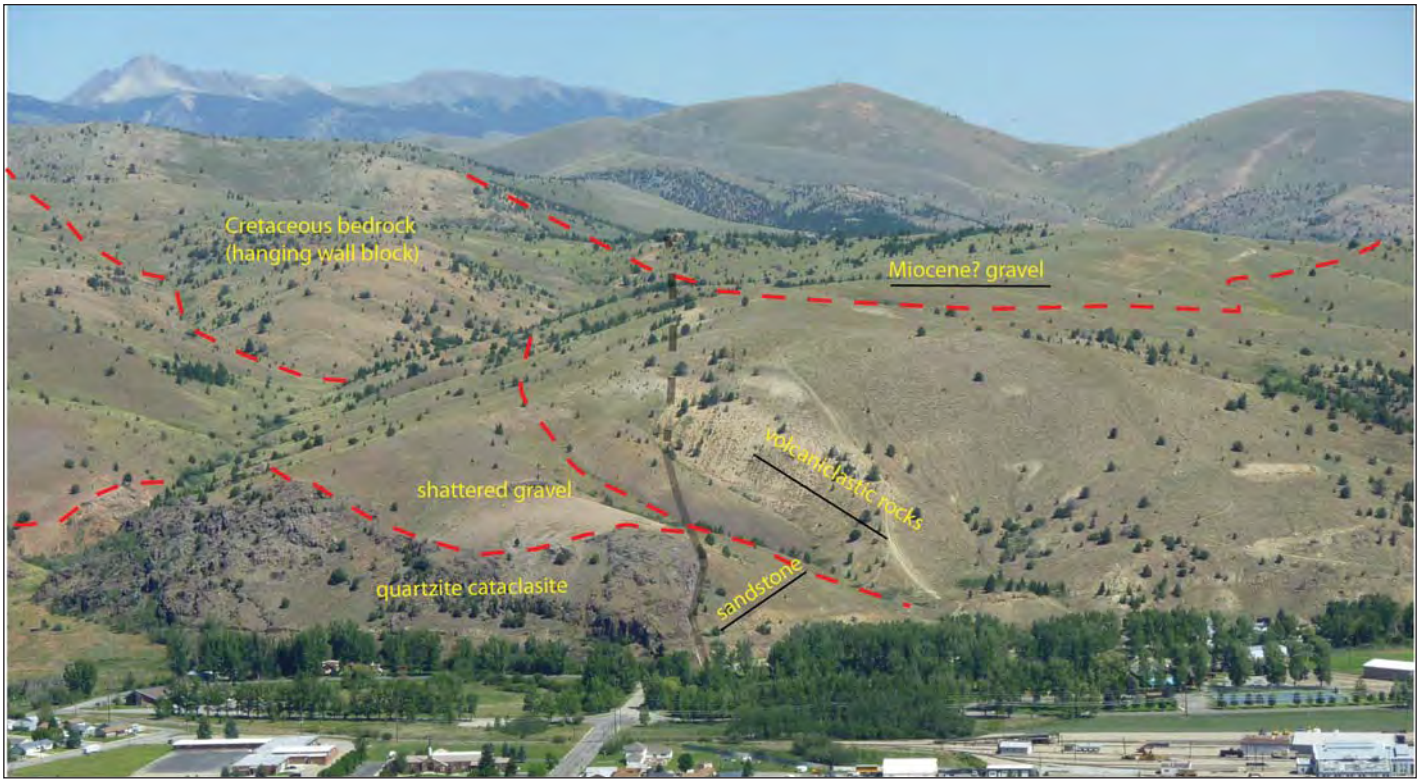

Figure 5. Oblique photo looking north towards Stop 2. Strongly brecciated quartzite on the lower left is overlain with brecciated gravel. Both are cut by a vertical fault that dropped west-dipping Eocene sandstone its east side. Cataclasite, gravel, sandstone, and fault are all overlain by gray tuff and volcaniclastic sediments.The entire sequence is overlain by unlithified cobble and boulder gravel that might be equivalent to the Miocene Sixmile Creek Formation. Thick gray line is a steep fault between quartz cataclasite and sandstone. Red dashed lines are unconformities. Black line segments are bedding traces.

Afternoon

Smelter Hill

Access to Smelter Hill is only by permission from the Atlantic Richfield Company (ARCO), who bought the Anaconda Company (and all its liabilities) in 1977. The hill is a Superfund site and undergoing remediation.

STOP 3. Sandstone at Base of Smelter Hill Tuffs (Upper Volcanic Sequence of fig. 2) (46.106247°, -112.908275°)

As we ascend Smelter Hill, we move up through a northeast-dipping sequence of well-lithified tuffaceous sandstone overlain by barely consolidated white tuff. The tuff correlates with what Dudás and others (2010) named the Upper Tuff of the Lowland Creek volcanics, which are 51–52 Ma (table 1).

Stop 3 is a road cut through the sandstone that is cut by west-dipping normal faults. The same Smelter Hill sequence is exposed on the west side of Sheep Gulch (fig. 6 and Stop 6). The sandstone at Stop 3 is equivalent to the sandstone shown in figure 6.

STOP 4. The Big Stack (46.110060°, -112.913721°)

The Washoe Smelter Stack (fig. 7) is 585 ft (178.3 m) tall, and is the tallest free-standing masonry structure in the world, or at least it was in 2017 (Gibson, 2017). It was built in 1918 in attempt to disperse sulfur- and arsenic-laden flue gases higher into the atmosphere than the older 300-ft stack at what is now the Old Works in Anaconda. The Washoe Smelter Stack operated until it was shut down by ARCO in 1980.

The Big Stack is surrounded by a gravel lag composed of well-rounded quartzite pebbles and cobbles mixed with angular clasts that include Lowland Creek porphyritic lava, garnet-bearing mylonite, and quartzite (fig. 8). The presence of mylonite clasts indicates that part of the Anaconda Detachment was already exposed and eroding when the rocks on Smelter Hill were deposited.

This is a good place to get an overview of the geology of the Anaconda area. Looking west, one can pick out the pale gray tuff that blankets the south side of the valley (fig. 6). The tuff correlates with tuff in the Lost Creek Valley that has a U-Pb detrital zircon maximum age of 51.84 ± 0.70 Ma (location f in fig. 2, table 1).

Table 1. Paleontologic and radiometric ages for Anaconda area.

Fig. 2 #	Unit/Location	Age	Age Type	Sample ID	Latitude	Longitude
a	Lower Renova Formation gravel, Old Works	**Probable Late Eocene to Early Oligocene**	Palynology	KC80816-1	46.137615°	-112.941251°
b	Lower Renova Formation gravel, Old Works	**Indeterminate Tertiary**	Palynology	KC80816-2	46.137131°	-112.944385°
c	Basal? Lowland Creek sandstone near top of Weather Hill	**Probable Tertiary**	Plant fossils	CEAS12-20	46.137131°	-112.944385°
d	Lowland Creek rhyolite intrusion, Old Works	**48.62 ± 0.09 Ma***	^{40}Ar-^{39}Ar sanidine	D1 [93-32]	46.13843°	-112.9328°
e	Lowland Creek rhyolite intrusion, Old Works	**49.17 ± 0.30 Ma**	^{40}Ar-^{39}Ar sanidine	CEAN-13	46.138624°	-112.926113°
f	Lowland Creek "upper tuff," north side Lost Creek Valley	**51.84 ± 0.70 Ma**	U-Pb zircon maximum age	CE16AN-1	46.162320°	-112.912121°
g	Dacite clast in Lowland Creek "upper tuff," Cabbage Gulch	**52.02 ± 0.2 Ma**	average of ^{40}Ar-^{39}Ar hornblende and biotite	D2 [93-06]	46.076756°	-112.925181°
h	Mill Creek, Lowland Creek sand at non-conformity above K granite	**52.1 ± 0.54 Ma**	U-Pb zircon maximum age	17DV0-4	46.08587°	-112.92746°
i	Mill Creek Highway hornblende granite	**76.3 ± 1.1 Ma§**	^{40}Ar-^{39}Ar biotite	DF02-114	46.073333°	-112.939444°

*Dudás and others, 2010.

§Foster and others, 2010.

Note. Ages are from Scarberry and others (in review) except those marked with a superscript. Locations a–i shown in figure 2.

Figure 6. Smelter Hill sequence as exposed on the west side of Sheep Gulch (Stop 6). The photo was taken from the hill on the south side of Anaconda marked on the ground by a giant "C" and looking west towards the hill marked with a giant "A." Both hills are underlain by intensely brecciated feldspathic quartzite that is probably from the Mesoproterozoic Belt Supergroup. Primary structures are locally still preserved. The yellow lines are parallel to bedding in tuffaceous sandstone that laps onto the breccia. Two sequences of more- and less-resistant sandstone are overlain by pale gray upper tuff of the Lowland Creek volcanic field.

Figure 7. The Anaconda smelter stack. It's big.

STOP 5. Weather Hill (46.097272°, -112.914842°)

Somewhere between Smelter Hill and Weather Hill we cross the contact between the northeast-dipping Upper volcanic sequence and the northwest-dipping Middle volcanic sequence, though the exact location is not clear. The maximum age of the Middle volcanic sequence is established by 52.1 ± 0.54 Ma detrital zircons from ashy sand at the nonconformity above Cretaceous granite at location h in figure 2 and table 1. The Middle volcanic sequence is therefore not much older than the Upper volcanic sequence. At Weather Hill, the Middle and Upper volcanic sequences are angularly discordant by more than 80° (fig. 9, indicating that uplift, tilting, and erosion between deposition of the two was rapid and extreme).

Outcrop at the top of Weather Hill includes marble, skarn, and jasperoid breccia with fluorite veins. Gravel surrounds Weather Hill on the west, north, and east. Yellow sandstone float near the south end of the hilltop contains plant fossil fragments that were identified as "probably Tertiary" (S. Manchester, written commun., 2013, table 1).

Figure 8. Gravels on Smelter Hill.

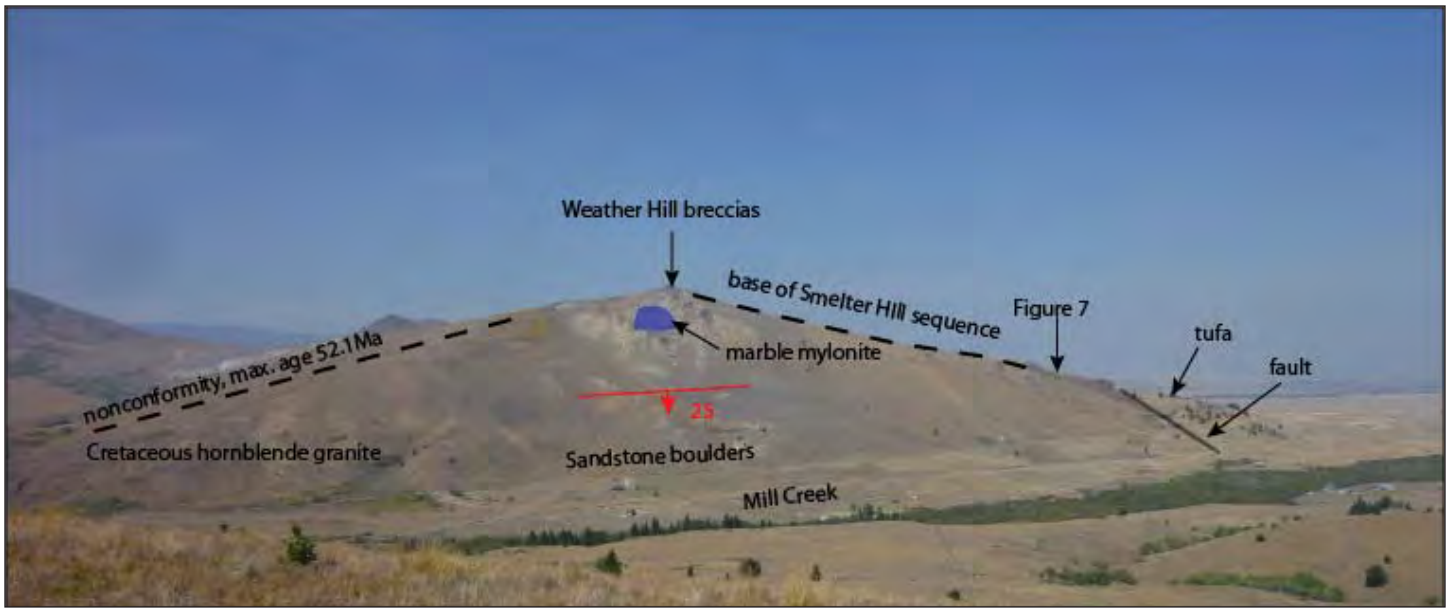

Figure 9. View of Weather Hill from the south side of Mill Creek. The dashed line on the left is the base of the earliest (?) clastic and volcaniclastic sequence. The youngest detrital zircons dated in the basal ashy sandstone are 52.1 ± 0.54 Ma (h in table 1). The blue polygon overlies an outcrop of marble with a mylonitic foliation dipping towards Mill Creek. The hillside below the marble is scruffy granite outcrops scattered with boulders of sandstone and conglomerate.

The N–S ridge at the top of Weather Hill is flanked on the west by west-dipping sediment and volcaniclastic rocks and on the east by east-dipping gravel at the base of the Upper volcanic sequence.

If there is time, let's walk down the southeast side of Weather Hill to the prominent outcrop above the railroad grade (fig. 10). The outcrop is a quartzite cataclasite overlain by broken gravel. The gravel sits on a

Figure 10. Sheared quartzite on the southeast side of Weather Hill, overlain by lag gravel, looking east. Kaleb Scarberry for scale. The inset is a close-up of the north–northeast-trending slickenlines on the top of the outcrop.

shallowly dipping surface with slickenlines plunging shallowly towards the north–northeast. This is similar to what we saw at stops 1 and 2.

The base of the east side of Weather Hill is covered by a thick layer of flat-lying tufa deposits. Tufa is a spongy calcareous rock that is the low-temperature equivalent of travertine. Tufa was once much more extensive around Weather Hill (Weed, 1905), but was mined out by the Anaconda Company. The conduit for the springs that deposited the tufa was a north-striking fault at the base of the quartzite. There is still a small active spring above the railroad grade that is forming calcite deposits.

The sequence of events represented on Weather Hill appear to be as follows:

1. Deposition of the Middle volcanic sequence after 52.1 Ma above an erosional surface on Cretaceous granite.
2. Extension on an east–northeast-dipping fault (probably the fault that forms the prominent scarp on the face of the ridge immediately west of Weather Hill), and tilting of the lower sequence.
3. Uplift and erosion, followed by deposition of the Upper volcanic sequence around 51.9 Ma.
4. Extension on an east–southeast–trending fault and tilting of both sequences.
5. South–southeast extension on the Mill Creek fault.

STOP 6. Sheep Gulch Road Sequence (46.118510°, -112.959902°)

This stop stands in for stops 3–5 for those who cannot access Smelter Hill.

From Washoe Park, follow West Pennsylvania Street east to Main Street (less than 1 mi). Drive south on Main Street for just over 0.5 mi to the T-junction at the Deer Lodge County Courthouse. Go around the west side of the court house and continue south along Sheep Gulch Road for another roughly 0.5 mi where there is a cross road and room to park on the east side of the road.

We will walk about 500 ft back towards town where a four-wheeler track leads west, skirting the base of a landslide or alluvial fan of light-colored tuff. The track leads to a quarry where there are good exposures of the same unit that is exposed on the road up Smelter Hill.

The quarry is visible near the lower left corner of figure 6.

Return to the parking spot and follow the four-wheeler track leading west. The track crosses a mound of tufa, which is well exposed past where the track curves to the left. Presumably this is the same tufa that is exposed at the base of Weather Hill. Scattered remnants of tufa can be found along the hillside on the east side of the gulch. We can debate whether the mound is really tufa (low-temperature spring deposits) or travertine (hot springs deposits).

The track follows the side of the hill, parallel to Sheep Gulch Road, and in less than 1,000 ft reaches a breccia zone that marks the base of the Smelter Hill sequence. Within the breccia are zones of broken sandstone and busted limestone, characteristic of the cataclastic deposits found along the length of the Anaconda Detachment Zone (shown as West Valley "chaos" in fig. 2). Mixed into the cataclasite are scattered, well-rounded, quartzite cobbles that weathered out of conglomerate. Some of the cobbles have been fractured and re-cemented, much like the gravels at stops 1 and 2.

The hillside steepens and trail degenerates, so we will have to backtrack a bit to find a place to scramble down to what was once a quarry along Sheep Gulch Road. There are more breccia exposures to examine near the road. There will be a large prize for anyone who finds kinematic indicators. So far I have found none, but speculate that the breccia zone marks a northeast-dipping extensional fault related to the speculative detachment exposed at Weather Hill.

STOP 7. Mill Creek Road at Cabbage Gulch (46.078823°, -112.922135°)

Retrace Main Street to West Park Street and turn right (east) at the lights. Continue east out of Anaconda and turn right onto the Mill Creek Road (MT 569) about 3 mi past the outskirts of town. In 3.4 mi angle left onto the Cabbage Gulch Road and park.

This stop allows us to look at Weather Hill and the geologic relationships exposed there (fig. 9). The south face of Weather Hill has some exposed granite and is covered near the base by boulders of coarse lithic sandstone and conglomerate.

The geometry of the hill requires that the sandstone either abutted the south face of the hill at a high angle and the contact was a fault, or it was parallel to the face of the hill and therefore dipped about 25° toward the viewer. I propose that the south face of Weather Hill is a dip slope of a detachment that extends southwest to connect to the Anaconda Detachment zone in the Big Hole Valley (fig. 1). This would represent the youngest phase of low-angle extensional faulting, with extension towards about 140°.

The quarry/shooting range near the mouth of Cabbage Gulch is a good place to examine the Lowland Creek Upper Tuff. A dacite clast within the tuff yielded ^{40}Ar-^{39}Ar ages of 51.90 ± 0.08 Ma (hornblende) and 52.06 ± 0.13 Ma (biotite), establishing the maximum age of the tuff (the upper tuff of the Lowland Creek volcanics of Dudás and others, 2010; location h in fig. 1; table 1).

REFERENCES

Berger, A., and Elliott, C.G., 2007, Detailed structural geology of the central part of the West Valley 7.5′ quadrangle, southwest Montana: Montana Bureau of Mines and Geology Open-File Report 560, 11 p., 1 sheet, scale 1:24,000.

Coney, P.J., 1980, Cordilleran metamorphic core complexes: An overview, *in* Crittenden, M.D., Coney, P.J., and Davis, G.H., eds., Cordilleran metamorphic core complexes: Geological Society of America Memoir, v. 153, p. 7–31.

Csejtey, B., 1962, Geology of the southeast flank of the Flint Creek Range, western Montana: Princeton, Princeton University, PhD dissertation, 208 p.

Dudás, F.Ö., Ispolatov, V.O., Harlan, S.S., and Snee, L.W., 2010, Ar Geochronology and geochemical reconnaissance of the Eocene Lowland Creek Volcanic Field, west-central Montana: The Journal of Geology, v. 118, p. 295–304, doi: 10.1086/651523.

Elliott, C.G., 2015, Geologic map of the Lower Seymour Lake 7.5' quadrangle, southwestern Montana: Montana Bureau of Mines and Geology Open-File Report 664, 11 p., 1 sheet, scale 1:24,000.

Elliott, C.G., and Lonn, J.D., in review, Geological map of the Long Peak 7.5' quadrangle, southwestern Montana: Montana Bureau of Mines and Geology Geologic Map, 1 sheet, scale 1:24,000.

Elliott, C.G., Smith, L.N., and Lonn, J.D., 2013, Geologic map of the Mount Powell 7.5' quadrangle, southwestern Montana: Montana Bureau of Mines and Geology Open-File Report 635, 22 p., 1 sheet, scale 1:24,000.

Emmons, W.H., and Calkins, F.C., 1913, Geology and ore deposits of the Philipsburg Quadrangle, Montana: U.S. Geological Survey Professional Paper 78, 271 p.

Foster, D.A., Doughty, P.T., Kalakay, T.J., Fanning, C.M., and Grice, W.C., 2007, Kinematics and timing of exhumation of metamorphic core complexes along the Lewis and Clark fault zone, northern Rocky Mountains, USA: Special Paper 434: Exhumation Associated with Continental Strike-Slip Fault Systems, v. 2434, p. 207–232, doi: 10.1130/2007.2434(10).

Foster, D.A., Grice, W.C., and Kalakay, T.J., 2010, Extension of the Anaconda metamorphic core complex: $^{40}Ar/^{39}Ar$ thermochronology and implications for Eocene tectonics of the northern Rocky Mountains and the Boulder batholith: Lithosphere, v. 2, p. 232–246, doi: 10.1130/L94.1.

Gibson, R.I., 2017, Mining City History: Washoe stack still the world's tallest free-standing masonry structure: Montana Standard, August 28.

Grice, W.C., 2006, Exhumation and cooling history of the Middle Eocene Anaconda metamorphic core complex, western Montana: Gainesville, University of Florida, MS thesis, 261 p.

Haney, E.M., 2008, Pressure-temperature evolution of metapelites within the anaconda metamorphic core complex, southwestern montana: Missoula, University of Montana, MS thesis.

Howlett, C.J., Reynolds, A.N., Laskowski, A.K., in review, Geologic map of the northern half of the Pintler Lake 7.5' quadrangle and the southern half of the Warren Peak 7.5' quadrangle, southwestern Montana: Montana Bureau of Mines and Geology Geologic Map, 1 sheet, scale 1:24,000.

Kalakay, T.J., Foster, D.A., and Thomas, R.C., 2003, Geometry and timing of deformation in the Anaconda extensional terrane, west-central Montana: Northwest Geology v. 32, p. 124–133.

Lonn, J., and Elliott, C.G., 2010, A walking tour of the Eocene Anaconda detachment fault on Stucky Ridge near Anaconda, Montana: Northwest Geology, v. 39, p. 81–90.

Lonn, J.D., and Elliott, C.G., 2011, Cretaceous synorogenic and Eocene post-orogenic extension in the Sevier hinterland, southwestern Montana: Geological Society of America, Rocky Mountain Section Annual Meeting, Logan, UT.

Lonn, J.D., McDonald, C., Lewis, R.S., Kalakay, T.J., O'Neill, J.M., Berg, R.B., and Hargrave, P., 2003, Geologic map of the Philipsburg 30' x 60' quadrangle, western Montana: Montana Bureau of Mines and Geology Open-File Report 483, 1 sheet, scale 1:100,000.

O'Neill, J.M., and Lageson, D.R., 2003, West to east geologic road log: Paleogene Anaconda Metamorphic Core Complex: Georgetown Lake Dam–Anaconda–Big Hole Valley: Northwest Geology, v. 32, p. 29–46.

O'Neill, J.M., Lonn, J.D., Lageson, D.R., and Kunk, M.J., 2004, Early Tertiary Anaconda metamorphic core complex, southwestern Montana: Canadian Journal of Earth Sciences, v. 41, p. 63–72, doi: 10.1139/e03-086.

Scarberry, K.C., Elliott, C.G., and Yakovlev, P., in review, Geologic map of the Butte North 30' x 60' quadrangle, southwestern Montana: Montana Bureau of Mines and Geology Geologic Map, 1 sheet, scale 1:100,000.

Scarberry, K.C., Korzeb, S.L., and Smith, M.G., 2015, Origin of Eocene volcanic rocks at the south end of the Deer Lodge Valley, Montana: Northwest Geology, v. 44, p. 201–212.

Wanek, A.A., and Barclay, C.S., 1966, Geology of the northwest quarter of the Anaconda quadrangle, Deer Lodge County, Montana: U.S. Geological Survey Bulletin 1222-B, p. B1–B28.

Weed, W.H., 1905, Economic value of hot-spring deposits, *in* Emmons, S.F., and Eckel, E.C., eds., U.S. Geological Survey Bulletin 260, p. 598–604, doi: https://doi.org/10.3133/b260.

Yonkee, W.A., and Weil, A.B., 2015, Tectonic evolution of the Sevier and Laramide belts within the North American Cordillera orogenic system: Earth-Science Reviews, v. 150, p. 531–593, doi: 10.1016/j.earscirev.2015.08.001.

THE DEATH AND REBIRTH OF SILVER BOW CREEK

Joe Griffin

Retired Superfund Project Manager, Montana Department of Environmental Quality, Helena

INTRODUCTION

This paper, which provides context for a companion 2019 TRGS field trip, explores the story of the Richest Hill on Earth and the extreme ecological devastation caused by over 100 years of unregulated mining, milling, and smelting on Silver Bow Creek. Between 1905 and 1917, Butte and Anaconda were producing a third of the copper used in the world. Of course, the story of mining copper continues to this day. But in a historical narrative full of superlatives, the greatest is the world-class environmental cleanup of Silver Bow Creek and the upper Clark Fork river basin under the Environmental Protection Agency's (EPA) Superfund program.

The tour will begin at the Diamond Mine, which overlooks the Berkeley Pit near what was the headwaters of Silver Bow Creek, and will end at the confluence of Silver Bow and Warm Springs Creeks, which marks the headwater of the Clark Fork of the Columbia River (fig. 1). Although the tour will end at the confluence, the mining damage and Superfund complex extends from Butte to Milltown, located 120 mi downstream near the city of Missoula.

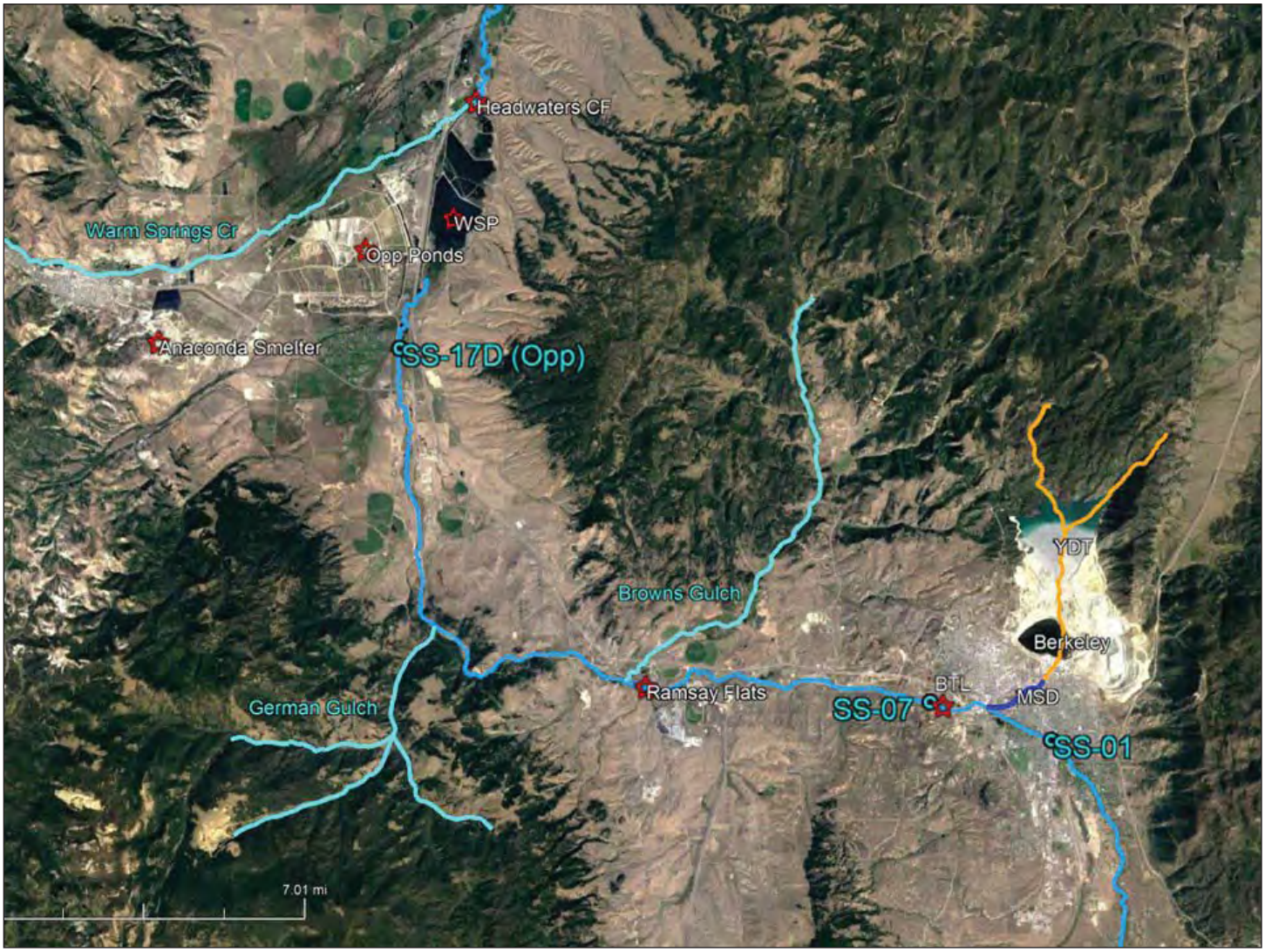

Figure 1. Google Earth image of Silver Bow Creek and location of environmental tour features. Yellow stream course is pre-mining course of SBC, lost forever in the mine. YDT, Yankee Doodle Tailings Impoundment; MSD, Metro Storm Drain (dark blue line); BTL, Butte Treatment Lagoons; WSP, Warm Springs Ponds; Opp Ponds, Opportunity Tailings Ponds; CF, Clark Fork River.

ENVIRONMENTAL PROBLEM

There are two fundamental sources of pollution that have affected Silver Bow Creek and the Clark Fork: tailings and acidic mine drainage. During the period from roughly the late 1880s to the earliest 1900s, most of the milling, concentrating, and smelting of the polymetallic ore from the Butte Hill also took place in Butte. The water used to carry ore through the milling and concentrating process helped slurry tailings directly to Silver Bow Creek and its floodplain. The Creek was a convenient industrial sewer. In 1908 the Clark Fork basin experienced the flood of record, flushing much of the tailings that had collected in the creek and floodplain downstream and redepositing them along Silver Bow Creek, the upper Clark Fork, and in the newly constructed Milltown Dam reservoir.

The other long-term insult to aquatic life was the substantial amounts of acid mine water, along with very high levels of toxic metals such as copper and zinc, that were discharged into the creek starting sometime in the 1880s and continuing until the Atlantic Richfield Company turned off the pumps on in 1982. As underground mining proceeded, eventually creating 10,000 mi of underground workings (Duaime and others, 2004), the mine complex worked as a groundwater drain system that captured an ever-expanding volume of water from the alluvial and bedrock aquifers. By the 1970s, the mine was discharging at an estimated rate of approximately 10 cfs (Spindler, 1977).

Although closing the pit and turning off the pumps was a reprieve for aquatic life in Silver Bow Creek, it was a blow to Butte and Anaconda. "It was a tough time in Butte," Fritz Daily told the Montana Standard. "They closed the smelter, the mines, the pit. It tipped the town over." (Montana Standard, April 22, 2015)

ENVIRONMENTAL MANAGEMENT

The first large-scale effort to manage the environmental damage was construction of the Warm Springs Ponds in response to the catastrophic flooding of 1908 and associated lawsuits from aggrieved downstream irrigators. The Anaconda Company built the first of the Warm Springs Ponds in 1911 to capture the downstream migration of tailings. Pond 2 was added in 1916, and finally in 1959 Pond 3 was added. In addition to acting as settling ponds, at some point, the operation began adding lime to remove dissolved metals. These ponds are still in service today—their fate is one of the last remaining questions of the Clark Fork Superfund Complex cleanup.

During the period between the 1890s and earliest 1900s, ore milling, concentrating, and smelting moved to Anaconda because Warm Springs Creek was a larger and more dependable source of process water than Silver Bow Creek. Ore processing was eventually consolidated on Anaconda's Smelter Hill and the first of the Opportunity and Anaconda Tailings Ponds were built in 1914 to capture tailings and keep them from reaching Silver Bow Creek and the Clark Fork. The Ponds continued to expand until 1964 when they covered roughly 6 mi^2.

As the rich veins that supplied ore stock to the Anaconda Smelter played out, the Company began mining low-grade ore in 1955 out of the Berkeley Pit. It was too costly to ship low-grade ore to the Anaconda Smelter, so in 1964 the Weed concentrator was built adjacent to the Berkeley Pit and only copper concentrate was sent to the Smelter. From that point on, tailings have been deposited in the Yankee Doodle Tailings Pond, located about a mile north of the Berkeley Pit (fig. 1).

Richard Nixon established the EPA in 1970, and in 1980 Congress passed the Comprehensive Environmental Response, Compensation and Liability Act, also known as the Superfund Law, which put real teeth into the EPA's ability to pursue the cleanup of Silver Bow Creek. Butte and Anaconda were added to the National Priorities List in the early 1980s, and so began a $1.4 billion cleanup that continues to this day.

THE BERKELEY PIT, 10,000 MILES OF UNDERGROUND MINE WORKINGS, AND ACID MINE DRAINAGE

The beginning of our tour and the most conspicuous feature in Butte's mining landscape, the Berkeley Pit (1955 to 1982), is at the headwaters for the Clark Fork of the Columbia (fig. 1). The pit is a mile and a half long, 1 mi across and approximately 1,200 ft deep measured from the lowest point on the pit rim (Duaime and others, 2018).

The Atlantic Richfield Company, who inherited the liability for the entire Clark Fork Superfund complex when they purchased the Anaconda Company in 1977, decided to abandon mining and turned off the mine

dewatering pumps, ironically on Earth Day (April 22) 1982. The Pit and underground workings began to flood with acidic (pH 2.5 to 6) and highly contaminated mine water. That massive mine complex posed a bit of a cleanup conundrum—how to deal with what is now 125 billion gallons of highly contaminated acidic water, with an inflow rate of approximately 5 million gallons per day.

EPA decided on a remedy based on a Technical Impracticability evaluation of four possible remedies (EPA, 1994). The most absurd solution that was considered was to remove the source of acid and metals, which meant removing the well-tunneled ore body, creating a pit 64 times larger than the Berkeley and costing $462 billion. EPA also considered drilling closely spaced holes and injecting grout to just plug up the mine workings or injecting lime to neutralize the aquifer and pit lake. Those two solutions would have cost between $9 and $13 billion, and EPA had little confidence of success—those options were also rejected. Ultimately, EPA determined that holding groundwater levels at a safe elevation by pumping and treating would be effective at managing groundwater and would cost somewhere between $27 and $213 million. Flooding would create a "wet closure" for most of the underground workings that would substantially reduce acid production over time. Treated water would eventually be released to Silver Bow Creek and would meet Montana's strict water-quality standards for both human and aquatic life. Pumping and treating will continue indefinitely, or in legal terms, in perpetuity—or in technical terms, a long damn time.

TAILINGS AND SILVER BOW CREEK

While the Pit is acting to contain acid mine drainage within the mining system, it is separated from the rest of the Silver Bow Creek drainage by a groundwater divide. The tour turns to the environmental problem of streamside tailings deposits and the massive effort to excavate those tailings and rebuild Silver Bow Creek and its floodplain. The instream tailings have had a direct effect on aquatic life but have also contaminated the alluvial aquifer associated with the Creek.

The most notorious, the Parrot Tailings, have created a groundwater plume that extends 1 mi downgradient and at the source has the highest concentrations of metals in the Superfund complex, sometimes exceeding 1,000,000 ppb copper (Tucci, 2010).

Within urban Butte, there has been a three-pronged approach to cleaning up Silver Bow Creek:

- Excavate the tailings from the stream and floodplain, rebuild the stream channel and floodplain;
- Capture and treat contaminated groundwater that is degrading stream water quality; and
- Manage urban stormwater runoff that is carrying mine waste contamination from the Butte Hill to the Creek.

Google Earth images from before and after remediation of the Colorado Tailings and Butte Reduction Works (fig. 2) show a vast makeover of the stream corridor along this 1-mi reach. In 1997, Atlantic Richfield excavated 1.1 million yd^3 and hauled them to a local waste repository where they were capped to form what is now the Copper Mountain sports complex.

Metals loading analysis had demonstrated that groundwater inflow through that 1-mi reach, also known as Lower Area One, was adding 72% of the total zinc load (Hydrometrics, 1990), so the final design included separating the water table from the creek by building an elevated floodplain and capturing and treating upwelling groundwater. Groundwater is treated by lime addition in the Butte Treatment Lagoons, a series of nine unlined settling ponds shown in the lower photo of figure 2. That treatment system currently meets Montana's strict water-quality standards at the end of the pipe.

Despite removal and revegetation of over 550 acres of waste rock dumps on Butte Hill (fig. 3), stormwater runoff is currently the worst source of contamination still finding its way to the creek. Stormwater ponds, which have a proven record in Butte of removing 95% of copper from runoff (Atlantic Richfield, 2010), will be located at the mouth of the Metro Storm Drain (fig. 1). The MSD channel, aligned along the pre-mining course of Silver Bow Creek, was built by local labor under the Work Project Administration during the Depression. Before the mine dewatering pumps were shut off in 1982, it served as a mine discharge sewer. Its only function now is to gather stormwater from six underground storm sewers and get it to Silver Bow Creek without flooding.

Figure 2. Google Earth images, before and after the environmental cleanup of the Colorado Tailings/Butte Reduction Works (CT/BRW) area. The CT is the rectangular light gray area on left with SBC outlining the northern boundary. In the post-reclamation image, SBC and its floodplain have been reconstructed to the south of its original location. The Butte Treatment Lagoons are a lime addition groundwater treatment system located at the former CT. The two circular clarifier tanks mark the Butte Sewage Treatment Plant.

Downstream of Butte, Montana,the Department of Environmental Quality took control of cleaning up the remaining 26 mi of Silver Bow Creek, a Superfund operable unit called Streamside Tailings (EPA, 2016). The project, which began in 1999 and was completed in 2015, entailed excavating tailings from the stream channel and floodplain and then reconstructing the entire riparian system. Capturing and treating contaminated groundwater was considered "not feasible" and will be left for time to eventually flush out the contaminated portions of the alluvial aquifer. DEQ hauled more than 6 million yd^3 of streamside tailings to the Opportunity Ponds Waste Management Area repository.

The single largest accumulation of streamside tailings was at Ramsay Flats—a before and after cleanup aerial photo is presented in figure 4. Tailings deposits were up to 12 ft thick but were typically 4 ft thick. This massive, unvegetated area often developed an aquamarine crust of copper and other metal salts in the summer, when hot dry days caused wicking and evaporation of soil moisture at the surface. Readily dissolved during summer thunderstorms, those metal salts would cause toxic spikes in Silver Bow Creek. Approximately 1.8 million yd^3 of streamside tailings were removed from the Ramsay Flats area alone. The morphology of this willow-lined reach of stream has continued to evolve and now has undercut banks that provide habitat for native cutthroat trout.

HOW WELL IS THE CLEANUP WORKING?

The United States Geological Survey has been collecting flow and water-quality data since 1989 at three strategically located stations (see fig. 1). Although arsenic, cadmium, copper, lead, and zinc have all

Figure 3. Before and after photographs of mine dump reclamation. The Diamond mine is marked by the prominent headframe.

been named contaminants of concern by the EPA, this discussion is focused on copper because it is the most problematic contaminant. A graph of copper data reads like a storyline of this massive Superfund cleanup.

Station SS-01 is located on Blacktail Creek at Harrison Avenue in Butte and upstream of the major mining impacts. Nonetheless, it should be considered an anthropogenically affected background site because the area was likely enriched in copper and other metals by smoke and dust from the Butte and Anaconda smelters.

Station SS-07 is located at the downstream boundary of urban Butte. Improvements in water quality generally reflect specific cleanup actions on the Butte Hill and along the Lower Area One stream corridor.

Station SS-OPP (SS-17D) is located close to the end of the Streamside Tailings Operable Unit and reflects cleanup progress from Butte to the Warm Springs Ponds.

In the 1970s, the EPA issued the Butte mining operation a National Pollutant Discharge Elimination System permit, which included a maximum allowed limit of 1,000 µg/L copper in their discharge (Spindler, 1976). For comparison, the current mine's discharge permit (MT DEQ, 2012) has a maximum daily limit of 14 µg/L. The Anaconda Company responded by treating their discharge with lime and coagulants. They also reduced their discharge flow rate by recirculating tailings water, thereby reducing the metal loads going to Silver Bow Creek. By these measures, Anaconda was able to reduce in-stream total recoverable copper levels from over 100,000 µg/L in 1971 to no more than 1,710 µg/L by 1975. During the early 1990s, when the mine was no longer discharging to the creek, the maximum values were less than 550 ppb.

Water-quality improvements during the Superfund cleanup period require a little explanation about water-quality standards. The yardstick of success and Su-

Figure 4. Before and after Google Earth images of SBC at Ramsay Flats. Whitish areas in 2002 photo are "slickens," areas devoid of vegetation because of acidic soils with phytotoxic levels of metals. The small stream entering from the north, and west of small village of Ramsay, is Browns Gulch, one of two major tributaries to SBC.

perfund's overarching objective is meeting Montana's numeric water-quality standards (Circular DEQ-7); they were selected by EPA to determine whether Silver Bow Creek is "in" or "out" of compliance. The copper standard is based on collecting an unfiltered sample, consisting of both dissolved and suspended fractions. For several metals, including copper, the standard is variable because it is based on the measured hardness (a function of calcium plus magnesium concentration) of the water sample. For long-term trend analysis, it is often more utilitarian to report data from Silver Bow Creek as a "compliance ratio" (CR), which is simply the measured concentration divided by the sample-specific regulatory standard. If the ratio is greater than one, the stream is out of compliance and likely affects aquatic health.

Using water quality at Station SS-01 as a background reference, Stations SS-07 and SS-OPP show dramatic improvements over the period from 1993 through 2013 (fig. 5). Before the cleanup, average annual copper levels were often 20 to 30 times the standard. The largest reduction in copper came from removing the Colorado Tailings and rebuilding the stream and floodplain in Butte in 1997. Water quality in Silver Bow Creek continued marked improvements in response to additional groundwater capture and treatment in Butte and from the Streamside Tailings cleanup until 2013. After 2013, the major remedy components were complete as reflected in the flattening of the copper compliance ratio curves.

Figure 6 focuses on copper trends since the beginning of 2013. Annual spikes in copper that exceed the standard consistently mark the spring runoff and rainy period in the Butte area. Over that 6-yr period there is little indication of improving water quality. However, in 2019 the EPA has stated they will require more work in Butte, including capturing and treating more groundwater, additional stormwater management, and

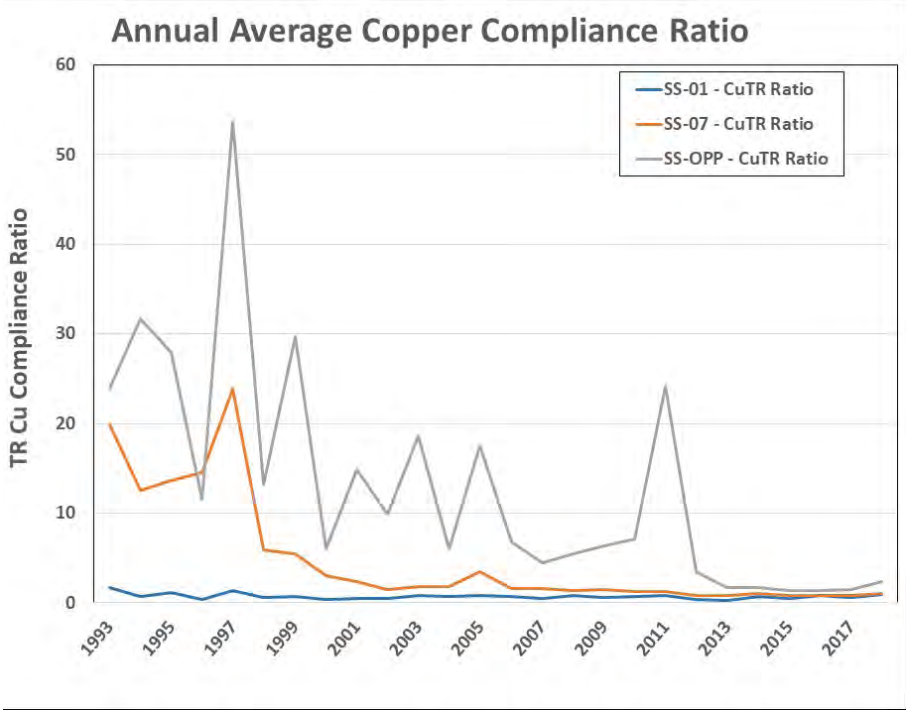

Figure 5. Plot of annual average, total recoverable copper compliance ratio (concentration ÷ standard) through time illustrates the effectiveness of stream restoration. SS-01 (blue), background location. SS-07 (orange), point of compliance for Butte portion. SS-Opp (gray), downstream portion of Streamside Tailings.

more in-stream cleanup (EPA, 2019). Downstream of Butte, DEQ expects that residual groundwater contamination, associated with the now removed tailings, will flush out over time. According to the USGS (Sando and others, 2013) those more subtle water-quality trends can take decades of monitoring to measure water-quality improvements.

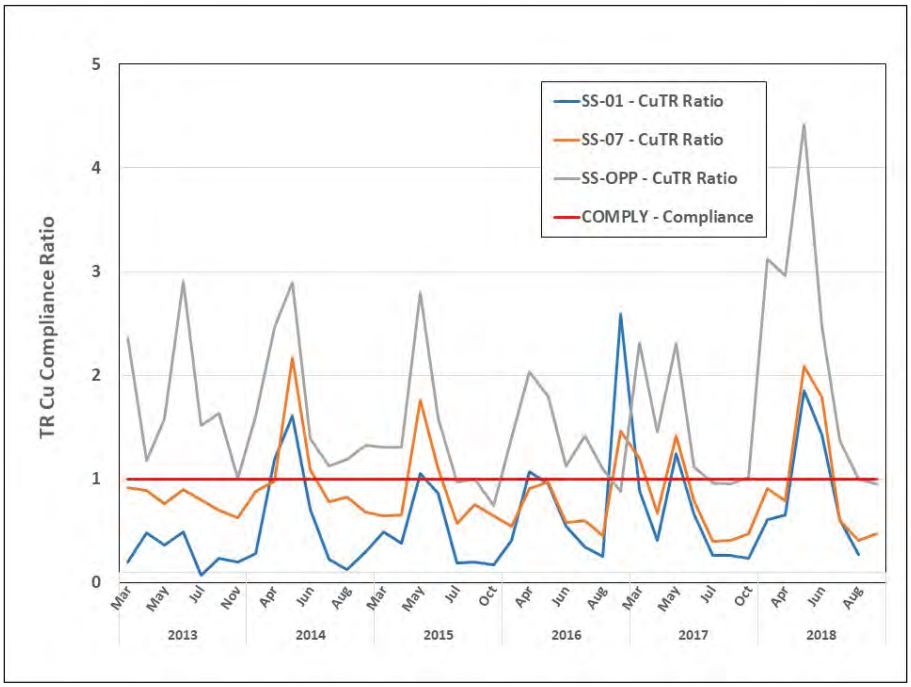

Figure 6. Plot of total recoverable copper compliance ratio at Stations SS-01, SS-07, and SS-OPP. All stations, including the background (SS-01), exceed the water-quality standard during seasonal high flow.

REFERENCES

Atlantic Richfield, 2010, Technical memorandum: Evaluation of storm water catch basins and sediment traps, Butte Priority Soils Operable Unit.

Duaime, T.E., Kennelly, P.J., and Thale, P.R., 2004, Butte, Montana: Richest hill on Earth, 100 years of underground mining: Montana Bureau of Mines and Geology Miscellaneous Contribution 19, 1 sheet, scale 1:9,000.

Duaime, T.E., McGrath, S.T., Icopini, G.A., and Thale. P.R., 2018, Butte Mine Flooding Operable Unit, Water-level monitoring and water-quality sampling 2016 consent decree update, Butte, Montana 1982–2016: Montana Bureau of Mines and Geology Open-File Report 700, 187 p.

EPA, 1994, Record of Decision for the Butte Mine Flooding operable unit, Silver Bow Creek/Butte area NPL site, Butte, Montana.

Hydrometrics, 1990, Colorado Tailings and Butte Reduction Works Project, Prepared for ARCO by Hydrometrics, Inc., February.

Montana Department of Environmental Quality, 2012, Authorization to discharge under the Montana Pollutant Discharge Elimination System from Montana Resources Facility No. MT0000191.

Sando, S.K., Vecchia, A.V., Lorenz, D.L., and Elliot, P.B., 2013, Water-quality trends for selected sites in the upper Clark Fork Basin, Montana, Water years 1996–2010, Scientific Investigations Report 2013-5217.

Spindler, J.C., 1977, The clean-up of Silver Bow Creek: Mining Congress Journal, June 1977.

Tucci, N.J., 2010, The Parrot Complex: A drilling investigation of historic mine waste left in place; Tailings and

overburden volumes, leachability and economic feasibility for recovery, and water quality along the upper metro storm drain in Butte, MT: Montana Bureau of Mines and Geology Open-File Report 590, 127 p.

RINGING ROCKS

Petr V. Yakovlev
Montana Bureau of Mines and Geology

INTRODUCTION

The Ringing Rocks of southwestern Montana are a geologic oddity, also known as lithophonic rocks or rock gongs, that produce a range of tones when struck (Loen, 1995). The site is located 15 mi southwest of Butte, on the western side of the Whitetail valley (fig. 1). The Ringing Rocks are a loosely stacked pile of rusty-brown weathering mafic boulders 1–5 m (3–16 ft) in diameter (Butler, 1983). Why the boulders at Ringing Rocks or other lithophonic rocks produce tones when struck remains a matter of scant scientific inquiry. How the Ringing Rocks formed is likewise unknown. However, the intrusion from which the Ringing Rocks boulders are sourced, referred to as the Ringing Rocks stock, presents an interesting example of magma mixing between mafic and felsic magmas (Johannesmeyer, 1999). The aim of this field trip is to showcase the Ringing Rocks, investigate magmatic relationships within the Ringing Rocks stock, and discuss possible formation mechanisms for the rock pile.

Some boulders at Ringing Rocks produce distinct musical tones when struck with a heavy object, like a stone or hammer (Loen, 1995). Similar lithophonic rocks or rock gongs have been found around the world, including at archeological sites (e.g., Bednarik, 1996; Kleinitz, 2004; Gibbons and Schlossman, 1970; "Ringing Rocks," Wikipedia, 2019). At Ringing Rocks, and an analogous site in Pennsylvania, boulders that lie on the ground do not ring, suggesting that their tonality is related to how the boulders are perched in the rock pile (Gibbons and Schlossman, 1970; "Ringing Rocks," Wikipedia, 2019). Gibbons and Schlossman (1970) proposed that ringing rocks in Pennsylvania produce sound due to a buildup of internal stresses during weathering, but this hypothesis has not been rigorously tested. This field trip presents an opportunity to discuss possible mechanisms that would cause the rocks to ring, and motivate further research on the subject.

Intrusion of the Ringing Rocks stock is thought to be related to formation of the Late Cretaceous Boulder Batholith (Protska, 1966). The Ringing Rocks stock lies ~800 m (½ mi) from the main body of the Boulder Batholith and is ~800 m (½ mi) in diameter (fig. 1; Prostka, 1966). The stock is composed of a felsic core of granite or quartz monzonite and a mafic rim of plagioclase shonkinite and olivine pyroxene monzonite (Butler, 1983; Johannesmeyer, 1999). The mafic rim is partially obscured by Quaternary colluvium, leading to interpretations that show the rim either completely or partially encircling the stock (figs 2, 3; Prostka, 1966; "Ringing Rocks," Wikipedia, 2019). The mafic rim has been locally eroded to form the Ringing Rocks. A prominent transition zone between the mafic rim and felsic core suggests that the two magmatic compositions were emplaced at roughly the same time, and were sufficiently hot to mix. Magma mixing is further supported by the presence of 5- to 30-cm-wide inclusions of the quartz monzonite core that may be found in the shonkinite rim, and vice versa (Johannesmeyer, 1999). Intrusions with a similar texture can be found in the Wilson Park quadrangle on the east side of the Whitetail valley (Scarberry, 2016).

The Ringing Rocks stock is likely associated with late Cretaceous magmatism found throughout southwestern Montana. The shonkinite rim of the stock was dated to 78.2 ± 3.1 Ma (Tilling and others, 1968) and 75.1 ± 2.8 Ma (Daniel and others, 1981) using the K-Ar technique. The felsic core of the Ringing Rocks stock has not been dated. The stock intrudes diorite porphyry of the Elkhorn Mountains volcanic field, which has a K-Ar age of 78 ± 1.7 Ma (Prostka, 1966; Daniel and Berg, 1981). More recent mapping in the Ratio Mountain quadrangle to the immediate north describes the diorite porphyry of Prostka (1966) as lavas and domes of pyroxene–hornblende dacite with an unpublished $^{40}Ar/^{39}Ar$ age of ~84.5 Ma (Olson and others, 2016). The 76.5 Ma Butte Granite of the Boulder Batholith (Olson and others, 2016) locally metamorphoses the diorite porphyry (Prostka, 1966).

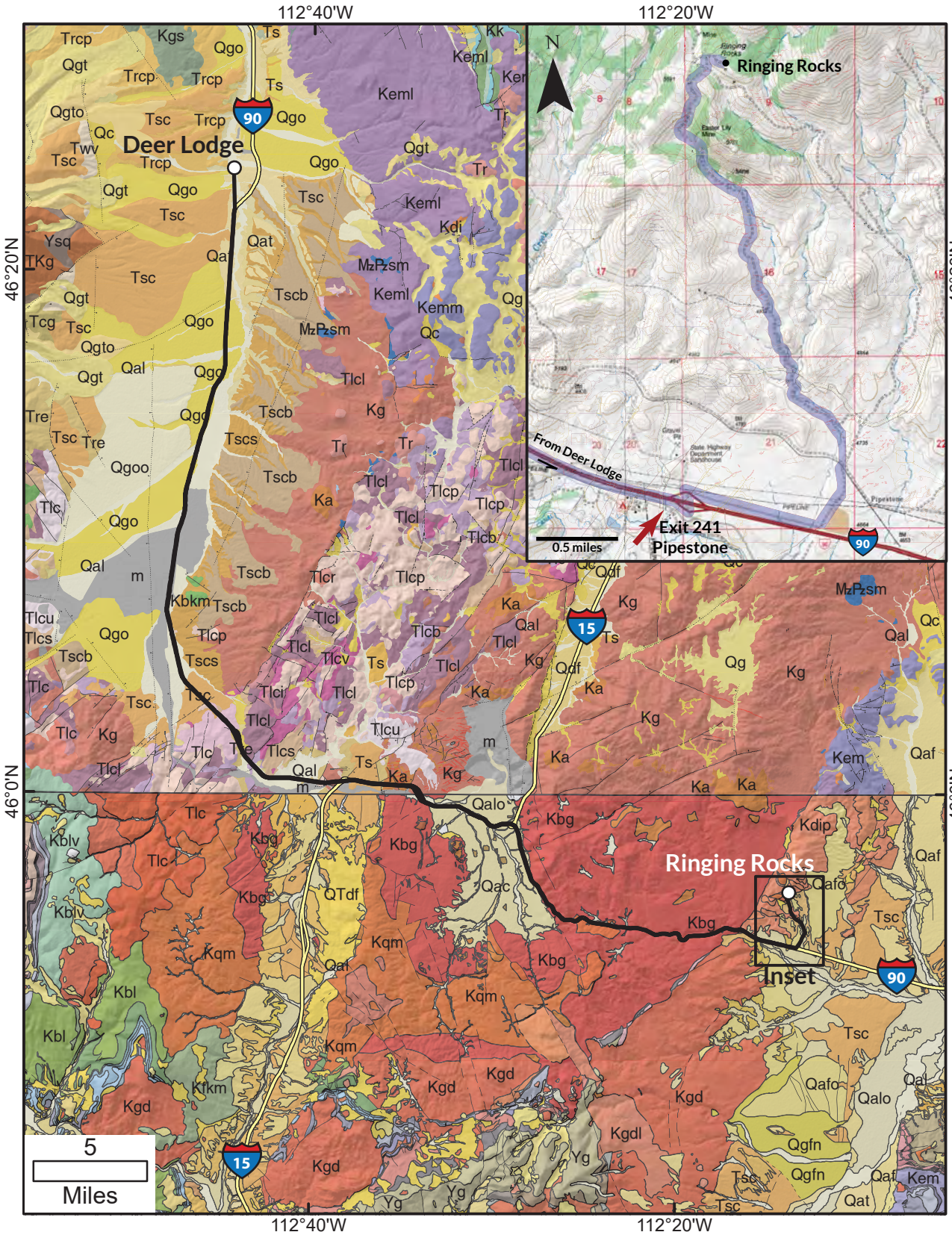

Figure 1. Geology of the vicinity of the Ringing Rocks stock, and field trip route.

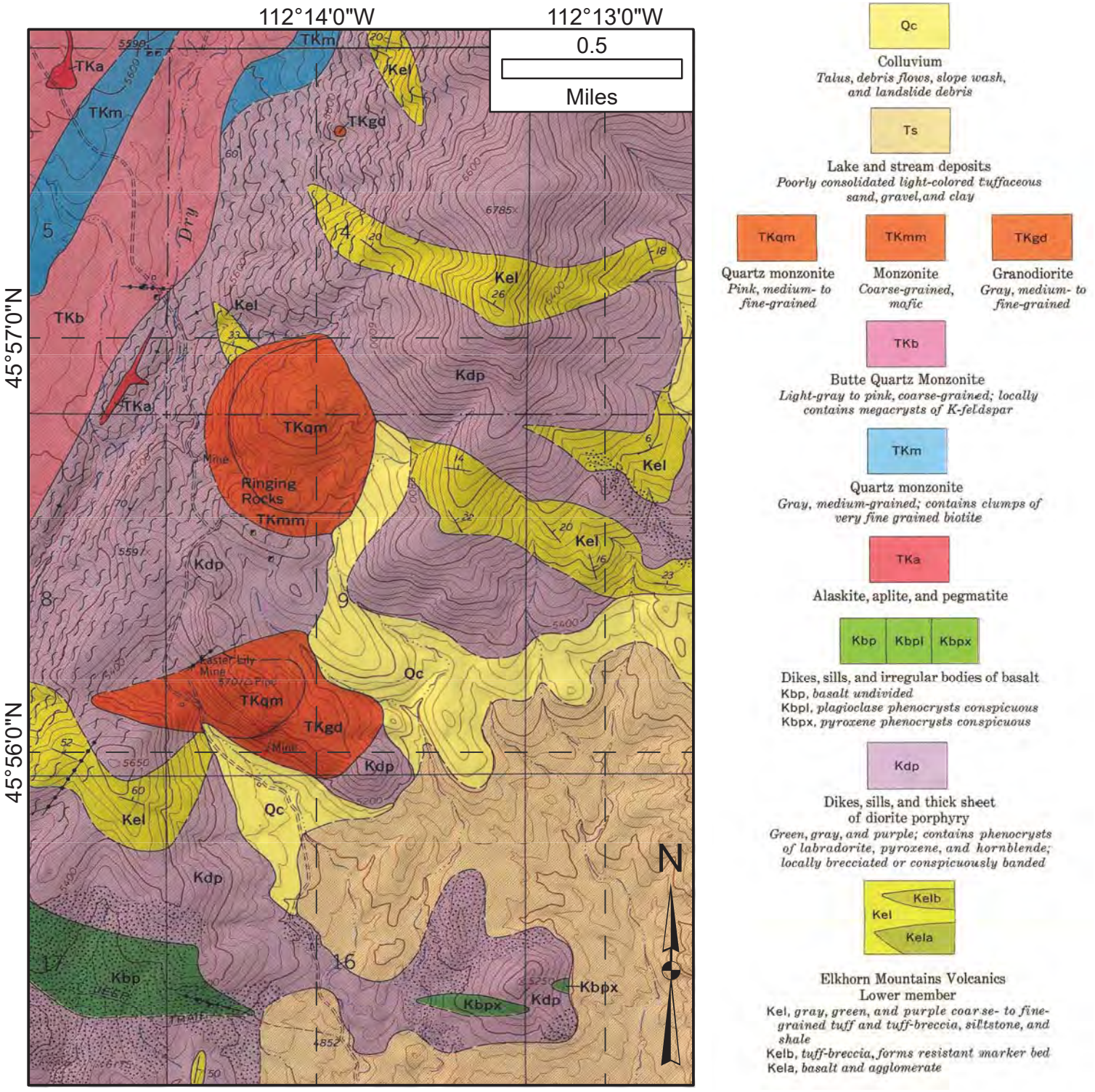

Figure 2. Geology of the area surrounding the Ringing Rocks stock. Modified from Prostka (1966).

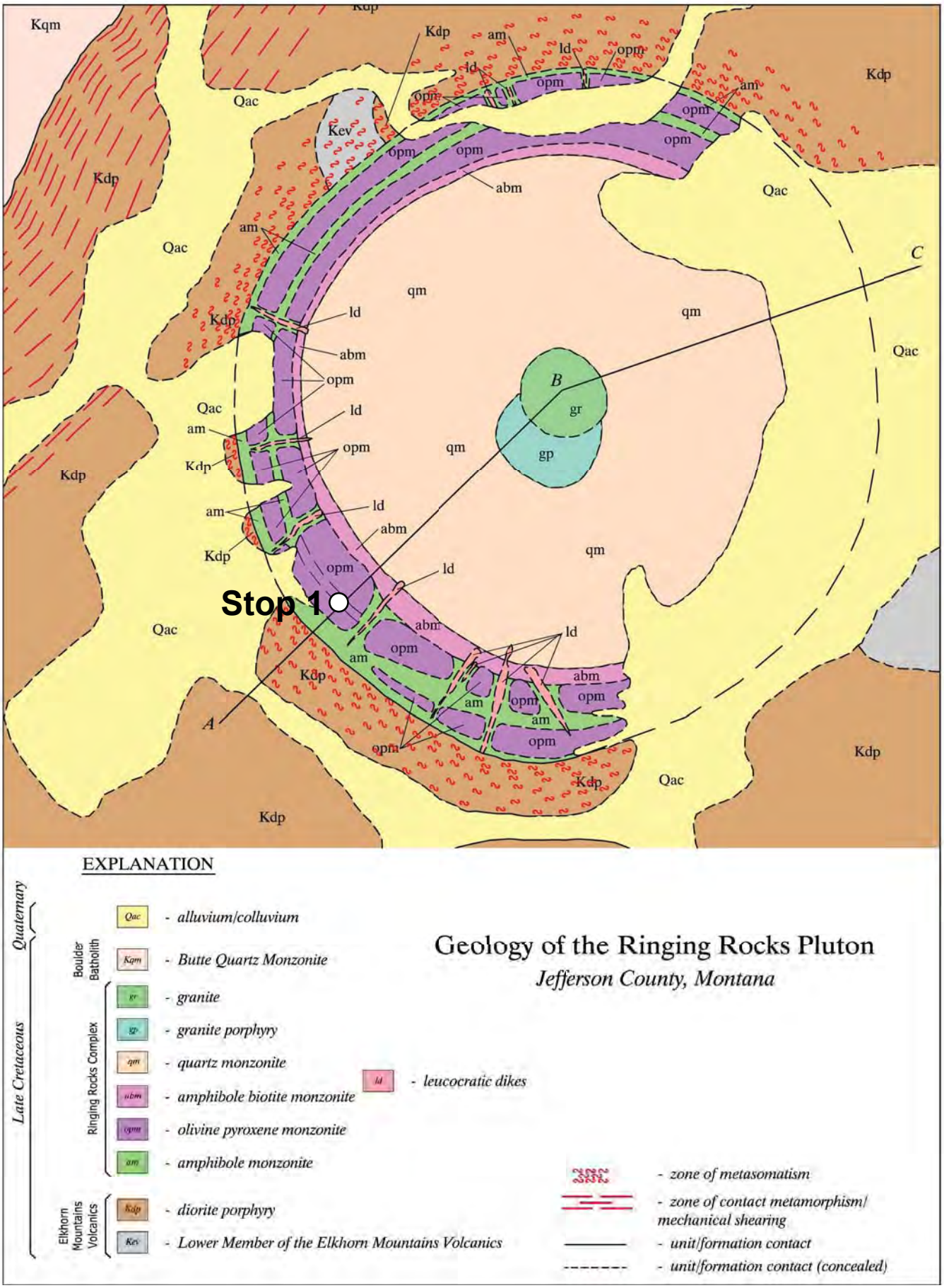

Figure 3. Geology of the Ringing Rocks stock. Figure modified from original by Andrew Stroud, Western Water Research & Mapping/History Mapping Services (“Ringing Rocks”,Wikipedia, 2019). Printed under the Creative Commons Attribution-ShareAlike license version 3.0.

However, the Ringing Rocks stock does not appear to metamorphose the surrounding diorite porphyry and is itself not metamorphosed (Prostka, 1966). These age dates indicate that the Ringing Rocks stock may be an early magma associated with the Boulder Batholith, emplaced soon after the Elkhorn Mountains volcanic sequence. More robust and modern dating techniques could help resolve the absolute ages of these units.

The quartz monzonite core of the Ringing Rocks stock is compositionally similar to the Butte Granite of the Boulder Batholith (See Scarberry and others, this volume, for an overview of the Boulder Batholith). However, the mafic outer rim is compositionally and petrologically distinct, and falls in the K-rich shoshonite series. Butler (1983) and Johannesmeyer (1999) infer that the felsic body of the pluton was generated by partial melting of the crust by injection of mafic alakali magmas compositionally similar to the mafic outer rim. The felsic magma differentiated at depth and was emplaced in the upper crust to form the core of the Ringing Rocks stock. The felsic core was then intruded and partially enveloped by the mafic alakali magma that now forms the rim of the stock (Johannesmeyer, 1999). Intrusions of similar composition to the Ringing Rocks stock can be found near the Boulder Batholith, with sites including the Kokoruda Complex southeast of Helena, dikes near Garrison, Montana (Kunz, 2003), and at Bull Mountain on the east side of the Whitetail valley (Scarberry, 2016).

Why this rock pile formed in a particular portion of the mafic margin of the Ringing Rocks stock, and nowhere else, is currently unknown. The boulder pile was initially described as a felsenmeer by Butler (1983). Felsenmeer are generally thought to have been produced by frost wedging and heaving of underlying bedrock, though mass wasting processes have also been proposed (Ritter and others, 2011). However, foliations can be easily followed between adjacent boulders in the pile, which implies that they have not moved significantly from their original orientation. The rock pile may instead be interpreted to be a tor or castle koppie, which are common throughout the Boulder Batholith. While both tropical and periglacial tor formation processes have been proposed, a defining feature of tors is in-place weathering and exposure (Twidale and Romani, 2005) like that inferred for the boulders at Ringing Rocks. Part of an unpublished Montana Tech BS thesis by Andrew Stroud now discussed on Wikipedia ("Ringing Rocks," Wikipedia, 2019) suggests that the tor formed as a result of preferential erosion of amphibole monzonite in the mafic rim of the Ringing Rocks stock and subsequent frost wedging of remaining olivine pyroxene monzonite outcrops to form the tor. Gabelman (2019) proposed that the tor formed as a result of gas-driven fracturing related to the Holocene emplacement of an amagmatic diatreme, though no evidence for such a diatreme has been found. Future investigations should address whether compositional differences are apparent in the rock pile, and investigate potential gravity anomalies associated with a subsurface diatreme.

ROAD LOG

(Miles Total/Miles this section)

(0.0) From the intersection of Main Street and Milwaukee Avenue in Deer Lodge, MT (46° 23.874' N, 112° 44.120'W), drive south on Main Street.

(1.9/1.9) Merge onto I-90 east.

(53.2/51.3) Take Exit 241 to Pipestone.

(53.3/0.1) Take a left. Go under the overpass. Follow signs to Ringing Rocks by turning right onto BLM-2, the first dirt road after the I-90 offramp.

(54.1/0.8) Drive on BLM-2, first parallel to I-90 then the road will curve north.

(54.5/0.4) Cross cattle guards at sign reading "Entering Public Lands."

(54.8/0.3) Bear left at the fork to continue on BLM-2.

(56.1/1.3) Rough road. This is the most difficult spot to cross. Sedans will likely need to stop here. If you can make it past this spot, you'll make it to Ringing Rocks.

(57.6/1.5) Cattle guard and sign for Ringing Rocks. Turn right on BLM-2.

(57.8/0.2) Parking area with route maps and sign for Ringing Rocks. Continue on BLM-2. The road from here is rough, but should be no problem for a small SUV.

(57.9/0.1) Arrive at Ringing Rocks (45° 56.596' N, 112° 14.343'W).

Ringing Rocks

We will explore the boulder pile of the Ringing Rocks and magma mixing relationships of the Ringing Rocks stock. Start by grabbing a hammer and banging on a perched boulder to hear it produce a sound. When finished, investigate the individual boulders in the pile. You should be able to see their generally mafic composition, inclusions of quartz monzonite, and a pervasive foliation that can be traced between adjacent boulders. The transition to the quartz monzonite core of the Ringing Rocks stock begins at the northeast corner of the boulder pile. The intrusive margin of the stock may be found in exploration pits southeast of the boulder pile, across the dirt road.

Questions for Discussion:

1. How are the structure and composition of the ringing boulders different from adjacent exposures?
2. How did the tor form?
3. Why do the rocks ring when struck?

REFERENCES

Bednarik, R.G., 1996, The cupules on Chief's Rock, Auditorium Cave, Bhimbetka: Artefact: The Journal of the Archaeological and Anthropological Society of Victoria, v. 19, p. 63.

Butler, B.A., 1983, Petrology and geochemistry of the Ringing Rocks pluton Jefferson County Montana: Missoula, MS Thesis, University of Montana.

Daniel, F., and Berg, R.B., 1981, Radiometric dates of rocks in Montana: Montana Bureau of Mines and Geology Bulletin 114, 144 p., 2 sheets.

du Bray, E.A., Aleinikoff, J.N., and Lund, K., 2012, Synthesis of petrographic, geochemical, and isotopic data for the Boulder batholith, southwest Montana: U.S. Geological Survey Professional Paper 1793, 39 p.

Gabelman, J.W., 2019, Ringing Rocks, Montana: A modern gas diapir?, *in* Scarberry, K.C., and Barth, S., eds., Proceedings of the Montana Mining and Mineral Symposium 2018: Montana Bureau of Mines and Geology Special Publication 120, p. 31–38.

Gibbons, J., and Schlossman, S., 1970, Rock music: Natural History, v. 79, no. 10, p. 36-41.

Johannesmeyer, T.C., 1999, Magma mixing and mingling in the Late Cretaceous Ringing Rocks pluton, Jefferson County Montana, and implications for the generation of the Boulder batholith: Missoula, MS Thesis, University of Montana.

Kleinitz, C., 2004, Rock art and 'rock gongs' in the Fourth Nile Cataract region: The Ishashi island rock art survey: Sudan & Nubia, no. 8, p. 12–17.

Kunz, R.S., 2003, The Alkalic intrusions of Garrison, Montana: A possible extension of the Central Montana Alkalic Province: Missoula, MS Thesis, University of Montana.

Loen, J.S., 1995, Geological curiosities of southwestern Montana: Northwest Geology, v. 25, p. 79–90.

Olson, N.H., Dilles, J.H., Kallio, I.M., Horton, T. R., and Scarberry, K.C., 2016, Geologic map of the Ratio Mountain 7.5' quadrangle, southwest Montana: Montana Bureau of Mines and Geology EDMAP portion of the National Geologic Mapping Program 10, 1 sheet, scale 1:24,000.

Prostka, H.J., 1966, Igneous geology of the Dry Mountain quadrangle, Jefferson County, Montana: U.S. Geological Survey Bulletin, v. 1221-F, 21 p.

Ritter, D.F., Kochel, R.C., and Miller, J.R., 2011, Process geomorphology, Fifth Edition: Long Grove, Ill., Waveland Press, p. 449-451.

Scarberry, K.C., 2016, Geologic map of the Wilson Park 7.5' quadrangle, southwestern Montana: Montana Bureau of Mines and Geology Geologic Map 66, 1 sheet.

Tilling, R.I., 1973, Boulder batholith, Montana: A product of two contemporaneous but chemically distinct magma series: Geological Society of America Bulletin, v. 84, p. 3879–3899.

Twidale, C.R., and Romani, J.R.V., 2005, Landforms and geology of granite terrains: Boca Raton, Fla., CRC Press, 354 p.

Wikipedia, 2019, Ringing rocks: Wikipedia, The Free Encyclopedia, https://en.wikipedia.org/w/index.php?title=Ringing_rocks&oldid=891977271 [Accessed April 16, 2019, 20:33].

FIELD GUIDE TO THE GEOLOGY AND METALLIC MINERAL DEPOSITS ALONG THE EASTERN CONTACT BETWEEN THE BOULDER BATHOLITH, THE ELKHORN MOUNTAINS VOLCANIC FIELD, AND CRETACEOUS–PALEOZOIC SEDIMENTARY ROCKS

Kaleb C. Scarberry,[1] Christopher H. Gammons,[2] and Ian M. Kallio[2]

[1]*Montana Bureau of Mines and Geology*
[2]*Geologic Engineering, Montana Technological University*

*Note that the odometer values were done using Google Earth, so may be slightly off.

INTRODUCTION

The Boulder Batholith and Elkhorn Mountains Volcanic field (EMVF–"Elkhorn Mountains Volcanics") represent a remarkably well-preserved record of continental magmatism and related metallic mineral deposits. The EMVF formed during Late Cretaceous Cordilleran arc volcanism (Rutland and others, 1989) between about 85 and 77.5 Ma (Tilling and others, 1968; Foreman and others, 2008) and was originally about 3.5 to 4.6 km thick (Tilling and others, 1968; Lageson and others, 2001). The Boulder Batholith consists of a compositionally diverse suite of stocks and plutons that were emplaced into the EMVF between about 79 and 76 Ma (Lund and others, 2002). Previous examinations of the eastern contact between the Boulder Batholith and the EMVF have produced differing conclusions regarding the nature of the contact zone. For example, does the contact zone represent a Sevier thrust-ramp that continued to move significantly (1–2 km) after the Butte Granite was emplaced (e.g., Tilling and others, 1968), or does the Butte Granite cut and post-date Sevier fold-thrust structures (e.g., Houston and Dilles, 2013)? Also of interest are a series of mineralized porphyry intrusions along the eastern margin of the batholith. Few of these porphyry intrusions have been dated, but contact relationships show that they are older than the Butte Granite.

This field trip guide is split into two parts. The road log for part 1 focuses on the structure of the Whitetail Valley, contact relationships between the Boulder Batholith and EMVF, and evidence for active Basin and Range faulting. Part 2 of the road log describes the setting of polymetallic mineral deposits, contact relationships between the Boulder Batholith and Cretaceous–Paleozoic sedimentary rocks, and the history of mining at Elkhorn, Montana.

GEOLOGIC SETTING: PART 1

The Late Cretaceous Boulder Batholith and the EMVF (fig. 1) formed in an evolving thrust wedge during Sevier fold-thrust belt deformation (Tilling and others, 1968; Hamilton, 1988; Lageson and others, 2001), and are a record of Cordilleran arc magmatism (Rutland and others, 1989; Gaschnig and others, 2011). Gentle NE tilting (20° ± 10°) in the Butte district accompanied uplift and extraordinary exhumation (6–9 km) of the magma system during Laramide compressional deformation between about 66 and 53 Ma (Houston and Dilles, 2013). The over-thickened fold-thrust belt collapsed during an episode of crustal extension beginning at around 52 Ma, with eruption of the Lowland Creek volcanic field (fig. 1), and perhaps continuing until around 20 Ma (Constenius, 1996; Houston and Dilles, 2013). Basin and Range block faulting initiated around 17 Ma, overprinted the earlier phase of extension, and continues today (Reynolds, 1979). Collectively, these processes have produced, exposed, and redistributed bedrock mineral deposits as stream placers throughout southwestern Montana (Foster and Childs, 1993; Lyden, 1948).

The EMVF (Klepper and others, 1957) covers 25,000 km^2 (9,650 mi^2) along the flanks and top of the Boulder Batholith north and east of Butte (fig. 1). Regional studies have identified lower, middle, and upper EMVF sequences (Klepper and others, 1957, 1971; Smedes, 1966). The lower EMVF is primarily basaltic andesite and dacite porphyry lavas and dome complexes (Prostka, 1966; Olson and others, 2016). The middle member EMVF (fig. 2) consists of andesite pyroclastic deposits and several large-volume rhyolite ignimbrites (Smedes, 1966; Scarberry and others, 2016; Olson and others, 2016). The upper sequence contains volcanogenic sediments, interstratified tuff and tuff breccia, and pyroclastic water-laid deposits. Only the lower and middle member EMVF succes-

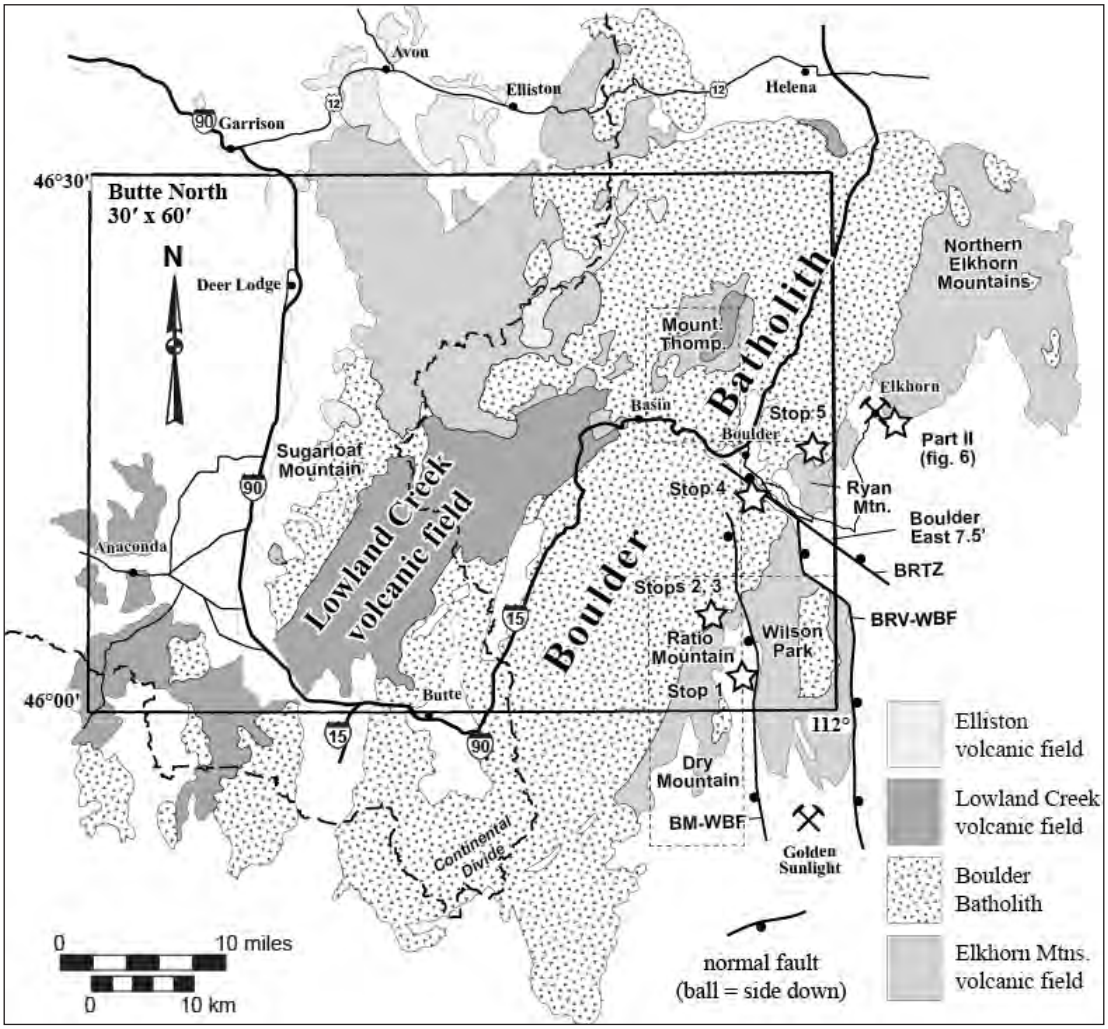

Figure 1. Simplified igneous geology of the Boulder Batholith–Elkhorn Mountains volcanic field magma system (after Vuke and others, 2007). The general location of field stops and the major Quaternary faults discussed on the field trip also shown. BM-WBF, Bull Mountain Western Border Fault; BRV-WBF, Boulder River Valley Western Border Fault; BRTZ, Boulder River Transverse Zone.

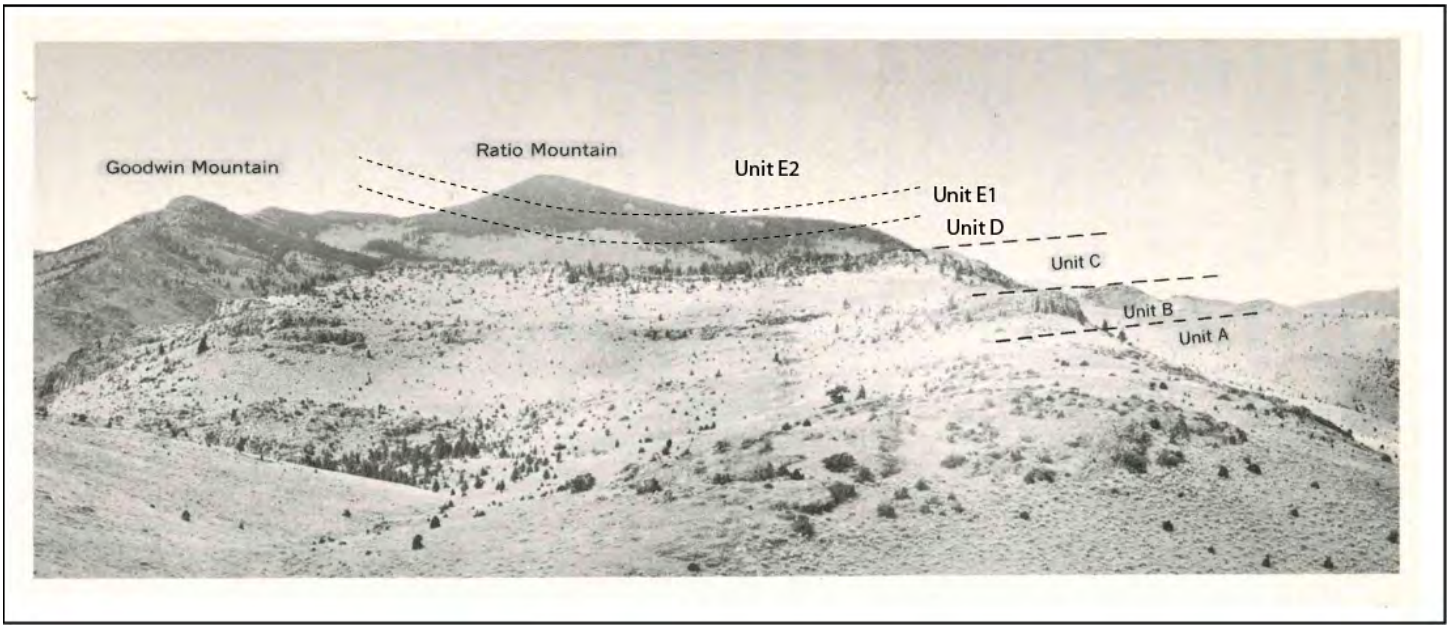

Figure 2. Photograph of the middle member EMVF ignimbrite section at Ratio Mountain, modified from Prostka (1966), who first described units A, B, and C. Recent work by Olson and others (2016) added units D, E1, and E2 to the section. View is to the north from the top of the ridge (sec. 30, T. 3 N., R. 4 W.) south of Ratio Mountain, in the Dry Mountain 7.5′ quadrangle.

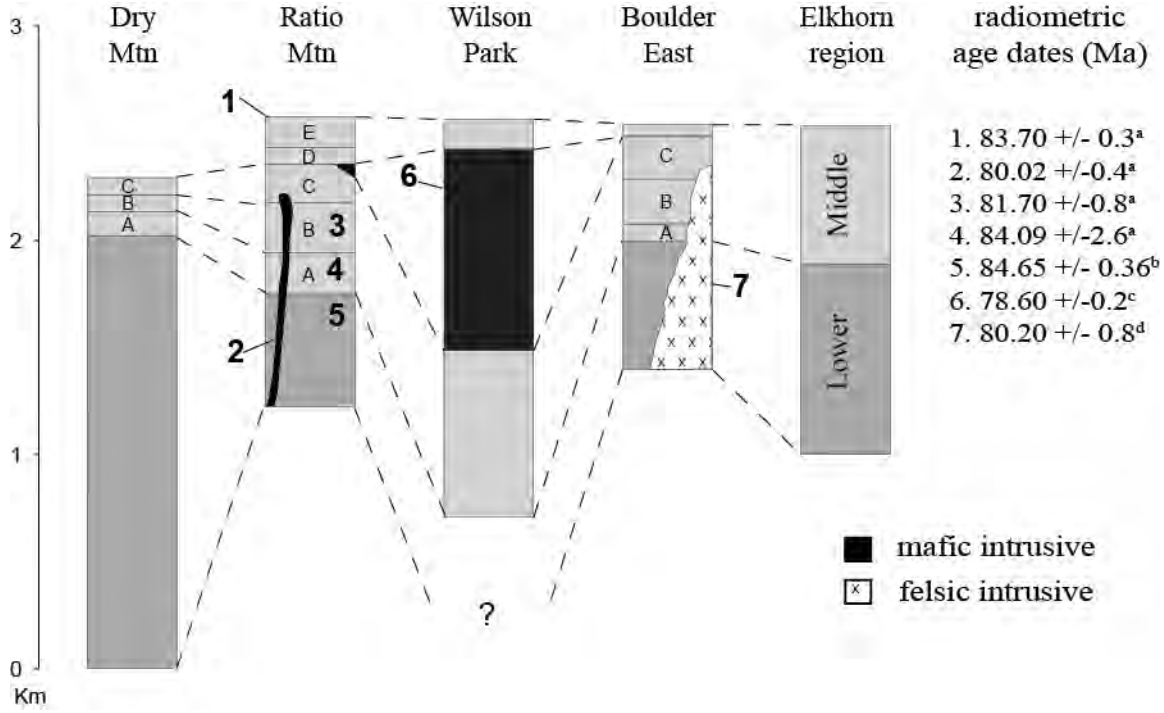

Figure 3. Correlation diagram showing the general stratigraphy of the EMVF and recent radiometric age determinations from the eastern margin of the Boulder Batholith–EMVF contact zone. Ar, $^{40}Ar/^{39}Ar$ age; Uz, U/Pb age from zircon. Data sources: (a) Olson and others (2016); (b) N. Olson, written commun., 2018; (c) Scarberry (2017) and J. Dilles, written commun., 2017; (d) Olson and others, 2017. Most of the radiometric age dates are not published, except on geologic maps, and in some cases the reported errors are not accurate (J. Dilles, written commun., 2019).

sions are exposed along the field trip route. Figure 3 shows the revised stratigraphy for EMVF and new age dates for units we will visit.

ROAD LOG: PART 1

The field trip begins after exiting I-90 eastbound at Whitehall (exit 249). Reset your odometer before turning left (north) onto Whitetail Valley Road (Route 399). The Boulder Mountains are on the west side of the road and Bull Mountain is on the east side. About 5 mi down the Whitetail Valley Road, a prominent block of rocks appears on the east side of the road. The base of the rock block consists of the Mesoproterozoic Greyson Formation of the Belt Supergroup, which is overlain by the Cambrian Flathead, Park, Meagher, and Pilgrim Formations. The Devonian–Cambrian Maywood and Red Lion Formations and the Devonian Jefferson Formation form the top of the block (McDonald and others, 2012). Although the Mesoproterozoic–Devonian section is clearly cut by, and dips east into, a Quaternary fault (Bull Mountain western border fault), the section also represents the eastern limb of a broad, north-plunging Sevier fold-thrust belt anticline. Another line of reasoning for the existence of the north-plunging fold is that the trip route cuts up-section, from south to north. The northbound Whitetail Valley Road essentially follows the fold axis down-plunge.

STOP 1: Overview of the Elkhorn Mountains Volcanic Field (Odometer: 10.2 mi; 46.02079°N, 112.10886°W)

New mapping in the Ratio Mountain (Olson and others, 2016), Wilson Park (Scarberry, 2016), and Boulder East (Scarberry and others, 2017) 7.5′ quadrangles has built on EMVF stratigraphic relationships described by Prostka (1966) in the Dry Mountain 7.5′ quadrangle (figs. 1–3). The middle member of the EMVF is exposed at Ratio Mountain on the west side of the road, and along Dearborn Creek on the east side of the road. Prostka (1966) mapped the Dry Mountain 7.5′ quadrangle south of Ratio Mountain, and divided the middle member of the EMVF into three welded tuff units (A, B, and C). Olson and others (2016) expanded Prostka's (1966) middle member stratigraphy in the Ratio Mountain 7.5′ quadrangle, and identified three additional units: (1) andesitic air-fall and reworked volcaniclastic deposits (unit D), (2) crystal-rich (30%) andesite–dacite ignimbrite (unit E1), and (3) relatively crystal-poor (15%) andesite–da-

cite ignimbrite (unit E2; figs. 2, 3). Units D (fig. 4A) and E1 and E2 (fig. 4B) of Olson and others (2016) are discontinuously exposed along the summit of Bull Mountain in the Wilson Park 7.5′ quadrangle (fig. 1), where Scarberry (2016) thought they were part of the Upper Member EMVF and mapped them as a single unit (Kemu).

Signs of active extensional tectonics are conspicuous throughout the Whitetail Valley. The Bull Mountain western border fault, the main structure on the east side of the Whitetail Valley, is an active Basin and Range normal fault that has a strike length of about 30 km (Stickney and others, 2000). If the fault were to rupture at once it could generate a 6.5M to 7.0M earthquake (e.g., Wells and Coppersmith, 1994). The Whitetail Creek Fault, on the southwestern side of the Whitetail Valley, strikes approximately N–S for a distance of about 7 km and has moved in the past 130,000 years (Stickney and others, 2000). Olson and others (2016) mapped the trace of an active fault to the north, near Ratio Mountain, that strikes roughly N–S and dips to the east. These observations suggest that the Whitetail Creek Fault may have a greater strike-length than is recognized, and that the fault forms the western boundary of a graben structure in the Whitetail Valley (fig. 4C).

Continue North on Whitetail Valley Road and be on the lookout for landslide and alluvial fan deposits that track the active range front fault (Bull Mountain western border fault; Stickney and others, 2000) along the east side of the road. After about 3.25 mi, turn left (west) onto Hay Canyon road (Odometer: 13.5 mi; 46.06745°N, 112.10588°W). Continue west on Hay Canyon road across Whitetail Deer Creek for another 2.1 mi.

STOP 2: Rhyolite Ignimbrite (unit A) of the Middle Member EMVF
(Odometer: 15.6 mi; 46.07056°N; 112.13873°N).

The base of ignimbrite A of the middle member EMVF is nicely exposed at this stop. Rheomorphic flow bands in the ignimbrite define its E–W strike and a 20° to 30°S dip. The following description of unit A is largely from Olson and others (2016): unit A is up to 160 m thick in the Ratio Mountain 7.5′ quadrangle (fig. 3) and displays strong rheomorphic deformation (fig. 4D) throughout the section except the basal 5–10 m. Rheomorphic textures include stretching lineations that are typically oriented NNE to SSW, and folded fiamme with aspect ratios of around 100:10:1. The unit is moderately welded and rheomorphic to its uppermost exposure, which suggests the top has been eroded away. Overall, the unit is crystal-poor (7 to 10 percent by volume). Phenocrysts include plagioclase (5 to 7 percent), with sparse but large biotite (1–3 mm) that is partially altered to chlorite, and traces of quartz and chlorite-altered pyroxene. A weighted mean U/Pb zircon age for the ignimbrite is 84.09 ± 2.6 Ma (fig. 3).

STOP 3: Aplite of the Boulder Batholith in Contact with Dacite of the Lower Member EMVF
(Odometer: 16.0 mi; 46.07110°N, 112.14637°W).

This stop is located at the contact between the Boulder Batholith and the Lower Member of the EMVF. Here you can see the Butte Granite and the thermal effects of aplite intruding the EMVF (fig. 4E). Some of the aplite dikes at this stop trend N35°E to N60°E, mimicking the Butte Granite contact with the EMVF, and are continuous for about 130 m. Hornblende compositions yield barometric estimates of 2.1 to 2.4 (± 0.2) kb pressure for Butte Granite at this field trip stop based on the calibration of Anderson and Smith (1995), suggesting emplacement depths of 7 to 8 km (J.H. Dilles, written commun., 2015). Schorl occurs in the Butte Granite at this stop and is likely associated with pegmatite pockets that are scattered throughout this area. U/Pb zircon ages for the Butte Granite are 74.5 ± 0.9 Ma (Lund and others, 2002) and 76.28 ± 0.14 (Martin and others, 1999). Korzeb and Scarberry (2018) dated an aplite dike on the west side of the Boulder Batholith (Oro Fino District) at 74.5 ± 0.6 Ma by using the ^{40}Ar-^{39}Ar method to date hydrothermal muscovite (sericite) from vein-altered host rock.

Batholith rocks intruded dacite flow-dome complexes that form the base of the EMVF section at this stop. Prostka (1966) mapped the dacite as intrusive porphyry in the Dry Mountain 7.5′ quadrangle to the south, but the presence of both auto-breccias and intercalated volcaniclastic sedimentary units as well as topographically high domes locally demonstrates an extrusive origin (Olson and others, 2016). Unfortunately, none of these geologic features are very clear at this stop because the dacite sequence has been thermally metamorphosed. Hornfels with conspicuous biotite is present within 500 m of the contact with the

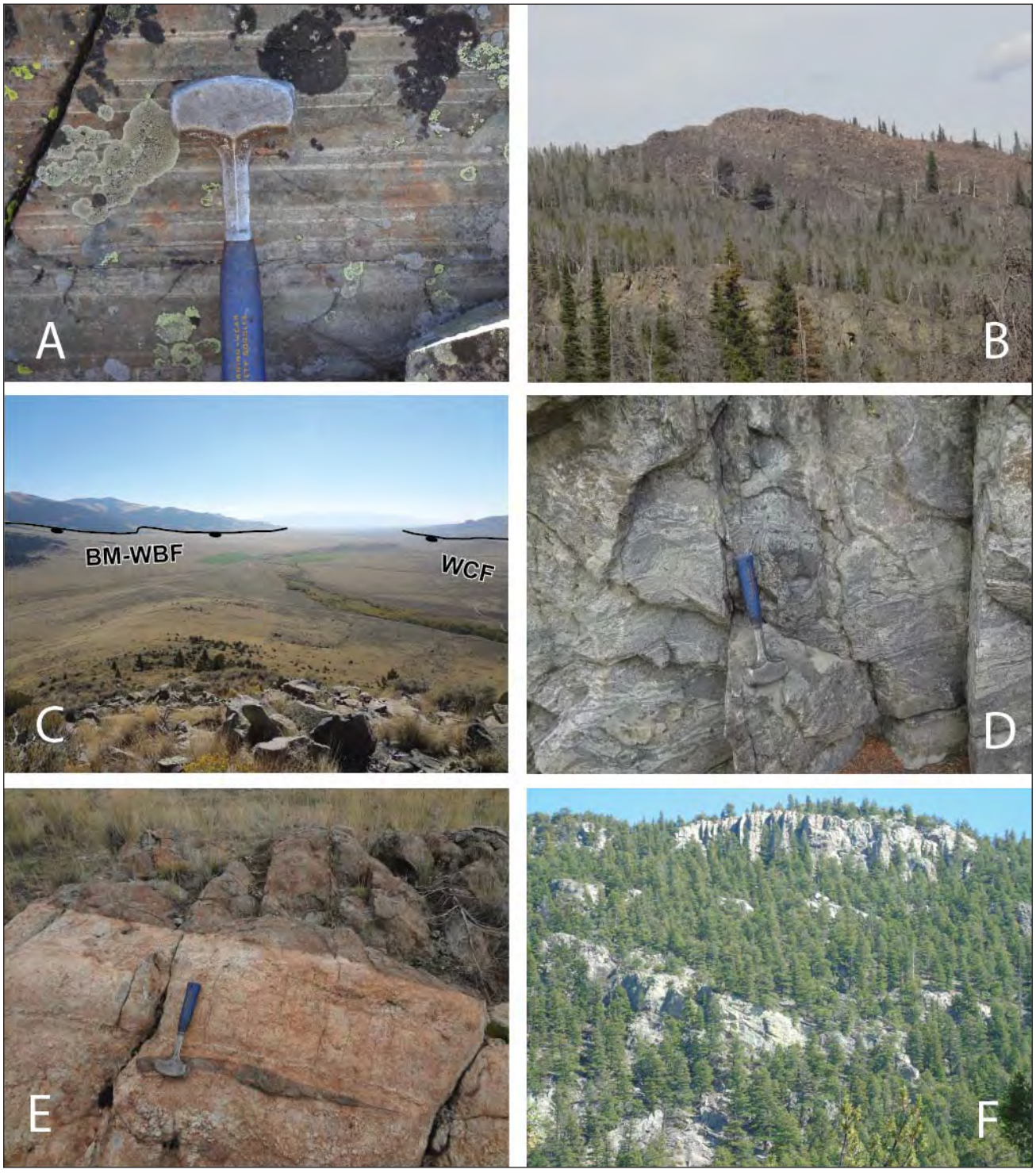

Figure 4. (A) Andesitic air-fall, likely water-lain, and reworked volcaniclastic deposits (unit D) near the summit of Bull Mountain in the Wilson Park 7.5′ quadrangle (Scarberry, 2017). (B) Crystal-rich (30%) andesite–dacite ignimbrite (unit E1), and relatively crystal-poor (15%) andesite–dacite ignimbrite (unit E2) near the summit of Bull Mountain. (C) View of the Whitetail Valley looking south from Fletcher Mountain (near Stop 2). BM-WBF, Bull Mountain Western Border Fault; WCF, Whitetail Creek Fault. (D) Rheomorphic deformation in unit A of the middle member EMVF in the Wilson Park 7.5′ quadrangle. Rheomorphism is caused by post-eruption flow of the pyroclastic density current through uneven topography. (E) Aplite dike intruding dacite porphyry flow-domes in the lower EMVF sequence at stop 2. (F) Middle member EMVF ignimbrites at the top of Ryan Mountain.

Boulder Batholith, and locally biotite extends up to 1,500 m outward from the contact (Olson and others, 2016). Units B, C, D, and E of the middle member EMVF were mapped by Olson and others (2016) in the hill to the east.

Return to Whitetail Valley Road via Hay Canyon road, then turn left (north) onto Whitetail Valley Road (odometer: 18.5 mi; 46.06745°N, 112.10588°W). Fletcher Mountain is on the north (left), and west (left) sides of the roads as you immediately head out. Fletcher Mountain is a big pile of thermally metamorphosed middle member EMVF rhyolite ignimbrite. As you continue north on Whitetail Valley Road, glance out the window and note the roughly N40°E contact between the Butte Pluton (white and blocky) and the EMVF (dark and forested) that strikes across the road (odometer: about 21.7 mi). Continue north on Whitetail Valley Road for another 10.1 mi (odometer: about 31.7 mi), turn right (east) onto Hot Springs Road, and continue another 0.8 mi to Boulder Hot Springs.

STOP 4: Boulder Hot Springs and the Boulder River Transverse Fault Zone (Odometer: 32.5 mi; 46.19997°N, 112.09527°W).

The Boulder Hot Springs occur at the northwest end of the Boulder River transverse zone (BRTZ), which is a roughly 750-m-wide transfer fault zone (Faulds and Varga, 1998) that marks the northern termination of both the Bull Mountain western border fault and the Boulder River Valley western border fault (Stickney and others, 2000) to the south (fig. 1). North of the Boulder River transverse zone, across the Boulder River Valley and just east of the hot springs, the range front normal fault at Ryan Mountain has a dip polarity opposite to the Bull Mountain western border fault. Therefore, the BRTZ may represent a regional accommodation zone that separates fault dip domains. Accommodation zones that separate fault dip domains are favorable structural settings for geothermal systems throughout the Basin and Range extensional province (Faulds and Hinz, 2015).

Surface-water temperature at the hot springs ranges from 54 to 74°C and water chemistry suggests that it originates from a 140°C subsurface reservoir (Metesh, 2000). These observations imply slow and deep (4.7 km) water circulation, assuming a regional geothermal gradient of 30°C/km (Sonderegger, 1984). The Boulder Hot Springs are actively depositing metallic minerals. Veinlet filling near the hot springs contains Au (0.05 oz/ton) and Ag (0.4 oz/ton), and hydrothermally altered granite is stained with Cu (Weed, 1900).

The BRTZ juxtaposes middle member EMVF ignimbrites at Ryan Mountain (fig. 1) to the north, with what is primarily lower member EMVF dacite flow-domes at Bull Mountain to the south (Scarberry and others, 2017). Olson and others (2016) obtained geochemical data from representative samples of the Ratio Mountain section (fig. 2). Kallio (2017) used geochemistry to correlate the Ryan Mountain ignimbrite sequence with units B and C at Ratio Mountain (fig. 5). These relationships suggest that Ryan Mountain has been faulted down along the BRTZ relative to Bull Mountain by a minimum of 500 m, which is roughly the exposed thickness of the dacite flow-dome

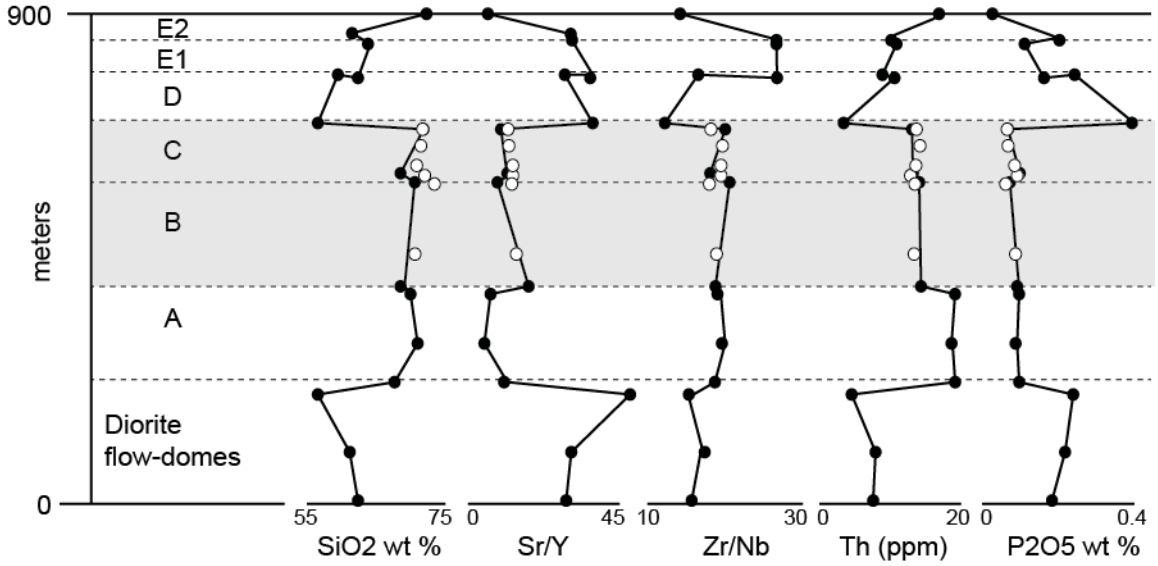

Figure 5. Geochemical stratigraphy of the top of the lower member, and the entire middle member EMVF, in the Ratio Mountain and Boulder East 7.5′ quadrangles (Kallio, 2017). Data from Olson and others (2016) and Scarberry and others (2017).

sequence at Bull Mountain that is missing at Ryan Mountain.

Scarberry and others (2017) calculated fault plane solutions for 16 small magnitude (0.5–3.5) earthquakes that occurred at depths of 0.6–17.8 km (0.4–11.1 mi) since 1982 in the Boulder region. Collectively, the stress orientations (P-axes and T-axes) for the earthquakes are consistent with NW–SE-directed extension. Therefore, the BRTZ is favorably oriented to accommodate NW–SE-directed extension, and perhaps right-lateral slip, similar to faults of the eastern Lewis and Clark line (Stickney, 2015).

Continue westbound on Hot Springs Road for about 0.3 mi and turn left (north) onto Montana Highway 69. After 0.6 mi (odometer: 33.4 mi; 46.21085°N, 112.09683°W) turn right (east) onto Upper Valley Road. Take Upper Valley Road across the Boulder River and continue for about 1.2 mi to the fork in the road. Take the left fork and follow the main gravel road for about 1 mi, until the road appears to fork again. This time, follow the right fork in the gravel road and head north and east towards Ryan Mountain. Follow the switchbacks in the road for about 2.5 mi and park in the turnout to the left (north).

STOP 5: Quartz-Eye Porphyry in the Boulder Batholith (Odometer: 37.2 mi; 46.22847°N, 112.02718°W)

The porphyry is characterized by blocky and jointed brown outcrops that contain conspicuous 2–4 mm, rounded quartz "eyes," potassium feldspar, and biotite. Groundmass is anhedral quartz, potassium feldspar, and micropegmatitic intergrowths of potassium feldspar and quartz, and in part orthoclase. Weeks (1974) assigned the unit to the late stage of Boulder Batholith formation. A U-Pb age of 80.2 ± 0.8 Ma (fig. 3; J. Dilles, written comm., 2015) indicates that the quartz-eye porphyry pre-dates the Butte Granite and is one of the older plutons in the Boulder Batholith. The quartz-eye porphyry is intriguing from an economic perspective because: (1) it is similar in composition to the Turnley Ridge stock near the Elkhorn Mine (Stop 8), and (2) it is similar in age and composition to the rhyolite breccia pipe at the Golden Sunlight Mine (DeWitt and others, 1996). It is speculated here that these 80 Ma porphyry intrusions may be genetically related to the middle member ignimbrite eruptions.

GEOLOGIC SETTING: PART 2

The Elkhorn mining district is located 8 mi northeast of Boulder, MT, in the southern Elkhorn Mountains. The district is of interest because it displays a wide variety of rocks and mineral deposit types in a relatively small area (fig. 6). Rock types include Mesoproterozoic through Mississippian sedimentary units locally metamorphosed to hornfels and calc-silicate skarn, the late Cretaceous EMVF, and at least three petrologically distinct late Cretaceous intrusions: (1) gabbro/diorite stocks, dikes, and sills; (2) quartz–feldspar and feldspar porphyry of the Turnley Ridge Complex (TRC); and (3) Butte Granite. Mineral deposit types include the important carbonate replacement Ag-Pb-Zn deposits of the historic Elkhorn Mine, Au-rich skarns, magnetite-rich skarns, porphyry-style Cu-Mo mineralization in the TRC, and polymetallic, tourmaline-rich breccia pipes. Descriptions of the geology and mineralization in the Elkhorn district can be found in Weed (1901), Pardee and Schrader (1933), Roby and others (1960), Everson and Read (1992), and Brown and others (2019).

ROAD LOG: PART 2

Part 2 of this field trip begins at the turnoff to the town of Elkhorn from Montana Highway 69 (46.17405°N, 112.03319°W), between mile markers 31 and 32. Reset odometers to zero at this turnoff.

0.3 mi—After crossing the Boulder River, bear right onto Lower Valley Road

2.2 mi—Bear left onto Elkhorn Road (dirt)

3.0 mi—Bear left; the low hills to the east are folded Paleozoic sediments.

7.4 mi—Immediately after a cattle guard, there is parking on the right. This is a good spot for anyone who wants to look at more rocks of the EMVF, which crop out 0.2 mi up the road as an impressive overhanging cliff.

9.0 mi—Outcrops on both sides of the road are EMVF.

STOP 6: Tourmaline Queen Mine (Odometer 9.5 mi; 46.25172°N; 111.96381°W)

Park at intersection of Elkhorn Road and Queen Gulch Road. Blasted cliffs on the west side of the road

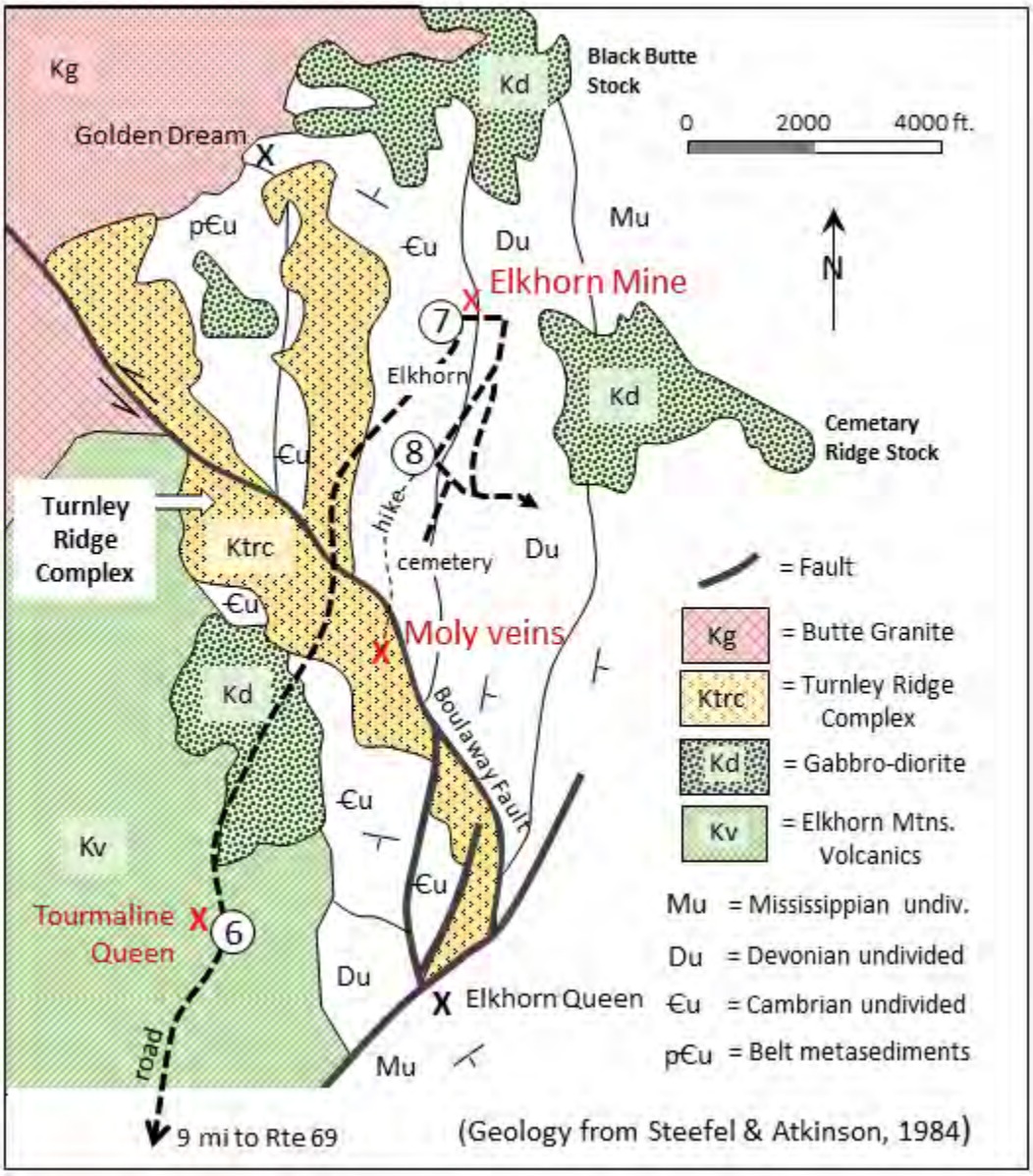

Figure 6. Simplified geologic map of the Elkhorn district (redrawn from Steefel and Atkinson, 1984), showing the locations of field trip stops 6, 7, and 8.

are the Tourmaline Queen Mine, and are worth a quick look. The Tourmaline Queen was a minor producer of gold and silver from a tourmaline-bearing breccia pipe that cut the EMVF. The tourmaline is a fine-grained schorl that is hard to see in hand sample. Hydrothermal alteration with disseminated pyrite and arsenopyrite is widespread. The rough road that leads east from the parking spot heads to the Elkhorn Queen Mine (high clearance 4WD needed). The Elkhorn Queen is another steeply plunging breccia pipe, in this case cutting Madison Limestone. Between 1905 and 1956, the mine produced an impressive 1.9M lbs of Pb, along with 150,000 oz Ag, 1,800 oz Au, 13,000 lbs Cu, and 355,000 lbs Zn (Roby and others, 1960). Mine dumps contain coarse-grained pyrite, arsenopyrite, galena, and sphalerite in a gangue of quartz and fine-grained schorl.

Return to vehicles and continue north towards Elkhorn.

10.5 mi—To the west is a large pile of mill tailings from the historic Elkhorn (Holter) Mine. The forested hillside further west is underlain by porphyry of the Turnley Ridge Complex.

10.8 mi—To the right, one sees foundations of the historic Elkhorn mill.

STOP 7: Elkhorn (Holter) Mine
(Odometer: 10.5 mi; 46.27651°N, 111.94346°W).

After passing through the picturesque town of Elkhorn, park near the top of the hill, where the main road takes a hard right turn. The mine dumps to the north and west are all that remains of the important Elkhorn (Holter) Mine. Mineralization was discovered in the late 1870s, and quickly led to development of what was, in its day, one of the largest underground Ag mines in Montana.

Between 1881 and 1900, 9.9M oz of Ag, 8,500 oz Au, and 4M lbs of Pb were produced (Roby and others, 1960). Although several attempts were made in the early 20th century to reopen the mine, the rich ore was evidently spent out.

The Elkhorn Mine was described in detail by Weed (1901), although the names of the formations have changed. The ore bodies, hosted in the Cambrian Pilgrim Formation, were crudely tabular in shape, dipping east at about 40°. The main ore body was in dolomitic marble immediately below the Red Lion shale, which in the mine area is metamorphosed to hornfels. Over 12,000 ft of mine workings was serviced by an inclined shaft that was driven to a depth of

1,439 ft below ground surface. The ore bodies consisted of sulfide minerals (galena, sphalerite, tetrahedrite) replacing marble along bedding planes and fractures. The lodes displayed very little in the way of wall-rock alteration, and skarn minerals are completely lacking in the mine dumps. The passive, replacement style of mineralization prompted McClernan (1983) to suggest that the Elkhorn Mine could be a Mississippi-Valley Type (MVT) deposit, perhaps having formed in the Paleozoic by migrating basinal brines. A recent study by Brown and others (2019) casts doubt on this hypothesis, and suggests the mineralization is related to late Cretaceous magmatic-hydrothermal processes.

In the hills west and north of Stop 7, numerous trenches, road cuts, and small open pits expose locally abundant skarn minerals, including grossular garnet, diopside, vesuvianite, magnetite, tremolite–actinolite, epidote, axinite, and other minerals. Zoned skarn mineralization around the north and east edge of the Black Butte stock was described in detail by Bowman and Essene (1982, 1984) and Bowman and others (1985). However, the gold-rich skarns of greatest economic interest (Everson and Read, 1992) are located further west, closer to the Turnley Ridge Complex (TRC). The recently active Golden Dream prospect sits near the intersection of the TRC, the Black Butte stock, and the Butte Granite (fig. 6). At this location, a small stockpile of auriferous massive sulfide (pyrite–pyrrhotite–chalcopyrite) sits adjacent to a modern portal, waiting to be milled. In an early paper, Knopf (1912) interpreted this site to be a magmatic massive-sulfide deposit similar to Sudbury, Ontario. However, discontinuous pods of Au-rich skarn extend from Golden Dream southward as far as the mine office near the main Elkhorn Road (Everson and Read, 1992). Most of the mineralization is hosted in metamorphosed Wolsey Shale and Meagher Limestone, and is clearly of metasomatic (hydrothermal) origin.

Return to vehicles, and continue on the Forest Service access road that loops around the top of the town of Elkhorn to the east.

11.7 mi—At an intersection in the trees, turn right (south). This road heads to the old Elkhorn cemetery and beyond.

11.9 mi—The road forks. Stay on the lower (right) fork.

STOP 8: Turnley Ridge Complex and contact Metamorphosed Cambrian Sediments (Odometer: 12.1 mi.; 46.27118°N, 111.94620°W).

Find parking on the right before the road takes a sharp left turn up a steep hill. From this spot, we will hike south down an old railroad grade to view outcrops of the TRC. The TRC consists of an older quartz–feldspar porphyry and a younger feldspar porphyry lacking quartz phenocryts. The TRC is older than the Butte Granite and is contact metamorphosed by it (Steefel and Atkinson, 1984), but no radiometric dates are available. It is interesting to speculate that the TRC could be similar in age to the Golden Sunlight porphyry and associated gold-rich breccia pipe, which was emplaced at about 80 Ma (DeWitt and others, 1996), or the 80.2 Ma quartz-eye porphyry (J. Dilles, written commun., 2015) described by Scarberry and others (2017) in the Boulder East 7.5′ quadrangle (Stop 5). Porphyry-style Cu-Mo mineralization associated with the TRC was investigated by the Anaconda Company, but was never aggressively drilled.

The first outcrops encountered on the hike are Cambrian metacarbonates and hornfelsed shale. Less than a mile from the start the trail crosses the Boulaway Fault, on the other side of which is intrusive porphyry of the TRC. Not far from the fault contact, the porphyry contains a quartz-vein stockwork with visible molybdenite, chalcopyrite, and pyrite. After examining this mineralization, return to vehicles and retrace path to Elkhorn.

STOP 9: Group Discussion at Elkhorn USDA-FS Picnic Area (46.27273°N, 111.94977°W).

Discussion questions:

- What is the nature of the contact between the Boulder Batholith and EMVF? Is it a fold-thrust belt type structure with significant post-batholith movement? Or might the contact be a Laramide type structure that cuts the fold-thrust belt?
- Which intrusive event are the gold-rich skarns related to? (Turnley Ridge, Black Butte stock, Butte Granite, all three?) How would you determine this?
- What is the relationship (if any) between carbonate-replacement mineralization at the

Elkhorn Mine and the Au-rich skarns? Could Elkhorn be an MVT deposit? If you wanted to look for more Ag-Pb-Zn deposits of this type in the district, how would you find them?

- What is the relationship (if any) between the breccia pipes at the two "Queen" mines and the Turnley Ridge porphyry? Could a Golden Sunlight-sized breccia pipe be concealed somewhere?
- The metasediments in figure 6 are folded into a dome, elongated N–S. Was this dome caused by intrusion of the Turnley Ridge Complex or is it due to Laramide type shortening?
- Some of these questions are addressed in Steefel and Atkinson (1984) and Brown and others (2019), although nobody really knows the answers!

REFERENCES CITED

Anderson, J. and Smith, D., 1995, The effects of temperature and *f*O2 on the Al-hornblende barometer: American Mineralogist, v. 80, p. 549–559.

Bowman, J.R., and Essene, E.J., 1982, PTX (CO_2) conditions of contact metamorphism in the Black Butte aureole, Elkhorn, Montana: American Journal of Science, v. 282, p. 311–340.

Bowman, J.R., and Essene, E.J., 1984, Contact skarn formation at Elkhorn, Montana: I, PT-component activity conditions of early skarn formation: American Journal of Science, v. 284, p. 597–650.

Bowman, J.R., O'Neil, J.R., and Essene, E.J., 1985, Contact skarn formation at Elkhorn, Montana: II, Origin and evolution of COH skarn fluids: American Journal of Science, v. 285, p. 621–660.

Brown, A., Gammons, C.H., and Poulson, S.R., 2019, New investigations of the economic geology of the historic Elkhorn mining district, Jefferson County, Montana, *in* Scarberry, K.C., and Barth, S., eds., Proceedings of the Mining and Mineral Symposium, Montana Bureau of Mines and Geology Special Publication 120, p. 101–112.

Constenius, K.N., 1996. Late Paleogene extensional collapse of the Cordilleran foreland fold and thrust belt: Geological Society of America Bulletin, v. 108, p. 20–39.

DeWitt, E., Foord, E.E., Zartman, R.E., Pearson, R.C., and Foster, F., 1996, Chronology of Late Cretaceous igneous and hydrothermal events at the Golden Sunlight gold–silver breccia pipe, southwestern Montana: U.S. Geological Survey Bulletin 2155, 48 p.

Everson, C.I., and Read, J.J., 1992, Gold skarn deposits of the Elkhorn district, Jefferson County, Montana: AIME-SME Annual Meeting, Preprint 92–105, 6 p.

Faulds, J.E., and Varga, R.J., 1998, The role of accommodation zones and transfer zones in the regional segmentation of extended terranes, *in* Faulds, J.E., and Stewart, J.H., eds., Accommodation zones and transfer zones: The regional segmentation of the Basin and Range Province: Boulder, Colo., Geological Society of America Special Paper 323.

Faulds, N.H., and Hinz, N.H., 2015, Favorable tectonic and structural settings of geothermal settings in the Great Basin Region, western USA: Proxies for discovering blind geothermal systems: Proceedings, World Geothermal Congress 2015, Melbourne, Australia.

Foreman, B.Z., Rogers, R.R., Deino, A.L., Wirth, K.R., and Thole, J.T., 2008, Geochemical characterization of bentonite beds in the Two Medicine Formation (Campanian, Montana), including a new $^{40}Ar/^{39}Ar$ age: Cretaceous Research, v. 29, p. 373–385.

Foster, F., and Childs, J.F., 1993, An overview of significant lode gold systems in Montana, and their regional geologic setting: Exploration Mining Geology, v. 2, p. 217–244.

Gaschnig, R.M., Vervoort, J.D., Lewis, R.S., and Tikoff, B., 2011, Isotopic Evolution of the Idaho Batholith and Challis Intrusive Province, Northern US Cordillera: Journal of Petrology, v. 52, p. 2397–2429.

Hamilton, W.B., 1988, Laramide crustal shortening, in Interaction of the Rocky Mountain Foreland and the Cordilleran Thrust Belt, Schmidt, C.J., and Perry Jr., W.J., eds., The Geological Society of America Memoir 171, p. 27–39.

Houston, R.A., and Dilles, J.H., 2013, Structural geologic evolution of the Butte District, Montana: Economic Geology, v. 108, pp. 1397–1424.

Kallio, I.M., 2017, Stratigraphic correlation of Late Cretaceous volcanic rocks along the eastern flank of the Boulder Batholith, southwestern Montana: Corvallis, Oregon State University, B.S. Thesis.

Klepper, M.R., Weeks, R.A, and Ruppel, E.T., 1957, Geology of the southern Elkhorn Mountains, Jefferson and Broadwater Counties, Montana: U.S. Geological Survey Professional Paper 292, 82 p.

Klepper, M.R., Ruppel, E.T., Freeman, V.L., and Weeks, R.A., 1971, Geology and mineral deposits, east flank of the Elkhorn Mountains, Broadwater County, Montana: U.S. Geological Survey Professional Paper 665, 1:48,000 scale.

Knopf, A., 1912, A magmatic sulphide ore body at Elkhorn, Montana: Economic Geology, v. 8, p. 323–336.

Korzeb, S.L., and Scarberry, K.C., 2018, Timing of pluton emplacement and mineralization of the Boulder Batholith, *in* Scarberry, K.C., and Barth, S., eds., Proceedings of the Montana Mining and Mineral Symposium 2017: Montana Bureau of Mines and Geology Open-File Report 699, p. 39–44.

Lageson, D., Schmitt, J., Horton, B., Kalakay, T., and Burton, B., 2001, Influence of Late Cretaceous magmatism on the Sevier orogenic wedge, western Montana: Geology, v. 29, p. 723–726.

Lund, K., Aleinikoff, J., Kunk, M., Unruh, D., Zeihen, G., Hodges, W., duBray, E., and O'Neill, J., 2002, SHRIMP U-Pb and $^{40}Ar/^{39}Ar$ age contrasts for relating plutonism and mineralization in the Boulder Batholith region, Montana: Economic Geology, v. 97, p. 241–267.

Lyden, C.J., 1948, The gold placers of Montana: Montana Bureau of Mines and Geology Memoir 26, 152 p.

Martin, M., Dilles, J., and Proffett, J.M, 1999, U-Pb geochronologic constraints for the Butte porphyry system [abstract]: Geological Society of America Abstracts with Programs, v. 31, no. 7, p. A380.

McClernan, H.G., 1983, Lead–zinc–silver deposits in carbonate host rocks in Montana: Mississippi Valley Type? Proceedings of the International Conference on Mississippi Valley Type Lead–Zinc Deposits, University of Missouri-Rolla, p. 516–525.

McDonald, C., Elliott, C.G., Vuke, S.M., Lonn, J.D., and Berg, R.B., 2012, Geologic map of the Butte South 30′ x 60′ quadrangle, southwestern Montana: Montana Bureau of Mines and Geology Open-File Report 622, 1 sheet, scale 1:100,000.

Metesh, J.J., 2000, Geothermal springs and wells in Montana: Montana Bureau of Mines and Geology Open-File Report 415, 29 p.

Olson, N.H., Dilles, J.H., Kallio, I.M., Horton, T.R., and Scarberry, K.C., 2016, Geologic map of the Ratio Mountain 7.5′ quadrangle, southwest Montana: Montana Bureau of Mines and Geology EDMAP 10, 1 sheet, scale 1:24,000.

Pardee, J.T., and Schrader, F.C., 1933, Metalliferous deposits of the greater Helena mining region, Montana: U.S. Geological Survey, Bulletin 842, 318 p.

Prostka, H.J., 1966, Igneous geology of the Dry Mountain quadrangle, Jefferson County, Montana: U.S. Geological Survey Bulletin 1221-F, scale 1:24,000.

Roby, R.N., Ackerman, W.C., Fulkerson, F.B., and Crowley, F.A., 1960, Mines and mineral deposits (except fuels), Jefferson County, Montana: Montana Bureau of Mines and Geology Bulletin 16, 120 p.

Reynolds, M.W., 1979, Character and extent of Basin-Range faulting, western Montana and east-central Idaho, *in* Newman, G., and Goode, H., eds., 1979 Basin and Range Symposium: Rocky Mountain Association of Geologists and Utah Geological Association, p. 185–193.

Rutland, C., Smedes, H., Tilling, R., and Greenwood, W., 1989, Volcanism and plutonism at shallow crustal levels: The Elkhorn Mountains Volcanics and the Boulder Batholith, southwestern Montana, *in* Henshaw, P., ed., Volcanism and plutonism of western North America; vol. 2, Cordilleran volcanism, plutonism, and magma generation at various crustal levels, Montana and Idaho, Field trips for the 28th International Geological Congress: American Geophysical Union, Monograph, p. 16–31.

Scarberry, K.C., 2016, Geologic map of the Wilson Park 7.5′ quadrangle, southwestern Montana: Montana Bureau of Mines and Geology Geologic Map 66, 1 sheet.

Scarberry, K.C., Kallio, I.M., Olson III, N., Dilles, J.H., Older, C.W., Horton, T., and English, A.R., 2016, Large-volume pyroclastic deposits along the eastern edge of the Boulder Batholith, southwestern Montana: Geological Society of America Abstracts with Programs.

Scarberry, K.C., Kallio, I.M., and English, A.R., 2017, Geologic map of the Boulder East 7.5′ quadrangle, southwest Montana: Montana Bureau of Mines and Geology Geologic Map 68, 1 sheet, scale 1:24,000.

Sonderegger, J.L., 1984, A summary of geothermal studies in Montana, 1980–1983: Montana Bureau of Mines and Geology Open-File Report 142, 45 p.

Steefel, C.I., and Atkinson, W.W., 1984, Hydrothermal andalusite and corundum in the Elkhorn district, Montana: Economic Geology, v.79, p. 573–579.

Stickney, M.C., Haller, K.M., and Machette, M.N., 2000, Quaternary faults and seismicity in western Montana: Montana Bureau of Mines and Geology Special Publication 114, 1 sheet, scale 1:750,000.

Stickney, M.C., 2015, Seismicity within and adjacent to the eastern Lewis and Clark Line, west-central Montana: Northwestern Geology, v. 44, p. 19–35.

Smedes, H.W., 1966, Geology and igneous petrology of the northern Elkhorn Mountains, Jefferson and Broadwater counties, Montana: U.S. Geological Survey Professional Paper 510, 116 p.

Tilling, R.I., Klepper, M.R., and Obradovich, J.D., 1968, K-Ar ages and time span of emplacement of the Boulder Batholith, Montana: American Journal of Science, v. 266, p. 671–689.

Vuke, S.M., Porter, K.W., Lonn, J.D., and Lopez, D.A., 2007, Geologic map of Montana: Montana Bureau of Mines and Geology Geologic Map 62A, scale 1:500,000.

Wells, D.L., and Coppersmith, K.J., 1994, New empirical relationships among magnitude, rupture length, rupture width, rupture area, and surface displacement: Bulletin of the Seismological Society of America, v. 84, p. 974–1002.

Weed, W.H., 1900, Mineral-vein formation at Boulder Hot Springs, Montana: U.S. Geological Survey Twenty-first Annual Report, part 2, p. 233.

Weed, W. H., 1901, Geology and ore deposits of the Elkhorn mining district, Jefferson County, Montana: U.S. Geological Survey Annual Report, v. 22, p. 399–510.